DOCTOR OF PHILOSOPHY

The use of subsurface physical barriers to control seawater intrusion in heterogeneous coastal aquifers

Experimental and numerical study

Abdoulhalik, Antoifi

Award date:
2017

Awarding institution:
Queen's University Belfast

The use of subsurface physical barriers to control seawater intrusion in heterogeneous coastal aquifers: Experimental and Numerical study

A thesis submitted to Queen's University Belfast

By

Antoifi Abdoulhalik

in partial fulfilment of the requirements for the Degree of

Doctor of Philosophy

School of Natural and Built Environment

29th September 2017

Abstract

The ever growing threat of seawater intrusion (SWI) has prompted water resources managers to establish practical countermeasures to mitigate its detrimental effects on coastal aquifers. With climate changes and sea level rises severely affecting coastal hydrology, the effort to preserve groundwater quality in coastal areas has promoted the deployment of various practical engineering applications affecting the hydrodynamic of the aquifer, often through physical alteration of the aquifer and/or groundwater recharge. Amongst these is the implementation of subsurface physical barriers. The main purpose of this thesis was to use laboratory and numerical modelling tools to provide an insight on the impact of subsurface physical barriers on seawater intrusion and flow dynamics incorporating commonly found aquifer heterogeneity effects and to assess the performance of the mixed physical barrier (MPB) as a new countermeasure for SWI control purposes. The laboratory experiments were completed in a two-dimensional laboratory tank where automated image analysis techniques were implemented to quantify the SWI parameters under transient conditions with high spatial and temporal resolutions. The numerical code SEAWAT was used for the numerical modelling simulations.

The first objective of this research was to examine the response of seawater intrusion and retreat to incremental water level variations under transient conditions. The saltwater wedge toe motion as well as the freshwater-saltwater transition zone dynamics were quantitatively analysed in response to both sea level and freshwater level fluctuations with high spatial and temporal resolution. The investigation involved the analysis of two homogeneous systems of different properties, and two additional cases incorporating an impermeable wall at different locations. The results showed that the expansion of the transition zone was negligible during the intruding phase of saltwater wedge whether it

resulted from freshwater level drop or saltwater level rise, regardless of the magnitude of the head change applied. By contrast, a substantial widening of the transition zone width was observed during the retreat process, with a peak magnitude and a peak time relatively similar in the scenario involving a rise of the freshwater level and the scenario involving a drop of the saltwater level, in cases of equivalent absolute head change magnitudes. The magnitude of the widening of the transition zone observed during saltwater retreat was larger and extended over longer time period in the aquifer of smaller hydraulic conductivity, whether the head change occurred at the freshwater or saltwater boundary. The experimental observations revealed that the widening mechanism was also enhanced by the presence of some possible freshwater sliding into the wedge during the saltwater retreat process, which was thereafter sucked upward towards the transition zone because of density difference effects, thereby exacerbating the widening. For equivalent freshwater level rise increment, the impact of the impermeable wall on the transition dynamics was different depending on the location of the wall with respect to the position of the toe in the base case. The transient analysis of the saltwater toe length revealed that in cases of equivalent saltwater level variations but opposite directions, the intruding wedge required up to twice longer time to reach steady state condition than the receding wedge, which evidence the timescale asymmetry between saltwater intrusion and retreat processes in scenarios involving sea level fluctuations. When comparing freshwater and saltwater change scenarios, the intruding and receding rates of the saltwater wedge as well as the time taken to reach steady state were fairly comparable. The steady state toe analysis enabled the correlation of logarithmic toe length to the boundary head difference by a simple linear equation with site-specific regression coefficients which vary with different hydrogeological parameter combinations, as shown in the sensitivity analysis.

The second objective of this research was to examine the response of seawater intrusion and retreat to freshwater abstraction through a well in laboratory-scale coastal aquifers under transient condition. The study provided for the first time a valuable insight on the effect of freshwater pumping on the shape and location of the upconing freshwater-saltwater transition zone through qualitative and quantitative analysis. The implemented image analysis enabled uncovering crucial details of some transient related phenomena occurring during the motion of the saline plume as it rises toward the well. The results showed that the vulnerability of the pumping well to salinization was higher for the low permeability aquifer system. The saltwater upconing process could be observed with an abstraction rate smaller in the lower hydraulic conductivity scenario. In addition, the inland penetration of the saline plume was larger in the lower permeability scenario relative to the higher permeability scenario, for equivalent pumping rate increment (up to 41% larger). The widening of the freshwater-saltwater transition zone was observed only as the saltwater wedge approached the well location and occurred especially along the upper part of the interface length, with a visibly more pronounced magnitude in the low permeability scenario. The results showed that the process of decay (following the interruption of the abstraction) of the wedge was slower in the low permeability aquifer system, which suggests a slower restoration of the salinized aquifer and thus a longer time required prior reusing freshwater from the restored aquifers. Flow velocity field analysis revealed that the local reduction of the magnitude of the flow velocity along the upper part of the interface was a major factor contributing to the upconing mechanism, as it allowed “free” vertical rise of the saline plume due to the subsequent reduced repulsion forces of the seaward freshwater flow. Sensitivity analysis showed that the critical pumping rate and critical time (defined as the time taken for 1% salt concentration isoline to reach the well) were more sensitive to the variations of the location than the depth of the well. The critical time increased with increasing location and

depth ratios following a relatively simple linear equation. For all the configurations tested, the lowest critical pumping rate was found for the lowest hydraulic conductivity, which further reflects the vulnerability of low permeability aquifer systems to salinization of pumping wells. Results showed that for the well configurations considered, higher saltwater densities would lead to smaller critical pumping rate and shorter critical time. The influence of the saltwater density on the critical time was more significant for wells located farther away from the initial position of the interface. Results showed that increasing the dispersivity only induced negligible effects on the critical pumping rate, but reduced the critical time for a fixed pumping rate.

The third objective of this research was to examine the effectiveness of cutoff walls in multi-layered heterogeneous coastal aquifers. Three different configurations were tested, including a homogeneous scenario for reference purpose, a stratified aquifer with high K-low K-high K pattern (case HLH) and another stratified aquifer with low K-high K-low K pattern (case LHL). The results show that the cutoff wall was effective in reducing the saltwater wedge in all the investigated cases of layered-aquifers with toe length reduction of up to 43%. The cutoff wall exhibited more saltwater wedge reduction in shallower than steeper hydraulic gradients. However, the aquifer stratification appeared to lessen the overall performance of cutoff walls compared to the homogeneous scenario. The presence of stratification disrupted the flow dynamics, and thus affected the freshwater velocity at the wall opening. The presence of an interlayer of low K (case HLH) inhibited the downward movement of the freshwater towards the wall opening, and thereby decreasing the repulsion ability of the cutoff wall. Moreover, the presence of an underlying low permeability layer (case LHL) was found to partially obstruct the freshwater flow in the lower part of the aquifer, thereby inhibiting the supposed increase of velocity through the wall opening. Numerical analysis of

other layering patterns of monotonically increasing/decreasing permeability from top to bottom showed that the cutoff wall remained effective in repulsing the seawater wedge.

The fourth objective of this research was to explore the impact of layered heterogeneity on the ability of subsurface dams to retain and to clean up SWI in coastal aquifers. Four different layering configurations were investigated, including a homogeneous case (case H), and three different layered cases where a low permeability layer was set at the top of the aquifer (case LH), at the middle part of the aquifer as interlayer (case HLH), and at the lower part of the aquifer (case HL). The subsurface dam was able to retain the saltwater wedge associated with a drop of the hydraulic gradient from 0.0158 down to 0.0095 in all the cases, thereby achieving up to 78% reduction in SWI. In cases LH and HLH, the start of the saltwater spillage was delayed compared to the homogeneous case, and the time taken for the freshwater zone to be fully contaminated (post-spillage) was twice and three times longer, respectively. By contrast, the existence of a low K layer at the bottom of the aquifer (case HL) considerably weakened the ability of dams to retain the intrusion, allowing for quicker saltwater spillage past the wall. The natural cleanup of SWI-contaminated coastal aquifers was, for the first time, evidenced in heterogeneous settings. Depending on the stratification pattern, the presence of stratified layers however prolonged, to various degrees, the cleanup time compared to the homogeneous scenario, particularly in case HL, where the cleanup time was nearly 50% longer.

The fifth and last objective of the study was to propose a new physical barrier system for seawater intrusion control purposes, referred to as the mixed physical barrier (MPB), which consist in the simultaneous implementation of a cutoff wall and a semi-permeable dam located on its seaward side. Four different configurations were investigated, including a base case (without barrier), and three cases which incorporating a subsurface dam, a cutoff wall

and the MPB, respectively. The performance of the MPB in controlling SWI was assessed and compared to that of the traditionally-used physical barriers. The results show that the MPB induced a visible lifting of the dense saline flux upward towards the outlet by the light freshwater. This saltwater lifting mechanism, observed for the first time, induced significant reduction to the saline water intrusion length. The use of the MPB yielded up to 62% and 42% more reduction of the saltwater intrusion length than the semi-permeable dam and the cutoff wall, respectively. The performance achieved by the MPB with a wall depth of 40% of the aquifer thickness was greater than that of a single cutoff wall with a penetration depth of 90% of the aquifer thickness (about 13% extra reduction). This means that the MPB could produce better seawater intrusion reduction than the traditionally used barriers at even lower cost.

Acknowledgments

Firstly, I wish to give all praises and thanks to God, The Most Merciful, to whom this work is exclusively dedicated, for His guidance, help and support throughout this long and lasting journey until completion.

I also wish to express my sincere, profound and hearty gratitude to my very dear mother for her lovely care, very strong encouragements, and countless supplications for me.

I would like to thank my wife for her sincere love and patience throughout the entire duration of my study. I also thank my beloved son for his patience during all this time I stayed away from him to do this work. Thanks also to my brothers for their support, as well as my dear sister.

From a research prospective, I cannot thank enough Dr Ashraf A. Ahmed for his great supervision and the trust that he placed in me, in times of ease and adversity. I sincerely appreciate his guidance, relentless support and countless advice he provided me until completion of my research.

I would like to thank Dr Abdelrahman M. Abdelgawad for his valuable help and the regular and fruitful conversations we had about the results. I also wish to thank Dr Salissou for constantly inviting me for discussion and for his willingness to offer help to further develop my research. Thanks also to Dr Gareth Robinson for his introductory training to the experimental methodology employed in this study.

I would like to rightfully acknowledge the anonymous reviewers of Journal of Hydrology and Journal of Environmental Management for their very constructive comments through the several publications that this work has yielded. Thanks to Dr. Georg Houben and Dr. Ulrich Ofterdinger for their careful examination of the thesis and the suggestions they provided.

Table of content

List of figures

List of tables

Chapter 1

Introduction

1.1 Background on seawater intrusion

1.1.1 Statement of the problem

Aquifers are essentially natural groundwater reservoirs which represent important sources of freshwater that are essential for human life. In simple terms, aquifers are basically water bearing geological formations from which large amount of water could be extracted (Bear, 1972). In overall, groundwater accounts for about a third of the worldwide freshwater use (Bear et al., 1999). For populations living in coastal zones, which represents about 70% of the world's population (Webb and Howards, 2011), groundwater represents the main, in some cases the only, source of water supply. In such areas, groundwater is particularly susceptible to degradation given its proximity with seawater as well as the intense water demand associated with ever increasing population densities (Werner et al., 2013). The subsequent over-abstraction of groundwater to satisfy an increasing demand ultimately leads to the landward incursion of oceanic saline water into fresh coastal groundwater commonly known as seawater intrusion (SWI). The contamination of fresh groundwater by SWI has already occurred in many coastal regions around the world (Bear at al., 1999).

In addition to unreasonable extraction of groundwater, climate change also greatly enhances the saltwater intrusion mechanism in coastal aquifers (Sheriff and Singh, 1999; Oude Essink et al., 2010; Ferguson and Gleeson, 2012). The reduction in freshwater recharge, resulting from changes in rainfall patterns, and sea level rises (SLR) are the two climate change-induced factors that cause a disruption of the hydraulic gradients between the land and the sea, subsequently leading to more pronounced SWI. The reduction of freshwater recharge into an aquifer induces a direct decrease of the magnitude of the seaward

groundwater discharge, which leads to a lesser resistance exerted on the intruding saline water. The rate of freshwater recharge into the aquifer and the magnitude of seaward groundwater discharge are considered the major controlling factors affecting SWI (Ketabchi et al, 2016).

The adverse impact of SLR on SWI has been well documented in the literature (Chang and Clement, 2011; Michael et al, 2013, Watson et al, 2010; Werner and Simmons, 2009). Hussain and Javadi (2016) showed that SLR significantly enhances the inland progression of saline water and caused a substantial reduction of the available fresh groundwater resources, particularly for flat-shoreline aquifer systems. The type of inland boundary condition was found to play a major role in determining the vulnerability of a coastal aquifer to SWI induced by SLR. In physical terms, substantially larger saltwater intrusion lengths have been observed in head-controlled aquifer systems compared to those observed in flux recharge controlled systems (Michael et al., 2013; Rasmussen et al., 2013; Werner and Simmons, 2009). Several studies gave a special attention to the overshooting mechanism (Morgan et al., 2013; Morgan et al., 2015; Watson et al., 2010), a process by which the saltwater intrusion length extends transiently beyond the final equilibrium position as a result of SLR, thereby questioning the steady-state as being the actual worst case scenario. Considering the forecasting of sea level rise of 0.82 m towards the end of the century (IPCC, 2014), SWI will continue to threaten freshwater resources in many countries along the worldwide coastlines in the near future.

SWI is generally characterized by quantitative indicators, which include external metrics that delineate the outward boundary of the saline plume and the freshwater-saltwater interface. A simplified diagram of a typical coastal unconfined aquifer is shown in Fig 1.1a. The external SWI metrics include the horizontal extent of intrusion, often called the toe length, and the vertical extent along the coastline boundary (Goswami and Clement, 2007,

Sebben et al., 2015). The freshwater-saltwater interface is a specific characteristic feature of coastal aquifers that occurs as a transition-zone where the salt concentration varies gradually from that of the freshwater to that of the saltwater in the seaward direction. These parameters outline the wedge-like shape of the plume that the intruding saltwater tend to form while encroaching homogeneous isotropic coastal aquifers, albeit aquifer heterogeneity may, to various degrees, severely affect this highly idealised shape.

The main detrimental effects of SWI are the contamination of production wells and the loss of the volume of available fresh groundwater sources. As saline water intrudes deeper into the aquifer system and approach the location of the pumping wells, large withdrawal of groundwater leads to the rise of the freshwater-saltwater interface below or within the vicinity of the well, a process known as saltwater upconing mechanism (Reilly and Goodman, 1987). A simplified diagram showing the saltwater upconing mechanism is shown in Fig 1.1b. A review of saltwater upconing investigations is provided in section 1.1.2. Incorrect management of freshwater pumping may eventually lead to the salinization of pumping wells, which would occur following the mixing of only 250 mg/l of chloride after which freshwater is considered undrinkable as per WHO regulations (WHO, 2011), which is equivalent to less than 1% of seawater. Mixing with 3-4% of seawater is sufficient to render groundwater unsuitable for irrigation purposes and rising this to 6% renders it unfit for all purposes except for cooling (Morris et al., 2003).

Once an aquifer is contaminated, the clean-up process is often very difficult and unreasonably costly (Simpson et al, 2014). The salinization of a groundwater supply not only causes considerable impacts on human health and the ecological system, but it also leads to considerable negative economic impact, due to the very high cost involved in the replacement of a water supply once groundwater is contaminated, which is very often associated with the close-down of water intensive businesses, i.e industries and farms relying mostly on

groundwater in coastal areas (Klassen and Allen, 2017; Simpson et al, 2014). Preventive measures should therefore be implemented to protect production wells and groundwater storages from salinization and thus enable sustainable and optimal exploitation of the available groundwater resources.

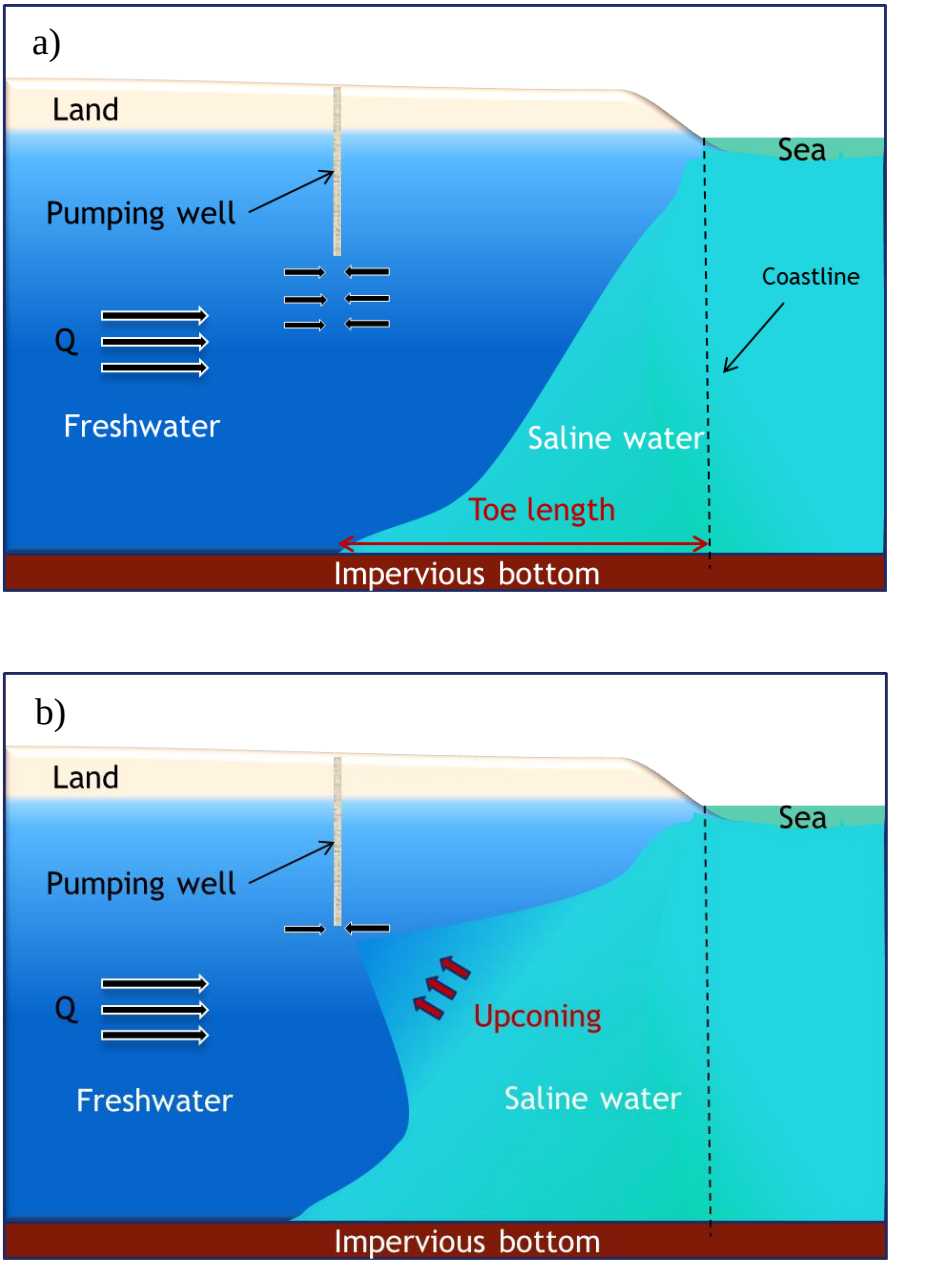

Figure 1.1 Simplified diagrams of a coastal unconfined aquifer showing a) the SWI mechanism and b) the saltwater upconing process. The transition-zone is shown as a sharp interface for the sake of simplicity

1.1.2 Saltwater upconing investigations

The issue of rising freshwater-saltwater interface towards pumping wells was addressed by Dagan and Bear (1968) who developed mathematical equations and verified their results using series of sand box model experiments. Based on the equations of Dagan and Bear (1968), Schmork and Mercado (1969) mathematically determined the critical pumping rate, which is defined as the highest rate at which the freshwater-saltwater interface can remain stable below the well without the discharge of rendering saline the discharge of the well (Reilly and Goodman, 1987). Kashef and Smith (1975) simulated the extent of saltwater intrusion interface resulting from freshwater abstraction considering different well design parameters and various aquifer properties. Factors controlling the critical pumping rate and the extent of saltwater upconing were investigated either experimentally or numerically; however most of these investigations were based solely on qualitative analysis. These controlling factors could be subdivided into two main categories: the first category includes the parameters related to the well and pumping characteristics such as: location, depth, rate and sequence of pumping; the second category includes parameters related to the physical and hydraulic properties of the aquifer, such as the hydraulic gradient, the hydraulic conductivity, the dispersivity, the porosity, the saltwater density and the initial position of the freshwater-saltwater interface.

Several numerical modeling studies have attempted to explore upconing problems in a field scale models. Diersch et al. (1984) investigated saltwater upconing process using an axisymmetric model assuming steady-state condition. Their results showed the influence of dispersion and demonstrated that density and dispersion coupling induced some new effects in the breakthrough behaviour of the concentration for the pumped water. Reilly and Goodman (1987) investigated steady-state upconing problems using the sharp-interface and the fluid-density-dependent solute transport methods. Their results showed that longitudinal

dispersion induced negligible effects on the concentration distribution, but evidenced the strong sensitivity of the upconing saltwater distribution to transverse dispersivity. Although considering steady-state flow condition is very convenient when investigating regional flow systems, investigating transient upconing conditions enable gaining a valuable insight on the movement of saline water toward the pumping well and enable the examination of the flow dynamics.

Several investigations have been conducted to simulate the upconing mechanism under transient conditions (Wirojanagud and Charbeneau, 1985; Johannsen et al., 2002; Zhou et al. 2005; De Louw et al., 2013). Most of these numerical studies focused on 3D and/or axisymmetric models. Johannsen et al. (2002) performed a 3D saltpool as a benchmark problem of saltwater upconing in a porous media. Oswald and Kinzelbach (2004) compared their numerical results with the experimental saltpool box and found that the upconing was more pronounced in the numerical model with the mixing zone being significantly wider. Shi et al. (2011) validated a steady-state 3D numerical model with a sandbox saltwater intrusion experiment under freshwater pumping condition. They conducted series of experiments which included scenarios with different combinations of freshwater pumping and injection and saltwater pumping. The freshwater–saltwater transition zone was considered abrupt in their experiments.

Few studies investigated the upconing mechanism within 2D laboratory-scale experiments (Werner et al., 2009; Mehdizadeh et al., 2015; Noorabadi et al., 2017). Werner et al. (2009) verified their experiments using the analytical equation of Dagan and Bear (1968). Their experiments were designed to evaluate saltwater movements subjected to different pumping rates and under different freshwater–saltwater density contrasts. The influence of density was shown to be minor in comparison to the influence of pumping rate. Jakovovic et al (2011) simulated the laboratory experiments of Werner et al. (2009) using fine

discretization and small dispersion coefficients. The results showed good agreement with those of the sandbox experiments for high pumping rates and low density contrasts, but the interface rise was over estimated for low pumping rates. Mehdizadeh et al. (2015) simulated saltwater upconing in a sharp interface model and compared their results to laboratory tank experiments and dispersive model results, in terms of salt wedge shape and well salinity. Noorabadi et al. (2017) conducted 2D laboratory upconing experiments in steady state condition, varying the saltwater concentrations, the extraction rates and the depth of the well. In most of the previous upconing laboratories studies, the variation of salt concentration within the freshwater-saltwater transition zone during the upconing was not explored mostly because measurements were only through visual observations. Thus, crucial details of transient related phenomena occurring within the freshwater-saltwater transition zone during the upward motion of the saline plume as it rises toward the well were often poorly described. In addition, the impact of aquifer hydraulic conductivity on the saltwater upconing and decay (following pumping shut-off) mechanisms has never been explored and is yet to be examined. Addressing these knowledge gaps is one of the objectives of this investigation.

1.1.3 Seawater intrusion control methods

Several practical measures to prevent or mitigate SWI have been suggested in previous studies (Oude Essink, 2001; Todd, 1959; Van Dam, 1999). These countermeasures have been classified into pumping rate reduction and/or well relocations, artificial aquifer recharge and underground barriers (Abarca et al., 2006). Modifying the pumping pattern is often not an effective solution and, is in most cases, unsuccessful in remediating SWI (Werner et al., 2013). The efforts of preserving the quality of ground waters in coastal zones has yielded the development of various practical engineering solutions that affect the flow hydrodynamic of coastal aquifers, through physical alteration of a portion of the aquifer and/or artificial groundwater recharge. These essentially consist in the implementation of

subsurface barriers, which may be of hydraulic or physical nature (Abarca, 2006; Oude Essink, 2001).

Hydraulic barriers can be divided into three types: positive, negative, and mixed barriers, as shown in Fig 1.2. In positive barriers (Fig 1.2a), freshwater is injected into the aquifer to raise the water table, which impedes the inland motion of the saltwater. The water is often injected through recharge wells installed in series along the coastline to create a freshwater ridge. Although the effectiveness of positive barriers has been argued in some studies (Abarca et al., 2006), recent studies have shown that an effective saltwater repulsion could only be achieved if the water is injected at the toe of the saltwater wedge (Botero-Acosta and Donado, 2015; Luyun et al. (2011). This highlights a significant limitation of positive barriers, considering that the saltwater wedge is never completely stationary in real-world scenarios but moves back and forth with seasonal oscillations (Michael et al., 2013).

Negative barriers (Fig 1.2b) involve the interception of the intruding saltwater by pumping near the coast. Although the landward motion of the saltwater could be slowed, it was found that these barriers extract more freshwater than saltwater which eventually leads to a decrease of the available groundwater resources (Pool and Carrera, 2010). In addition, this method is only effective if the saltwater abstraction rate exceeds the freshwater pumping rate, thus involving a considerable and continuous amount of energy (Sriapai et al., 2012). The disposal of the abstracted saline groundwater could also be a source of concern (Kumar, 2006). A mixed hydraulic barrier (Fig 1.2c) combines a positive barrier and a negative barrier. Freshwater is injected inland to repulse the saltwater wedge, while saltwater is extracted near the shore to slow its encroachment (Basdurak et al., 2007; Pool and Carrera, 2010). In addition to the limitations mentioned above, this measure would require significant operational and maintenance costs due to the high risk of clogging and reduction of filtering area of the screen generally involved in the use of wells (Bear, 1979).

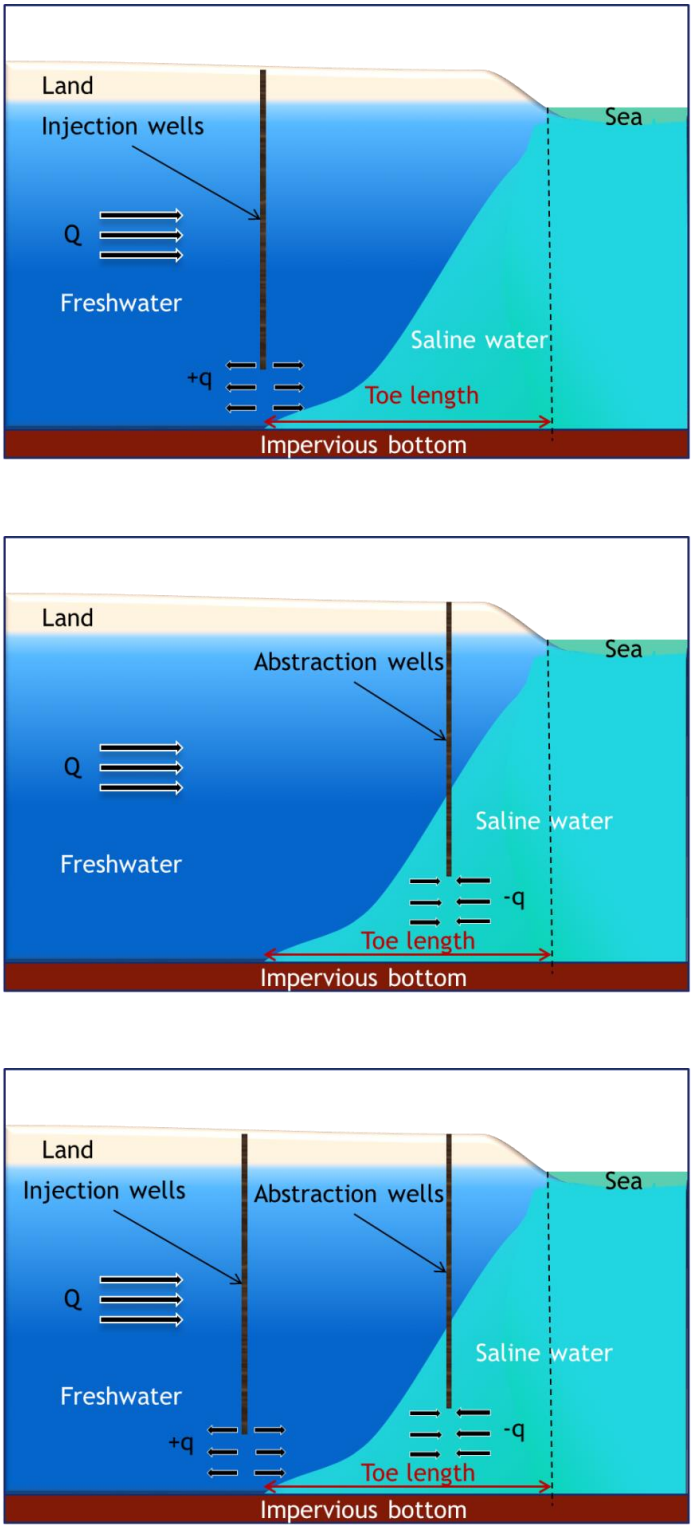

Figure 1.2 Simplified diagrams showing the various hydraulic barriers; a) Positive barrier, b) Negative barrier and c) Mixed hydraulic barrier.

The use of physical barriers as a SWI control method has been the focus of several studies (Archwichai et al., 2005; Sugio et al., 1987; Hasan Basri, 2001; Anwar, 1983; Kaleris and Ziogas, 2013; Luyun et al., 2009, 2011; Strack et al., 2016). Physical barriers are subsurface impermeable or semi-permeable structures constructed parallel to the coast. Two main types of physical barriers are described in the literature: the subsurface dams and the cutoff walls. The construction of barriers often involve sheet piles, cement grout, or chemical grout. Fig 1.3 presents simplified diagrams showing the main subsurface barriers used for seawater intrusion control. Another "excavation free" method was recently suggested by Strack et al. (2016), which consists in reducing the hydraulic conductivity of the upper part of the aquifer by injecting precipitate at the surface downstream from production wells to mitigate SWI.

The subsurface dam is embedded at the impervious bottom layer of the aquifer and obstructs its lower part only, leaving an opening above it to allow the natural discharge of freshwater to the ocean (Fig 1.3a). This method has met great success in Japan, where seven out of fifteen subsurface dams were specifically designed to prevent landward incursion of saltwater and preserve fresh groundwater storage (Luyun et al., 2009; Japan Green Resources Agency, 2004). Advanced construction procedures have been deployed allowing noticeable saving in construction cost generally involved in the implementation of this countermeasure (Luyun, 2010). Luyun et al. (2009) demonstrated that subsurface dams with smaller height could achieve faster removal of inland residual saltwater as well as more reduction of the expected increase of the saltwater wedge height along the coastline boundary than higher dams. The dam height only needs to exceed the height of the saltwater wedge at the desired construction location.

The second type of physical barrier is cutoff walls, which extend from the top of the aquifer to a predefined depth (Fig 1.3b). The effectiveness of cutoff walls increases when

they are closer to the coastline and have greater penetration depth (Luyun et al., 2011). The closer the cutoff wall is installed to the coast, the larger the fresh groundwater volume would be. Kaleris and Ziogas (2013) found that the performance of cutoff walls located at distances from the coastline of the order of half of the aquifer height depends not only on the penetration depth, but also on the ratio of the groundwater inflow velocity over the density driven saltwater velocity. The results reported in Kaleris and Ziogas (2013) suggest that increasing the velocity ratio would not only better help to repulse saltwater intrusion, but it would also allow an increased freshwater storage thus allowing a more optimal exploitation of the available freshwater resource. One objective of this study addresses this point by proposing a new barrier system, as described below.

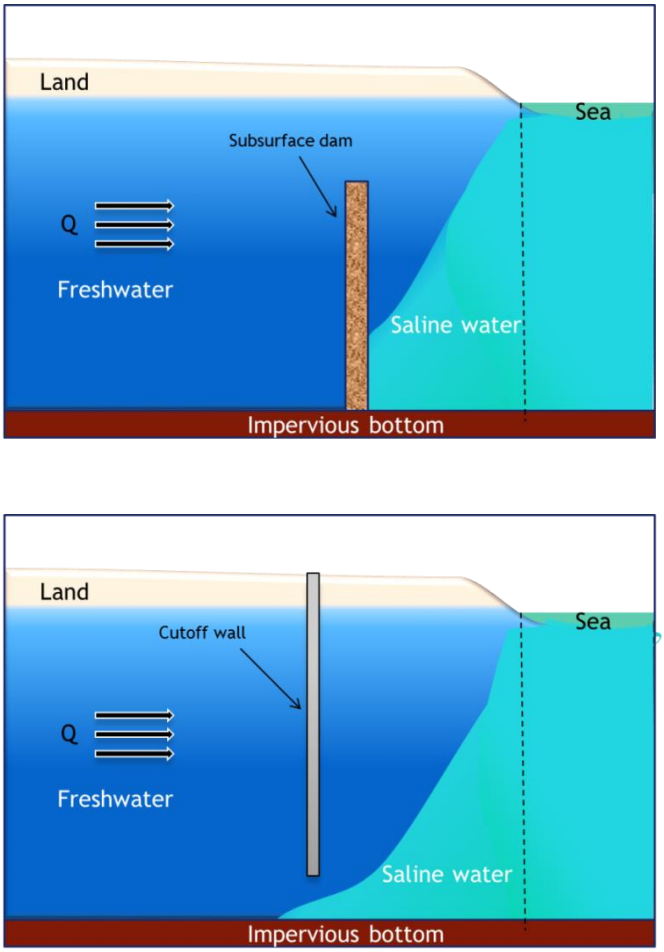

Figure 1.3 Simplified diagrams showing the various physical barriers; a) subsurface dam and b) cutoff wall

1.1.4 Impact of heterogeneity on seawater intrusion

The presence of spatial variation in the hydraulic conductivity within a geologic structure causes disruptions of the flow over various length scales and plays an important role in density-dependent flow systems (Simmons et al., 2001). A few well documented field studies have highlighted the impact of inherent heterogeneity on groundwater flow dynamics and solute transport. Compte et al (2017) provided quantification of the impact of volcanic dykes on groundwater flow and seawater intrusion in a coastal sandstone aquifer in Northern Ireland using multi-physics hydrogeological approach. Their results showed that the existence of the dykes induced preferential paths of flow and salt transport, whereby flow occurred parallel to the observed dyke orientations. Kim et al (2006) explored the impact of tidal fluctuations on freshwater–saltwater interface motion and groundwater flow in a heterogeneous layered coastal aquifer on Jeju Island (Korea). Their results revealed strong dependency of the freshwater-seawater locations to the presence of geological layers. Oki et al., (1998) examined a layered coastal aquifer system in Oahu, (Hawaii, USA) and reported that the freshwater flow direction, the water level distribution and salinity are primarily controlled by variations in hydraulic conductivity.

Despite that the variability of possible geological structures encountered in real world cases does not allow generalizing the heterogeneity effects, a sound understanding can be gained from analysing SWI in various simplified heterogeneous configurations (Werner et al, 2013). One of the most prevalent forms of subsurface heterogeneity commonly encountered in real coastal aquifer systems is the layered heterogeneous structures, which consist of simulating various stratified layers of different hydraulic conductivities. Such representations of heterogeneous aquifer systems have been simulated in several previous SWI studies (e.g. Ketabchi et al., 2014; Liu et al., 2014; Dose et al., 2014; Mehdizadeh et al., 2014). Mehdizadeh et al, (2017) explored the impact of gradual and instantaneous SLR on SWI

within field-scale layered aquifers of different hydraulic conductivity ratios. Strack et al., (2015) provided an analysis for modelling interface flow in a stratified aquifer using a comprehensive potential. Their results revealed that a significant seaward shifting of saltwater wedge toe position could be observed in the scenario where a highly conductive zone covered the bottom part of the system, whereby the freshwater-saltwater interface was displaced toward the sea. Lu et al, (2013) examined steady-state freshwater-saltwater transition zone behaviour within multi-layered coastal aquifer systems with various layering patterns using physical experiments. They observed a noticeable distortion and a widening of the transition zone at different locations along the interface length depending on the stratification pattern simulated. Their results also revealed a significant displacement of the location of the freshwater-saltwater interface toe position for all their investigated heterogeneous configurations relative to their homogeneous scenario.

A serious and common limitation in the (limited) previous studies on physical barriers is the assumption of homogeneous and isotropic conditions (e.g. Anwar, 1983; Luyun et al., 2009, 2011). The widely accepted representation of porous media using a single homogeneous layer does not represent a true reflection of the reality. This simplification results from our limited ability to derive detailed characterisation and observation of hydraulic conductivity distributions in real world settings over large spatial scale (Simmons et al., 2001). It is expected that simulating SWI within various typical layered configurations in subsurface barrier controlled environments through laboratory and numerical modelling would not only provide a valuable insight on the influence of such typical geological formations on the workability of these physical barriers, but it would also help better understand the impact of physical barriers on the flow dynamics and solute transport within typical layered heterogeneous coastal aquifers.

1.2 Objectives of the study

The main purpose of this work was to provide an insight on the impact of subsurface physical barriers on seawater intrusion and flow dynamics in typical heterogeneous coastal aquifer settings using laboratory and numerical modelling tools and to assess the performance of the MPB as a new countermeasure for SWI control purposes. This was subdivided into 5 research objectives that were addressed in five distinct chapters.

The first objective of this study was to provide an analysis of the response of seawater intrusion and retreat to incremental water level variations and freshwater abstraction under transient condition. The saltwater wedge toe motion as well as the freshwater-saltwater transition zone dynamics were quantitatively analysed during the intrusion and retreat processes in response to both sea level and freshwater level fluctuations under transient condition using physical experiments.

The second objective of this study was to investigate the response of seawater intrusion to freshwater abstraction under transient condition. The key influential factors affecting the saltwater upconing mechanism were examined in laboratory-scale coastal aquifer system, thereby providing a valuable insight on the effect of freshwater pumping on the shape and location of the upconing of the saltwater wedge and on the freshwater-saltwater transition zone through qualitative and quantitative analysis.

The third objective of this study was to examine the effectiveness of cutoff walls in multi-layered coastal aquifer settings. Multi-layered coastal aquifer settings with stratification patterns high permeability-low permeability-high permeability and low permeability-high permeability-low permeability were simulated within the physical model and additional layering patterns of monotonically increasing/decreasing permeability from top to bottom were analysed using numerical modelling.

The fourth objective focused on exploring the impact of a low-permeability layer on the ability of subsurface dams to 1) restrict the saltwater spillage towards the landward side of the wall and 2) clean up the landward freshwater zone from residual saline water. Three layered configurations where a low permeability layer was set at the top part, in the middle part and at the bottom part of an aquifer were analysed. An insightful transient analysis of the spillage and flushing processes of saline water over the subsurface dam was therein provided in these various heterogeneous configurations.

The fifth objective of this study was to investigate the concept of combined actions of cutoff wall and subsurface dam on seawater intrusion. A new physical barrier system was proposed, referred to as the mixed physical barrier (MPB), which consists in the simultaneous application of an impermeable cutoff wall located close to the shore, and a short semi-permeable subsurface dam placed at the seaward side of the wall. The main feature of this MPB system is to increase the ratio of the seaward freshwater flow velocity over the intruding saline water velocity, and hence further enhance the capability of the barrier to repulse the seawater wedge and allow a more optimal use of the freshwater resources.

In overall, the thesis is subdivided into 8 chapters. The first chapter provides some relevant literature pertaining to this research, lists the research objectives, and provides a brief preview of each chapter. The second chapter presents a description of the general methodology adopted in this research as well and the details of the experimental settings investigated. The third chapter addresses the first objective of this research, which is the response of seawater intrusion and retreat to incremental water level variations. It yielded one journal publication (currently under review in Hydrological processes). The fourth chapter addresses the dynamics of seawater intrusion in response to well abstraction, from which a publication was derived (currently under review in Journal of Hydrology). The fifth chapter addresses the effect of cutoff walls on SWI in multi-layered heterogeneous aquifers. It

yielded a publication in Journal of Environmental Management (Abdoulhalik and Ahmed, 2017a). The sixth chapter covers the fourth research objective (the use of subsurface dams to control SWI in layered aquifers), from which a publication was derived in the Journal of Hydrology (Abdoulhalik and Ahmed, 2017b). The seventh chapter discusses the new proposed physical barrier system (fifth objective). The outcome of this chapter has been communicated to Journal of Hydrology (Abdoulhalik et al, 2017). The eighth and final chapter summarizes the main findings of this research and offers some recommendations for future work.

Chapter 2

General methodology

2.1 Experimental methods

2.1.1 Description of the apparatus

A laboratory flow tank of dimension 0.38 m x 0.15 m x 0.01 m representing a cross section of an unconfined coastal aquifer was used for the experiments. Fig 2.1 shows a schematic diagram of the flow tank. The flow tank was subdivided into three distinct compartments: a central chamber and two circular reservoirs located at either side. The central chamber was filled with clear glass beads from Whitehouse Scientific® to simulate the porous medium. Two fine mesh acrylic screens with aperture diameter of 0.5 mm were located at each side of the central chamber to separate the porous medium from the side reservoirs. The aperture of these meshes were small enough to contain the glass beads and sufficiently large to allow circulation of water flowing from the side reservoirs. The bottom of the central viewing chamber was located 5 mm below the visible bottom edge of the central chamber. Therefore, to allow direct comparison between experimental and numerical results, this offset was accounted for in all the forthcoming experiments.

The two reservoirs were used to provide constant-head boundary condition at either side of the porous media. The left and right side reservoirs were filled with freshwater and saltwater, respectively. The freshwater reservoir was filled with cold tap water. Adjustable overflow outlets were placed within each reservoir to maintain the water levels by draining any excess water to waste. Each of the overflow outlets was connected to a flexible hose that was plugged at the bottom of each reservoir as shown in Fig 2.1. The saltwater filling the right side reservoir was sourced from a 200 L saline water solution prepared prior the experiments.

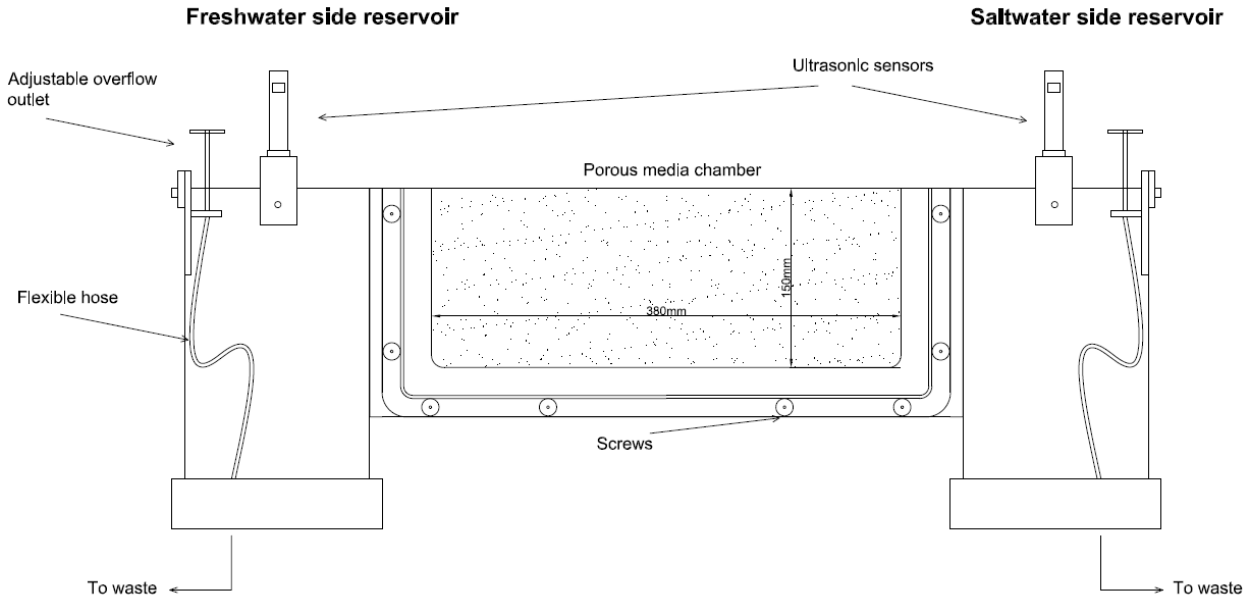

Figure 2.1 Schematic diagram of the porous media tank

2.1.2 Measurements of porous media properties

As previously stated, glass beads were used to simulate the porous media. To simulate heterogeneity effects, different bead sizes were used, namely 780 µm, 1090 µm and 1325 µm. The hydraulic conductivity of each of these was estimated using in situ measurement within the experimental flow tank. Various hydraulic gradients were successively imposed to the system, and the corresponding volumetric freshwater discharge was measured. The average hydraulic conductivity value was then subsequently derived using Darcy's law, as described in Oostrom et al., (1992). The average hydraulic conductivity value of the porous media was estimated at 36 cm/min, 85 cm/min and 108 cm/min, for the beads 780 µm, 1090 µm and 1325 µm, respectively. The porosity of porous media was measured using volumetric method and an average value of 0.38 was considered for all the beads.

2.1.3 Fluids measurements

The saltwater solution was prepared by dissolving commercial salt into freshwater to achieve a density of 1025 kg/m^3. A batch of 200 L was prepared before each set of experiments. The density of the saltwater solution was monitored using a hydrometer H-B Durac plain-form polycarbonate and through manual measurements using mass/volume ratio. In order to distinguish it from the freshwater, red food colour was added to the saltwater at concentration of 0.15 g/L. The scale used for the measurement of salt and dye quantities was accurate to 0.01g. For each set of experiments, the saltwater was primarily sourced from the initial 200 L batch in order to reduce any possible risks of density or colour discrepancies between each experiment to a minimum.

The water levels in both freshwater and saltwater reservoirs were monitored using ultrasonic sensors Microsonic - mic+25/DIU/TC with ± 0.2 mm accuracy. The reading was shown by a digital display integrated into the sensors. The sensor display was programmed to show readings as percentages over a 20 mm range, such that each 1% increment was equivalent to a change in water level of 0.2 mm. The increments of 0.2 mm allowed to accurately measure the water levels and to adjust the overflow outlets accordingly.

2.2 Experimental procedure

2.2.1 Preparation of the experimental set-up

A photograph of the whole experimental set up used in this study is shown in Fig 2.2. The glass beads were packed into the central chamber under saturated conditions to avoid air bubbles development. The beads were packed in successive even-sized layers and each layer was carefully compacted to ensure homogeneity of the packing. Two LED lights (Camtree 600) were placed behind the experimental set-up to illuminate the porous media and a

diffuser was fixed to the back of the tank to ensure homogeneity of the light throughout the aquifer.

A high speed camera IDT MotionPro X-Series was used to capture images of the experiments. The camera was equipped with a capture resolution of 1280x1024 pixels and an 8-bit grayscale pixel depth. The resolution enabled for a pixel size of about 0.3 mm and the grayscale pixel depth provided a range of 256 available light intensities. The IDT Motion Studio software was used for the acquisition of the images. The IDT Motion Studio software enabled to trigger the camera externally by using a flashing LED bulb connected to a variable analogue timer which allowed a control over the sample rate, which was set to 30 s for all the experiments. Each time the camera was triggered, 10 images were recorded. The average of these images was then used in the analysis procedure. The images were taken at a rate of 100 Hz, which means that each image was taken in 0.01s (i.e. 0.1s for all 10 images).

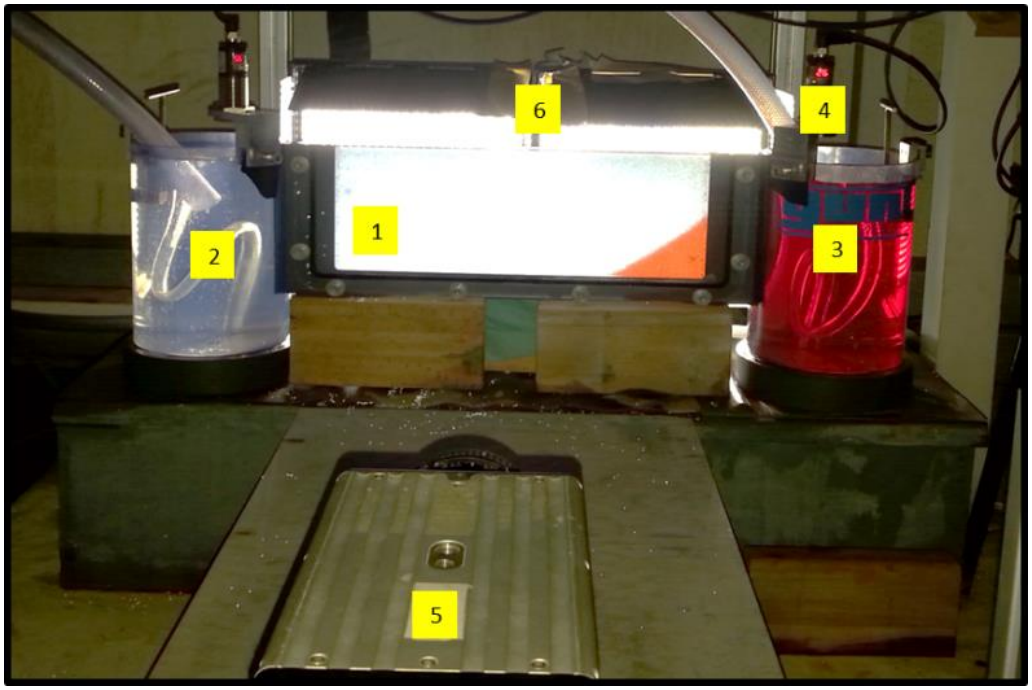

Figure 2.2 Photograph of the experimental set up; 1) porous media chamber; 2) freshwater reservoir; 3) saltwater reservoir; 4) ultrasonic sensors; 5) high speed camera; 6) LED lights

2.2.2 Calibration procedure

To allow the determination the key SWI parameters, each experimental configuration was preceded by a calibration procedure allowing correlation of the saltwater concentration to the intensity of the light transmitted through the main chamber. This calibration is described in thorough details in Robinson et al. (2015). A summary of the main steps is given below.

The purpose of the calibration was basically to correlate the saltwater concentration to the intensity of the light transmitting through the main chamber. The calibration procedure consisted in flushing the entire system with various saltwater solutions at known concentrations and recording the image of each saturated aquifer. In all, eight solutions were used to flush the system, with a concentration of 0% (i.e. freshwater), 5%, 10%, 20%, 30%, 50%, 70% and 100% of the total saltwater concentration. For every concentration, the light intensity of every single pixel of the system was recorded. In other words, eight light intensities were recorded for eight known concentrations. The known concentrations and corresponding light intensities were used to derive, through regression analysis, the coefficients a, b and c of a power law curve expressed by: $C = aI^b - c$, adopted to relate the light intensity I and the concentration. The regression analysis was performed through a MATLAB code developed for the purpose (Robinson et al., 2015)

The images recorded over the course of the experiments could then be analysed through another MATLAB code which applied the derived regression coefficients determined in the calibration and analysed each single image to calculate the intrusion parameters (i.e. toe length and width of transition zone) and provided post-processed images displaying the distribution of salt concentration throughout the system for clear visualisation. The toe length was taken as the distance between the 50% concentration isoline and the saltwater boundary along the bottom boundary, and the width of the transition zone was measured as the average

of the vertical distance between the 25% and 75% saltwater isolines within the range 20% and 80% of the toe length.

2.2.3 Data acquisition procedure

Prior to the experiments, freshwater was injected at constant rate from a large tank located above the left side reservoir. The freshwater level was set high enough to allow the entire porous media to remain fully saturated with freshwater. Freshwater flux transited through the system from the inland boundary and exited at the coastal boundary without overflowing. The freshwater exiting the system was rapidly drained out through the overflow outlet of the saltwater reservoir. The later was adjusted such that to maintain a constant saltwater head of 129.7 mm. Excess amount of saltwater was supplied from another large tank into the right reservoir to ensure the prompt flushing out of any freshwater floating at the surface. The density in the saltwater reservoir was continuously monitored using a hydrometer. The saltwater intrusion experiment was initiated only after stabilisation of the density measurements.

The experiments were initiated by lowering the overflow outlet of the freshwater reservoir such that to impose an initial constant freshwater head of 135.7 mm. This initial head boundary difference dh = 6 mm which allowed the dense saline water to penetrate into the porous media up to nearly a fourth of the total aquifer length, as shown in Fig 2.2. This head difference was used in all the experiments as initial head boundary conditions. The steady state condition was assumed when no substantial changes could be visually observed in the freshwater-saltwater interface position. Various hydraulic gradients were thereafter applied to the system to simulate changes in the hydrological conditions. This was done by varying the freshwater level such that to impose various head differences ranging from dh = 6 mm to dh = 2 mm, corresponding to hydraulic gradients of 0.0158, and 0.0053, respectively. These values were within the range of hydraulic gradients values commonly used in previous

similar laboratory studies (Goswami and Clement, 2007; Chang and Clement, 2012) as well as within the range of values measured in some real coastal aquifers (Ferguson and Gleesson, 2012; Attanayake and Michael, 2007).

2.2.4 Experimental settings investigated

The details of the experimental procedure pertaining to each experimental set are provided in their respective chapter. The study on the transience of seawater intrusion response to incremental water level variations (Chapter 3) included a total of 54 experiments. All the experiments were therein performed for the two bead sizes 1090 µm and 1325 µm. This set included 34 experiments (17 hydraulic gradients for each bead size) for advancing and receding saltwater wedge experiments as a result of freshwater level variations, while maintaining the saltwater boundary constant. Another set of 20 experiments (ten hydraulic gradients for each bead size) were conducted for the advancing wedge and receding wedge experiments where the saltwater level was changed while the freshwater boundary was held constant.

The investigation of the saltwater upconing mechanism in homogeneous coastal aquifer system (Chapter 4) included 11 experiments. These comprehended seven experiments (six different pumping rates plus one initial case without pumping) for the beads 1090 µm and four experiments (including three different pumping rates plus one initial case without pumping) for the beads 790 µm. Each test was initiated by establishing first the initial head difference (dh = 6 mm) to allow the intrusion of saline water until steady state prior to the start of the abstraction process. The abstraction rate was thereafter increased in a stepwise fashion such that the number of pumping rates applied to each experiment corresponded to the number of pumping rates used until saltwater upconing mechanism was observed.

The investigation of the effectiveness of cutoff walls in layered heterogeneous coastal aquifers (Chapter 5) included in total 18 experimental cases. These included nine experimental cases (three physical experiments x three different hydraulic gradients), where saltwater intrusion dynamics was investigated in each aquifer setting prior to wall installation (base cases), and nine others experimental cases (three physical experiments x three different hydraulic gradients) where the performance of cutoff walls was examined in each corresponding aquifer setting. Three different aquifer configurations were analysed in this investigation, including two stratified aquifers of pattern High K-Low K-High K and Low K-High K-Low K and a homogeneous scenario for reference purpose. Additional aquifer settings were analysed using numerical modelling experiments.

The study on the impact of heterogeneity on the performance of subsurface dams comprehended a total of 48 experimental cases (Chapter 6). These included 20 different experiments (four physical experiments x five different hydraulic gradients) for the base cases i.e. where the saltwater wedge was analysed in advancing and receding conditions in an aquifer free of barrier; and 28 different experiments (four physical experiments x seven different hydraulic gradients) for the subsurface dam cases, where the ability of subsurface dams to retain SWI and clean up contaminated aquifers from previously intruded saline water was assessed in the various aquifer settings. The investigated settings included a homogeneous case and three different layered cases where a low permeability layer was set in the top part of the aquifer (Low K-High K), in the middle part of the aquifer (High K-Low K-High K) and along the aquifer bottom (High K-Low K).

The investigation of the impact of the MPB on saltwater intrusion dynamics was investigated in homogeneous conditions using the beads 1090 μm (Chapter 7). This set of experiments comprehended a total of 12 experimental cases, which included one base case experiment where three different hydraulic gradients were tested and three physical barrier

experiments where three different hydraulic gradients were applied. The physical barrier experiments included the investigation of the effect of a semi-permeable subsurface dam, a cutoff wall case and the MPB on SWI dynamics.

2.3 Description of the numerical model

The MODFLOW family variable density flow code SEAWAT (Guo and Langevin, 2002) was used to perform the numerical modelling experiments. SEAWAT combines the modified MODFLOW (Harbaugh, et al., 2000) and MT3DMS (Zheng and Wang, 1999) into a single program that solves the coupled groundwater flow and solute-transport equations. SEAWAT has been widely used to solve various variable-density groundwater flow, such as the Henry problem, the Elder problem, and the HYDROCOIN problem (Guo and Langevin, 2002; Langevin et al., 2003). SEAWAT has also been successfully used for modelling SWI experiments involving freshwater head boundary variations (Goswami and Clement, 2007; Chang and Clement, 2012). The purpose of performing numerical simulations was primarily to assess the consistency of the experimental data with the numerical predictions and thereafter used the developed models to better explain underlying phenomena, through series of sensitivity analyses and/or by exploring the flow velocity field throughout the various aquifer systems investigated.

For each study, the dimensions of the two dimensional vertical simulation area corresponded to the dimensions of the porous media chamber of the flow tank. The model domain was evenly discretised with a grid size of 0.2 cm. A no flow boundary condition was set at the top and bottom of the model domain. The longitudinal dispersivity was estimated after trial and error process and was eventually estimated at 0.1 cm and the transverse dispersivity was 0.05 cm, which is within the range of dispersivity values reported in Abarca and Clement (2009). The spatial discretization satisfies the criterion of numerical stability, i.e. grid Peclet number was less or equal to four (Voss and Souza, 1987). The porosity was

set to 0.38. The molecular diffusion was neglected in all the numerical simulations (Riva et al., 2015). The specific storage was set at 10^{-6} cm^{-1}. The freshwater density was set to 1000 kg/m^3 and the saltwater density was set to 1025 kg/m^3. Considering the standard density-concentration slope factor of 0.7, a concentration of 36.16 g/L was used for the seawater boundary.

At the start of the simulation, the model domain corresponded to an entirely fresh aquifer. In all the simulation, the freshwater and the saltwater boundary were initially set at 135.7 mm and 129.7 mm, respectively, same as in the experiments. This allowed the penetration of saline water into the model domain until it reached steady state condition. The head and concentration values obtained at each cell of the domain after this initial simulation were used as the initial condition for the following simulations. More details of the numerical simulation procedure pertaining to each set of modelling experiments are provided in their respective chapter.

Chapter 3

Seawater intrusion dynamics in response to incremental water level variations

This first chapter provides an analysis of the response of the external SWI metrics (toe length and height along the coastline) and freshwater-saltwater transition zone dynamics to various incremental water level fluctuations. The saltwater toe migration rate was examined during intruding and receding phases following both freshwater and saltwater fluctuations and for various head change magnitudes. The logarithmic toe length was correlated to the boundary head difference by a simple linear equation and the effect of various hydrogeological parameter combinations on the linearity was assessed. The study also presents a comparison of the effect of freshwater and sea level fluctuations on the transition zone dynamics during intrusion and retreat phases using physical experiments. To further demonstrate the applicability of results and to examine the effect of different aquifer properties on the toe migration and the transition zone response to water level changes, the experiments were carried out twice for two different bead sizes. The analysis also included an investigation of the temporal response of the transition zone to changes in the freshwater flow regime through an abrupt flow disruption caused by an impermeable wall, for an equivalent magnitude of freshwater level change and hydraulic conductivity.

3.1 Experimental procedure

In the investigation of the SWI external metrics, a total of 54 experiments were carried out, as shown in table 3.1. The experiments were performed using two different bead sizes, namely 1090 μm and 1325 μm. For each bead size, 10 experiments were completed for the advancing wedge experiment and receding wedge experiment as a result of gradual freshwater head drop and rise, respectively, while the saltwater boundary remained constant. Seven additional experiments were completed where the magnitude of the freshwater level change was varied.

Another set of 10 experiments were carried out for the advancing wedge and receding wedge experiments where the saltwater level was changed while the freshwater boundary was held constant. The five head differences applied to the system in the advancing wedge experiment were dh = 6 mm, 5.2 mm, 4.4 mm, 3.6 mm. and the head difference was then returned to the initial value (dh = 6 mm). In the receding wedge experiment, the head difference were applied in reverse order i.e. dh = 3.6 mm, 4.4 mm, 5.2 mm and back to dh = 6 mm. The set of experiments involving freshwater head variations with constant saltwater boundary are referred to as FW in the forthcoming figures. The sets of experiments where the saltwater level was changed while the freshwater boundary was held constant are referred to as SL. The head differences applied in the experiments involving variations in the magnitude of head change were similar to the others: the different head change magnitudes used therein included: 0.8 mm (dh = 6 to 5.2 mm), 1.6 mm (dh = 6 to 4.4 mm) and 2.4 mm (dh = 6 to 3.6 mm).

Table 3.1 Experimental case investigated in the study, where dh and ΔH refer to the head boundary difference and the head change magnitude, respectively. In total, 54 experimental cases were carried out.

Experiment	Advancing wedge (FW/SL)	Receding wedge (FW/SL)	Magnitude of inland head change (FW)
Case 1090	dh = 6, 5.2, 4.4 , 3.6 mm	dh = 6, 3.6, 4.4, 5.2, 6 mm	ΔH = 0.8, 1.6, 2.4 mm
Case 1325	dh = 6, 5.2, 4.4 , 3.6 mm	dh = 6, 3.6, 4.4, 5.2, 6 mm	ΔH = 0.8, 1.6, 2.4 mm

In the freshwater-saltwater transition zone investigation, two sets of two experiments were completed; the first set included the analysis of two homogeneous cases of two different

mean diameters. In the second set of experiments, a cut off wall was installed into a homogeneous aquifer at two different locations (Fig 3.1), using the beads of diameter 1090 µm. The purpose of these tests was primarily to explore how a disruption of the freshwater flux transmitting through the system would affect the dynamics of the transition zone, for equivalent inland freshwater boundary head change.

The cutoff wall was made of impermeable material (plasticine) and was installed prior to the siphoning and packing of the beads in the tank. In the first scenario, the cutoff wall was placed at a distance equivalent to the height of the aquifer from the coastline boundary (13.6 cm). This test was referred to as case H. In the second scenario, the wall was located at about twice the height of the aquifer from the coastline boundary (27.2 cm). This test was referred to as case 2H. In both case H and case 2H, the wall was set such that to leave an opening of 2.8 cm from the bottom boundary such that the wall penetration depth was greater than 60% of the aquifer height to ensure effective repulsion of saline water (Kaleris and Ziogas, 2013).

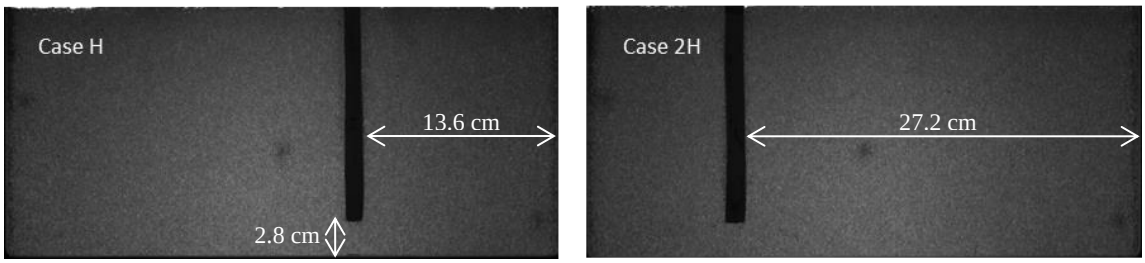

Figure 3.1 Photograph of the additional investigated configurations including the barrier

As per usual practice, the experiment was initiated after dropping the freshwater head to 135.7 mm such that the first head difference dh = 6 mm was imposed to the system, which subsequently allowed the saline water to enter the system. Once the steady state condition was established, the freshwater level was directly dropped down to 133.3 mm to impose a head difference dh = 3.6 mm, to analyse the transition zone dynamics during the advancing

wedge phase. The head difference was thereafter increased back to dh = 6 mm to allow the analysis of the transition zone behaviour during the receding wedge phase.

3.2 Numerical procedure

The case 1090 in the FW scenario was adopted for the numerical simulation. After allowing penetration of the saline water into the aquifer until steady state (following the application of a head of 135.7 mm and 129.7 mm at the freshwater and saltwater boundary, respectively), the freshwater head was thereafter successively decreased to establish the head differences dh = 5.2 mm, 4.4 mm and 3.6 mm in three successive stress periods. A fourth stress period was used to reset the head difference to the initial value (dh = 6 mm) by increasing the freshwater head back to 135.7 mm, which forced the retreat of the saltwater wedge towards the boundary.

In the transition-zone analysis, the simulation procedure involved two additional transient stress periods after establishing the initial condition, where the head differences dh = 3.6 mm and dh = 6 mm were successively imposed in the first and second stress period, respectively, which was achieved by dropping the freshwater head down to 133.3 mm (t = 0 - 50 min) and thereafter increasing it back to 135.7 mm (t = 50 -100 min), respectively.

3.3 Results and discussion

3.3.1 External SWI metrics

Transient analysis

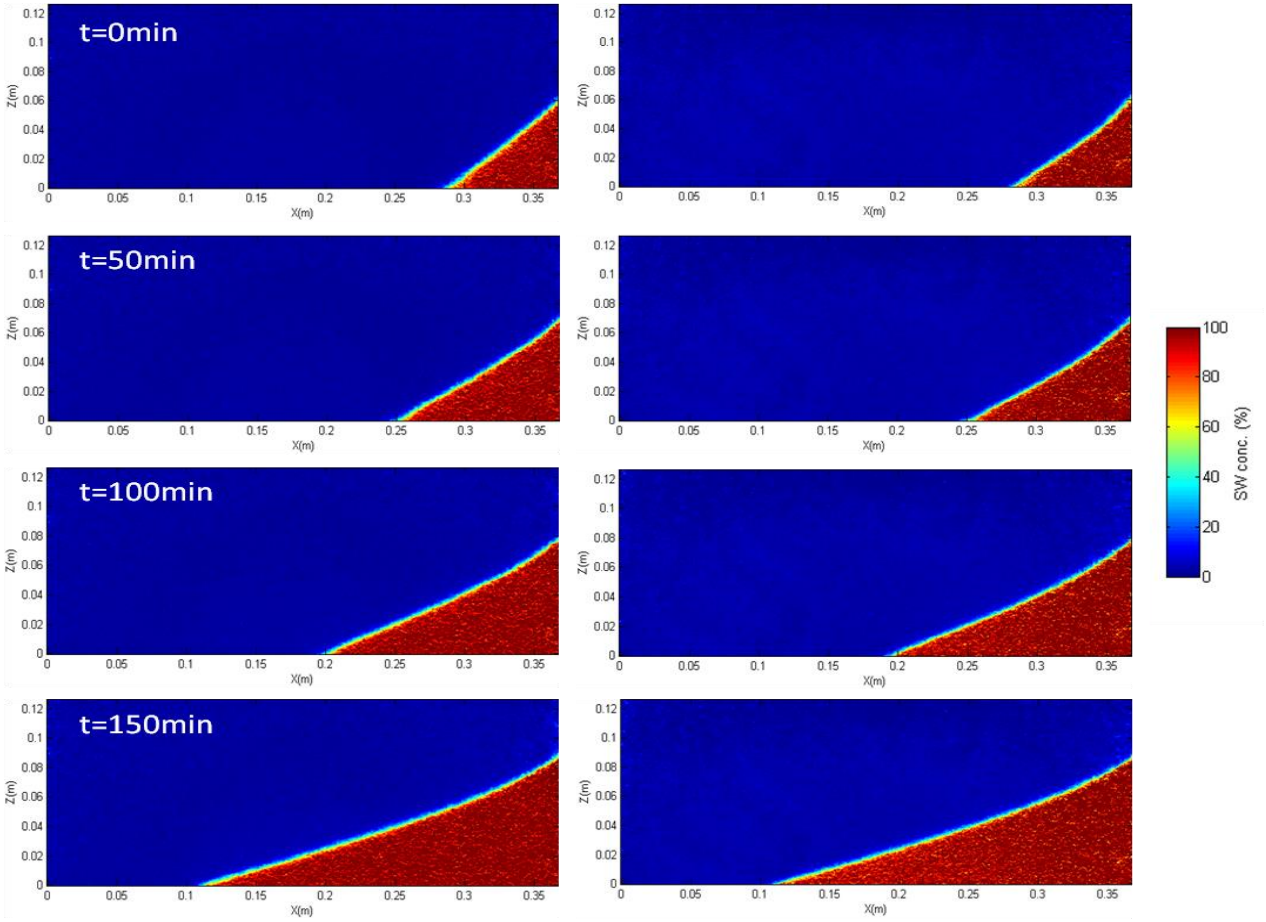

Figure 3.2 Experimental images of the saltwater wedge in case 1090 (left) and case 1325 (right)

The experimental images of the steady state saltwater wedge for the two cases are shown in Fig 3.2. In the first experiment, the head difference was varied as a function of the freshwater head boundary, while the head at the seaside boundary remained fixed at 129.7 mm. As discussed earlier, the first steady state saltwater wedge after the freshwater boundary head was dropped to 135.7 mm (dh = 6 mm), was considered as the initial condition of the experiment (t = 0.0 min). The saltwater intrusion lengths TL were 7.9 cm and 8.4 cm in cases

1090 and 1325, respectively. The freshwater level was thereafter successively decreased down to 134.9 mm, 134.1 mm and 133.3 mm, i.e using a constant decreasing step of 0.8 mm. This drastically reduced the freshwater flow through the system, which allowed the saline water to penetrate further inland. The recorded saltwater wedge toe lengths TL were 11.3 cm, 16.5 cm and 24.9 cm in case 1090, and 11.5 cm, 17.2 cm and 25.5 cm in case 1325, for dh = 5.2 mm (t = 50 min), 4.4 mm (t = 100 min) and 3.6 mm (t = 150 min) respectively. The freshwater level was then increased back to the initial value of 135.7 mm (dh = 6 mm), thereby forcing the saltwater wedge to recede toward the coastline boundary, until the system reached the final steady state.

The steady state of the first stress period (dh = 6 mm) was also considered as the initial condition in the sea level rise experiments. The inland freshwater level was maintained constant at 135.7 mm, and the saltwater level was successively raised up to 130.5 mm, 131.3 mm and 132.1 mm to maintain the same head difference decrement pattern as in the freshwater change scenario. This rise of the saltwater level induced an increase of the supply of saline water into the aquifer. The buoyancy forces that drive the intrusion were subsequently increased, thereby enforcing the saltwater wedge to intrude up 11.4 cm, 17.6 cm and 26.7 cm in case 1090; and 11.8 cm, 18.3 cm and 28.2 cm in case 1325, following the application of dh = 5.2 mm, 4.4 mm and 3.6 mm, respectively. Likewise, the saltwater wedge was then forced to retreat towards the coastline after the sea level was instantaneously dropped down to the initial value of 129.7 mm.

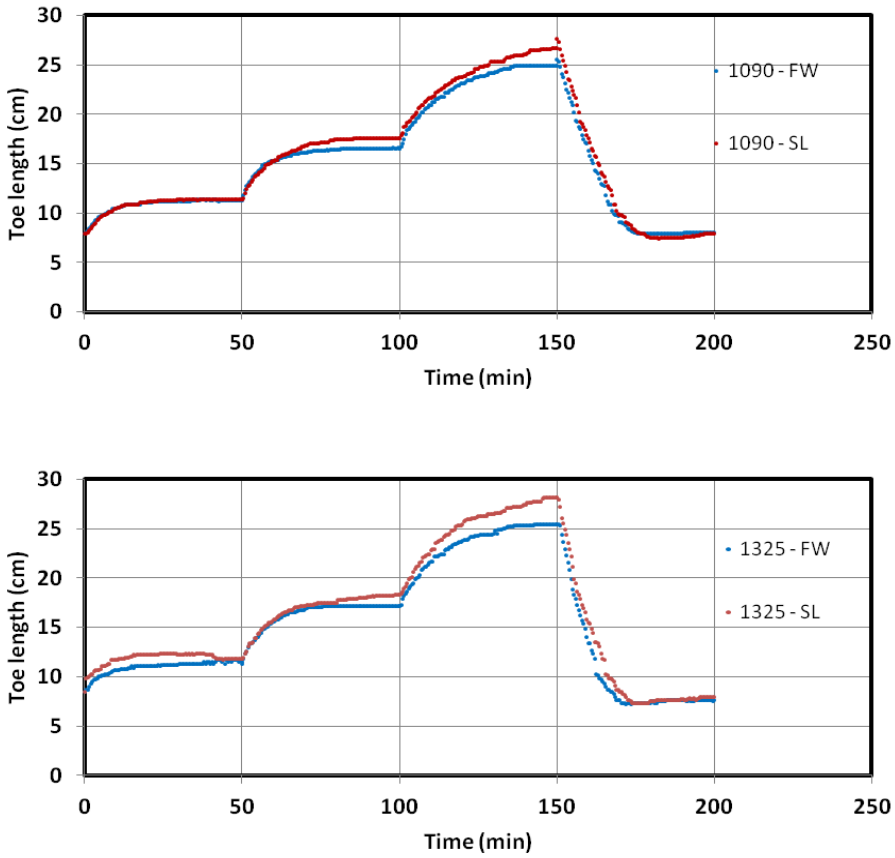

Figure 3.3 Transient experimental toe length data in advancing scenario in case 1090 (top) and case 1325 (bottom) for both freshwater (FW) and sea level change (SL) experiments

The transient toe length data for the two cases are shown in Fig 3.3. As expected, the saltwater intrusion process caused by sea level changes induced faster and larger intrusion length than that caused by freshwater fluctuations, for the same absolute head change magnitude. Unlike confined aquifers, sea level rise in unconfined aquifers is associated with an increase of the transmissivity (average saturated thickness) of the system. While the transmissivity continuously increases with incremental increase of the coastal head boundary, it decreases when dropping the inland head boundary, for equivalent absolute head change. The increase of transmissivity has been found to induce larger inland intrusion length in unconfined aquifers in Chang et al. (2011), which comforts the current observations.

The intruding and receding rates of the wedge were quantified and compared in order to assess the difference in timescale of intrusion and retreat resulting from inland and coastal head changes. The parameter ∆TL was employed to characterise the relative distance to be travelled by the toe before reaching its steady state value, such that $\Delta TL_i(t) = abs[TL(t) - TL_f]/TL_f$ and $\Delta TL_r(t) = abs[TL(t) - TL_f]/TL_0$ for the intruding and receding cases, respectively; where TL(t) is the toe length at time t, TL_f is the final steady state toe length, and TL_0 is the toe length prior to the application of the head change. The time to reach steady state corresponds to the time at which ∆TL become smaller than 1%. The curves of ∆TL of the intruding and receding wedge phases for the various water level changes are shown in Fig 3.4 and the times required for the saltwater toe to reach steady state are presented in table 3.2.

Table 3.2 Time required for the wedge to reach steady state condition for both freshwater (FW) and sea level (SL) changes between dh = 6 mm and dh = 3.6 mm (ΔH = 2.4mm)

Cases	SL-SWI	FW-SWI	SL-SWR	FW-SWR
Case 1090	45.5 min	47.5 min	25.5 min	23.5 min
Case 1325	44.5 min	46 min	21 min	19 min

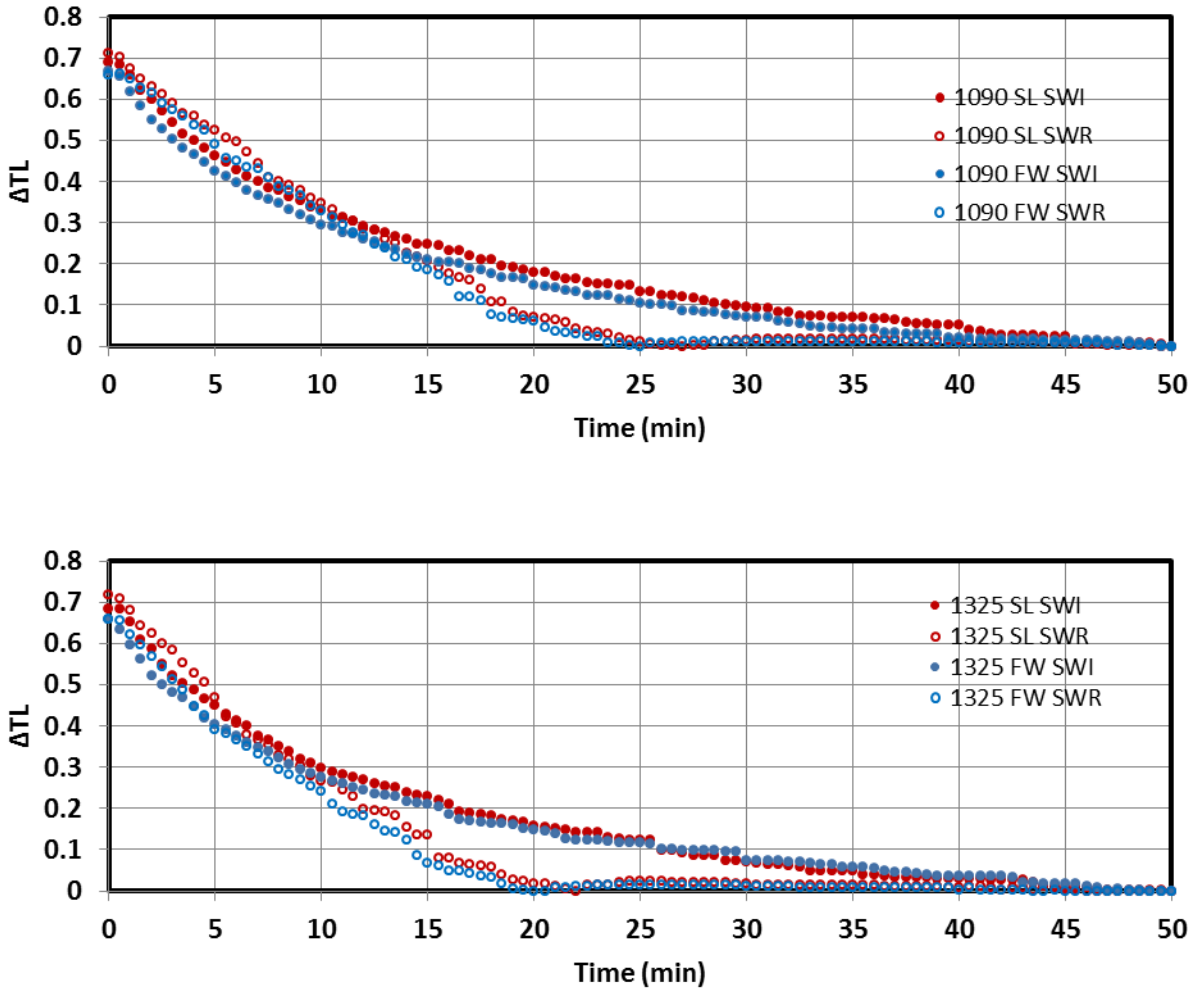

Figure 3.4 Comparison of the toe intruding (SWI) and receding (SWR) rates following both freshwater (FW) and sea level (SL) changes between dh = 6 mm and dh = 3.6 mm (ΔH = 2.4mm) in case 1090 (top) and case 1325 (bottom).

The intruding wedge was here prompted by decreasing the head difference decrement from dh = 6 mm to dh = 3.6 mm for both freshwater (FW) and sea level changes (SL), designated as FW-SWI and SL-SWI in the figure, respectively, while the retreat was prompted by re-increasing the head difference from dh = 3.6 mm back to dh = 6 mm, designated as FW-SWR and SL-SWR. The data show that the intruding and receding rates of the wedge as well as the time taken to reach steady state are fairly comparable in SL and FW scenarios. Based on a numerical conceptual model study, Lu and Werner (2013)

demonstrated than in confined aquifer systems, inland head change would promote similar transient toe motion and timescale of toe response as coastal head changes, in cases of comparable head variations, but opposite direction. These results provide thus experimental evidence of the applicability of their findings to unconfined coastal aquifer systems.

The data show that the receding rate of the saltwater wedge was relatively faster than the intruding rate in both SL and FW scenarios, with an intruding wedge requiring up to twice longer time than the receding wedge to reach steady state condition in case 1325. While previous studies demonstrated the asymmetry of timescale between intruding and receding processes following inland head variations (Chang and Clement, 2012; Robinson et al., 2015), the present results suggest that timescale asymmetry would also apply in scenarios involving sea level fluctuations. The data show that the receding migration rate was relatively faster in case 1325 than in case 1090 in both SL and FW scenarios, while the intruding rates remain relatively comparable. This can readily be observed in the steepness of the slope at t = 0 min in case 1325, as well as the shorter time taken to reach steady state condition in both SL and FW fluctuation scenarios in table 3.2. This means that for equivalent magnitude of freshwater level rise/saltwater level drop, faster seaward motion of the saltwater wedge would occur in higher hydraulic conductivity media, which is in agreement with Robinson et al (2016). This trend was also confirmed in Fig 3.5 and table 3.3, where the ΔTL results recorded for two different inland head change magnitudes but similar head difference are presented.

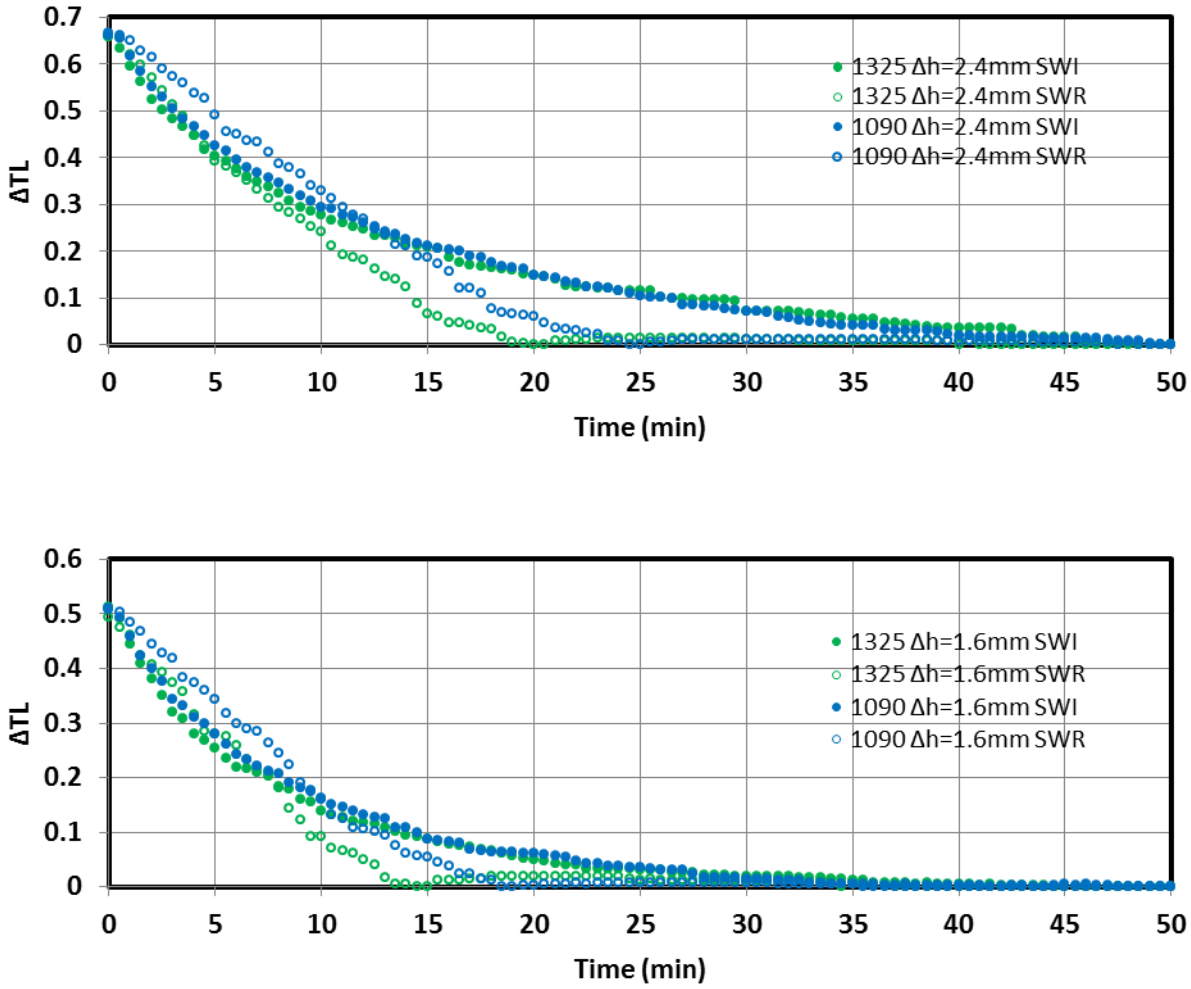

Figure 3.5 Comparison of the toe intruding (SWI) and receding (SWR) rates for various inland head change magnitudes. ΔH = 2.4mm and ΔH = 1.6mm were simulated by varying dh between dh = 6 mm to dh = 3.6 mm, and between dh = 6 mm to dh = 4.4 mm, respectively.

Table 3.3 Time required for the wedge to reach steady state condition for various head changes magnitude ΔH.

Cases	ΔH	Timescale SWI	Timescale SWR
Case 1090	**1,6 mm**	**33 min**	**18.5 min**
	2,4 mm	**47.5 min**	**23.5 min**
Case 1325	**1,6 mm**	**35 min**	**13.5 min**
	2,4 mm	**46 min**	**19 min**

Steady state analysis

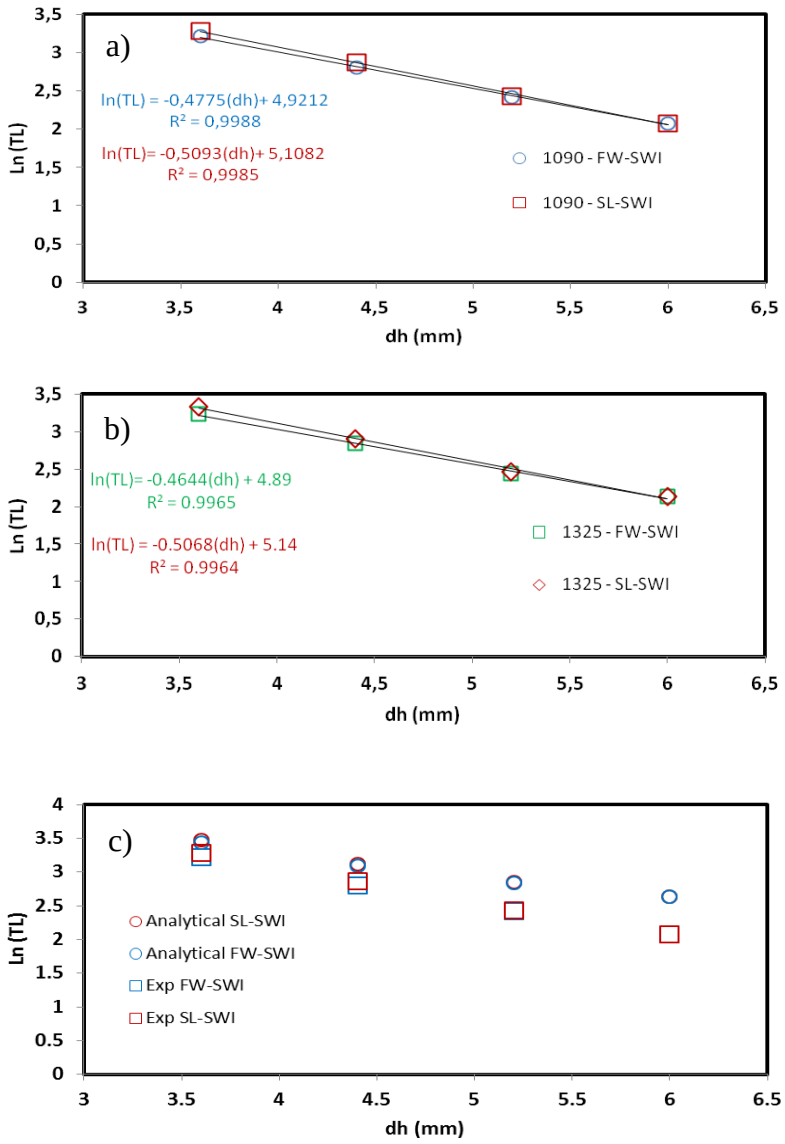

Figure 3.6 Steady state-to steady state toe length data against the head difference dh in advancing condition for both freshwater (FW) and sea level change (SL) experiments; a) case 1090 and b) case 1325; c) Comparison with the analytical solution (for case 1090).

The logarithm of the steady state toe length of the wedge was correlated to the head difference by linear equation of the type *ln (TL) = a(dh)+ b*, with a and b being the linear regression coefficients (Fig 3.6a and 3.6b). The values of the coefficients *a* and *b* for the current system are shown in the figure. These coefficients are strongly dependant of the

hydrogeological parameters of the system, as evidenced in the forthcoming sensitivity analysis. The negative value of *a* simply indicates that lower dh values induces larger toe length penetrations. The coefficient *b* is found to be slightly larger in the sea level scenarios, as expected. The strong linearity of the correlations is characterized by the relatively high coefficient of determination $R^2 > 0.99$.

The experimental results were compared with the analytical solution provided in Lu et al (2015), which was initially derived using Strack (1976) single potential theory (Fig 3.6c). The results show that the linearity of the correlation was also well demonstrated with the analytical solution. As expected, the toe length values predicted by the analytical model were slightly overestimated compared to the experimental data. This is because the analytical model assumes sharp-interface condition, whereby dispersion effects are neglected, while these significantly affect the saltwater wedge dynamics in the physical model and cause the breakdown of density contrast effects, subsequently inducing smaller intrusion lengths. That is why the mismatch was more pronounced for dh = 6 mm, where the flow velocity (which promotes dispersion) was the highest.

The linearity of this correlation was also tested during saltwater retreat in the experiment, whereby the head difference was first set to dh = 3.6 mm (t = 0-50 min) and then successively increased up to dh = 6 mm, following both inland and coastal variations (Fig 3.7). It was found that almost no changes were observed in the regression coefficients as well as in the linearity of the equations (Fig 3.8).

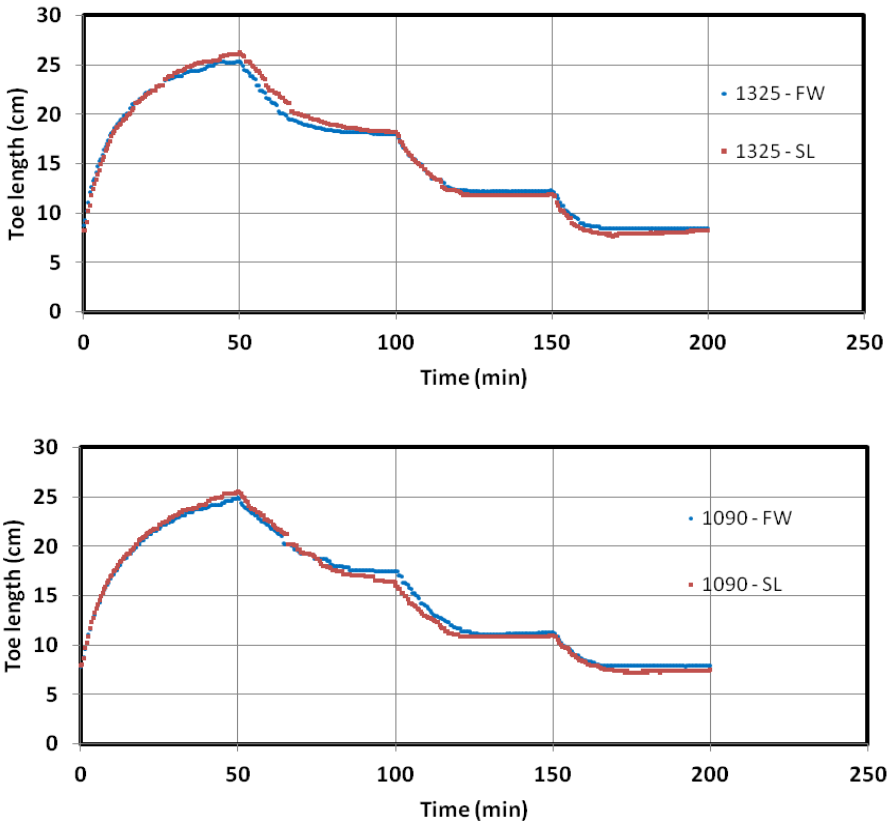

Figure 3.7 Transient experimental toe length data in receding scenario in case 1090 (top) and case 1325 (bottom) for both freshwater (FW) and sea level change (SL) experiments

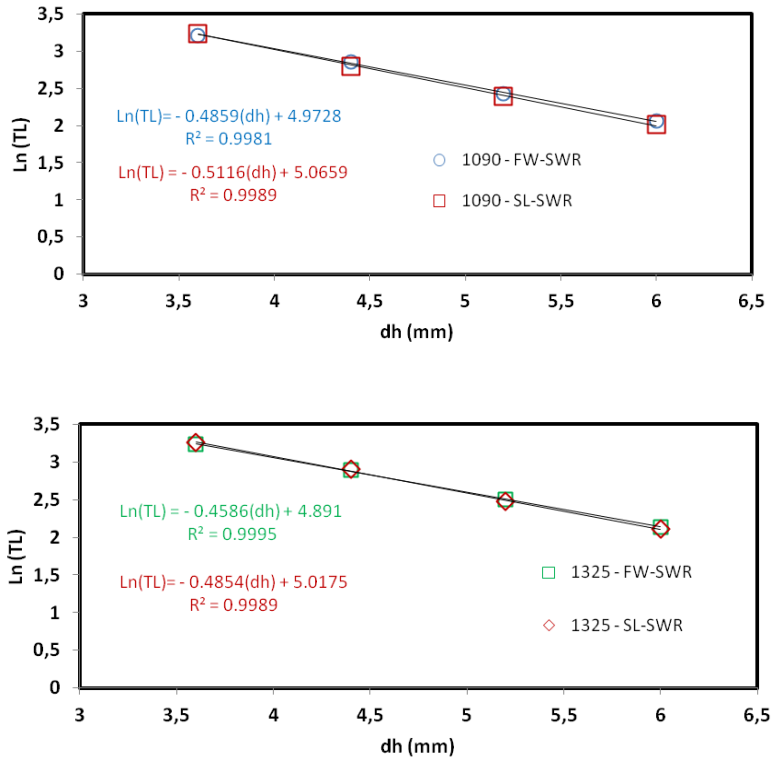

Figure 3.8 Steady state-to steady state toe length data against the head difference dh in receding scenario in case 1090 (top) and case 1325 (bottom) for both freshwater (FW) and sea level change (SL) experiments

The height of the saltwater wedge along the coastline *Hs* is also an important metric quantifying SWI in coastal aquifers (Goswami and Clement, 2007; Sebben et al., 2015). The current experimental data show that *Hs* increases linearly with the head difference in both FW and SL scenarios (Fig 3.9). Again, a simple linear correlation of type $Hs = c(dh) + d$ could be derived, with c and d being constants depending on the system. The values of *c* and *d* for the current configuration are shown in Fig 3.9, with c being negative as the decreasing value of *dh* would obviously lead to an increase in the height of the saline water along the coastline. Intuitively, decreasing the freshwater level at the inland boundary would induce a lower resistance to the buoyancy forces driving the inflow of saline water at the top end of the saltwater boundary. The coefficient *d* is a limiting value corresponding to the value of *Hs* for *dh* = 0 mm (freshwater and saltwater heads are equal). It is found that there is almost no

difference in the coefficients in the case 1325 (not shown for brevity) for similar head change, which suggests that the rise of the intruding saltwater along the coast line was little affected by the increase of the hydraulic conductivity of the porous media, but solely on the difference between the inland freshwater head and the saltwater head.

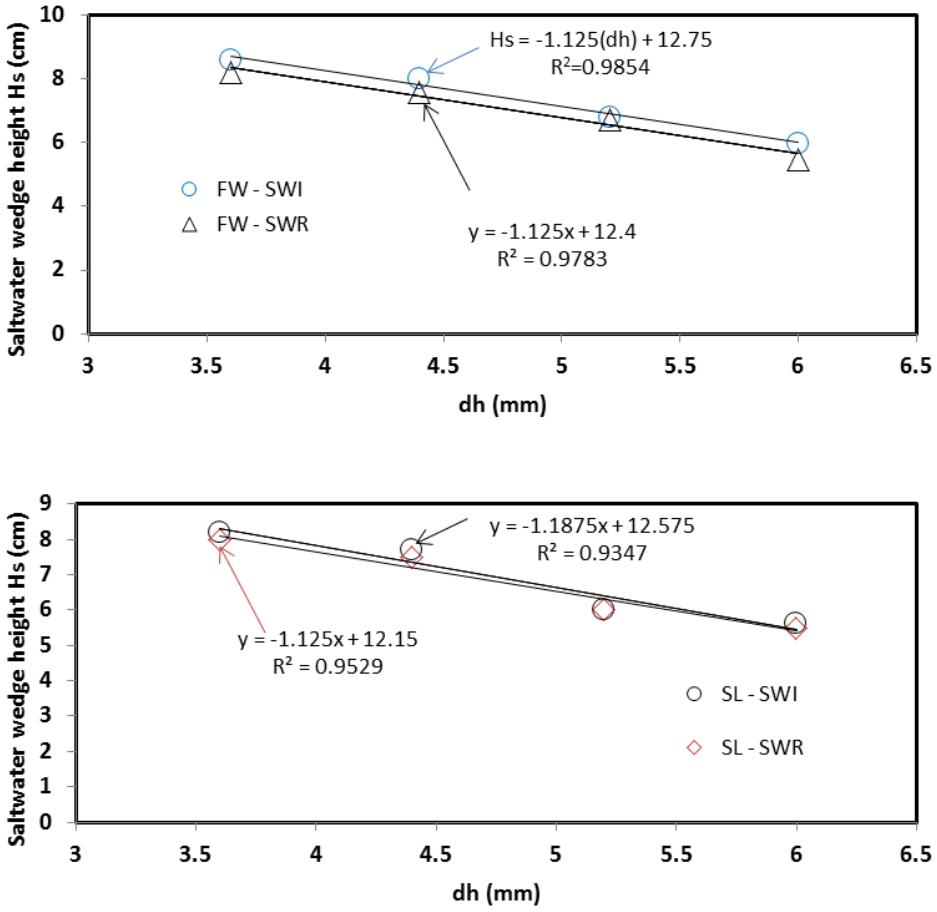

Figure 3.9 Steady state-to steady state saltwater wedge height against the head difference dh in case 1090, following fluctuations of the freshwater head boundary (top) and saltwater boundary (bottom).

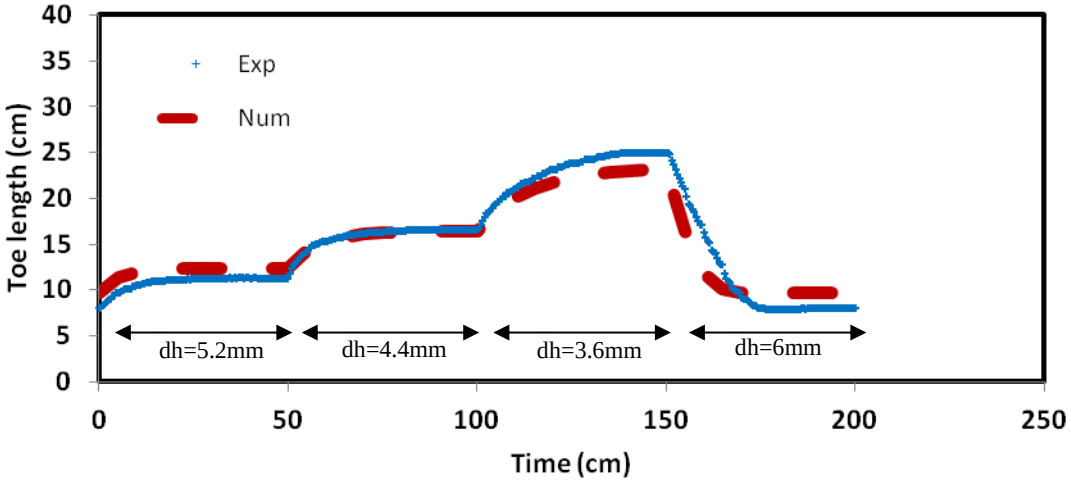

Figure 3.10 Comparison between transient experimental and numerical toe length data

In overall, the results show that the transient toe movement was reasonably well predicted by the numerical model (Fig 3.10). The maximum percentage difference was 10%, 1% and 7% for dh = 5.2 mm, 4.4 mm and 3.6 mm, respectively. Some mismatch could be observed in the retreat, where the toe movement predicted by the numerical was slightly faster than in the physical model, as observed in previous similar studies (Chang and Clement, 2012; Robinson et al. 2015, 2016), with a maximum percentage difference recorded at the end of the retreat (nearly 21%). Additional simulations were conducted to explore the effect of some important hydrogeological parameters on the coefficients of the derived empirical equation. The sensitivity analysis was performed based on the case 1090. Only the scenario involving inland freshwater variations was considered.

The magnitude of head incremental change ΔH was the first parameter that was investigated. The data show that varying the rate of inland head change induced no changes in the regression coefficient values as well as in linearity of the correlation of the derived equations (Fig 3.11). Three ΔH values were tested, namely 0.2 mm, 0.4 mm and 0.8 mm (same as in the experiment). The values of *a* and *b* remain nearly identical for all the Δ*H*

values. The coefficient R^2 was superior to 0.99 in all cases. The linearity of the correlation is independent of the rate of head change, which is particularly important considering that coastal systems are associated with great variations in the water table resulting from seasonal variations and/or from intermittent sea level fluctuations (tides) in the opposite scenario.

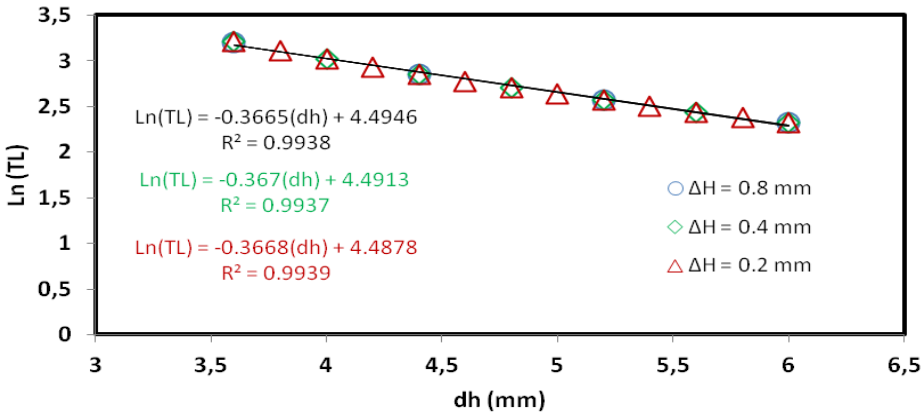

Figure 3.11 Change of the logarithmic toe length with the head difference for different head change magnitudes

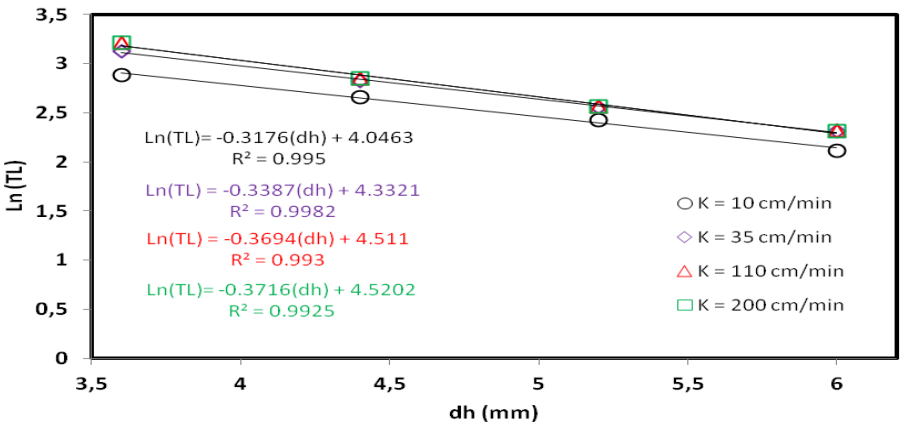

Figure 3.12 Change of the logarithmic toe length with the head difference for different hydraulic conductivity values

The sensitivity of the regression parameters to the hydraulic conductivity K was investigated over a range of 10-200 cm/min. The data show that increasing the hydraulic conductivity induced a slight increase of the intrusion length and then settle for higher K

values (Fig 3.12). Observing the trend of the coefficients, it appears that the increase of K primarily induced a continuous decrease of the constant *a* from -0.3176 for K = 10 cm/min to -0.3716 for K = 200 cm/min, respectively. The sensitivity of the toe length is higher for lower values of dh. The vertical movement of the slope is reflected by the coefficient *b*, which also increases with increasing K, but becomes constant for higher K values, which indicate faster and larger intrusion for increasing K, for equivalent dh decrement. These results are consistent with previous studies (Hussain and Javadi, 2016). The linearity of the relationship could be exhibited for all the K values tested here, as reflected by the relatively high correlation coefficient R^2 values.

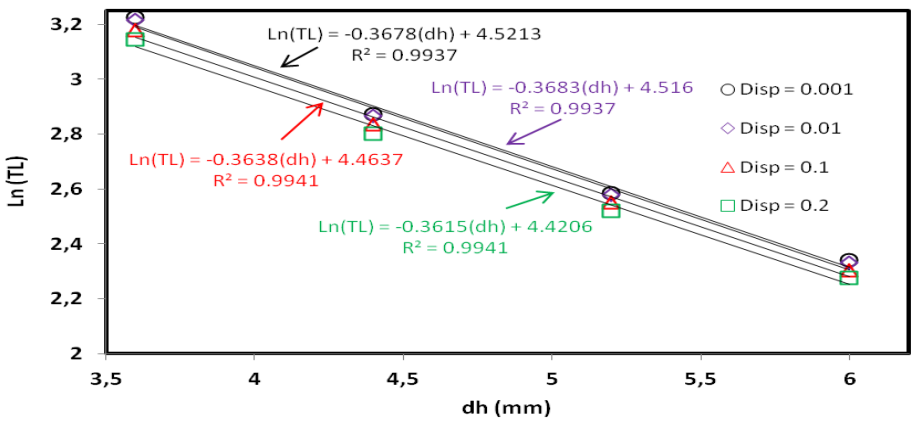

Figure 3.13 Change of the logarithmic toe length with the head difference for different dispersivity values

The sensitivity of the coefficients of dipersivity was also explored. The data show strong linearity of the equations derived for all the various values of dispersivity tested here (Fig 3.13). The equation again is of the form *Ln(TL)=a(dh)+b*. The decrement of the dispersivity values yielded an increase of the intrusion length, as expected. The dispersivity was varied over the range 0.001-0.2 cm, from which four values were selected. The longitudinal to transverse dispersivity ratio remained constant. Modifying the dispersivity did not affect the slope of the regressions lines in all cases, which is manifested by a relatively

steady constant *a*. The coefficient b was however found to slightly decrease with increasing dispersivity, indicating that in response to the same head difference dh applied, smaller toe length values would be exhibited for larger values of dispersivity, which is in agreement with previous studies (Abarca et al., 2007; Kaleris and Ziogas, 2013; Lu and Werner, 2013).

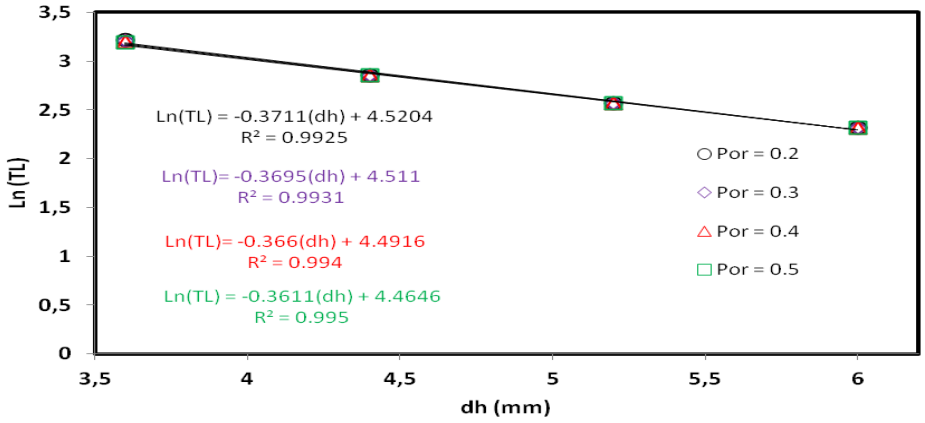

Figure 3.14 Change of the logarithmic toe length with the head difference for different porosity values

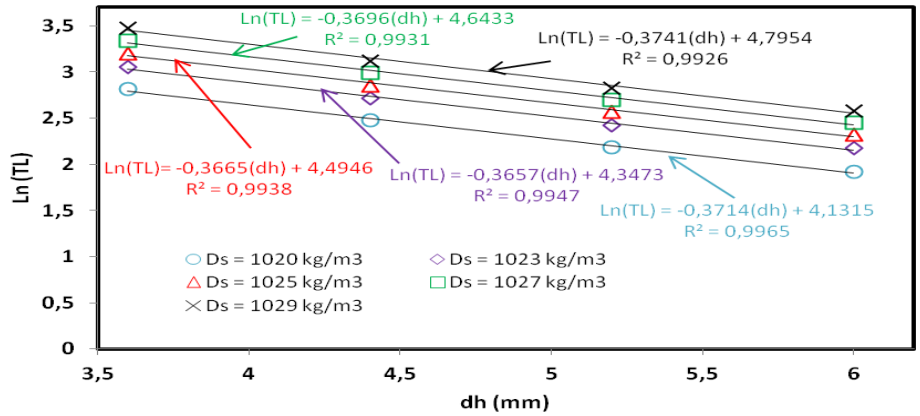

Figure 3.15 Change of the logarithmic toe length with the head difference for different saltwater density values

The influence of the porosity on the regression coefficients was explored over the range 0.2-0.5 (Fig 3.14). The regressions coefficients remain nearly the same for all the values tested and no specific trend was observed, albeit coefficient *a* very slightly increases with decreasing porosity values, indicating very slightly larger saltwater wedge toe penetration as a result of decreasing the porosity of the system for equivalent dh decrement.

This very little change however confirms that varying the porosity of the system has negligible affect the extent of the seawater wedge, as it was confirmed in previous studies (Hussain and Javadi, 2016). Again, the linear relationship was established for the derived equation for all the values of porosity tested, which is reflected by the high values the coefficient of determination R^2.

The effect of the saltwater density on the regressions coefficients was explored over the range 1020-1029 kg/m^3 (Fig 3.15). The results demonstrate the linearity of the equations established, for the all the density values tested. The regression coefficients as well as the coefficient of determination are shown in the figure. The slope of the regression line was nearly the same in all cases, while the coefficient *b* continuously increased with increasing density. This result means that the intrusion length would be substantially larger for higher density values, in response to a similar head difference, as expected. Likewise, the linear relationship was established for the derived equations for or all the values of density tested.

3.3.2 Freshwater-saltwater transition zone

Base cases

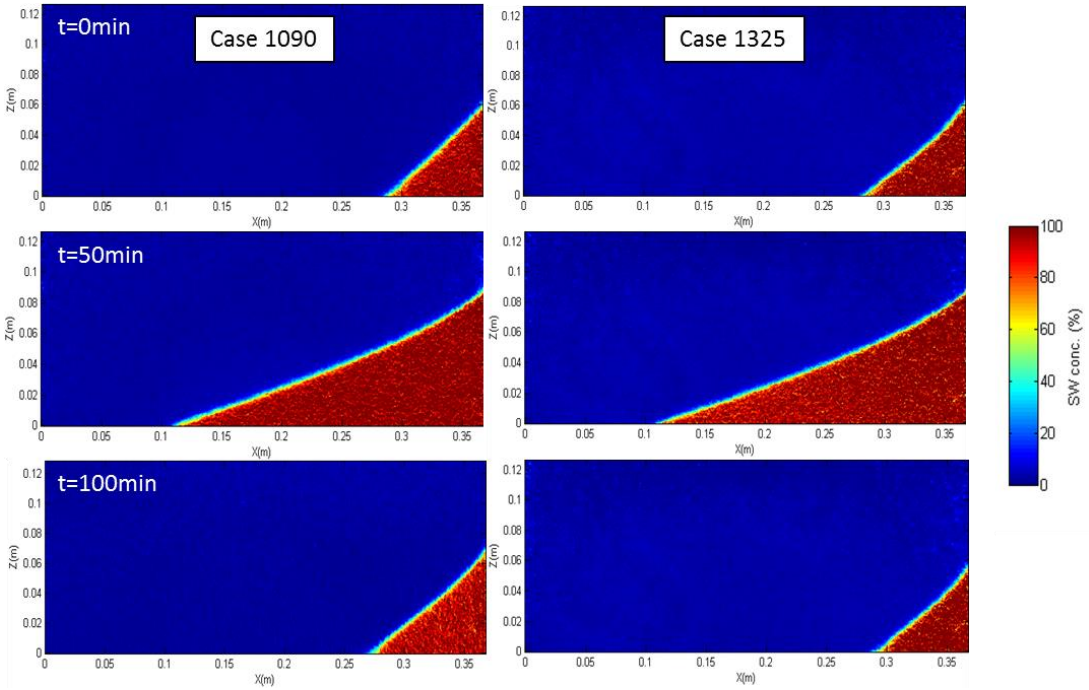

Figure 3.16 Concentration colour maps of the steady state saltwater water wedges in case 1090 and case 1325 at t = 0 min and 100 min (dh = 6 mm); t = 50 min (dh = 3.6 mm)

Fig 3.16 shows the steady state concentration colour maps showing the saltwater wedge at the various stages. The saline water initially entered the system following the first inland head drop to 135.7 mm, which prompted the saltwater wedge toe to move up to 7.9 cm and 8.4 cm inland, in cases 1090 and 1325, respectively. After the second head drop (dh = 3.6 mm), the toe further penetrated into the system up to 24.2 cm and 25.3 cm, in cases 1090 and 1325 respectively. The saltwater wedge was then forced to move seaward to the same initial location after rising freshwater head back to 135.7 mm. The comparison between the transient experimental and numerical results presented in Fig 3.17. The shape of the saltwater wedge was relatively well depicted in the numerical model, although the width of the transition zone (TZ) appears slightly thicker in the numerical model compared to the experimental observations. The width of TZ was the same for the two head differences in the

experiments, while it slightly increased in the model after the head difference was decreased. The comparison of the transient experimental and numerical toe length data shows nonetheless good agreement for both the advancing and receding wedge conditions, albeit the retreat of the saltwater wedge was once again slightly faster in the numerical model. The values of maximum percentage difference calculated were 9% and 13%, for dh = 3.6 mm and dh = 6 mm, respectively.

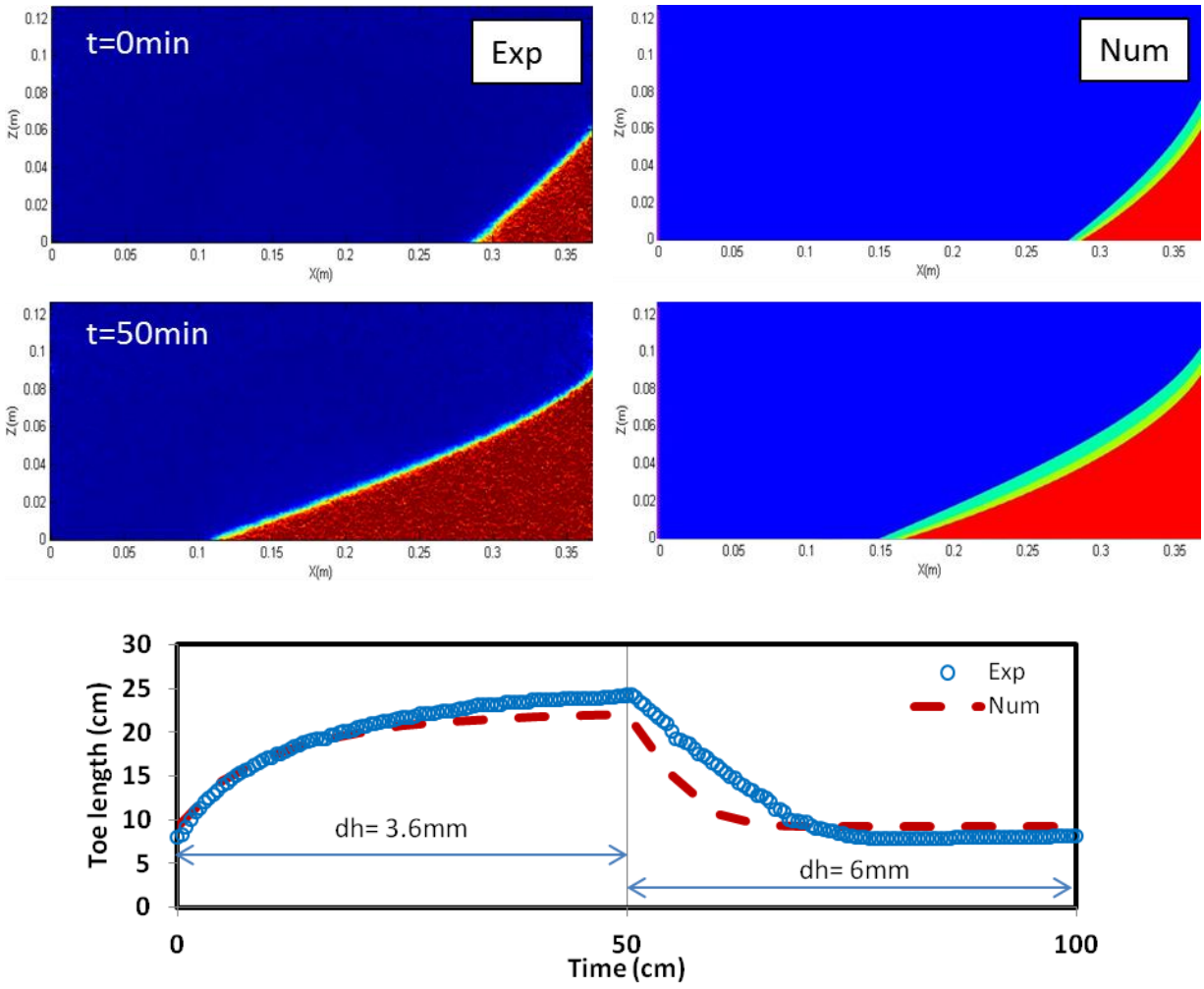

Figure 3.17 Comparison between transient experimental and numerical saltwater wedge for the case 1090, Steady state (top) and transient toe length (bottom)

Experimental observation showed that under transient condition, the width of TZ was not only narrow, but remains constant throughout the entire advancing-wedge phase, regardless of the inland head change magnitude applied (Fig 3.18). These observations are

analogous to that reported in Robinson et al. (2015) who demonstrated the constancy of the transition zone width throughout seawater intrusion following change in hydraulic gradient. These results further confirms that the widening of TZ width would be little affected by the drop of the freshwater level causing the inland advancement of the saltwater wedge, regardless of the head change magnitude applied. In addition, the width of the TZ was very similar in cases 1090 and 1325, fluctuating within the range of 0.3-0.5 cm, which indicates that the change in aquifer hydraulic conductivity induced insignificant effects on TZ over the course of the intrusion phase, regardless of the inland head drop magnitude applied.

Conversely, Fig 3.18 shows that the width of the TZ exhibited a noticeable widening during the saltwater retreat process, with a magnitude increasing with increasing freshwater level increment. The peaks of the widening along with their time of occurrence are shown in table 3.4. The results not only confirm that the widening process is primarily a transient phenomenon, but also confirms that the occurrence of the widening may be limited to the seawater retreat process, which agrees with Robinson et al (2016). The magnitude of the head change prompting the seaward motion of the freshwater-saltwater interface is one of the controlling factors of the extent of the widening. The results show that the width of the TZ was nearly three times greater from ΔH = 0.8 mm to ΔH = 2.4 mm in both case 1090 and case 1325. This is because a higher magnitude of head change would promote higher flow velocity, which implies more dispersion along the interface thus further increasing the width of the transition zone. The results also show that the TZ occurring during the retreat was also larger when the grain size was smaller (case 1090). The data show that from the highest (case 1325) to the lowest grain size (case 1090), the peak of the widening increased by 33%, 21% and 43 %, for ΔH = 0.8 mm, 1.6 mm and ΔH = 2.4 mm, respectively.

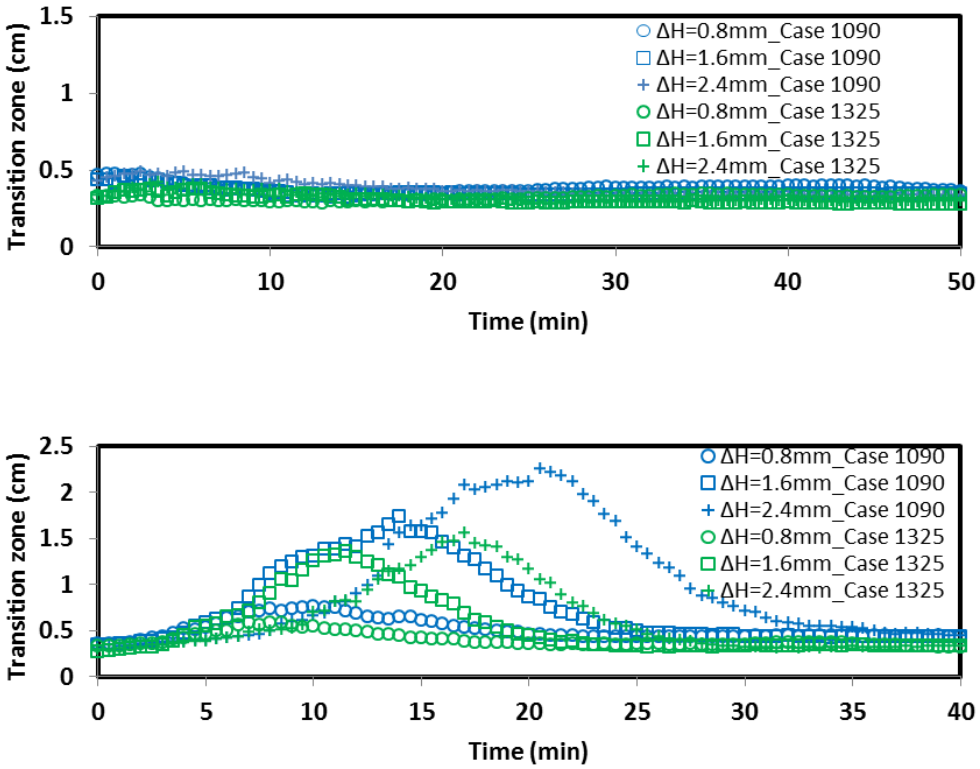

Figure 3.18 Transient transition zone data in a) advancing phase (top) and b) receding phase (bottom)

Table 3.4 Summary of the maximum values of the transition zone width and their associated time of occurrence

Cases	ΔH	Peak value	Time to peak
Case 1090	0.8 mm	0.8 cm	10 min
	1,6 mm	1.7 cm	14 min
	2,4 mm	2.3 cm	20.5 min
Case 1325	0.8 mm	0.6 cm	7 min
	1,6 mm	1.4 cm	11.5 min
	2,4 mm	1.6 cm	17 min

The response of the width of the transition zone to freshwater and saltwater level fluctuations was analyzed and the results are presented in Fig 3.19**.** The results revealed that there was very little change in the width of TZ throughout the seawater intrusion process in both scenarios involving freshwater and saltwater head changes. In both cases 1090 and 1325, the results show that the width of TZ was fluctuating around 0.3 cm during the entire intrusion process for both head boundary changes. The small variations may solely be due to possible minor fluctuations in the water levels occurring at the boundaries. These observations appear to suggest that the expansion of the transition zone would not be significant during the intruding phase of seawater wedge resulting from water table drop or sea level rise, regardless of the magnitude of the head change.

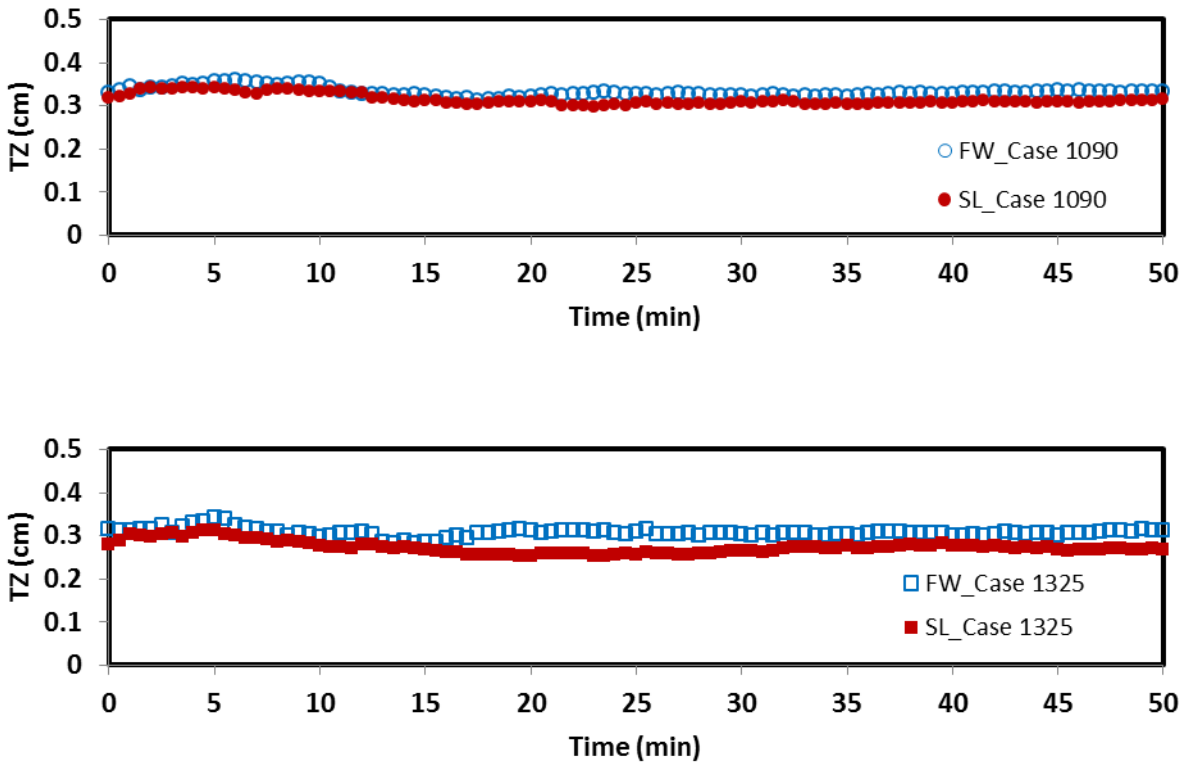

Figure 3.19 Response of the width of the transition-zone to decrement of dh from 6mm to 3.6mm (ΔH = 2.4 mm) from both freshwater side (FW) and sea level side (SL) in case 1090 (top) and case 1325 (bottom)

The transient response of the transition zone width TZ exhibited, again, a significant widening of the transition zone during the receding phase, with a relatively similar peak magnitude and peak time in both sea level drop and freshwater rise scenarios (Fig 3.20). The results therefore give initial indication that the widening of the transition zone during the retreat would exhibit the same amplitude in scenarios involving the rise of the water table and a drop of the sea level rise, in cases of equivalent head change magnitudes but opposite directions. Again, the magnitude of the peak greater and extended over longer time period in the case of smaller grain size (case 1090), which further extends the results presented in Fig 3.18 for scenarios involving sea level fluctuations.

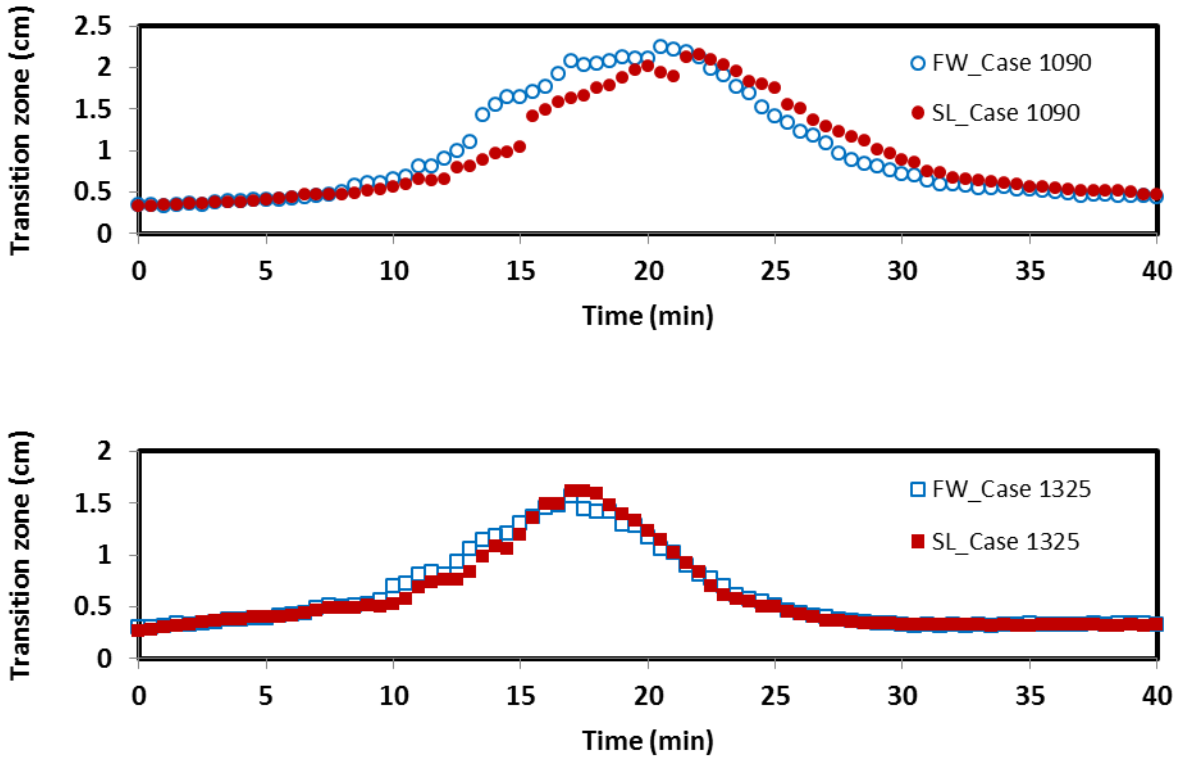

Figure 3.20 Response of the width of the transition-zone to increment of dh from 3.6mm to 6mm (ΔH = 2.4 mm) from both freshwater side (FW) and sea level side (SL) in case 1090 (top) and case 1325 (bottom).

Fig 3.21 shows the concentration colour maps of the saltwater wedge during the retreat in both experimental and numerical models. The experimental observations revealed

the existence of a yellowish pulse (of relatively low salt concentration) travelling upwards inside the receding saltwater wedge and spreading along the interface, thereby substantially exacerbating the widening of the transition zone. This yellowish pulse could be observed about 5 min following the head change and started spreading along the interface at around t = 10 min. The image taken at t = 20.5 min shows the saltwater wedge when the width of TZ reached the maximum peak value. Note that this interesting phenomenon was repeatedly observed in the two experiments (i.e. case 1090 and case 1325), and in the receding wedge scenarios involving both freshwater as well as saltwater level fluctuations. Such observations have never been reported in previous studies.

The discrepancies in the toe position between the numerical and physical model results are simply due to the faster retreat observed in the numerical model compared to the physical model, as previously observed in Fig 3.17. The numerical model reproduced the widening of the transition zone width occurring saltwater retreat, although the peak value occurred earlier in the numerical model (within the first 10 min) compared to the physical model (about t = 20.5 min). The widening ended faster in the numerical model compared to the physical experiment, with no noticeable changes observable in the wedge after t = 20 min in the numerical model, while changes could still be observed until t = 30 min in the physical experiments. The yellowish pulse could not be reproduced by the numerical simulation, where the widening of the transition zone is primarily caused by dispersion along the interface. This further highlights the key role of laboratory experiments in the investigation of density-driven flow in porous media and the evaluation of numerical models (Stoeckl et al., 2015).

It is hypothesised that this yellowish pulse observed in the experiments may have been the results of some freshwater “sliding” into the receding saltwater wedge along the bottom boundary, which was thereafter diluted and sucked upwards towards the interface due

to density contrast, thereby exacerbating the widening. This possible sliding freshwater into the wedge may have been caused by the rather sudden rise of the freshwater head that induced in great change of the freshwater flow velocity in the system, thus abruptly pushing seaward the saltwater wedge and creating a perturbation allowing a tiny portion of freshwater to leak along the aquifer bottom. This experimental observation was not an artefact of any wall effects (i.e. 2D versus 3D transport) given the relatively small width of the tank (10 mm).

Such mechanism could conceivably occur in real coastal aquifer systems especially where the non-uniformity aquifer bedrocks may enhance preferential flow, although observations of such effect have not been reported in previous investigations. Further works would nonetheless be required to examine the reproducibility of the observed phenomenon within systems involving preferably larger scale models. These very interesting observations was the main motivation to examine in the next section how the disruption of the freshwater flux transmitted through the system caused by an impermeable wall would affect the dynamics of the transition zone (widening and narrowing) as well as the above observed phenomenon.

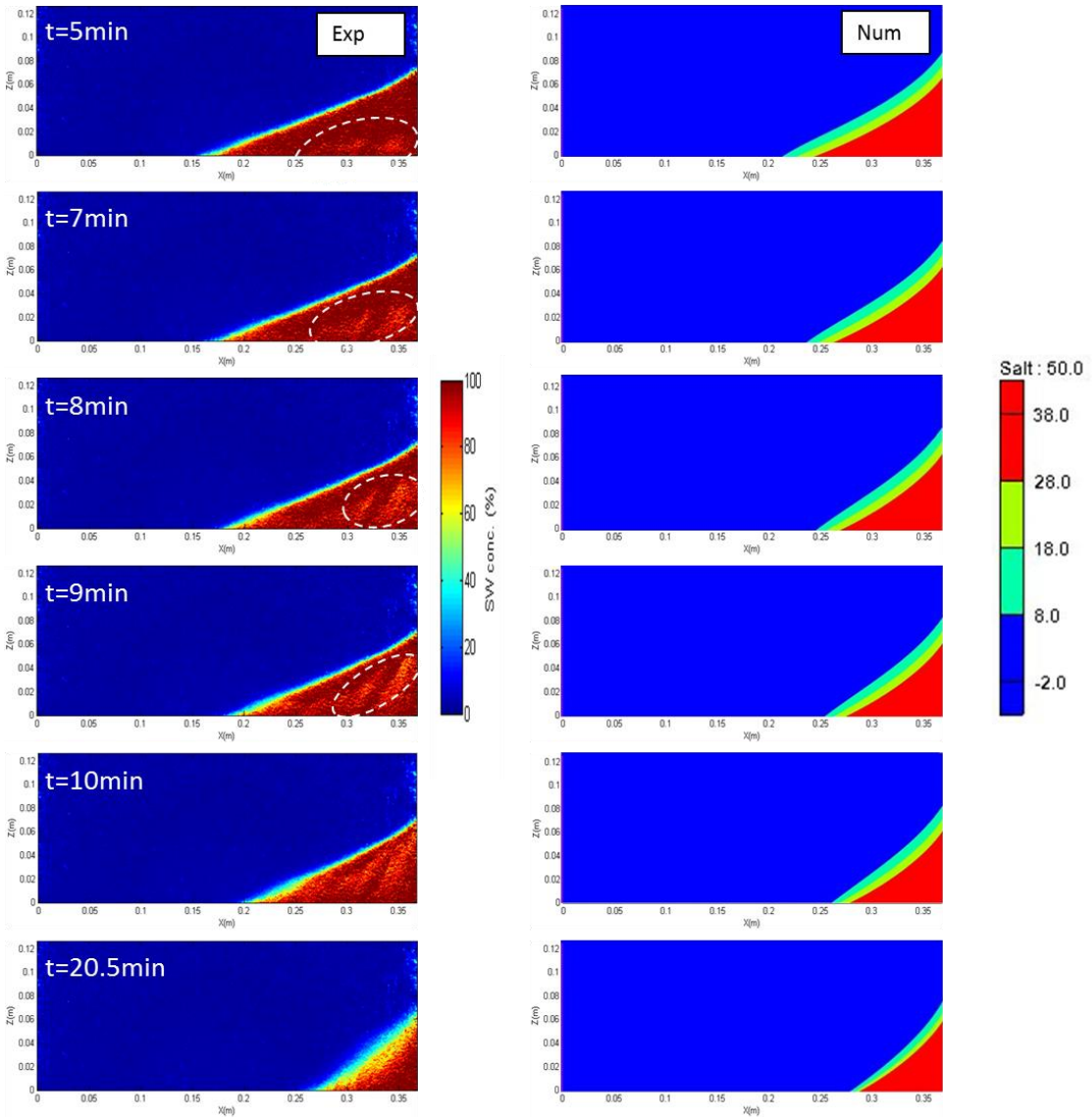

Figure 3.21 Transient experimental and numerical receding saltwater wedge during the receding phase in case 1090

Cutoff wall cases

As stated above, the purpose of these tests was primarily to explore how a disruption of the freshwater flux transmitting through the system would affect the dynamics of the transition zone, for equivalent hydraulic conductivity and inland freshwater boundary head change. The beads used in these two cases were the same beads used in case 1090. Thus the base case of these cutoff wall experiments corresponds to case 1090.

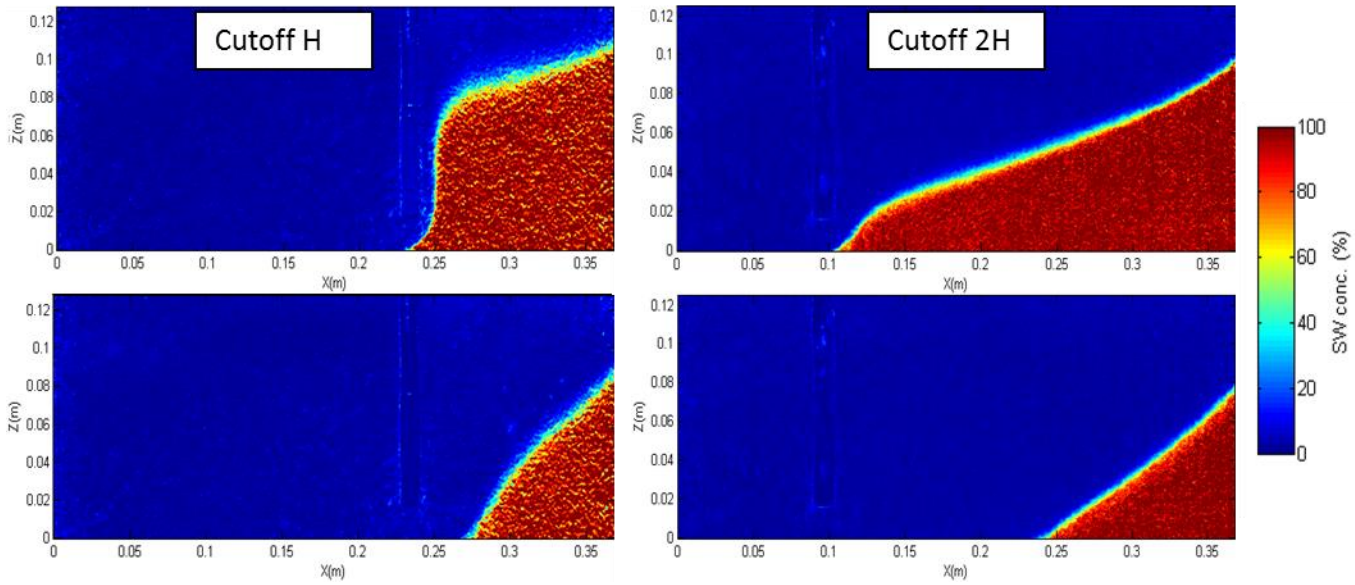

Figure 3.22 Concentration colour maps of the steady state saltwater water wedges in case H and case 2H after application of dh = 3.6 mm (top) and after increasing to dh = 6 mm (bottom)

Fig 3.22 shows the concentration colour maps of case H and case 2H. Following the application of dh = 3.6mm, the saltwater wedge intruded inland up to 13.7 cm and 26.3 cm in case H and case 2H, respectively. This represents a reduction to the initial saltwater intrusion length of case 1090 by 43% and -9%, in case H and case 2H respectively (compared to the toe length of the base case shown in Fig 3.16). This negative reduction value means that the toe length in case 2H was greater than that of the base case 1090. The comparison between the numerical and experimental data steady state saltwater wedge of both cases is presented in Fig 3.23 and the transient experimental and numerical toe length data are shown in Fig 3.24. The results show that the numerical models predicted relatively well the overall shape of the wedge in all cases, albeit the thickness of the saline plume near the wall was slightly underestimated compared to the experimental observations in case H at t = 0 min. Fig 3.24 shows that the transient toe length data obtained from the numerical model matches relatively well with the experimental results, particularly in case H where the maximum percentage difference was 7%, albeit a slightly greater toe length could be observed towards the end of

the retreat in the numerical model in case 2H (nearly 23% difference).

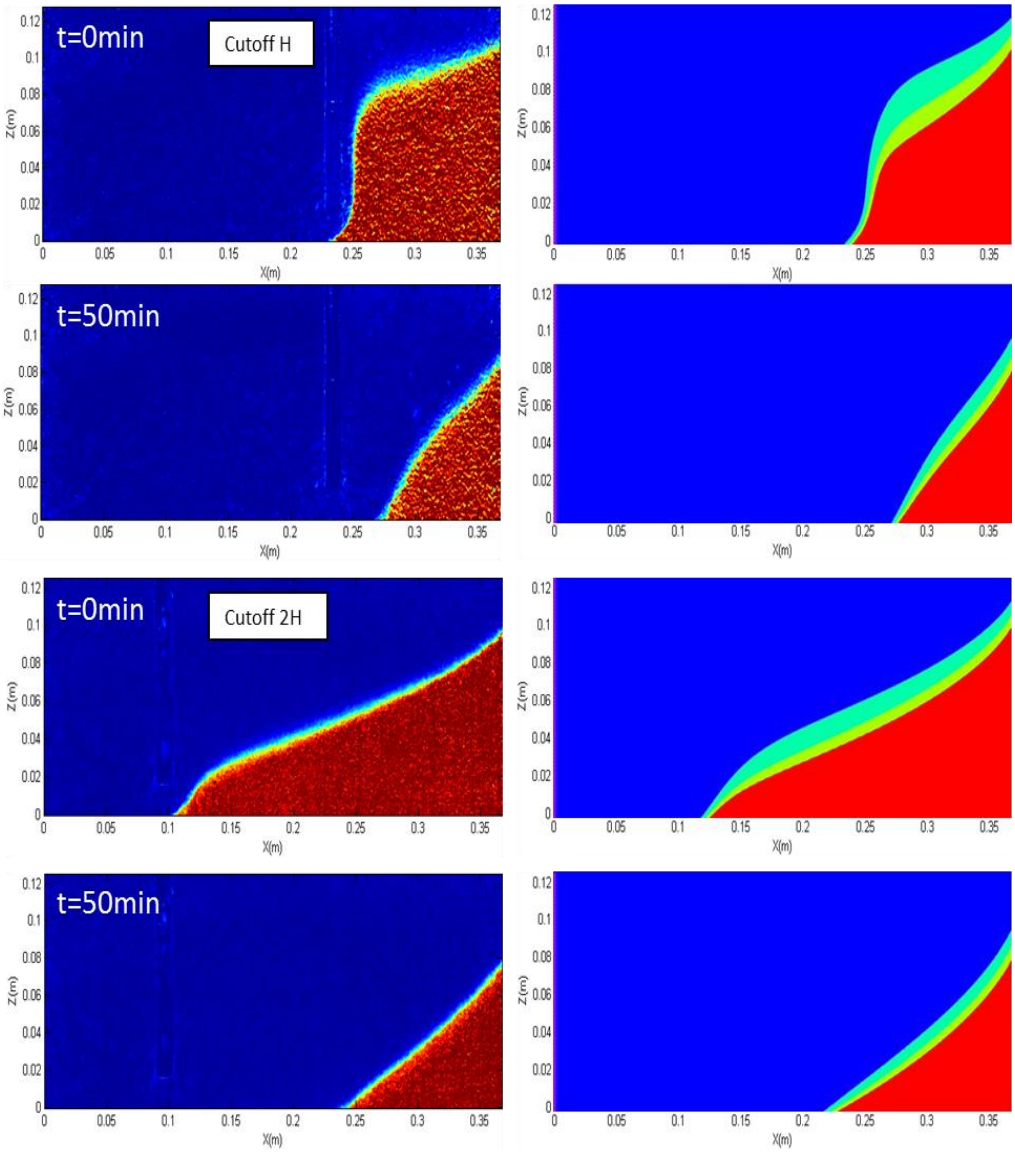

Figure 3.23 Comparison between experimental (left) and numerical (right) steady state saltwater wedge in case H (top) and case 2H (bottom)

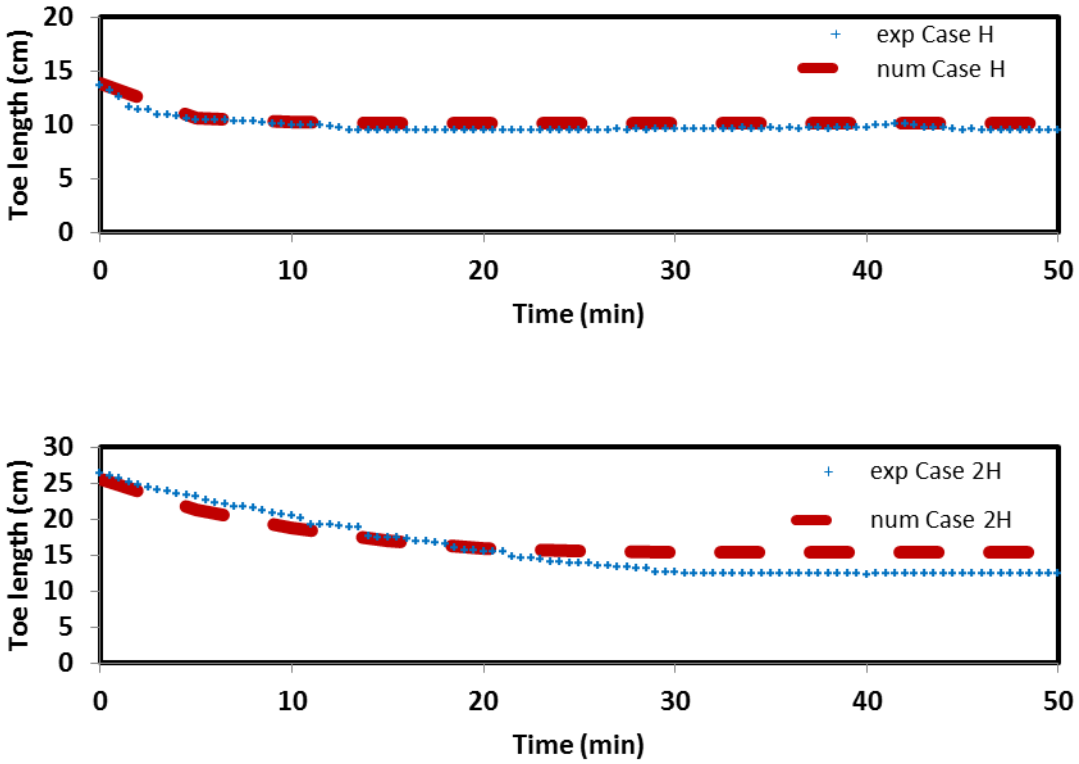

Figure 3.24 Comparison between transient experimental and numerical receding saltwater wedge toe length data in case H (top) and case 2H (bottom)

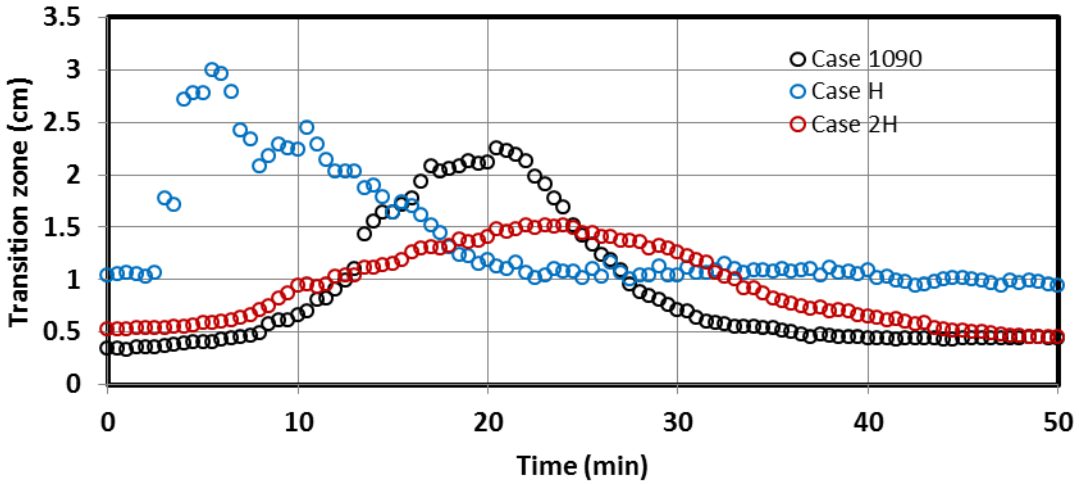

Figure 3.25 Transient transition zone data in receding phase in case H and case 2 H following freshwater level rise increment from dh = 3.6mm to dh = 6mm (ΔH = 2.4 mm)

Fig 3.25 presents the transient TZ width data following the freshwater head rise of ΔH = 2.4 mm. The data clearly show that the magnitude of the widening exhibited in case H was greater than in the base case (case 1090), while it was noticeably attenuated in case 2H. The results show that the peak value was about 3 cm and 1.5 cm, in case H and case 2H, respectively, compared to 2.3 cm previously recorded in case 1090. In other words, the peak magnitude of the widening was about 30% greater in case H compared to the base case, while it was about 35% smaller in case 2H. In addition, the peak value of the widening was recorded at 5.5 min and 22 min in case H and case 2H, respectively, while it occurred at about t = 20.5 min in the base case. Fig 3.25 shows that the widening reached the peak value nearly 4 times quicker in case H than in the base case, while it was slightly slower in case 2H compared to the base case, for equivalent increment freshwater level rise.

These results therefore suggest that in case of equivalent freshwater level increment, the magnitude of the transition zone widening was strongly affected by the position of the wall from the seaside boundary. This may be because in case H, the cutoff wall was located relatively close to the coastline and within the initial location of the saltwater wedge, i.e. in the base case (24.2 cm). Thus, most of the inland freshwater that is driven downwards below the wall opening flows with increased velocity and repulses the saline water seaward (Luyun et al., 2011). This repulsion of the saltwater wedge was characterised by a reduction of 43% compared to the base case toe length, as previously shown in Fig 3.22. In such condition, the sliding of freshwater flux into the receding saltwater wedge would be expected to be substantially faster, thus inducing quicker widening. This appears to be confirmed in the transient concentration colour maps presented in Fig 3.26, where the yellowish pulse diluted was observable after only one minute following the freshwater level increment. The high flow velocity induced the rapid upward motion of the pulse, which then travelled quickly along the interface and promoted a rather sharp widening.

Conversely, in case 2H the cutoff wall is further away from the seaside and outside the initial location of the saltwater wedge (base case). In this case, the cutoff wall is known to partially prevent the freshwater flow from effectively impacting the saltwater wedge (Luyun et al., 2011; Abdoulhalik and Ahmed 2017a). This was manifested by the negative reduction of -9% estimated in this case, as mentioned above (Fig 3.22), which means that is such configuration the toe length could penetrate deeper inland than before the installation of the wall. Therefore, in such condition the sliding of freshwater into the receding saltwater wedge would be expected to be slowed down, thereby inducing a slower widening than in the base case. This was confirmed in the transient concentration colour maps shown in Fig 3.26, which shows a rather single yellowish pulse travelling upwards within the receding wedge (Fig 3.26). This pulse appeared within five minutes following the freshwater level increment and travelled rather obliquely until reaching the interface at about t = 7 min. The figure shows that the subsequent widening of TZ was less uniform and less pronounced, because the single pulse did not spread evenly along the interface as observed in the base case, but the impact on the interface was instead more localised. These very interesting observations appear to further confirm the possible existence of some freshwater sliding along the aquifer bottom into the saltwater wedge over the course of the retreat, which thereafter participated in enhancing the TZ widening mechanism.

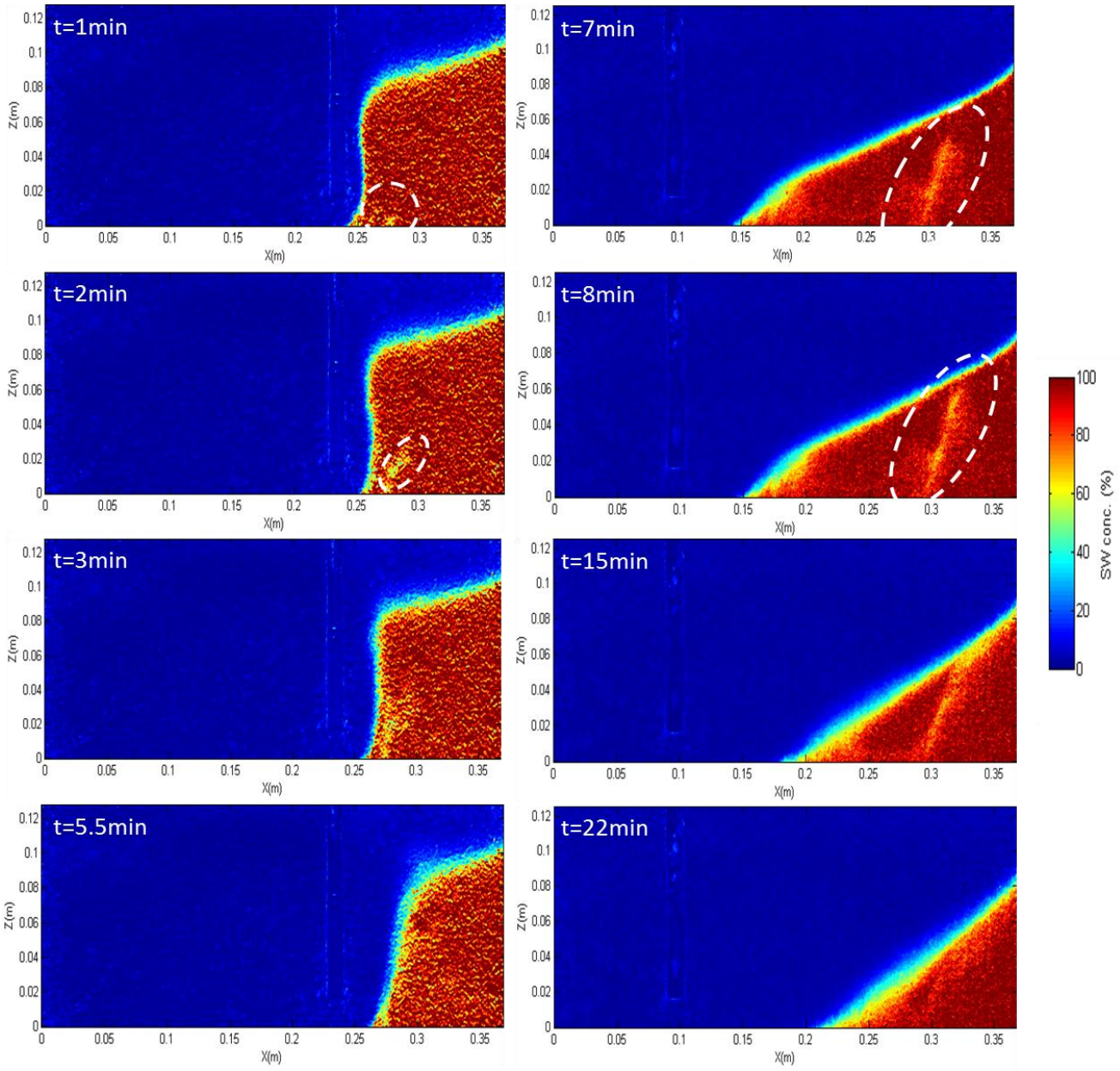

Figure 3.26 Transient concentration colour maps of the receding phase in case H (left) and case 2H (right)

3.4 Summary and conclusions

This study provided a quantitative and qualitative analysis of the effect of boundary water level variations on saltwater intrusion dynamics and the temporal response of freshwater-saltwater transition zone. Two homogeneous cases of different bead sizes (and hence different hydraulic conductivity) were analysed; and two other cases where an

impermeable wall was set at different locations where thereafter examined, whereby the impact of flow disruption on the widening process was explored. The main findings of the study are:

- The expansion of the transition zone did not occur during the intruding phase of saltwater wedge whether it resulted from freshwater level drop or saltwater level rise, regardless of the magnitude of the head change. This finding gives initial indications that in coastal aquifer systems, the widening of the transition zone width may not be substantial during the landward displacement of freshwater-saltwater interface, whether it occurs as a result of water table drop or sea level rise, regardless of the magnitude of the boundary head change.
- By contrast, a substantial widening of the transition zone width was observed during the retreat process, with a peak magnitude and a peak time relatively similar in the scenario involving a rise of the freshwater level relative to the scenario involving a drop of the saltwater level, in cases of equivalent absolute head change magnitudes. This finding suggests that in coastal aquifer systems, receding saltwater wedges induced by a rise of the water table would tend to exhibit transition zone expansions of the same magnitude and same timescale of occurrence as when following a drop of the sea level, provided that the head change magnitudes are comparable but opposite directions.
- The magnitude of the widening of the transition zone observed during saltwater retreat was larger and extended over longer timeframe in homogeneous aquifers with smaller hydraulic conductivity, irrespectively of whether the head change occurred at the freshwater or saltwater boundary.
- The experimental observations revealed that the widening mechanism was also enhanced by the presence of some freshwater sliding and into the wedge during the saltwater retreat process, which was thereafter sucked upward because of density difference effects and

eventually travelled along the transition zone toward the outlet, thereby promoting further widening. The observed phenomenon could not be reproduced by the numerical simulation, where the widening is primarily caused by dispersion along the interface. This underlines the importance of physical model experiments for the investigation of density-driven flow in porous media in improving general process understanding. Despite field evidence of such mechanism have never been documented in previous studies, it is reasonable to hypothesise that such mechanism could conceivably occur in real coastal aquifer systems especially where the non-uniformity aquifer bedrocks may enhance preferential flow. Further investigations would nonetheless be required to examine the reproducibility of this mechanism within larger scale coastal aquifer models which would enable easier examination transition zone dynamics

- The installation of the cutoff wall affected the transition dynamics in different ways, depending on the location of the wall. In the case where the wall was located within the area of the base case toe length, the magnitude of the transition zone widening was about 30% greater and four times quicker than in the base case, for equivalent freshwater rise increment. Conversely, when the wall was located outside the area of the base case toe length, the magnitude of the widening was about 35% smaller and was slightly slower compared to the base case, for equivalent increment freshwater level rise. Experimental observations showed that the hypothesised freshwater pulse could also clearly be observed in presence of the impermeable wall in the two investigated cases.

- The transient analysis of the saltwater toe length revealed that in cases of equivalent saltwater level variations but opposite directions, the intruding wedge required up to twice longer time to reach steady state condition than the receding wedge. This observation shows that timescale asymmetry between saltwater intrusion and retreat processes would also occur in scenarios involving sea level fluctuations. When comparing freshwater and

saltwater change scenarios, the intruding and receding rates of the saltwater wedge as well as the time taken to reach steady state were fairly comparable.

- The steady state toe length analysis enabled correlation of logarithmic toe length to the boundary head difference by a simple linear equation with site specific regression coefficients which vary with different hydrogeological parameter combinations. This finding suggest that for such (highly) simplified homogeneous coastal aquifer system, a reasonable estimate of the logarithmic extent of the saltwater intrusion could be obtained based on the difference between the water table and the sea level. For prediction purposes, a minimum of two values of toe lengths associated with two water level differences would be required to estimate the regression coefficients. It is important to underline that this finding is not meant to, and could not, be directly extrapolated to practical management situations. Future works involving the of larger and/or 3D aquifer models would nonetheless be beneficial in enabling using more data points to further verify the linear relationship suggested herein.

Chapter 4

Transient investigation of saltwater upconing mechanism in laboratory-scale coastal aquifer

The aim of this chapter was to explore the key influential factors affecting the saltwater upconing mechanism in a laboratory-scale coastal aquifer system. In most of the previous upconing laboratory studies, the variation of salt concentration within the freshwater-saltwater transition zone during the upconing was not explored since measurements were only through visual observations (e.g. Mehdizadeh et al., 2015; Noorabadi et al., 2017; Shi et al., 2011). This study provides a valuable insight on the effect of freshwater pumping on the shape and location of the upconing freshwater-saltwater transition zone through qualitative and quantitative analysis for various abstraction rates. Unlike most of the previous laboratory studies which investigated upconing at steady-state condition, this study provides transient analysis uncovering crucial details of transient related phenomena occurring during the upward motion of the saline plume as it rises toward the well with high spatial and temporal resolution. The impact of aquifer hydraulic conductivity on the saltwater upconing and decay (following pumping shut-off) mechanisms was also examined. The sensitivity of the critical pumping rate and the critical time (defined as the time needed for the upconing saltwater to reach the lower part of well) to the well design parameters (pumping rates, depth and location) and the main aquifer properties (hydraulic conductivity, dispersivity and saltwater density) was explored in further numerical modeling simulations

4.1 Experimental procedure

The investigation of the saltwater upconing mechanism in homogeneous coastal aquifer system included 11 experiments. To examine the effect of hydraulic conductivity changes on the saltwater upconing process, the experiments were conducted for two beads

sizes, namely 1090 µm and 790 µm. These comprehended seven experiments (six different pumping rates plus one case where the pumping was switched off) for the beads 1090 µm and four experiments (including three different pumping rates plus case without pumping) for the beads 790 µm.

Prior to initiating the experiment, the overflow outlet in the saltwater reservoir was adjusted such that to maintain a constant head of 129.7 mm. The density of the saltwater solution herein was 1020 kg/m^3. The experiment was initiated by lowering the overflow outlet of the freshwater reservoir to impose an initial constant freshwater head of 135.7 mm. This initial head boundary difference (dh = 6 mm) allowed the dense saline water to penetrate into the porous media until the system reached steady state conditions. This first steady state was considered as the initial conditions of the experiments.

The pumping well was simulated using a Terumo Neolus hypodermic needle connected by a flexible hose (Maprene) to a peristaltic pump Watson Marlow 101 U/R. The needle was 50 mm long with an outside and inside diameter of 1.1 mm and 0.7 mm, respectively. The internal diameter of the hose was 4.8 mm. The hose was maintained outside the porous media by a clamp supported by retort stand placed behind the flow tank. The hose was carefully adjusted such that the tip of the needle was located 85 mm above the bottom of the tank, and 190 mm away from the seaside boundary. The needle was kept at the same position in all the experiments. The choice of a single point abstraction (from the tip of a thin needle) was preferred over the more realistic use of a well screen due to practical reasons and because using a screened tube within the relatively thin width of the porous media chamber (10 mm) would cause significant disruption of the flow and thus impact the behaviour the upconing wedge.

The abstraction was thereafter initiated, using an initial abstraction rate set at Q = 0.09 mL/s. The abstraction rate was increased in a stepwise fashion using an incremental step of 0.1 mL/s. Each time the abstraction rate was incremented, the system was allowed to reach steady state condition. The experiment was completed when the upconing mechanism was observed. The abstraction was thereafter stopped to observe the behaviour of the receding wedge post upconing. It is important to note that pumping from aquifer is a radial flow problem and therefore a pumping well could solely be properly considered in an aerial two-dimensional model or a fully three-dimensional model. The purpose of this investigation is not to simulate the behaviour of saltwater wedge for a specific real system; rather it is to provide an insight on the temporal upconing mechanism and assess its dependency on the permeability of the aquifer. Since all the experiments used the same geometry and properties, the results are thus deemed reliable for comparison, albeit the walls of the tank would probably hinder the development of the cone of the depression in the third dimension, thereby affecting the saltwater upconing behaviour. A quantification of the influence of the third dimension on the cone of depression and upconing dynamics is outside the scope of the study.

4.2 Numerical procedure

The case 1090 was adopted for the numerical validation (K = 85 cm/min). The freshwater and saltwater head boundaries were set at 135.7 mm and 129.7 mm, respectively, to allow penetration of saline water until steady state. The abstraction was initiated from a well simulated at the specified location with a discharge rate initially set at 5.4 cm^3/min for duration of 50 min, to allow the system to reach a new steady state condition. The discharge rate was then gradually increased using an increment of 6 cm^3/min and each time the system was allowed to remain an additional 50 min. The final abstraction rate applied to the system was 29.4 cm^3/min, which is the same as that used in the physical experiment. The last stress

period was dedicated for the retreat of the saltwater water wedge, following the interruption of the pumping.

4.3 Results and discussion

4.3.1 Saltwater upconing experiment

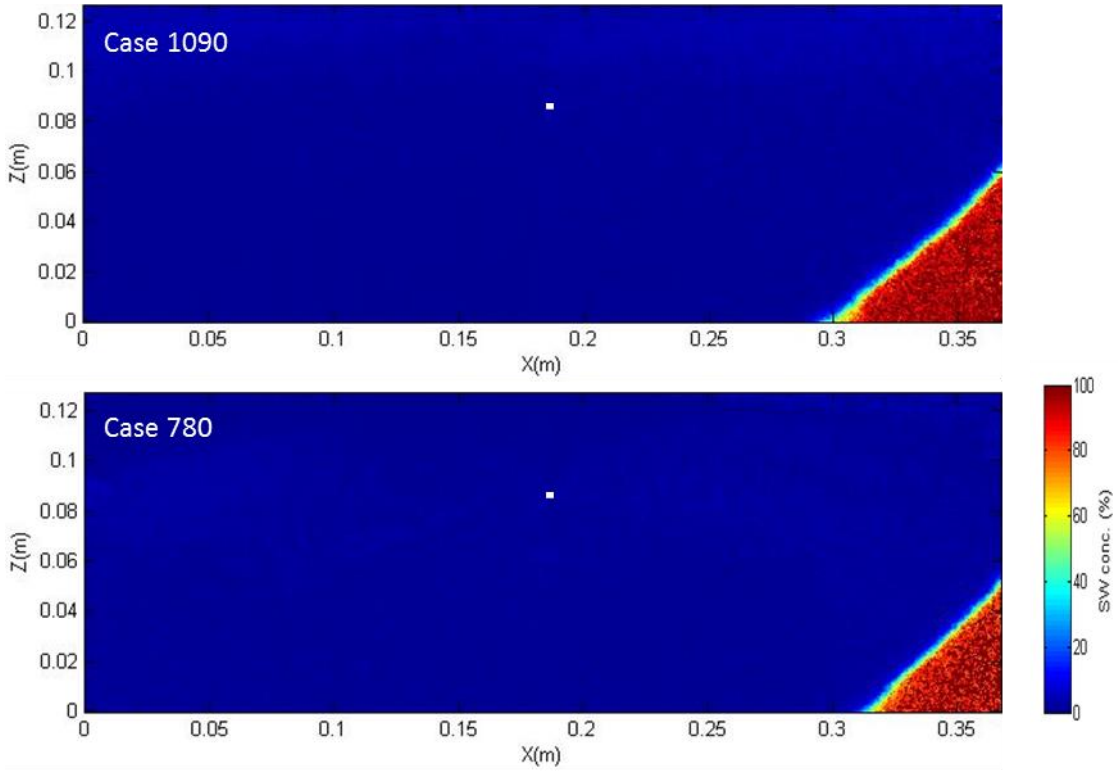

Figure 4.1 Initial steady state saltwater wedge after application of dh = 6 mm

Following the drop of the freshwater level down to 135.7 mm which decreased the head difference to dh = 6 mm, the saline water was allowed to enter the aquifer system and extend inland until it reached steady state condition. Fig 4.1 shows the concentration colour maps of the saltwater wedges at the initial steady state condition. Experimental observations showed that it took relatively less time for the system to reach steady state in case 1090, where it occurred only after 23 min following the head change, while it was reached after

about 45 min in case 780. As expected, the lower permeability media induced relatively slower migration of the denser fluid through the system, in the previous chapter (Fig 3.5).

The pumping rate was thereafter gradually incremented up until the observation of the saltwater upconing mechanism. Fig 4.2 and Fig 4.3 shows the concentration colour maps of the saltwater wedge at each steady state condition, in case 1090 and case 780, respectively. The results show that the abstraction rate required for observation of the upconing process was smaller in case 780 compared to case 1090. In case 1090, Fig 4.2 shows that the freshwater-saltwater interface started to curve upward in a concave-like shape following the increment of the pumping rate to Q = 0.29 mL/s and a further rate increment to Q = 0.39 mL/s led the saline plume to pre-upconing stage, where the saline water was stabilized below the well. At this phase, the buoyancy force induced by density contrast effects is able to stabilise the wedge below the well without causing salinization of the latter. The upconing was completed following the further increment of the rate to Q = 0.49 mL/s. In case 780, the upconing was already initiated after the pumping rate was set to Q = 0.19 mL/s, as shown in Fig 4.3. A further increase of the pumping rate to Q = 0.29 mL/s was sufficient for the saline water to intercept the bore of the well. These experimental observations suggest that the risk of pumping well salinization through saltwater upconing increases with decreasing hydraulic conductivity of the system. Hence, these results underline the vulnerability of production wells to salinization in low permeability aquifer systems whereby the saltwater upconing process is expected to be facilitated.

At first glance one may observe that the width of the transition zone remained relatively constant from one steady state to another before the initiation of the upconing, i.e. before the upward motion of the saltwater (up to Q = 0.29 mL/s and Q = 0.09 mL/s in case 1090 and 780, respectively). This indicates that during the phase prior to upconing, the width of the transition zone was little sensitive to the rate of groundwater abstraction. The widening

of the transition zone was only initiated as the freshwater-saltwater interface approached the vicinity of the well, after setting Q = 0.39 mL/s in case 1090 and Q = 0.19 mL/s in case 780. The transition zone appeared slightly wider in case 780, probably due to the higher spreading along the interface as the saline water flows through finer grain size. The widening was visibly more pronounced in the upper part of the freshwater-saltwater interface. Once the upconing was completed, the width of the transition zone became very thin. Similar observations were reported in previous studies (Mehdizadeh et al., 2015. Werner et al., (2009) also observed similar dispersion effects in the early stage of the up-coning, particularly during the "prefinal" stage of the upconing, whereby they observed a rise of a "dilute salt spike", after which the saltwater plume became non-dispersive at final up-coning stage.

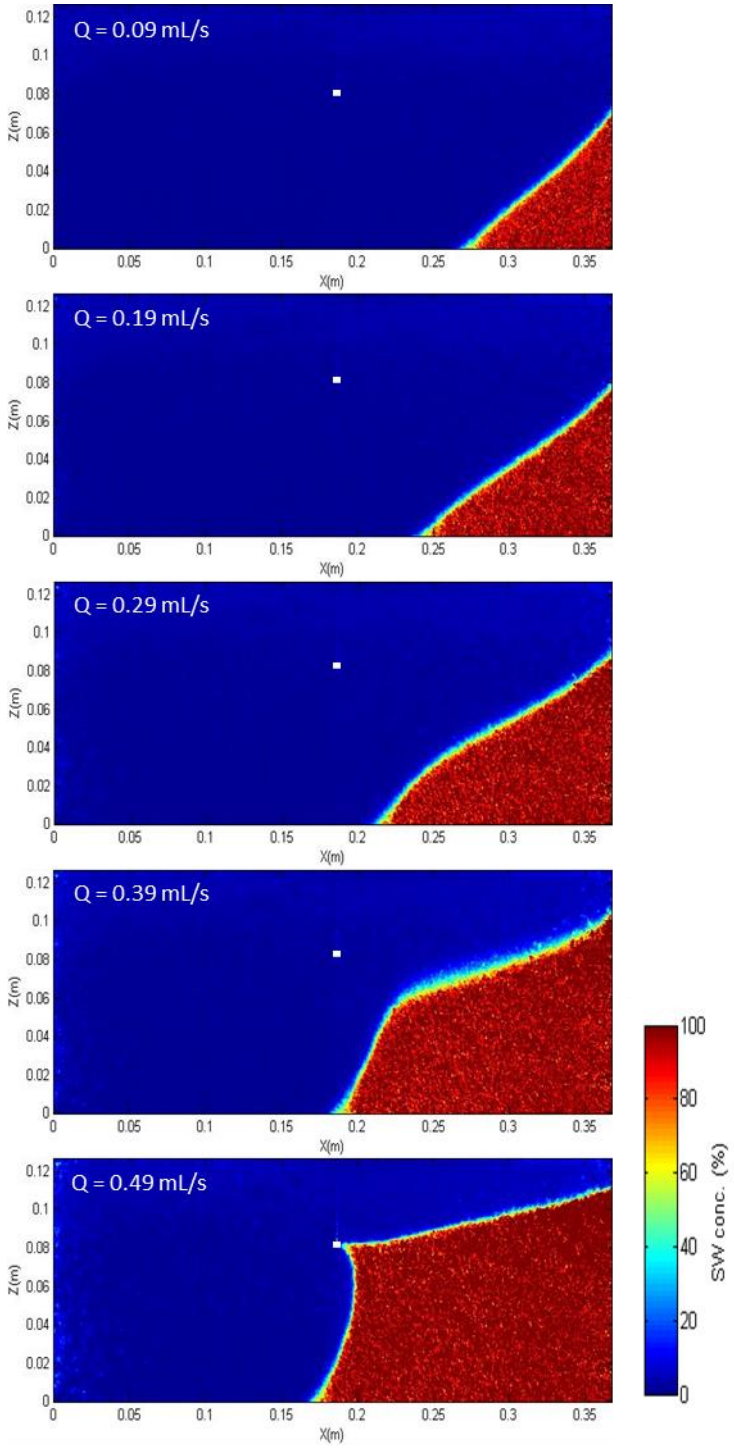

Figure 4.2 Concentration colour maps showing the saltwater upconing process in case 1090

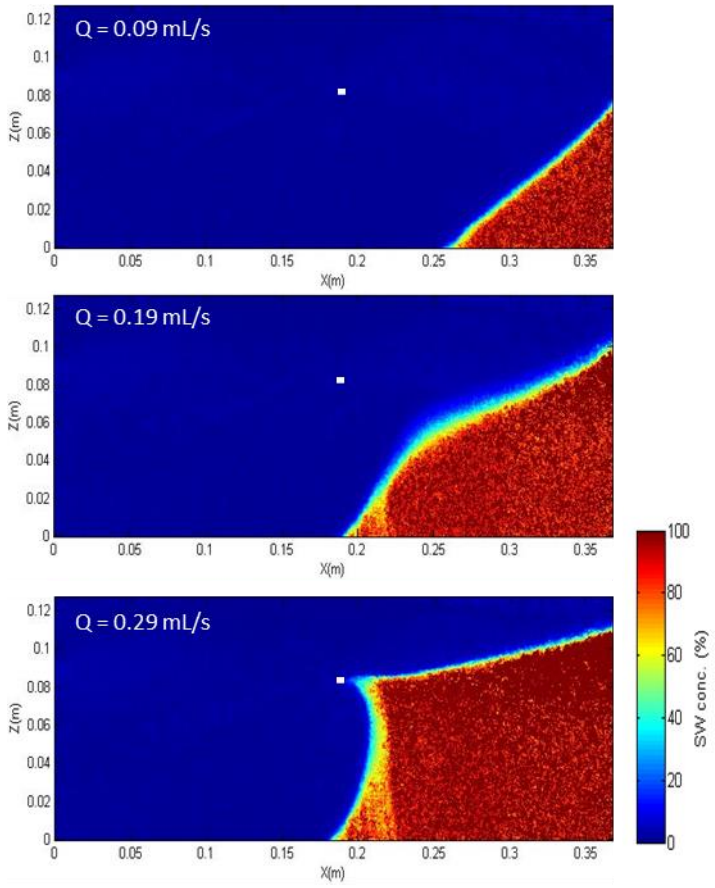

Figure 4.3 Concentration colour maps showing the saltwater upconing process in case 790

The transient toe length data of both cases are presented in Fig 4.4 and the steady state toe length values are shown in table 4.1 and table 4.2, for case 1090 and case 780, respectively. The toe intrusion length (obviously) increased with increasing pumping rate. Prior to upconing, the data show that for equivalent pumping rate increment, the saline water intruded faster in case 780. The results show that the intrusion length was 7% and 41% greater than the toe length recorded in case 1090 for the rates Q = 0.09 mL/s and Q = 0.19 mL/s, respectively. In addition, for equivalent pumping rate increment, the net increase in toe length was more pronounced in the early phase of the upconing process, but it reduced significantly as the saltwater wedge approached the well location, i.e. after setting Q = 0.39 mL/s in case 1090 and Q = 0.19 mL/s in case 780. These results show that for equivalent

pumping rate increment, the landward toe migration rate resulting from freshwater withdrawal was faster in the lower hydraulic conductivity system.

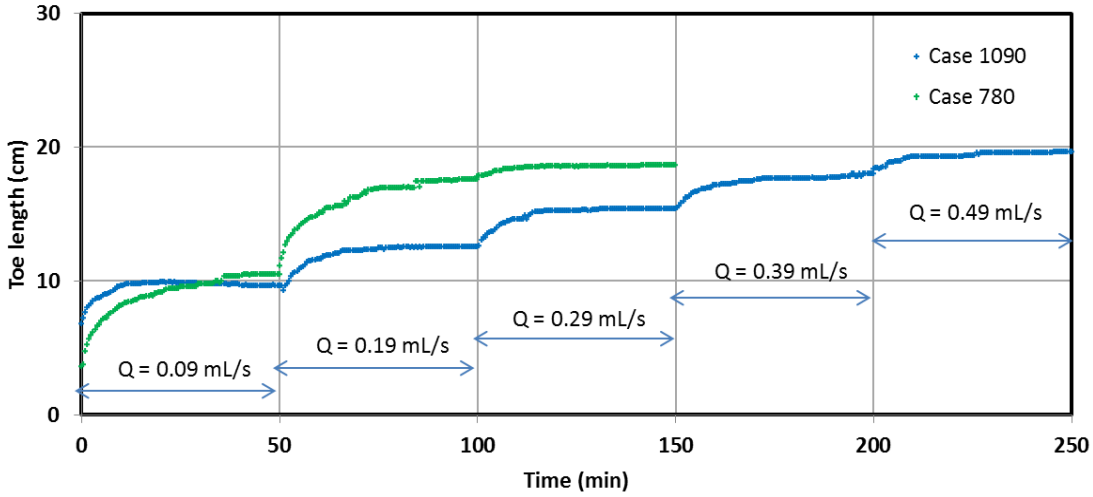

Figure 4.4 Transient experimental toe length data during the upconing in both cases

Table 4.1 Steady state toe length data in case 1090

Pumping rate (mL/s)	0.09	0.19	0.29	0.39	0.49
Toe length (cm)	9.8	12.5	15.4	18.0	19.6

Table 4.2 Steady state toe length data in case 780

Pumping rate (mL/s)	0.09	0.19	0.29
Toe length (cm)	10.5	17.6	18.6

Fig 4.5 shows the transient images of the early phase of the saltwater receding wedge phase. The saltwater receding phase was initiated after the pump was turned off. Following the interruption of the abstraction, Fig 4.5 shows that the tip of the cone moved rapidly away from the well towards the seaside and the freshwater-saltwater interface subsequently regained its natural (relatively) straight shape. This mechanism was visibly faster in case 1090, probably because the higher permeability of the system could promote faster seaward fluid motion. Fig 4.5 shows that a substantial widening of the transition zone was observable over the course of the retreat, which appears to be more pronounced in the low permeability media. The seaward migration of the saltwater toe was also faster in case 1090, as observed in Fig 4.6. The results show that the saltwater toe reached steady state within 20 min and 29 min, in case 1090 and case 780, respectively. This result suggests that the process of decay of the upconed saltwater wedge that follows the interuption of pumping would be slower in low permeability aquifer system, which implies a slower restoration of salinized aquifers and thus longer time required before the freshwater (from the restored aquifers) could possibly be reused again.

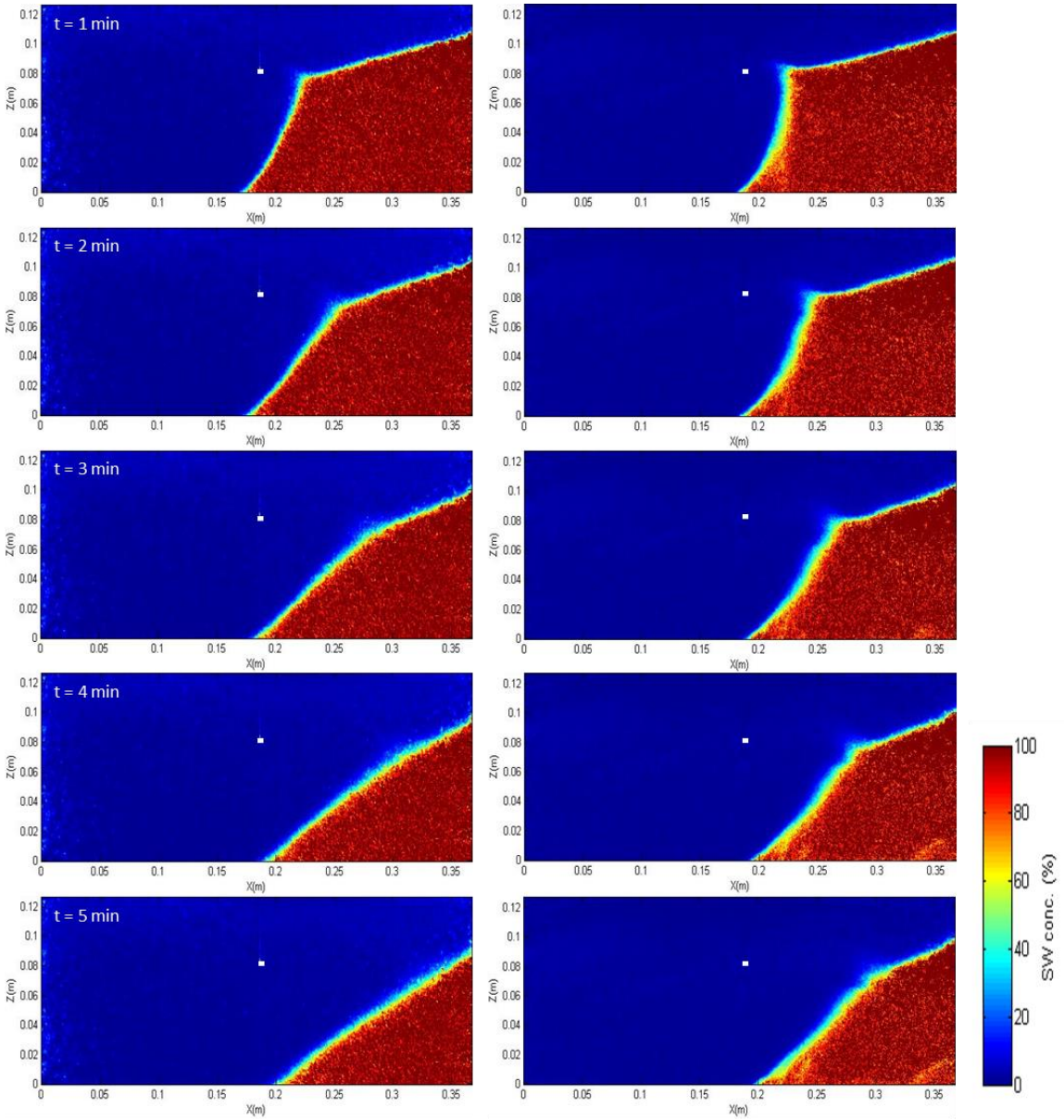

Figure 4.5 Concentration colour maps showing the receding saltwater wedge after interruption of the pumping in case 1090 (left) and case 790 (right)

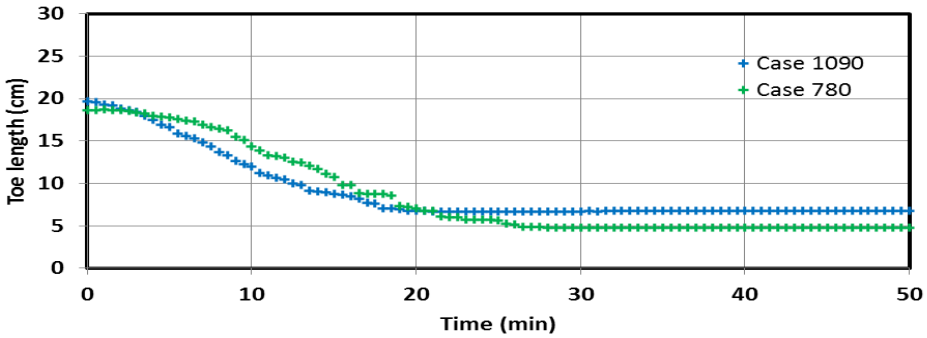

Figure 4.6 Transient toe length data during the retreat process

4.3.2 Numerical modelling

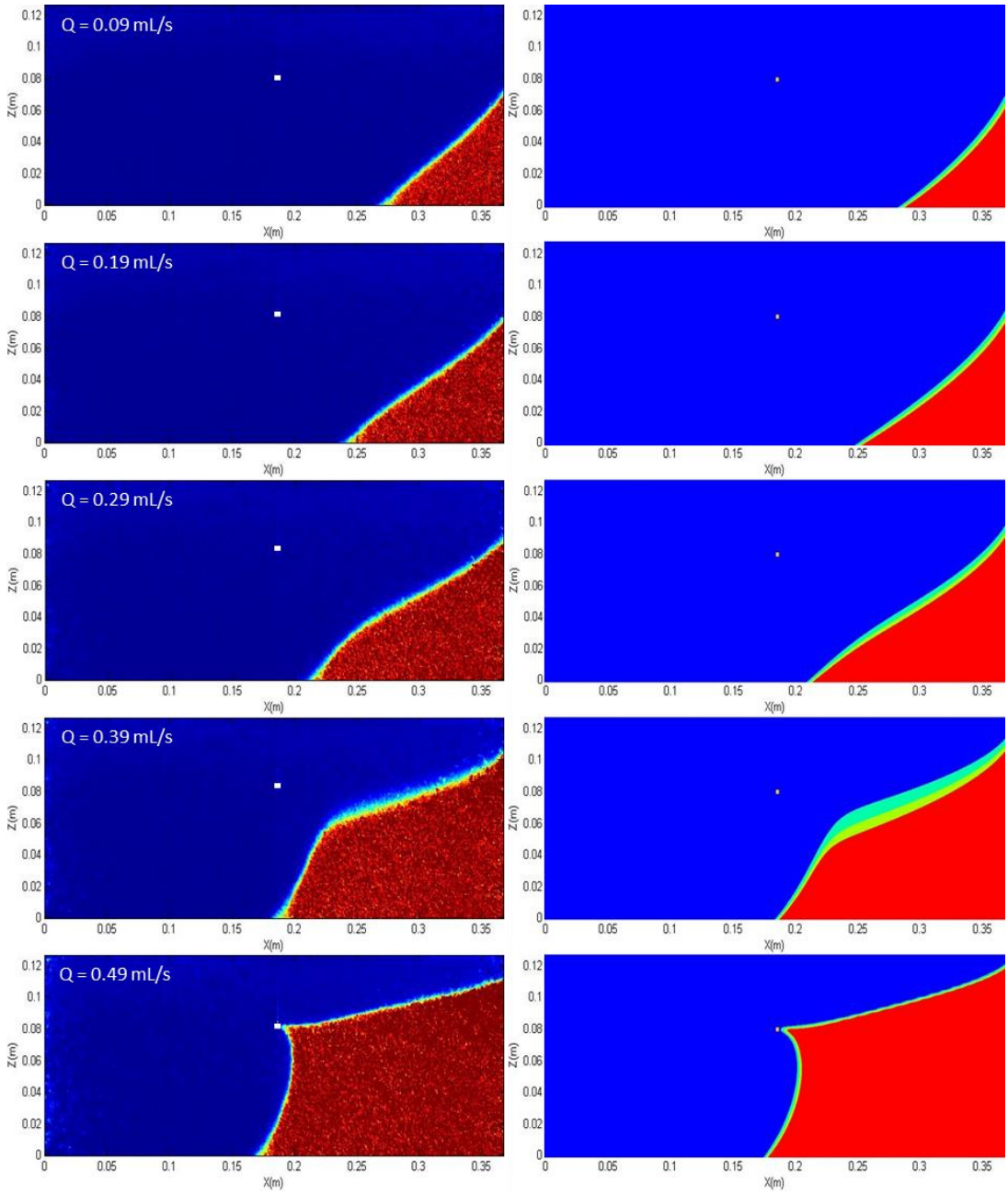

Figure 4.7 Comparison between experimental (left) and numerical (right) saltwater upconing process

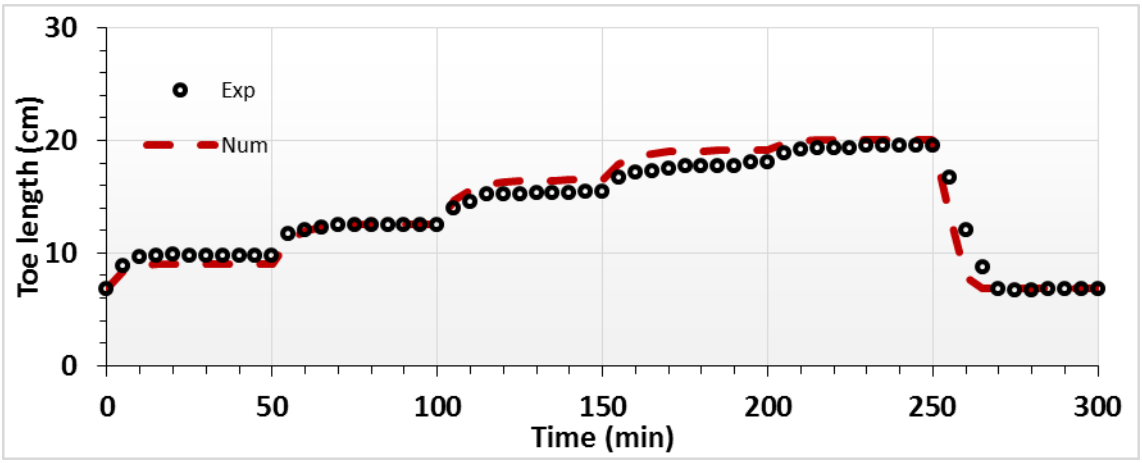

Figure 4.8 Comparison between transient experimental and numerical toe length data

The experimental case 1090 was adopted for the numerical simulations. Unlike most of the previous studies that only rely on qualitative analysis of the shape of the wedge; the numerical validation was herein through both qualitative comparison of the shape of the saline plumes as well as quantitative comparison of the transient toe length data. This adds extra feature to this study. Fig 4.7 shows that the numerical model reproduced very well the shape of the steady state saltwater wedge throughout the different phases of the upconing process. The curved shape of the freshwater-saltwater interface prior to upconing was well reproduced in the numerical model. The widening of the upper portion of the interface observed as the saltwater wedge approached the well (after setting Q = 0.39 mL/s) was also well depicted, albeit slightly overestimated in the numerical model. The model could predict relatively well the evolution from thin to wide transition zone conditions (Q = 0.09 - 0.39 mL/s) that was observed in the physical experiment. The final shape of the wedge during the upconing was also very well depicted, despite some minor discrepancies at the seaside boundary. At upconing stage, i.e. after the saline water intercepted the well, the transition zone in the model became relatively thin than at earlier stages, in agreement with experimental observations.

Fig 4.8 shows the comparison between the transient experimental toe length results and the numerical data. The results show that the experimental data match very well with the numerical prediction. The toe length was slightly under predicted at the start of the pumping (t = 0-50 min), while slightly over predicted after application of the pumping rates Q = 0.29 mL/s and Q = 0.39 mL/s. These minor discrepancies may be attributed to several factors, including possible minor source of heterogeneity associated with the packing of the beads, while the numerical model assumes perfect homogenous condition. Other factors such as tiny fluctuations in the water levels caused by surrounding vibrations may also contribute to this slight mismatch. Nonetheless, comparison shows in overall good agreement in the saltwater toe behaviour in response to the abstraction. The maximum percentage difference between experimental and numerical results was 8%, 1%, 7%, 6%, 2 % and 1% for Q = 0.09 mL/s, 0.19 mL/s, 0.29 mL/s, 0.39 mL/s and 0.49 mL/s, respectively.

The maps of the flow velocity vectors are presented in Fig 4.9 to better understand the impact of the abstraction well on the flow and solute transport processes. The data show that prior to abstraction, the magnitude of the flow vectors is identical throughout the system, except in the top right zone where the freshwater exits with higher velocity, which is in agreement with other studies (e.g. Chang and Clement, 2012, Abdoulhalik and Ahmed, 2017a,b). The saltwater plume could be readily delineated by the vectors of very low magnitude at the bottom right corner. The initiation of the abstraction caused the flow domain to be subdivided into three distinct zones, each of which exhibiting different flow patterns in response to the withdrawal. These three zones are respectively located at the landward side of the well, in the vicinity of the well and the seaward side of the well (above the saline plume).

When the abstraction was initiated, the magnitude of the vectors at the landward side of the well gradually increased from the inland boundary up to the vicinity of the well. The further increment of the pumping rate led to higher velocity within this region. In the vicinity

of the well, a rather circular shape was initially formed within which the velocity substantially increased. The magnitude of the vectors reached very high values as the rate was further increased and the associated initial circular shape started to spread inland, with velocity increasing radially towards the well.

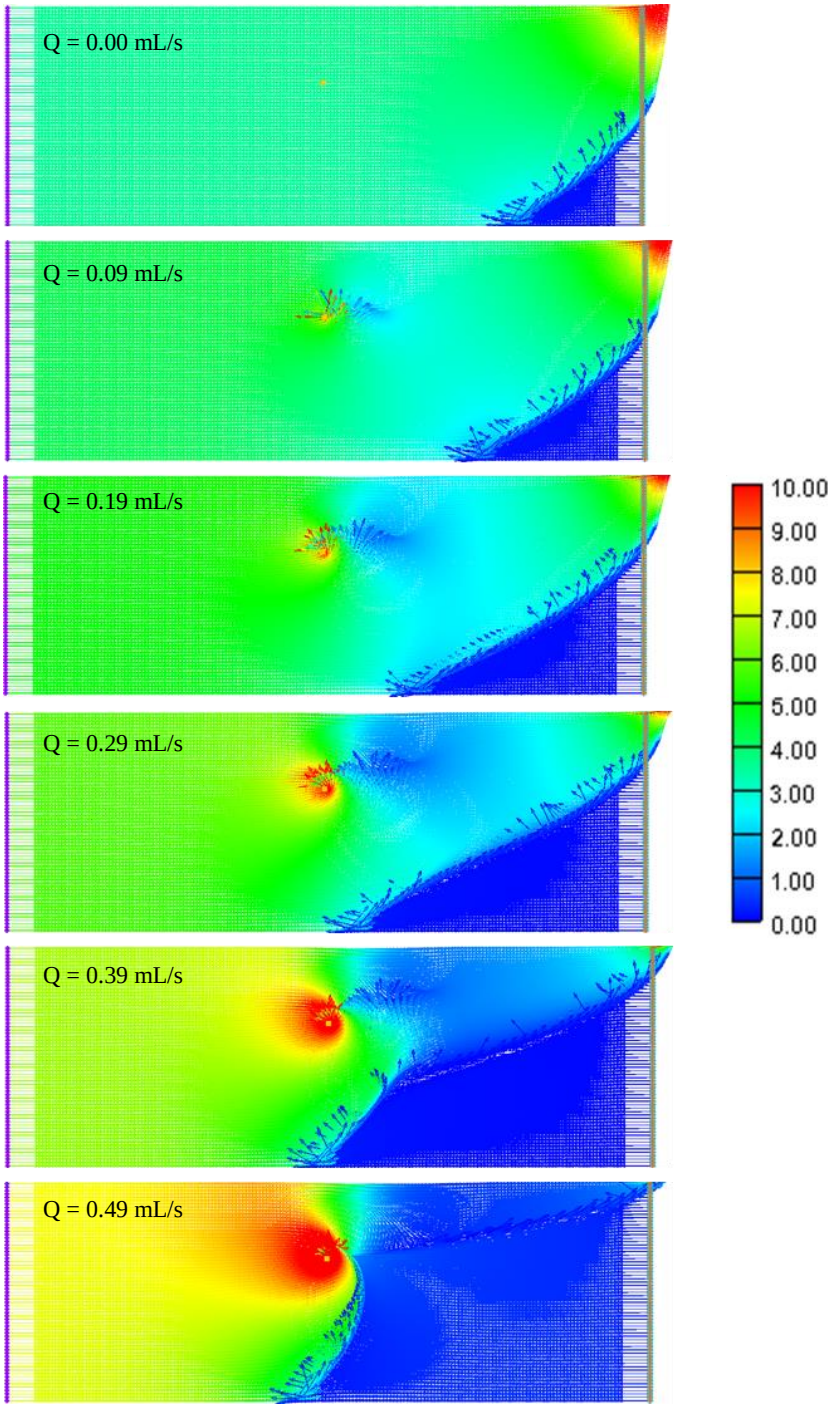

Figure 4.9 Maps of the flow velocity field of the steady state saltwater wedges after application of each pumping rate until observation of the upconing mechanism. The unit of the velocity cm/min

By contrast, the magnitude of the flow velocity in the seaward side of the well decreased noticeably, especially right beyond the well position. The flow velocity within this

zone was even more reduced as the pumping rate was increased, thereby causing the inland advancement of the saline wedge and the rise of the saline plume along the coastline. The upconing saline plume was thus bounded on the top part by very low flow velocity and on the landward side by relatively high flow velocity. This results in this outward dipping shape of interface (t = 250 min). The upconing was completed as the dipping part of the interface reached the zone of high velocity around the well, where the water is abstracted.

4.3.3 Sensitivity analysis

The objective of this sensitivity analysis was to provide insights on the impact of the main aquifer parameters on the upconing process for different well design configurations. In all the simulations, the initial condition (prior to abstraction) corresponded to that of a steady state saltwater wedge associated with a head difference dh = 6 mm. Table 4.3 shows the aquifer parameters and the well design parameters of the base case, which were similar to those of the physical and numerical models. The well location was expressed by the dimensionless location ratio L_w/L, where L_w is the well distance from the coastline and L is the length of the aquifer. The well depth was expressed by the dimensionless depth ratio Z/H, where Z is the height of the well from the aquifer bottom and H is the thickness of the aquifer.

Table 4.5 presents a summary of the different scenarios tested, involving various well locations, depths and pumping rates. Five different well locations and four well depths were tested. For the different locations and depths, the pumping rates were selected through trials and errors using an incremental step of 0.005 mL/s. The investigated aquifer parameters were the hydraulic conductivity, the saltwater density, the longitudinal and the transversal dispersivity values, as indicated in Table 4.4.

Table 4.3: Parameter combinations used in the base case

Parameters	Values ranges
Well configurations	
Well distance, L_w (cm)	19.0
Location ratio L_w/L	0.5
Well depth, Z (cm)	8.5
Depth ratio Z/H	0.625
Aquifer parameters	
Head differences (mm)	6
Saltwater density (kg/m^3)	1025
Hydraulic conductivity K (cm/min)	85
α_T/α_L	0.5
α_L (cm)	0.1
Porosity	0.38

Table 4.4: Summary of the parameters tested in the sensitivity analysis

Parameters	Values ranges
Well configurations	
Location ratio, L_w/L	0.25, 0.375, 0.5, 0.625, 0.75
Depth ratio, Z/H	0.375, 0.5, 0.625, 0.75
Pumping rate Q_P (mL/s)	Increment every 0.005
Aquifer parameters	
Hydraulic conductivity K (cm/min)	36, 55, 70, 85, 108
Saline water density (kg/m^3)	1020, 1025, 1030
α_T (cm)	0.005, 0.01, 0.05, 0.1
α_L(cm)	0.001, 0.01, 0.05, 0.1, 0.2

A simplified diagram of the upconing wedge including the investigated parameters is shown in Fig 4.10. In addition to the toe length (T_L), three other quantifying parameters were considered in order to examine the influence of the above-mentioned parameters on the upconing mechanism. These are described as follows:

- The upconing distance (X_U), which refers here to the horizontal distance between the apex of upconing at 1% salt contour line and the bottom of the well.

- The critical pumping rate (Q_c), defined as the maximum permissible pumping rate which does not allow saline water to reach the well (Reilly and Goodman, 1987). In this study, the critical pumping rate was considered as the well discharge value that produced steady-state upconing such that the 1% salt contour line of the cone apex just reached the well. Therefore, disruption of the steady-state interface resulting to saltwater motion causing partial salinization of the well discharge could all be consequences of the abstraction rate exceeding the critical pumping rate.

- The critical time (t_c), described as the time taken for the cone apex at 1% salt contour line to reach the well. This parameter gives an idea of how fast the well would be salinized, for equivalent pumping rate. A smaller critical time indicates thus faster upconing rate, therefore faster well salinization.

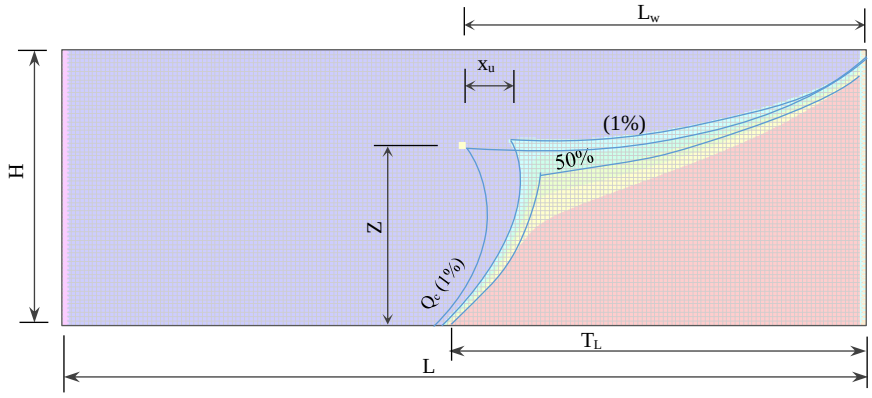

Figure 4.10 schematic diagram of the upconing wedge

Effect of the pumping rate at different well locations and depths

As stated above, the pumping rates were first selected through trials and errors process where the rate was gradually increased with an increment of 0.005 mL/s for the different well locations and depths, in order to investigate the effect of pumping rate on the dynamics and movements of the upconing process.

Figure 4.11 depicts the motion of the upconing wedge towards the well for some selective pumping rates at three different well locations. Obviously, increasing the pumping rate induced faster upconing motion movement towards the well, characterized by decreasing X_u values. The results show that the upward movement of the saline water was much faster in the early stage of the upconing process, and slows down as it approached the well. For each specific location, the critical pumping rate corresponded to the pumping rate at which $X_u = 0$, i.e. the 1% salt contour line of the cone apex reached the well. For instance, for a location ratio $L_w/L = 0.5$ and Q = 0.36 mL/s, the steady state equilibrium was attained before the upconing wedge reached the well, while for Q = 0.38 mL/s, the upconing wedge reached the well in even lesser time. A further increment of the rate to Q = 0.4 mL/s caused faster salinization of the well. That is because when the freshwater extraction was initiated, the pressure exerted by freshwater on the interface was reduced, which allowed rapid upward

motion of the saline water. This upward motion was then slowed down as the saline reached the vicinity of the well. When the steady-state was reached before the saline water reached the well, the seaward freshwater flow and the density contrast effects act jointly to stabilize the saltwater wedge.

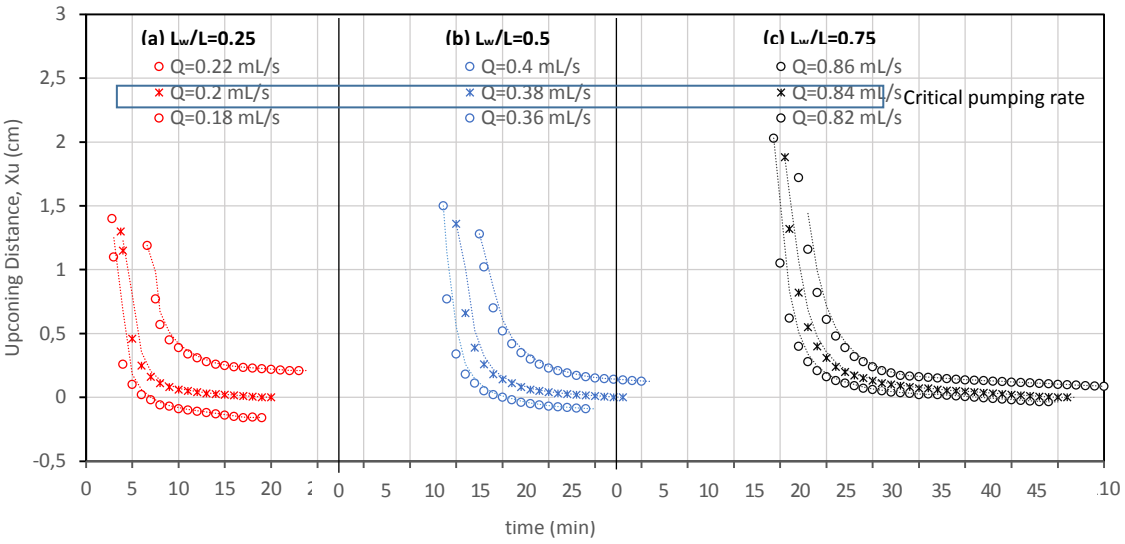

Figure 4.11 Effect of pumping rate on the movement of the upconing wedge

As expected, the results show that the critical pumping rate varied with the locations and the depths of the well, as shown in Figure 4.12a. The closer the well was located to the initial saltwater wedge position, the lower was the critical pumping rate, which would imply a faster salinization of the well. The critical pumping rate was more sensitive to the variations of the location than to the depth of the well. The farther the well was located from the seaside, the longer was the distance to be travelled horizontally by the saltwater, with the seaward freshwater flow slowing down its motion. At fixed depth, the motion of saline water toward the well was mainly vertical, while most of the flow along the upper part of the interface was reduced because of the abstraction, as previously observed in Fig 4.9.

Similarly, the impact of changing the well location had more influence on the critical time than changing the depth, as shown in Figure 4.12b. The distance from the coastline is an

important parameter to consider the maximum permissible pumping rate. It is very interesting to note that the critical time increases almost linearly with increasing location and depth ratios following a relatively simple linear equation of type $t_c = aX + b$, with a and b being the linear regression coefficients and X being either the L_w/L or Z/H. The values of a and b for the current system are shown in the figure. The strong linearity of the correlations is evidenced by the relatively high coefficient of determination $R^2 > 0.99$.

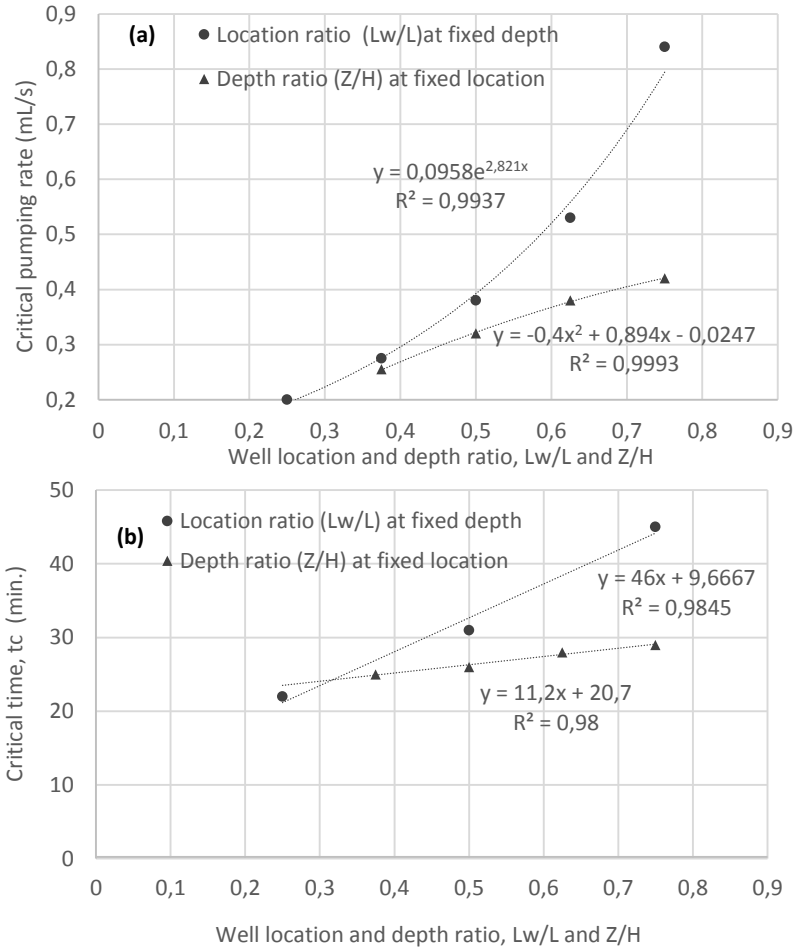

Figure 4.12 Effect of varying well location and depth ratios a) on the critical pumping rate and b) on the critical time, where the pumping rate is the maximum critical pumping rate for every well location (Q = 0.84 mL/s) and every well depth (Q = 0.42 mL/s)

Effect of the hydraulic conductivity

In this section, the influence of the aquifer hydraulic conductivity on the critical pumping rate and critical time was analysed for different well locations. The pumping rate was gradually increased by an increment of 0.005 mL/s for five values of hydraulic conductivities within the range 36 - 108 cm/min. This was done for three different well locations (with fixed depth) and three different well depths (at fixed location), as shown in Figure 4.13.

The results showed that the critical pumping rate was very sensitive to the hydraulic conductivity (Figure 4.13a). For all the well configuration tested, the lowest critical pumping rate was found for the lowest hydraulic conductivity, which reflects the vulnerability of low permeability aquifer system to saltwater upconing process and thus to well salinization. This may be because the freshwater flow contributing in the seaward repulsion of the saltwater wedge would be reduced as the hydraulic conductivity of the aquifer system is lowered, thus the horizontal and vertical migration of the saltwater wedge caused by the abstraction would subsequently be facilitated. These results are well supported by the experimental observations presented above.

The results show that for all the well locations tested, the critical time also decreased with decreasing aquifer hydraulic conductivity (Fig 4.13b). In these simulations, the critical pumping rates observed for the maximum K tested (here K = 85 cm/min) was applied to the other four (lower) hydraulic conductivity values such that to ensure that the upconing wedge reached the well in all cases. From the lowest to the highest conductivity values tested, the critical time was increased by 19 min, 26 min and 37 min, for L_w/L = 0.25, 0.5 and 0.75, respectively. This suggests that the sensitivity of the critical time to hydraulic conductivity was more significant for wells located farther away from the initial interface position.

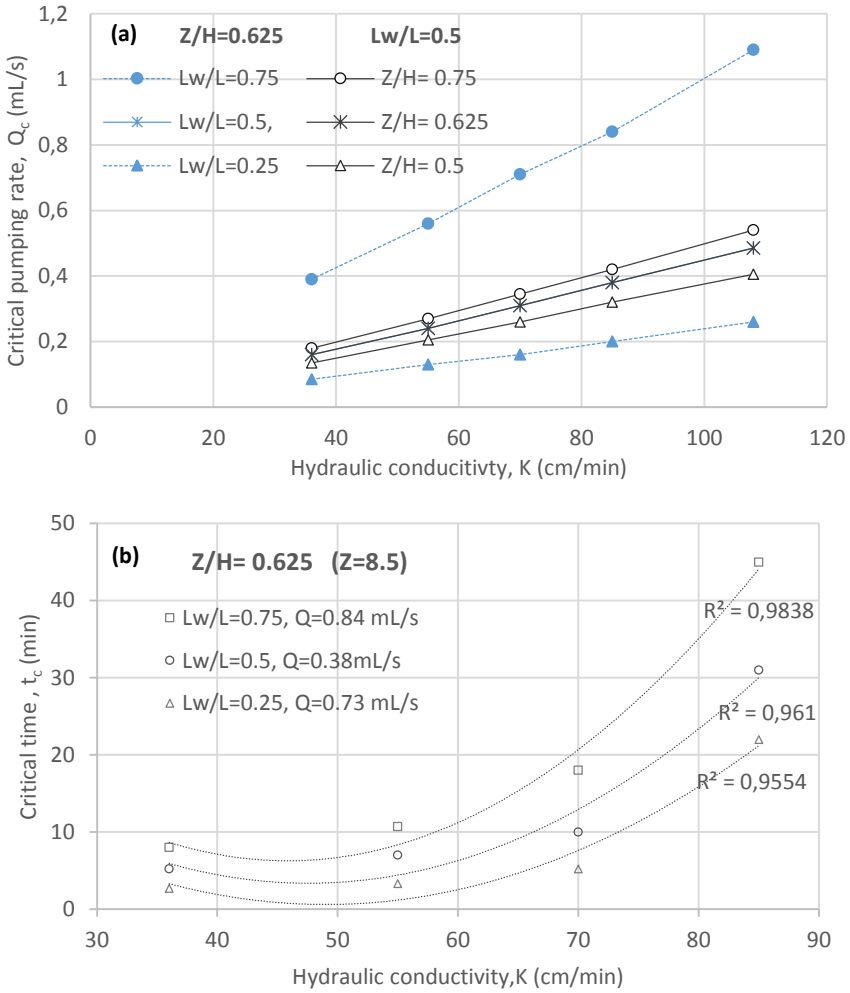

Figure 4.13 Impact of the hydraulic conductivity a) on the critical pumping rate b) on the critical time

Effect of the saltwater density

The sensitivity of the critical pumping rate to the saltwater density was explored for three different saltwater densities values ρ, namely 1020, 1025, and 1030 kg/m^3, as shown in Fig 4.14.This was performed for three different well depths ratios Z/H = 0.5, 0.625 and 0.75 and for a fixed well location.

As shown in Figure 4.14a, increasing the saltwater density induced a smaller critical pumping rate. This means that denser saltwater would require lower pumping rate for the

upconing to occur. By contrast, lighter saltwater density induced greater critical pumping rate. These results show that for the well configurations considered, higher saltwater densities would tend to facilitate the saltwater upconing mechanism. This is probably because increasing the density of the saltwater leads to increasing density contrast effects which enforce the lateral motion of the saltwater wedge in the early stage of the upconing. The results also showed that for a fixed saltwater density, the critical pumping rate decreased with increasing well depth, as expected.

The saltwater density also influenced the critical time, as shown in Fig 4.14b, where the density effect was tested for two different locations ratios (L_w/L = 0.5 and 0.25) and the three different depths ratios. The results clearly show that for equivalent pumping rate, higher saltwater density would induce faster upconing. This is because higher density values yield faster landward horizontal motion of the saline water before it starts to rise upwards toward the well. These finding differs from that reported in Werner et al., (2009) who observed the most rapid and significant up-coning occurred in their scenario involving high pumping and low density difference. This is because their analysis was based on an axisymmetric model, thus neglecting the horizontal motion of the saline water. In this scenario, the critical pumping rate applied to all density values was that of the case where ρ = 1020 kg/m^3 such that to ensure that the upconing wedge could reach the well in all the other cases. The influence of the saltwater density on the critical time was more significant for wells located farther away from the initial position of the interface. In such case, for ρ = 1020 kg/m^3 and L_w/L = 0.5, the critical time was relatively high for all well depths, but decreased substantially as the density was increased to 1030 kg/m^3, where the critical time became nearly twice smaller. This difference was less pronounced in the case where the well was closer (L_w/L = 0.25). This is because in the case where the well was farther away from the initial location of the interface, the horizontal motion of the saltwater wedge preceding the

upconing mechanism was significantly faster for higher density values, thus subsequently reducing the critical time. By contrast, when the well was located closer to the initial position of the interface, this horizontal motion was limited since the motion of the saline in such case was mostly vertical, thus the impact of the density change on the critical time was less pronounced.

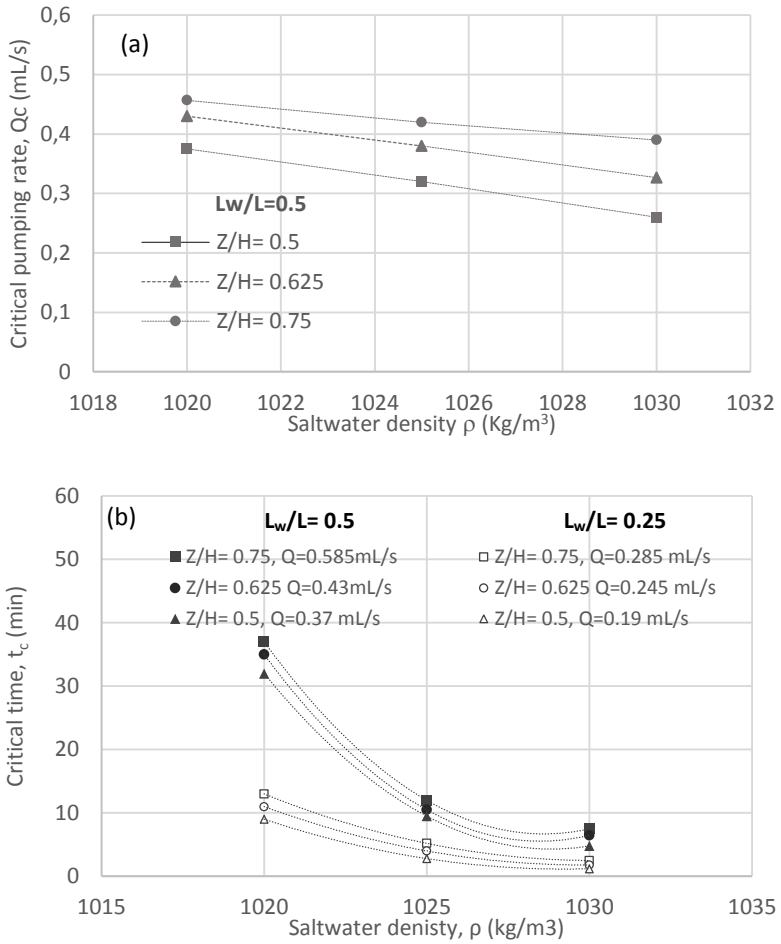

Figure 4.14 Effect of the saltwater density on a) the critical pumping rate and b) the critical time

Effect of the dispersivity

The sensitivity of the upconing mechanism to dispersivity was explored to understand the contribution of dispersivity to well salinization. In this section, two sets of simulations were performed by varying both longitudinal (α_L= 0.001, 0.01, 0.05, 0.1, 0.2 cm) and

transversal (α_T= 0.05, 0.1, 0.5, 1.0 cm) dispersivities for three different hydraulic conductivities (K = 55 cm/min, 70 cm/min and 85 cm/min). The location and depth of the well were maintained constant. The results are shown in Figure 4.15. Generally, the results showed that the effect of dispersion on the critical pumping rate was relatively small (4.15a). Increasing the dispersivity only induced very slight decrease of the critical pumping rate, albeit more visible when decreasing the transversal dispersivity. The results presented in Fig 4.15b further shows that for a fixed pumping rate, the critical time decreased with increasing dispersivity. This could be because high dispersivity induces more mixing along the interface which would lead to subsequent widening of the transition zone. In such conditions, less time would be required for the low concentration isoline of the dispersive zone to reach the well. Thus for equivalent pumping rate, these results suggests that higher dispersive systems would tend to induce faster upconing mechanism.

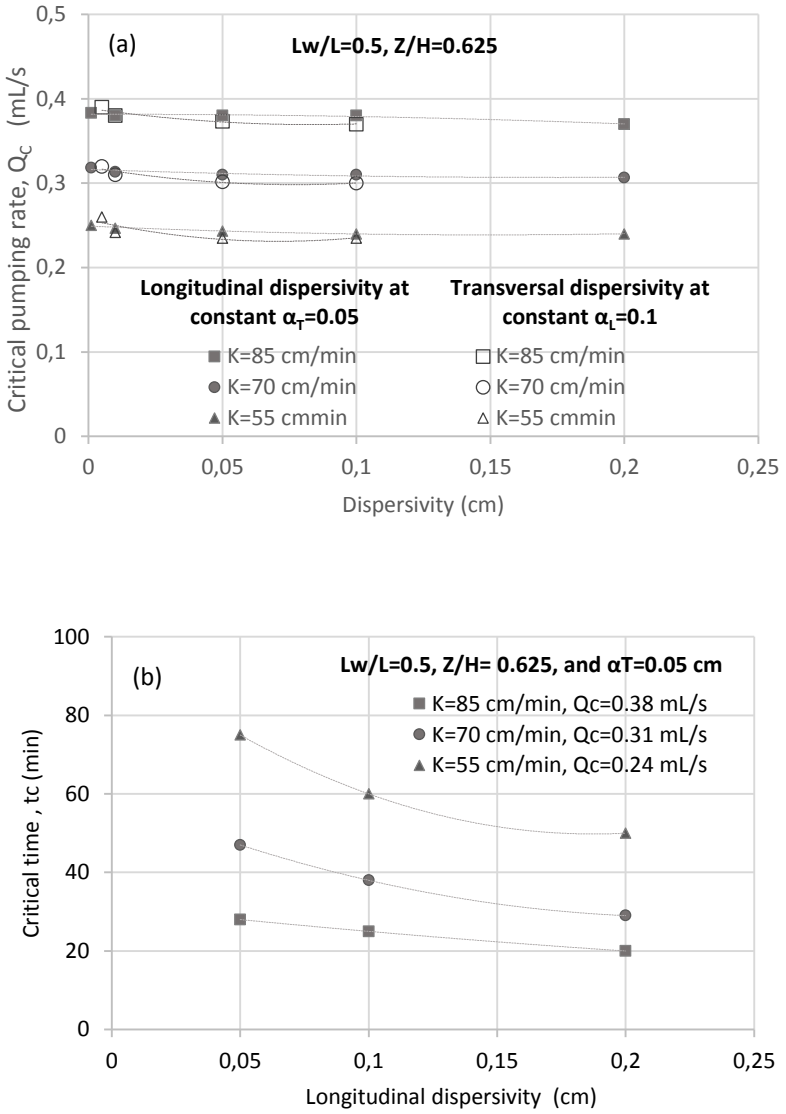

Figure 4.15 Effect of the dispersivity on a) the critical pumping rate and b) the critical time

4.4 Summary and conclusions

Experiments were conducted within laboratory flow tank to examine saltwater upconing and decay (following pumping shut-off) mechanisms in coastal aquifers under transient condition. The investigation involved the analysis of two homogeneous aquifer systems using two different bead sizes to examine the impact of aquifer hydraulic conductivity. The study provided a qualitative and quantitative analysis of the effect of

freshwater pumping on the saltwater upconing mechanism using image analysis techniques, thereby uncovering crucial details of the associated behavior of the freshwater-saltwater interface shape and location as well as the dynamics of the transition zone with high spatial and temporal resolution. The numerical simulation results showed very good agreement with the experimental data for both the transient toe length data and the shape of the saltwater wedge at the various steady states. The resulting model was used to examine the sensitivity of the critical pumping rate and the critical time (defined as the time needed for the upconing saltwater to reach the lower part of well) to the well design parameters and the main aquifer properties. The main findings of the study are:

- The vulnerability of the pumping well to salinization was higher for the low permeability aquifer system. The results showed that the saltwater upconing process could be observed with an abstraction rate smaller in the lower hydraulic conductivity scenario. In addition, the inland penetration of the saline plume was larger in the lower K scenario relative to the higher K scenario, for equivalent pumping rate increment. The widening of the freshwater-saltwater transition zone was observed only as the saltwater wedge approached the well location and occurred especially along the upper part of the interface length, with a more pronounced widening in the low K scenario.
- The process of decay (following the interruption of the abstraction) of the upconed wedge was slower in the low permeability aquifer system, which implies a slower restoration of the salinized aquifer and thus a longer time required before reusing freshwater from the restored aquifers. The experimental observations showed that following the interruption of the abstraction, the tip of the wedge moved relatively slower away from the well towards the seaside in the lower K scenario, which was associated with slower seaward motion of the toe of the saltwater wedge

- Flow velocity field analysis revealed that local reduction of the magnitude of the flow velocity along the upper part of the interface was a major factor contributing to the upconing mechanism, as it allowed “free” vertical rise of the saline plume due to the subsequent reduction of the repulsion forces of the seaward freshwater flow. The relatively high flow velocity below the well resulted in this outward dipping shape of interface which yielded upconing when the tip reached the zone of high velocity around the well, where the water is abstracted.
- Sensitivity analysis results showed that the critical pumping rate and the critical time were more sensitive to the variations in the well location than the well depth. The critical time increased with the increasing location and depth ratios following relatively simple linear equation.
- For all configurations tested, the lowest critical pumping rate was found for the lowest hydraulic conductivity, which further shows that the saltwater upconing mechanism was facilitated with decreasing permeability of the system. This further supports the experimental results and further reflects the vulnerability of low permeability aquifer systems to salinization of pumping wells.
- Results showed that for the well configurations considered, higher saltwater densities would tend to facilitate the saltwater upconing mechanism. The influence of the saltwater density on the critical time was more significant for wells located further away from the initial position of the interface.
- Results showed that increasing the dispersivity only induced very little change on the critical pumping rate. For a fixed pumping rate, the critical time decreased with increasing dispersivity, which suggests that for equivalent pumping rate, higher dispersive systems would tend to induce faster upconing mechanism.

Chapter 5

The effectiveness of cutoff walls to control saltwater intrusion in multi-layered coastal aquifers

Amongst the very limited SWI studies related to physical barriers, Anwar (1983) provided an analytical relationship to determine the location of the interface after installation of a cutoff wall, where the coefficients were derived through laboratory experiments. More recently, Kaleris and Ziogas, (2013) presented an extensive numerical analysis on the effect of cutoff walls in controlling SWI and protecting groundwater withdrawals for an extensive range of parameter combinations that include the wall geometry and hydraulic properties as well as the properties of the aquifer. They provided graphs and empirical equations suitable for field application purposes to evaluate the performance of cutoff walls.

In this chapter, the effectiveness of cutoff walls to control SWI was examined in heterogeneous coastal aquifers (stratified formations) to offer a more realistic insight on their performance. The experimental configurations included a homogeneous aquifer and typical heterogeneous aquifers with various stratification patterns. Additional layering patterns of monotonically increasing/decreasing permeability from top to bottom were also analysed numerically. A valuable insight on the flow dynamics imposed in each investigated aquifer setting was presented. Sensitivity analysis was also conducted to evaluate the influence of the design parameters and aquifer parameters on the ability of cutoff walls to control SWI in heterogeneous setting.

5.1 Experimental procedure

Three different aquifer configurations were analysed in this investigation, including two stratified aquifers (case HLH and case LHL) and one homogeneous scenario (case H) for reference. The two heterogeneous scenarios were composed of three quasi uniform layers. The case H was performed using glass beads of mean diameter 1325 µm and the low K layer was simulated using the glass beads of mean diameter 780 µm.

Fig 5.1 presents the photographs of all the investigated cases. In all, two sets of experiments were completed. The first set represented the saltwater intrusion scenarios occurring in each aquifer setting prior to the installation of the barrier, considered as base cases. In the second set, a cutoff wall was installed into the system. The cutoff wall was made of impermeable material (plasticine) and was installed prior to the siphoning and packing of the beads in the tank (Abdoulhalik et al., 2017). To ensure that the cutoff wall was located within the original zone of the saltwater wedge for good effectiveness (Luyun et al., 2011), the cutoff wall was designed based on the delineation of the saltwater wedge in the homogeneous scenario (case H). The cutoff wall was placed prior to the beads packing at 6.8 cm from the seaside boundary, considering that cutoff walls are generally located within a distance of twice the aquifer height from the coastline or closer (Allow, 2012; Japan Green Resources Agency, 2004). An opening of 2.8 cm was left between the tip of the wall and the bottom of the tank, such that the penetration depth was greater than 60% the aquifer, to ensure effective seaward saltwater repulsion (Kaleris and Ziogas, 2013)

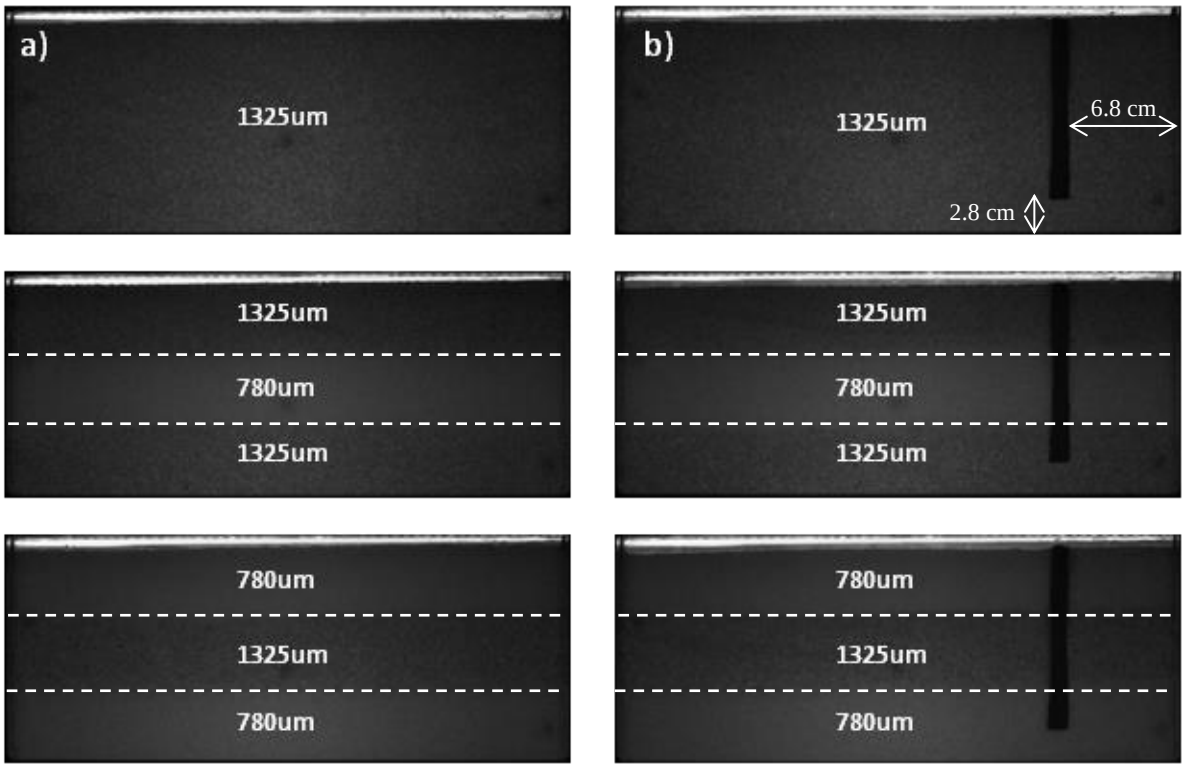

Figure 5.1 Investigated scenarios: case H (top); case HLH (middle) and case LHL (bottom); Base cases b) Cutoff wall cases

At the start of each experiment, a saltwater level of 129.7 mm was imposed while the freshwater level was set high enough to allow the entire porous media to remain fully saturated with freshwater. Various hydraulic gradients were applied to the system to simulate changes in the hydrological conditions by varying the freshwater level such that to impose head differences dh = 6 mm, 5.2 mm and 4.4 mm, corresponding to hydraulic gradients of 0.0158, 0.0137 and 0.0116, respectively.

5.2 Numerical procedure

After setting the freshwater and saltwater heads to 135.7 mm and 129.7 mm, respectively, which allowed the intrusion of the saltwater into the model domain (t = 0 – 50 min), two other stress periods were performed where the freshwater head was dropped down to 134.9 mm (t = 50-100 min) and 134.1 mm (t = 100-150 min). In other words, the head differences dh = 6 mm, 5.2 mm and 4.4 mm were successively imposed in the first, second and third stress period, respectively. The simulation procedure of the cutoff wall cases was similar to that of the base cases. The simulation of the cutoff wall was done by rendering the cells occupied by the wall as inactive in the models.

5.3 Results and discussion

5.3.1 Prior to cutoff wall installation

Saltwater intrusion dynamics was first analysed within each aquifer setting prior to the installation of the barrier, to examine of the performance of cutoff walls and attempt to better understand the flow dynamics and solute transport associated to each layering pattern. The concentration colour maps of the base cases are presented in Fig 5.2. The drop of the freshwater level to 135.7 mm generated a disturbance in the equilibrium of the system, allowing the saline water to enter and form a saltwater wedge in the lower right corner. The further decrement of the head difference to 5.2 mm and 4.4 mm led to further reduction of the hydraulic forces, allowing density contrast effects to further enforce the saltwater wedge deeper into the system. A summary of the experimental toe length values recorded in the base case is presented in table 5.1. The data show that the net increase of the saltwater intrusion length resulting from a head decrement of 1.6 mm (from dh = 6 mm to dh = 4.4 mm) was 8.72 cm, 8.90 cm and 7.19 cm in cases H, HLH, and LHL respectively.

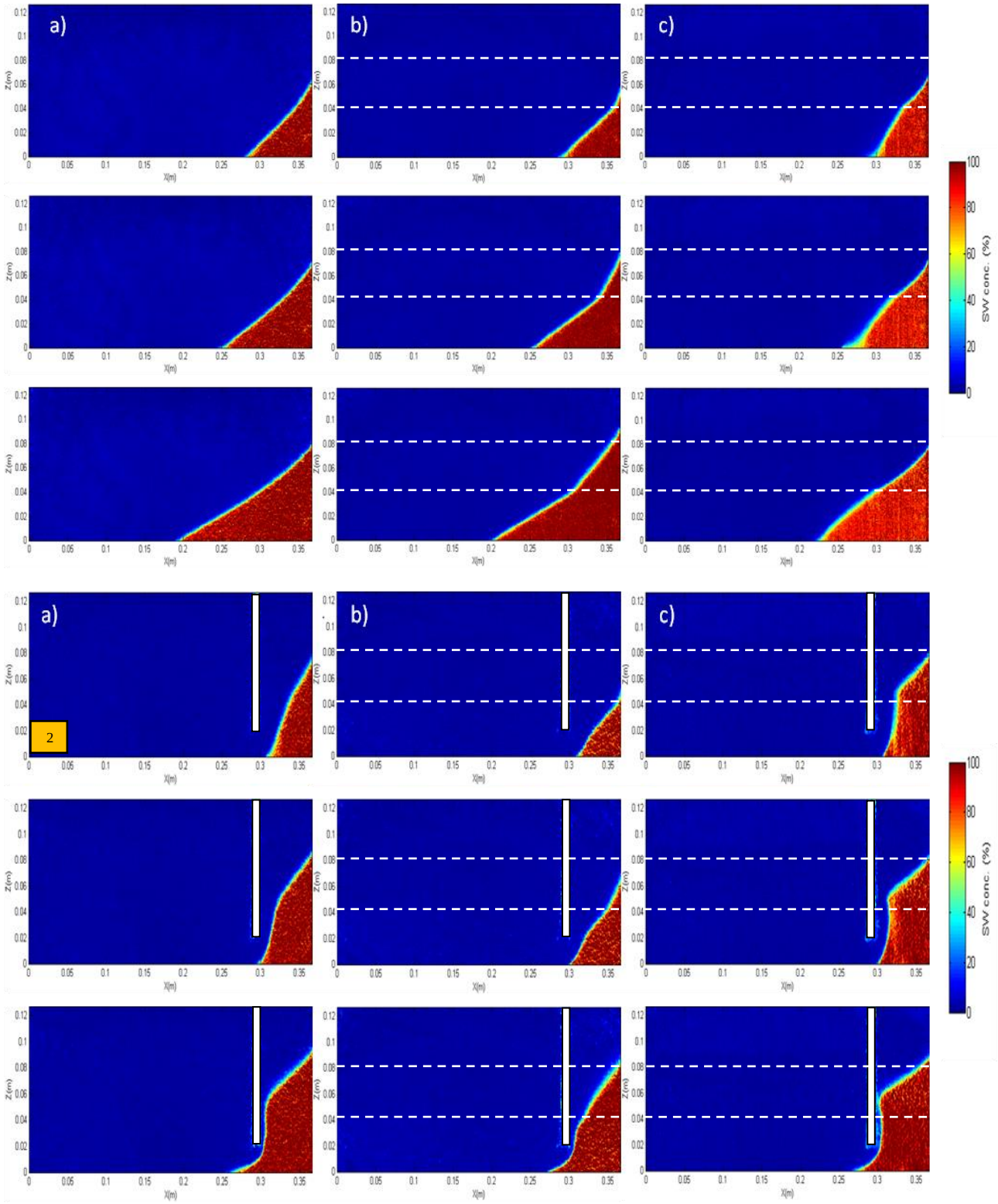

Figure 5.2 Concentration colour maps of the 1) bases cases (prior to wall installation) and 2) cutoff wall cases; a) case H; b) case HLH and c) case LHL. From top to bottom, dh = 6 mm, 5.2 mm, and 4.4 mm

Table 5.1 Experimental toe length values in the base cases

Head difference	Case H	Case HLH	Case LHL
dh = 6 mm	8.4 cm	7.4 cm	6.9 cm
dh = 5.2 mm	11.7 cm	11.2 cm	10.4 cm
dh = 4.4 mm	17.2 cm	16.3 cm	14.1 cm

The data show that the presence of stratification induced a seaward retreat of the saltwater wedge associated with a substantial distortion of the freshwater-saltwater interface, for all the hydraulic gradients tested. The seaward shifting of the interface observed in case LHL compared to the homogeneous scenario was due to the decrement of the buoyancy forces as the saline water is forced to flow through the finer beads, where dispersion and diffusion effects are relatively higher and tend thus to weaken density contrast effects. In case HLH, the middle layer of low K enhances the freshwater flow in both the upper and lower parts of the aquifer, thereby causing also the seaward retreat of the interface, albeit the freshwater flowing in the top part of the system has little contribution in repulsing the saltwater wedge, but rather flows mostly above the wedge towards the outlet. These observations are in good agreement with the observation reported by Lu et al. (2013), where similar heterogeneous settings were investigated at steady-state condition for a single head boundary condition.

5.3.2 Post cutoff wall installation

After wall installation, one may, at first glance, readily observe that the cutoff wall induced considerable repulsion of the saltwater wedge in all the investigated cases (Fig 5.2). As expected, the cutoff wall disrupted the normal flow dynamics and forced the freshwater to flow downwards through the small opening with substantially higher velocity, resulting in the

consequent repulsion of the saline water (Abdoulhalik et al, 2017). It is interesting to note the noticeable distortion of the overall shape of the wedge exhibited in the different layered configurations. The inward dipping freshwater-saltwater interface observed in case HLH relative to the homogeneous case suggests that the seaward freshwater flow was relatively greater in the former than in the latter. By contrast, the outward dipping interface observed in case LHL suggests here that the opposition force of the flow was relatively lowered compared to the homogeneous case.

Table 5.2 Experimental toe length and associated reduction values in the cutoff cases

Head difference	Case H		Case HLH		Case LHL	
	TL	R	TL	R	TL	R
dh = 6 mm	6 cm	29.5%	5.6 cm	25.1%	6 cm	13.9%
dh = 5.2 mm	7.1 cm	39.7%	6.8 cm	38.9%	6.7 cm	35.6%
dh = 4.4 mm	9.71 cm	43.4%	9.34 cm	42.8%	9.44 cm	33.1%

The toe length data along with the associated percentage reductions achieved by the cutoff wall are shown in table 5.2. The data show that the presence of the layer stratifications generally lowered the effectiveness of the cutoll wall. In case HLH, the seaward shifting caused by the low K layer in the middle part of the system prior wall installation induced a reduction of the difference TL_0 - TL_b, whereas TL_b remains nearly the similar (limited at the position of the wall). Likewise, in case LHL the effectiveness of the cutoff wall was even more reduced, given that the shifting observed prior to wall installation was even greater in this configuration. In addition, the flow velocity through the opening of the wall may also be reduced by the underlying low K layer, which also contributes in reducing the effectiveness of the cutoff walls in such setting. This will be further supported by the maps of the flow

velocity provided below. These results nonetheless show the workability of cutoff walls in heterogeneous layered aquifer systems in preventing SWI, but demonstrate that that neglecting the existence of stratification pattern by assuming perfect homogeneous conditions may lead to erroneous estimation of the wall performance.

5.3.3 Numerical modelling results

The numerical toe length results of the three investigated scenarios are shown in Fig 5.3. The transient experimental toe lengths in the base cases were reasonably well predicted by the SEAWAT model in the three scenarios, albeit the toe motion was at some points slightly over predicted. The maximum percentage difference between the experimental and numerical results was about 10%, 1% and 9% in case H; and 15%, 1% and 5% in case HLH, for dh = 6 mm, 5.2 mm and 4.4 mm, respectively. The toe length was most over-predicted in case LHL, where the maximum percentage difference reached nearly 39% for dh = 6 mm, but decreased to 16% and 12% for dh = 5.2 mm and 4.4 mm, respectively. The simulation results for the cutoff wall experiments yielded almost perfect agreement with the experimental data. The maximum percentage difference was 3%, 4% and 11% in case H; 1%, 2% and 1% in case HLH; and 1%, 5% and 2% in case LHL; for dh = 6 mm, 5.2 mm and 4.4 mm, respectively. The numerical model confirmed that the cutoff wall was effective in retaining the saline water on the seaward side of the wall for all the head differences tested and in all the investigated configurations, in agreement with the experimental observations.

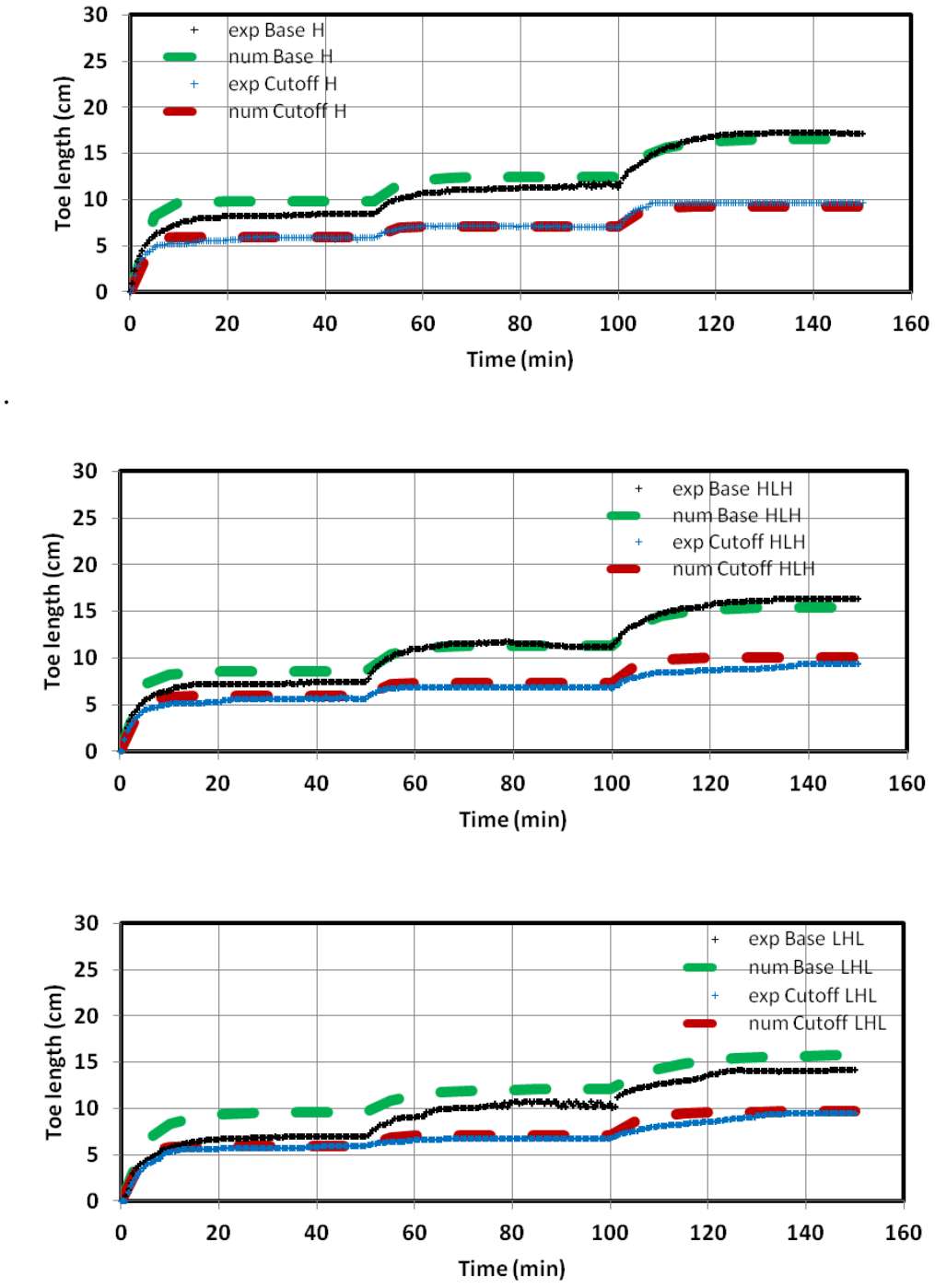

Figure 5.3 Comparison between transient experimental and numerical toe length data in the base and cutoff wall cases; case H (top); case HLH (middle) and case LHL (bottom)

Flow velocity analysis

To better understand the flow dynamics imposed by the layer stratification prior and post to installation of the cut wall, a flow velocity analysis was completed for each scenario (Fig 5.4). As expected, the magnitude of the flow velocity vectors was relatively even throughout the model domain, reaching maximum values when freshwater exiting the sytem in the top right part of the model domain and very low values within the saltwater wedge in the homogenous scenario, which agrees with results of Chang and Clement (2012). The decrement of the hydaulic gradient, obviously, led to a decrease of the freshwater flux transmitted to the system, manifested by velocity vectors of lower magnitude, which can clearly be seen in the gradual decreasing of red area in the top right part of the model, utlimately leading to further horizontal and veritcal extension of the saltwater wedge. In the cutoff case, this well homogeneized freshwater flow is driven downward towards the reduced cross section of the opening below the wall, thereby causing a significant increase of the flow velocity through the opening, which decreases with as the hydraulic gradient becomes smaller or shallaower.

In case HLH, the magnitude of the flow velocitiy vectors was low through the interlayer of low K, as expected, causing the confinement of the flow in the upper and lower parts of the aquifer. After cutoff wall installation, the middle low K layer restricted the downward movement of the freshwater toward the bottom layer and hence the flow velocity through the opening was reduced. This could clearly be seen in the figure where the magnitude of the velocity vectors through the opening in the HLH case was smaller than that of the homogeneous scenario.

In case LHL, the high velocity vectors are confined into the higher permeablity zone in the middle part of the aquifer due to the presence of both the overlying and underlying low

K layers. Most of the freshwater flow exited below the bottom boundary of the overlying low K layer where the magnitude of the velocity vectors was the highest. After the cutoff wall installation, the downard movement of the freshwater imposed by the cutoff wall was partly inhibited by the underlying low K layer, causing a substantial decrease of the magnitude of the flow velocity through the wall opening.

While the saltwater intrusion process is primarily controlled by the freshwater flow through the aquifer (Chang and Clement, 2012; Ketabchi et al., 2016), the results demonstrate that the presence of the layers of various permeability substantially disrupt the natural flow dynamics, thereby strongly affecting the response of the saltwater wedge to various degrees, depending on the layer stratification pattern. Specifically, the presence of layers of relatively low permeability induce the "channelling" of freshwater flow preferably towards the higher permeability layers, which affect both horizontal and vertical extension of the saltwater wedge and the associated distortion of the freshwater-saltwater interface.

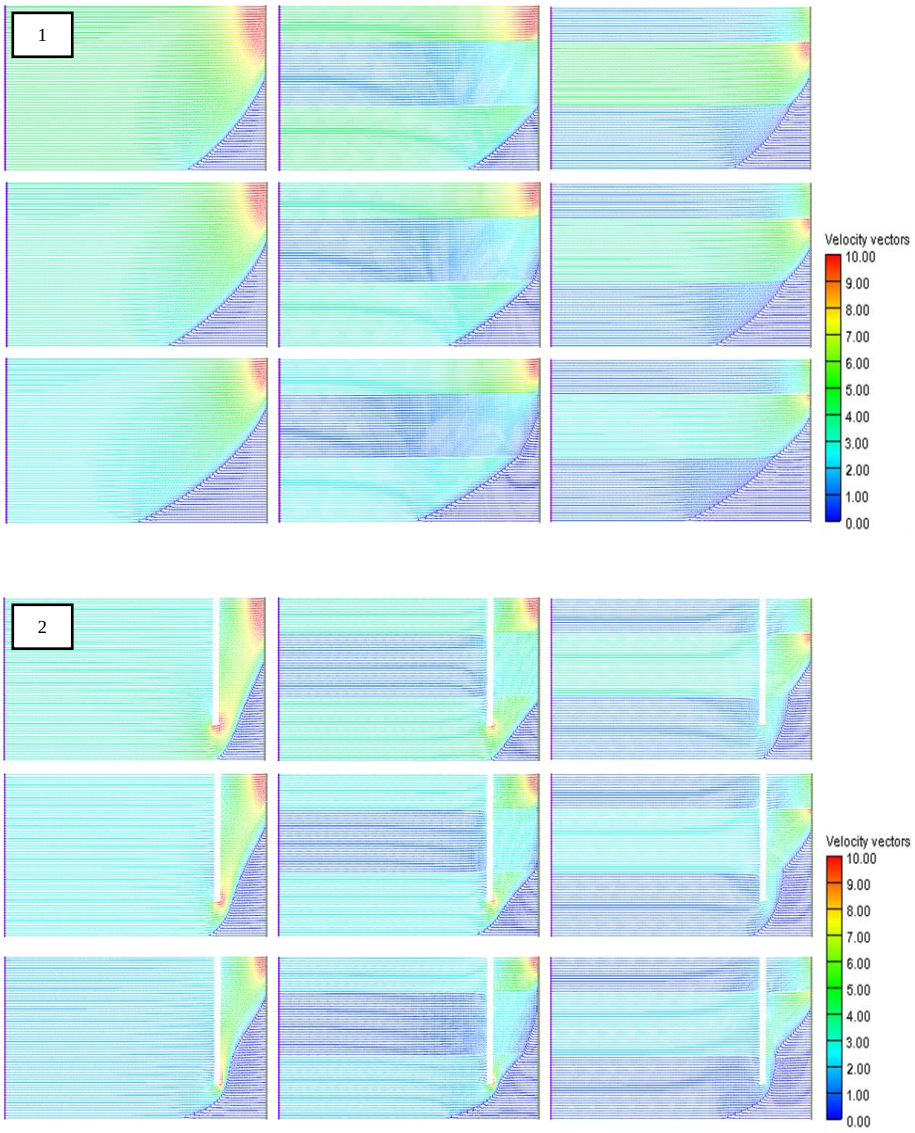

Figure 5.4 Flow velocity field in 1) the base and 2) cutoff wall cases; (left) case H; (middle) case HLH and (right) case LHL. From top to bottom, dh = 6 mm, 5.2 mm and 4.4 mm. The velocity vectors are in cm/min.

Two additional layering setting were investigated to gain more insights on how the soil stratification dissrupts the flow dynamics in heterogenous aquifers before and after wall installation. Fig 5.5 shows the flow velocity field of two additional layer settings, one with an monotonically increasing hydraulic conductivity from top to bottom referred to as case I and the other with monotonically decreasing hydraulic conductivity referred to as case D. The highest and lowest hydraulic conductivity values in case I and case D corresponded to those

of the previous cases (108 cm/min and 36 cm/min), and the middle layer was set to 85 cm/min (corresponding to the hydraulic conductivity of other beads size used in our lab). Therefore, the hydraulic condictivity values were 36-85-108 cm/min 108-85-36 cm/min in case I and case D respectively.

In case I, the overlying layer of low K, again, forced the freshwater flow in the lower part of the aquifer facing the saltwater wedge before it exited the system on the top corner of the middle layer, at high velocity. The magnitude of the flow velocity vectors at the tip of wall was significantly relatively higher in this case. By contrast, in case D the presence of the underlying low K layer redistributed the flow mainly in the upper part of the system, especially in the top layer where it was the highest, through which most of the freshwater rapidly exited the system without affecting substantially the wedge, which explains the faster horizontal and vertical intrusion of the saltwater wedge, compared to the preceding scenario. The magnitude of the flow velocity vectors at the tip of wall was significantly smaller in this case, allowing more building up of the saline plume on the seaward side of the wall. Nonetheless, the results demonstrate that the length of the saltwater wedge was also noticeably reduced by the cutoff in these extra heterogeneous settings, for all the hydraulic gradient considered.

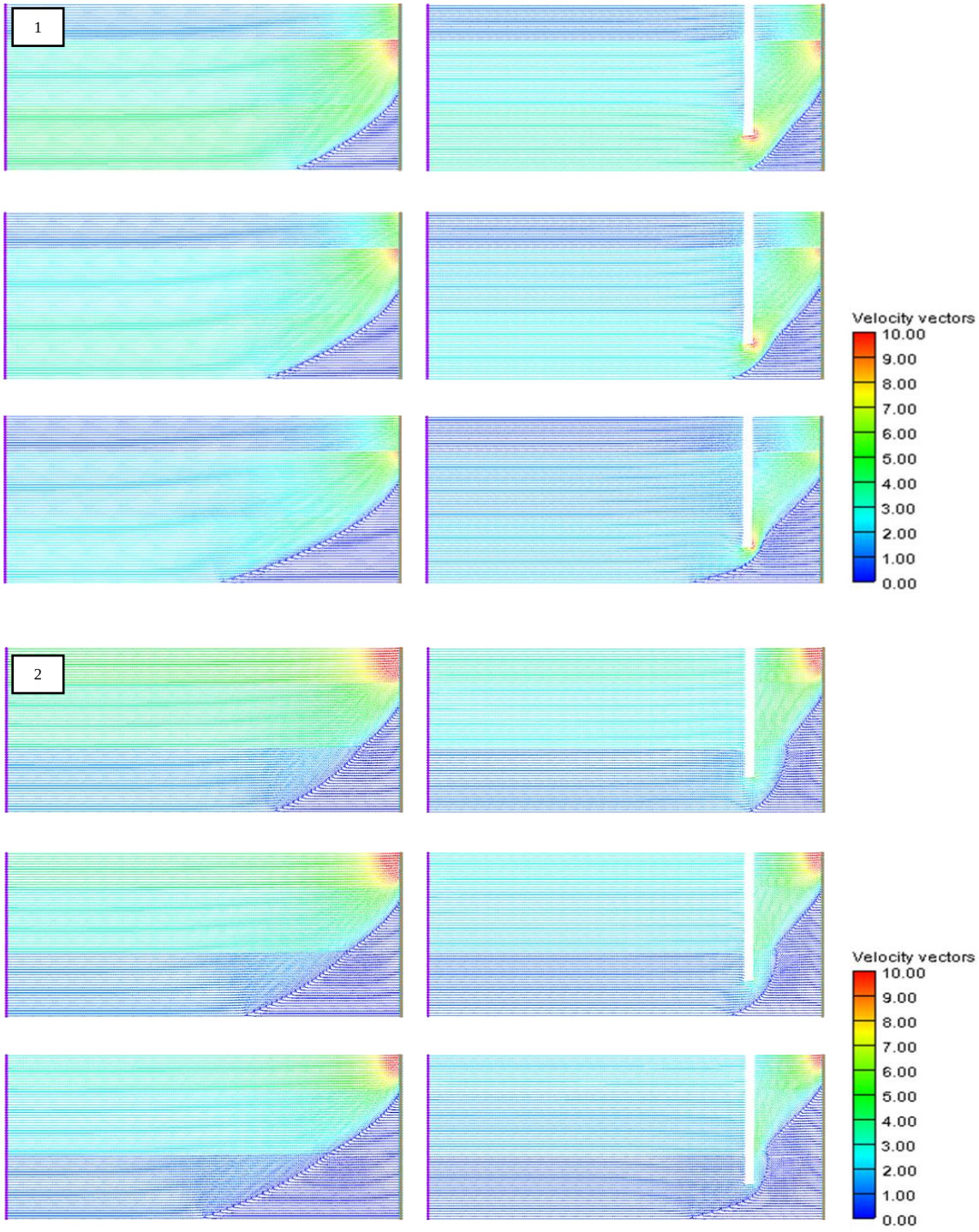

Figure 5.5 Flow velocity field in the additional cases; 1) case I; 2) case D; (left) base cases, (right) cutoff case. From top to bottom, dh=6mm, 5.2mm and 4.4mm. The velocity vectors are in cm/min.

5.3.4 Sensitivity analysis

Additional simulations were then performed to examine the influence of various relevant parameters on the effect of cutoff walls in stratified coastal aquifers. The stratified case HLH was considered in this section, considering the cutoff wall relatively less effective in case LHL, in light of the above an results. Also, the simulation was solely performed for dh = 4.4 mm which produced the extreme SWI scenario considered in this study. The parameters assessed in this section include the properties of the middle low K layer, the wall design parameters and the saltwater density.

Sensitivity to wall location and opening size

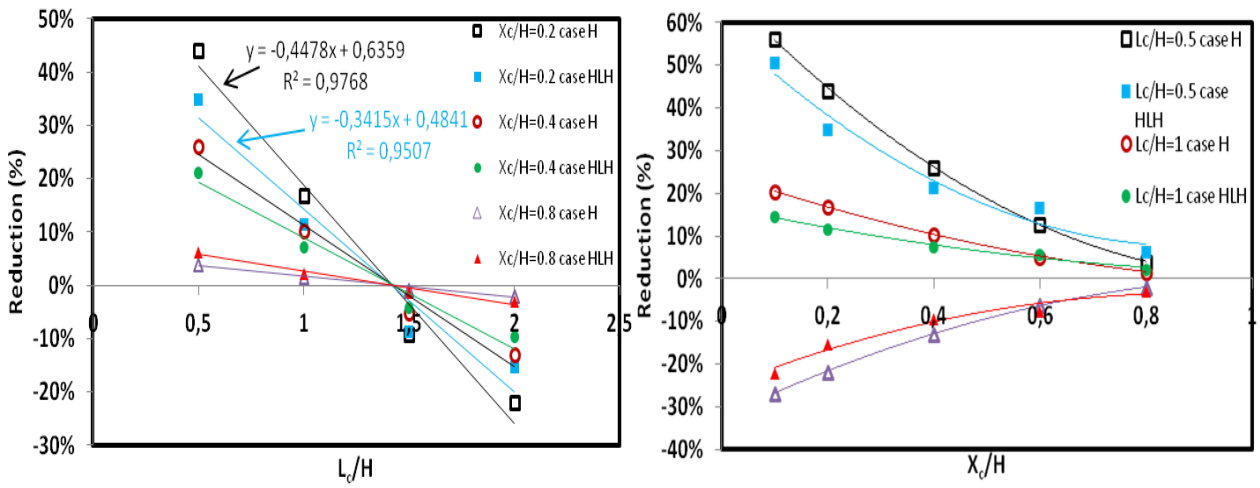

Figure 5.6 Sensitivity of the reduction to the wall location (left) and to the wall opening size (right).

The effect of the geometrical design parameters of the wall, namely the wall location and depth, on the effectiveness of cutoff wall was first investigated. The location of the wall was characterised by the dimensionless ratio L_c/H, where L_c is the distance between the wall and the coastline and H is the saturated aquifer thickness. The location of the wall was investigated for four different ratios L_c/H = 0.5, 1, 1.5 and 2. These values are within the typical range of dimensionless distance for cutoff wall installation in practical applications (Japan Green Resources Agency, 2004).

The reduction achieved by the cutoff wall increases with decreasing the distance from the coastline, with lower rate of increase in the presence of the low K layer (Fig 5.6). The simulation was performed for three different wall opening sizes, namely X_c/H = 0.2, 0.4, 0.8, where the tip of the wall was located below, within and above the low K layer, respectively. For $L_c/H<1.4$, the reduction values were smaller in the heterogeneous scenario, indicating that the effectiveness of the cutoff wall was lower under the presence of the low K layer than in the homogeneous scenario, for equivalent wall location. This is because without the cutoff wall, the low K layer causes the original length and thickness of the wedge to decrease. Thus, the saltwater wedge is less squeezed by the cutoff wall in the presence of the low K layer. As the opening becomes wider, the squeezing effect applied by the wall weakens gradually and the effect of the low K layer becomes smaller.

For $L_c/H>1.4$, the reduction became negative since at such distance, the cutoff wall was located outside the original area of the saltwater wedge. In such situation, the cutoff wall essentially prevents the freshwater from repulsing the saltwater wedge (Luyun et al, 2011). Hence, given that the reduction is higher in case HLH, the results implies that that this adverse effect was reduced under the presence of the low K layer. The results show that in both scenarios, a simple linear relationship of type $R = -a(L_c/H) + b$ could be derived, where a and b are the regression coefficients (see equation for X_c/H=0.2 in figure, where a, and b are

inherent to the present system). The strong linearity of the correlation is manifested by the high coefficient of determination R^2 exhibited in all cases. While Luyun et al. (2011) presented similar conclusion for homogeneous systems, the present results extend the applicability of their findings to cases where a low K layer is incorporated into an aquifer system.

The depth of the wall was expressed as a function of the opening ratio X_c/H, where X_c is the wall opening size. The influence of the depth of the wall was investigated for various opening ratios X_c/H in the range 0.1-0.8. Fig 5.6 shows that the effectiveness of the cutoff wall increased with decreasing the ratio X_c/H in both homogeneous and heterogeneous scenarios. For relatively small opening sizes ($X_c/H \leq 0.4$), the reduction achieved by the cutoff wall was lower in case HLH relative to the homogeneous scenario, for an equivalent opening size. For wider opening sizes ($X_c/H > 0.6$), this difference was reversed ($L_c/H = 0.5$, 1) or became negligible.

When the wall was located farther away from the coastline boundary ($L_c/H=2$), its effectiveness increased with increasing the ratio X_c/H, since at such distance, the cutoff wall obstructs the path of the freshwater flow as noted above, thus a wider opening would allow a greater freshwater discharge, and hence more reduction. In such conditions, the seaward discharge in the lower part of the aquifer is further enhanced under the influence of the low K layer, which explains higher reduction values found in case HLH, for equivalent opening size. Installing the wall at such distance from the coastline is nonetheless not recommended in any case as it leads to negative effect considering the increase of the toe length compared to the case with no wall in place. It is interesting to note that the reduction increased following a polynomial trend in the layered configuration. A similar observation was derived by Luyun et al. (2011) in their homogeneous isotropic setting. For relatively small wall

opening ($X_c/H<0.4$), any slight increase of X_c/H led to significant drop in the toe length reduction.

Sensitivity to the hydraulic conductivity contrast ratio and middle layer thickness

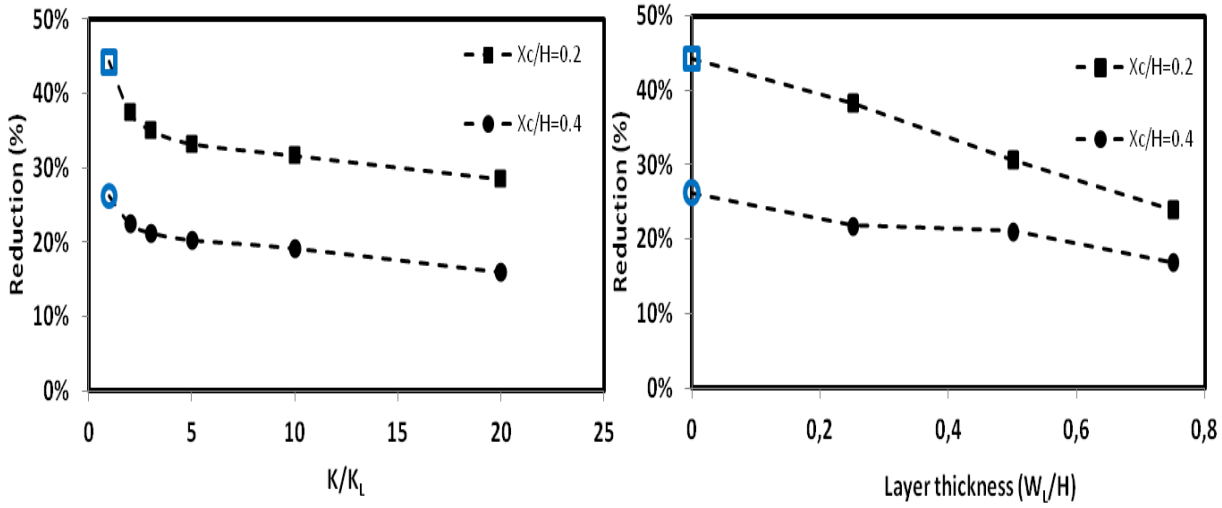

Figure 5.7 Sensitivity of the reduction to the hydraulic conductivity contrast ratio (left) and to the thickness of the middle layer (right)

The influence of the low K layer was characterised by (1) the hydraulic conductivity contrast between layers and (2) the thickness of the low K layer. The former was characterized by the ratio K/K_L, where K is the hydraulic conductivity of the aquifer (108 cm/min) and K_L represents the hydraulic conductivity of the low K layer, while the latter was characterised by the ratio W_L/H, where W_L is the thickness of the low K layer. The location of the wall was fixed at $L_c/H=0.5$, where the cutoff wall was found to exhibit the most reduction.

The influence of the dimensionless ratio K/K_L was explored over the range 1-20. In general, the reduction achieved by the cutoff wall decreased with increasing the ratio K/K_L (Fig 5.7). The blue points represent the reduction achieved by the cutoff wall for $K/K_L/ = 1$, i.e the homogeneous case. For $X_c/H = 0.2$, the reduction dropped from 44% for contrast ratio

K/K_L = 1 to 28% for K/K_L = 20, and for X_c/H = 0.4, the reductions dropped from 26% to16%, as K/K_L moved up from 1 to 20, respectively. In other words, the net decrement of R associated with the increment of K/K_L from 1 to 20 was 16% and 10%, for an opening ratio of 0.2 and 0.4, respectively.

In such configuration, the change in the effectiveness of the cutoff wall associated with the increment of the ratio K/K_L (or the decrement of K_L) is attributed to two opposed processes. The first one is the redistribution of the freshwater flow in the lower and upper parts of the aquifer because of the middle low K layer, leading to more repulsion of the saltwater wedge prior to wall installation. This first process results in an increase in the flow velocity at the opening of the wall and thus is expected to enhance the wall effectiveness. It is interesting to note that this process resulted in the total obstruction of the upper part of the seawater wedge below the middle layer for high ratios K/K_L, which resulted in a small intrusion in the upper part of the aquifer (Fig 5.8).

The second factor is the inhibition of the downward freshwater flow from the upper part to the lower part of the aquifer by the middle layer due to its lower K. This second factor will tend to reduce the performance of the cutoff wall. The decreasing trend of the reduction values observed here suggests that that the second process appears to have more influence on the overall performance of the cutoff wall relative to the first in such configurations.

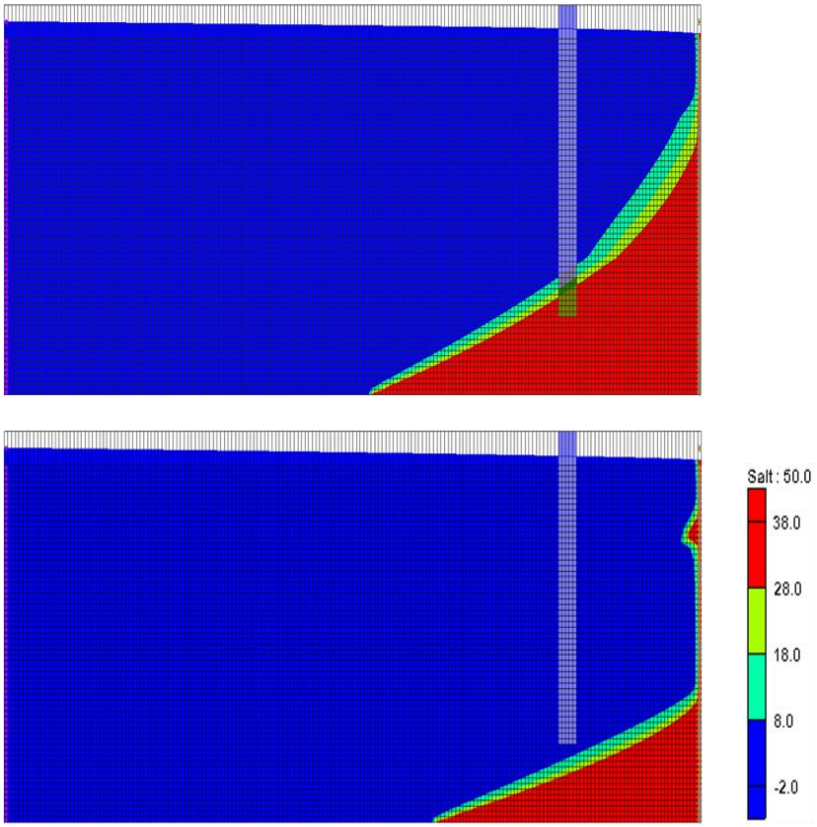

Figure 5.8 Saltwater wedge prior to wall installation; (top) K/K_L= 2; (bottom) K/K_L= 20. The dark cells indicate the desired position of the wall before construction

The influence of the low K layer thickness was examined for three values of W_L/H, namely 0.25, 0.5 and 0.75. Fig 5.7 shows that increasing the thickness of the low K layer reduced the effectiveness of the cutoff wall. The blue points represent the reduction achieved by the cutoff wall for $W_L/H = 0$, i.e. no middle low K layer (homogeneous aquifer). For $X_c/H = 0.2$, the percentage reduction went down from 44% for the homogeneous case to 24% for $W_L/H = 0.75$. The reduction decreases with W_L/H in a nearly linear trend. Fig 5.9 shows that prior to wall installation, the increase of the middle layer thickness induced not only the seaward retreat of the interface, but also a more elongated transition zone widening over the length of the interface, which agrees with results of Lu et al. (2013).

The tip of the wall penetrated into the wedge for $W_L/H = 0.25$, while it was located into the dispersive zone for $W_L/H = 0.75$, yielding a reduction in the wall effectiveness to halt

the saltwater wedge. For $X_c/H = 0.4$, the maximum and minimum values were 22% and 17%, corresponding to a ratio W_L/H of 0.25 and 0.75, respectively. The further decrement of the wall reduction as the low K layer thickness becomes greater may be because it becomes more difficult for the downward movement of the freshwater and hence the effect of the cutoff wall subsequently weakens.

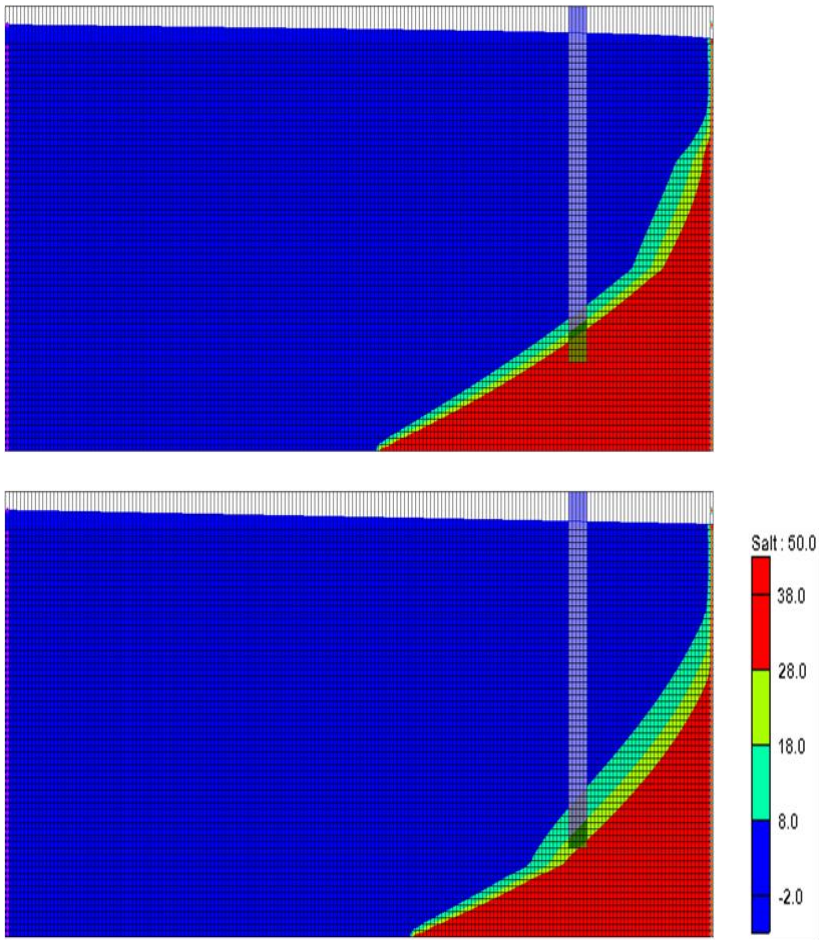

Figure 5.9 Saltwater wedge prior wall installation; (top) W_L/H of 0.25; (bottom) W_L/H of 0.75. The dark cells indicate the desired position of the wall before construction

Sensitivity to saltwater density

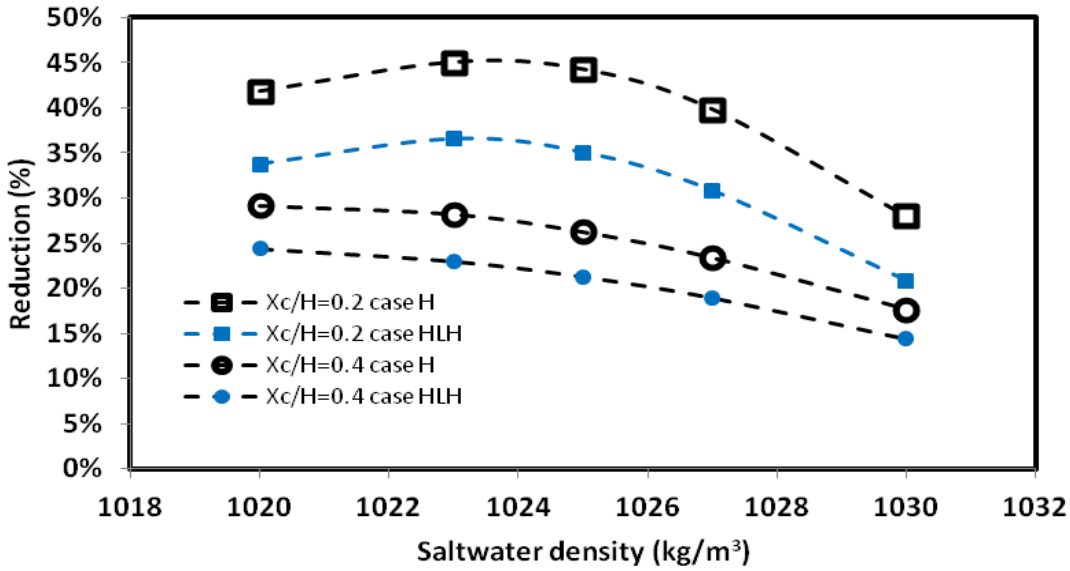

Figure 5.10 Sensitivity of the reduction to the saltwater density

The influence of the saltwater density was then finally investigated for a typical range of seawater density. The influence of the saltwater density was investigated for a typical range of seawater density ρ of 1020-1030 kg/m^3. In overall, the performance of the cutoff wall in reducing the saltwater intrusion length decreased with increasing saltwater density (Fig 5.10). In all the simulations, the location of the wall was fixed at L_c/H = 0.5 from the saltwater boundary, for the opening ratios X_c/H = 0.2 and 0.4 only.

For the homogeneous case with opening ratio X_c/H = 0.2, the reduction achieved by the cutoff wall ranged from 42% for seawater density of 1020 kg/m^3 down to 28%, for seawater density of 1030 kg/m^3. For the layered case, the reduction ranged from 34% to 21%, as the density went up from 1020 to 1030 kg/m^3 respectively. For opening ratio X_c/H = 0.4, the cutoff wall achieved a reduction of 29% and 18%, in case H; and 24% and 14%, in case HLH, as the density increased from 1020 to 1030 kg/m^3, respectively. The presence of the

low K layer caused a deviation of the interface, thus partly weakening the effect of the wall on reducing the toe length of the wedge.

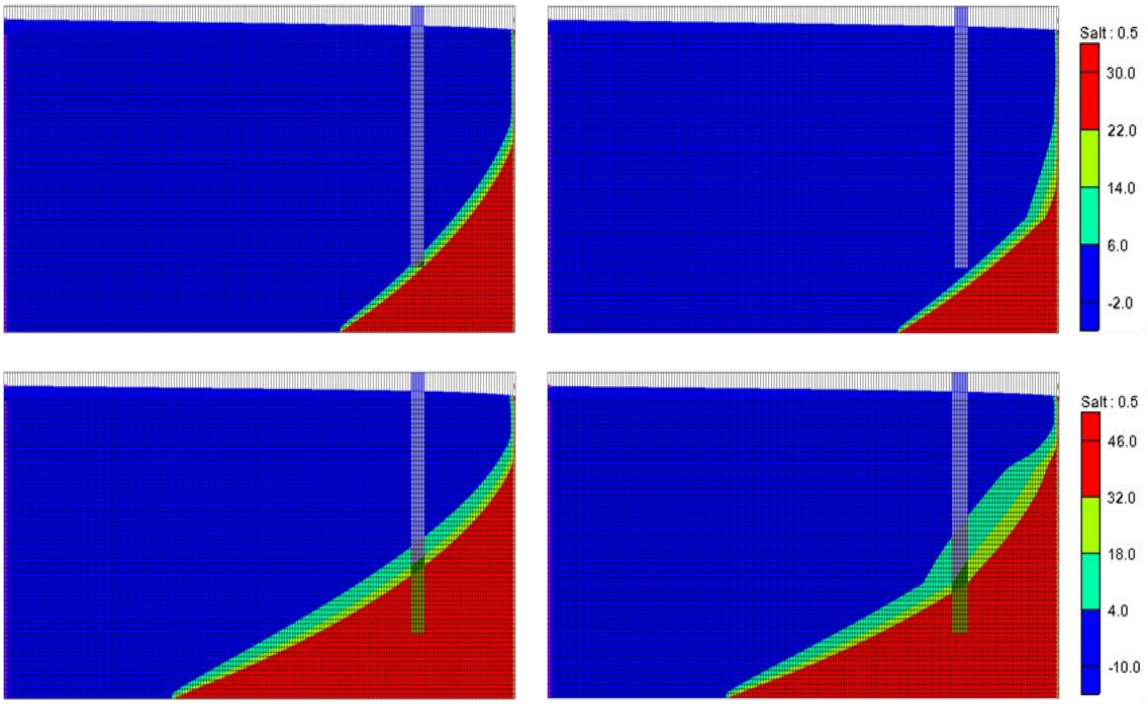

Figure 5.11 Saltwater wedge prior installation of the wall; (top) ρ =1020Kg/m^3; (bottom) ρ =1030Kg/m^3, (left) case H and (right) case HLH. The dark cells indicate the desired position of the wall before construction

Note that for X_c/H = 0.2, the reduction reached maximum values for average density values (1023-1025 kg/m^3) due to the compression effect exerted by the cutoff wall on the saltwater wedge that is stronger than for lower density values, where the extent and thickness of the saltwater wedge are relatively smaller. In any case, as the density further increases (>1023 kg/m^3), the saltwater of very high concentration invades the spacing between the wall and the coastline. Hence, this high density drives the incursion of the saline water by buoyancy forces through the wall opening and the extension of the wedge on the landward side of the wall (Fig 5.11), subsequently resulting in a loss of the cutoff wall effectiveness.

5.4 Summary and conclusions

In this work, we used laboratory experiments and numerical simulations to investigate the effectiveness of cutoff walls in heterogeneous coastal aquifers. Three different aquifer configurations were investigated, including a homogeneous, a stratified aquifer with high K–low K–high K pattern (HLH) and another stratified aquifer with low K–high K–low K pattern (LHL). The transient intrusion toe length data derived experimentally were relatively well predicted by the SEAWAT code.

The results demonstrated that the cutoff wall was effective in reducing the saline water intrusion length in all the stratified scenarios investigated here, for all hydraulic gradients considered. The stratification imposed a disruption of the flow dynamics, and thus affected the freshwater velocity at the wall opening, thereby altering the performance of the cutoff wall to various degrees, depending on the layering pattern considered. The presence of an underlying low permeability layer (case LHL) was found to obstruct the freshwater flow in the lower part of the aquifer, which caused a local reduction of the flow velocity at the wall opening, thereby decreasing the repulsion ability of the cutoff wall.

The interlayer of lower permeability exhibited in case HLH was found to affect the downward movement of the freshwater usually associated with the installation of cutoff calls. This resulted in lowering the flow velocity at the wall opening relative to the homogeneous scenario, and thus reducing the repulsion force facing the saltwater. Sensitivity analysis performed in such setting revealed that the cutoff wall was nonetheless able to achieve good reduction of the saline water despite the presence of the low K layer, especially for smaller opening size and shorter distance between the wall and the coastline. In such configurations, the effectiveness of the wall was found to decrease noticeably with decreasing the hydraulic conductivity and increasing thickness of the middle layer as well as the saltwater density.

Albeit the stratification patterns found in real field applications may be more complex than the rather simplified and idealised approached adopted herein, our study provides nonetheless for the first time a valuable first-hand insight on the expected impact of layering heterogeneity on the performance of cutoff walls to control SWI. Given that most of the real field sites exhibit prevalently layering stratification patterns, our results emphasizes therefore the necessity to consider ground variability prior to planning and designing of cutoff walls for saltwater intrusion control purposes, for a more realistic assessment of their performance.

Chapter 6

The impact of layered heterogeneity on the ability of subsurface dams to resist SWI and clean up SWI-contaminated coastal aquifers

This chapter presents an analysis on the impact of layered heterogeneity on the performance of subsurface dams in controlling SWI. The results presented in Luyun et al., (2009) greatly contributed towards improving the understanding on the impact of subsurface dams on the flow dynamics and the intrusion process. Their study not only considered only homogeneous conditions, but the investigation was therein restricted to the analysis on the saltwater removal process This third chapter explores the impact of typical layered heterogeneity on the ability of subsurface dams to retain saltwater spillage and to clean up the landward freshwater zone from residual saline water. This study provides for the first time a quantitative and qualitative analysis of the spillage and clean-up of saline water over the subsurface dam, which has not been captured in previous studies.

6.1 Experimental procedure

In total, two sets of four experiments were completed (Fig 6.1), which included one set of base cases (without barrier) and another set incorporating a subsurface dam. The four base cases included a homogeneous case with relatively high permeability (K), designated hereafter as case H, and three different layered cases where a low K layer was set at three different locations: case Low K-High K (LH) presented a scenario where a low K layer was set in the top part of the aquifer; case High K-Low K-High K (HLH) referred to the case where a low K layer was located in the middle part of the aquifer; and case High K-Low K (HL) presented a scenario where a low K layer was set along the aquifer bottom. In all the cases, the thickness of the low K layer was about one third of the total saturated thickness of the homogeneous. The nominal diameter of the glass beads used to simulate the porous media and the low K layer was 1325 μm and 780 μm, respectively.

The second set of experiments included a subsurface dam installed prior to siphoning of the beads into the tank. The subsurface dam was simulated using 12 mm wide PVC material covering the thickness of the tank. The dam was located at 50 mm from the seaside boundary, and has a height of 66 mm from the bottom boundary of the tank. The effect of the subsurface dam was examined within each of the four different aquifer settings, similar to the base cases.

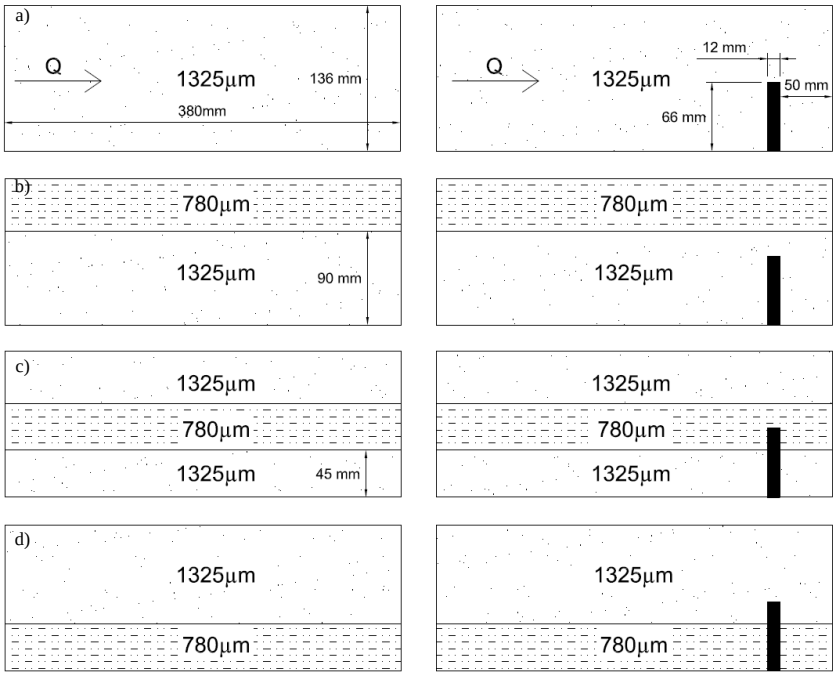

Figure 6.1 Schematic design of the investigated cases; the base cases (left) and after subsurface dam installation (right): a) case H; b) case LH; c) case HLH and d) case HL.

In total, 48 experimental cases were carried out in this investigation. These includes 20 different experiments (four physical experiments x five different hydraulic gradients) for the base cases where the saltwater wedge was analysed in advancing and receding conditions; and 28 different experiments (four physical experiments x seven different hydraulic gradients) for the subsurface dam cases, where the ability of subsurface dams to retain SWI

and clean up aquifers from previously intruded saline water was assessed in the various aquifer settings.

The various hydraulic gradients were simulated by varying the freshwater level such that various head differences were successively imposed to the system. In all the investigated cases, the initial condition was set by forcing a head of 135.7 mm at the freshwater boundary to impose a first head difference dh = 6 mm to the system, corresponding to a hydraulic gradient of 0.0158. The dense saltwater solution was allowed to intrude into a fully freshwater aquifer, until the system reached the first steady state condition.

In the base cases, three head differences were applied thereafter, including dh = 5.2 mm, dh = 4.4 mm, dh = 3.6 mm, corresponding to hydraulic gradients of 0.0137, 0.0116 and 0.0095, respectively. The final head difference was eventually reset to the initial value dh = 6 mm to allow the analysis of the seaward motion of the saltwater.

In the subsurface dam cases, two additional head differences were imposed to the system, specifically dh = 2.8 mm and dh = 2 mm, corresponding to a hydraulic gradient of 0.0074 and 0.0053, respectively, before returning the head to dh = 6 mm. The application of these additional head difference was primarily to ensure the spillage of the saline water over the wall, which is primordial in this investigation. The highest and lowest head differences applied to the system dh = 6 mm and dh = 2 mm corresponded to hydraulic gradient values of 0.0158 and 0.0053, respectively.

The investigation of the effect of the subsurface dam on saltwater intrusion dynamics was subdivided into two mains phases, namely the advancing-wedge and the receding-wedge phases. The advancing-wedge phase included the period prior to spillage where saltwater builds up in the seaward side of the wall, and the period post-spillage where saline water overflowed the crest of the subsurface dam and penetrated into the freshwater zone. The

receding-wedge phase related to the removal of the residual saline water from the freshwater zone, after restoration of the initial freshwater head boundary condition.

The effectiveness of subsurface dams was characterized by two different criterions, depending on the phase analysed. The first criterion, used in the advancing-wedge phase, was the ability to restrict the SWI mechanism, which was identified differently depending on the location of the saltwater wedge toe on either side of the wall. When located on the seaward side of the wall (prior to spillage), the percentage reduction of the saltwater wedge length R was used, where $R = (X_0 - X_d)/X_0$, with X_0 and X_d are the intrusion length before and after the dam installation.

When the toe was located on the landward side of the wall, the ability to restrict SWI was identified by T_{spil} and T_{crit}, corresponding respectively to the time taken for the saline water to start spilling over the wall and the time taken to reach the critical point X_{crit}, which was arbitrarily located at 90% of the total aquifer length from the seaside, at which the freshwater was considered completely contaminated. In the current system, the critical point X_{crit} was located at 34 cm from the coastline. For the sake of convenience, the time of spillage T_{spil} was defined as the time at which the overflowing saline water reached the aquifer bottom in the landward side of the dam.

The second criterion used to characterise the performance of subsurface dams was the ability to completely flush out residual saline water in the seaward side of the wall during the receding-wedge phase. It was characterized by the time required for the freshwater zone to be completely cleaned up T_{flush}.

6.2 Numerical procedure

As per usual practice, the first stress period was used to set the first steady state condition, whereby the freshwater and saltwater boundary were set at 135.7 mm and 129.7

mm, respectively, allowing penetration of saline water into a fully fresh model domain. In the next three stress periods, the freshwater head was dropped such that to successively impose the head differences dh = 5.2 mm and 4.4 mm, 3.6 mm to the system. The last stress period was dedicated for the retreat of the saltwater water wedge, following the rise of the head difference to its initial value (dh = 6 mm).

The SEAWAT models were then used to perform numerical simulations incorporating the subsurface dam. The later was simulated by rendering the cells occupied by the wall as inactive. Two extra stress periods were added (dh = 2.8 mm and dh = 2 mm) in the subsurface dam simulation to reproduce the spillage after the head difference was set to dh = 3.6 mm. The models were then used again to perform the numerical simulations of the receding phase of the saline water in presence of the subsurface dam. The initial condition of the receding phase corresponded to the final wedge for dh = 2 mm. A single stress period was thereafter used to initiate the saline water flushing process, following the rise of the inland freshwater head boundary to 135.7 mm to reset the initial head difference dh = 6 mm.

6.3 Results and discussion

6.3.1 Base cases

The assessment of the effectiveness of the subsurface dam and the understanding of the flow dynamics imposed by each layering pattern required first the analysis of saltwater intrusion dynamics in each aquifer setting, with no barrier. Fig 6.2 presents the concentration colour map of the base cases at the initial condition, i.e. after the application of the initial head difference dh = 6 mm. This first head change disrupted the equilibrium of the system and allowed the penetration of the saline water into the porous medium, forming an idealized wedge-like shape of the plume in homogeneous conditions, while slightly distorted in the heterogeneous cases HL and HLH, where the freshwater-saltwater interface crossed the

boundary between two layers of contrasted permeability (Abdoulhalik and Ahmed, 2017). Such distortion of the wedge does not however occur in case LH, as the wedge penetrated "freely" into the high permeability zone, which accounts for about two thirds of the aquifer height.

The further decrement of the head difference down to dh = 3.6 mm induced a reduction in the freshwater flux transmitted to the system and thus allowing deeper inland encroachment of the saltwater wedge. The toe length data of all the investigated cases are presented in table 6.1. The subsequent increase of the freshwater flow after resetting the initial head difference to dh = 6 mm forced the retreat of the saltwater toward the coastline boundary (Fig 6.3). The toe reached the same position as in the initial condition in all cases, which indicates that no hysteresis occurred in the system.

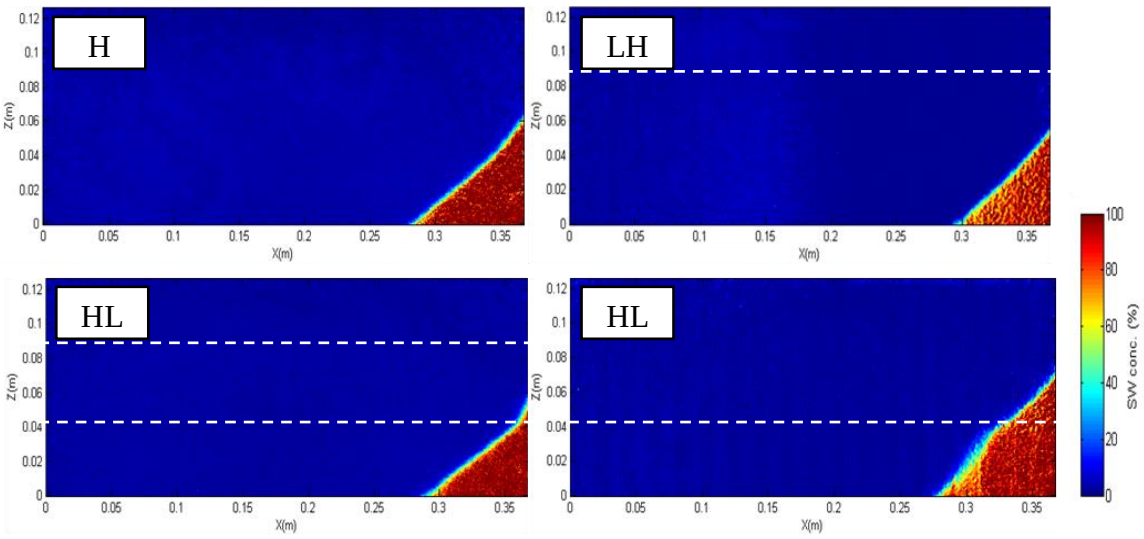

Figure 6.2 Concentration colour map of the experimental toe length at steady state after setting dh = 6 mm (t = 0 min) in the base case. The dashed lines represent the approximate location of the layer boundaries

Table 6.1 Experimental toe length values (cm)

Head difference	Case H	Case LH	Case HLH	Case HL
dh = 6 mm	8.4	6.6	7.4	8.6
dh = 5.2 mm	11.7	9.2	11.2	11.1
dh = 4.4 mm	17.2	13.5	16.3	16.7
dh = 3.6 mm	25.5	20.8	25.0	22.9

The data show that the shortest saltwater intrusion toe length was exhibited in case LH for all the inland head differences applied. In such configuration, the existence of the low K on the top of the aquifer forced part of the freshwater flow into the bottom layer that has greater hydraulic conductivity, i.e. directly facing the saltwater wedge, thereby obstructing its inland penetration. In other words, the freshwater flow is increased in the lower part of the aquifer, which leads to a greater repulsion of the saltwater wedge back towards the coast. This result is in agreement with the steady state analysis presented by Strack et al. (2016), where similar configuration was examined. The transient data provided in Fig 6.3 shows that the receding toe motion in this setting was noticeably faster compared to the homogeneous scenario, which indicate higher freshwater flow velocity, thus promoting faster repulsion of the saline wedge.

The toe length was also shorter in case HLH relative to the homogeneous case, albeit the difference was less obvious here. The low K layer in the middle portion of the aquifer is expected to force the freshwater to flow on the top and bottom parts of the aquifer. While the freshwater flowing in the top high K layer exits the system without substantial contribution in the saltwater wedge repulsion, the flow in the bottom layer of high K has greater impact to push the wedge in the seaward direction resulting in shorter wedge compared to the

homogeneous scenario. This observation is analogous to that reported in Abdoulhalik and Ahmed (2017) and Lu et al. (2013) where saltwater intrusion mechanism in such typical heterogeneous aquifer setting was also analysed.

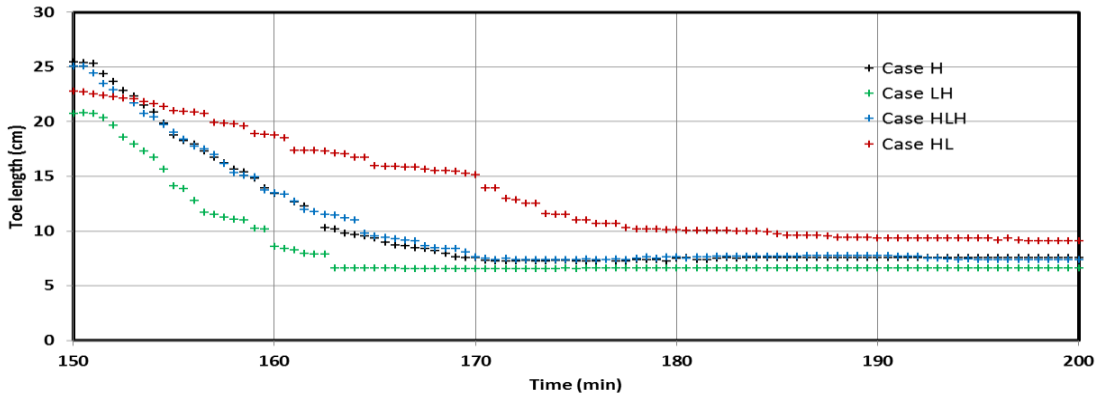

Figure 6.3 Experimental transient toe length data during saltwater retreat

The larger toe length values recorded in case HL compared to those observed in case LH are consistent with Strack et al. (2015) where the saltwater intrusion length in their dual-layered aquifer with underlying low K layer was up to twice longer than the opposite scenario. The transient data shows that the toe motion exhibited in this setting is considerably slower compared to the other cases. While the saltwater intrusion process was mainly controlled by the freshwater flow transmitted through the system (Chang and Clement, 2012), the freshwater flow transiting in the lower part of the aquifer was considerably slowed through the underlying low K layer, which resulted in inhibiting the effective seaward repulsion of the saline water. The subsequent increase of the flow velocity in the upper part of the aquifer is little involved in the repulsion effort, but rather directly exits at the outlet.

The comparison between the experimental and numerical toe length results of the base cases are shown in Fig 6.4. The transient experimental toe length data were very well predicted by the SEAWAT model in all the cases. The values of the maximum percentage

difference were: 1% 9% 13% and 22% in case H; 11%, 2%, 2% and 19% in case LH; 5% 11% 15% and 9% in case HLH; and 18%, 1%, 3% and 15% in case HL; for the head difference dh = 5.2 mm, 4.4 mm, 3.6 mm and 6 mm, respectively. The largest toe length was however observed in case HL compared to the other numerical cases. This may be because in the experiment, case HL had not reached complete steady-state condition, as the penetration of the wedge was very slow through the underlying low K layer. The numerical results nonetheless show that the minimum intrusion length was occurred in case LH, in agreement with the experimental observations. The resulting models were then used to simulate the subsequent subsurface dam experiments for each respective aquifer setting, as shown below.

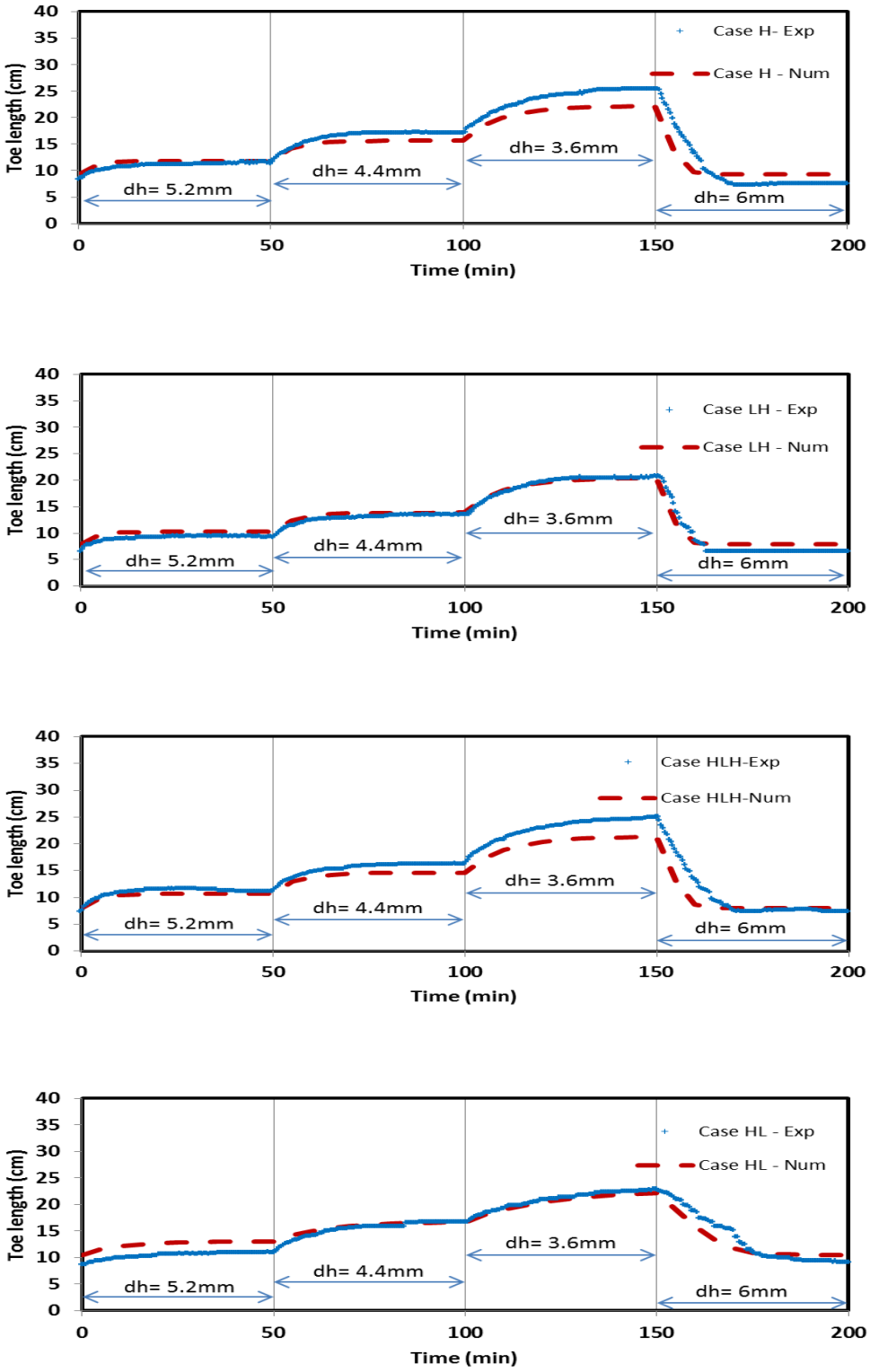

Figure 6.4 Comparison of the transient experimental and numerical toe length results of the base cases

6.3.2 Subsurface dam cases

Advancing-wedge phase

Fig 6.5 shows the concentration colour maps of the subsurface dam experiments at the initial conditions, i.e after applying dh = 6 mm. In all the investigated cases, the subsurface dam was able to retain the intrusion of saline water for all the head differences applied to the base cases, i.e. up to dh = 3.6 mm, which means that the subsurface dam could withstand the saltwater intrusion process associated with a decrement of the gradient from 0.0158 down to 0.0095. This was expected because the height of the saltwater wedge in the base cases at the location of the wall was slightly smaller than the height of the subsurface dam (Luyun et al., 2009; Abdoulhalik et al., 2017). The values of the percentage reduction of intrusion length R achieved by the subsurface dam are presented in table 6.2. The lowest values of reduction are recorded in case LH for all the head differences tested. This is because the difference $X_0 - X_d$ is the smallest in case LH, given that it exhibited the smallest toe length values prior to wall installation, while X_d is limited by the location of the subsurface dam in all the cases.

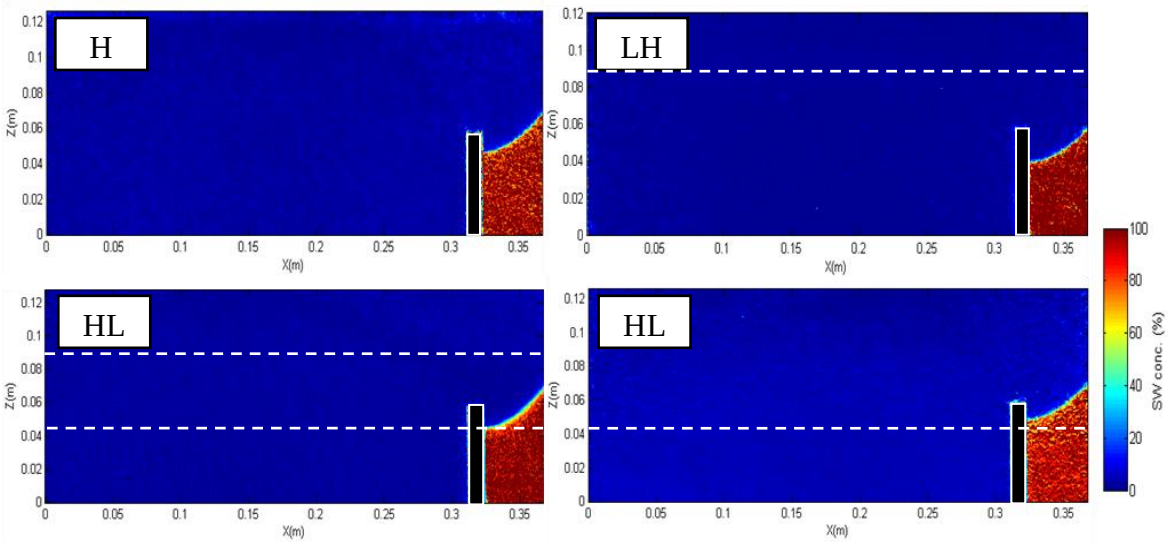

Figure 6.5 Concentration colour map of the experimental saltwater wedge at the steady state in the subsurface dam case after setting dh = 6 mm.

Table 6.2 Percentage reduction R of saltwater intrusion length achieved by the subsurface dam

Head difference dh (mm)	Case H	Case LH	Case HLH	Case HL
dh = 6 mm	41%	25%	33%	42%
dh = 5.2 mm	57%	46%	55%	55%
dh = 4.4 mm	71%	63%	69%	70%
dh = 3.6 mm	80%	76%	80%	78%

In order to observe the spillage of saline water over the wall, the head difference was thereafter gradually decreased by maintaining a step head difference decrement of 0.8 mm. The initial condition of this experiment (t = 0 min) corresponded to the steady state saltwater wedge under dh = 3.6 mm. The spillage process was first observed following the application of dh = 2.8 mm in case HL (Fig 6.6), while an additional inland head drop (dh = 2 mm) was needed in cases H, LH and HLH (Fig 6.7). In other words, the spillage of saline water occurred following the application of a hydraulic gradient 0.0074 in case HL, and 0.0053 in the other cases.

In case HL, the spillage occurred 12 min following the application of dh = 2.8 mm, and it took nearly 100 min for the saltwater length to extend up to 21.6 cm from the sea boundary (or 15.4 cm from the left edge of the wall) where it became quasi steady. A significant widening of the transition zone occurred during the spillage in all cases, due to the excessive dispersion and diffusion occurring along the freshwater-saltwater interface. The further decrement of the head difference to dh = 2 mm prompted the saline water to extend up to the critical point X_{crit} within 29 min. This observation shows that the ability of the subsurface dam to retain the saltwater intrusion process was significantly weakened in presence of the low permeability at the bottom part of the aquifer.

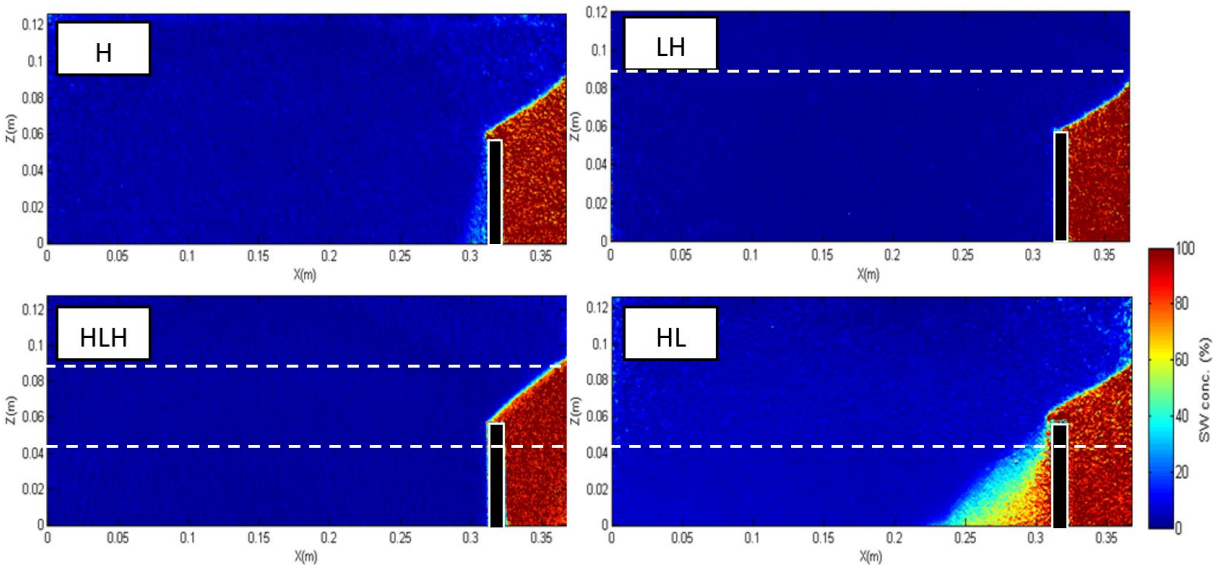

Figure 6.6 Concentration colour map of the experimental saltwater wedge at steady state in the subsurface dam case at = 50 min after decreasing the head difference from dh = 3.6 mm to dh = 2.8 mm

After decreasing the head difference from dh = 2.8 mm to dh = 2mm, Fig 6.7 shows that, at first glance, the inland progression of the saltwater wedge was inhibited in presence of a low K layer in the middle (case HLH) and top part of the aquifer (LH). The spillage process also exhibited different pattern depending on the layer arrangement. In case LH, the saline water almost dripped into the landward side of the wall with an interface exhibiting a slightly curved shape compared to the homogeneous case. In cases LH and HLH, the transition zone was noticeably wider than the homogeneous case with the case HLH exhibiting greatest transition zone and slowest spillage. Nevertheless, the spillage caused substantial widening of the transition zone in all cases even in case H, especially near the location of the dam, caused by the excessive dispersion along the interface. It is very interesting to note in case HLH the substantial reduction of the salt concentration of the residual saline water in the landward side of the wall, probably caused by much stronger dispersion in the lower portion of the aquifer, where the flow was increased due to the middle low K layer.

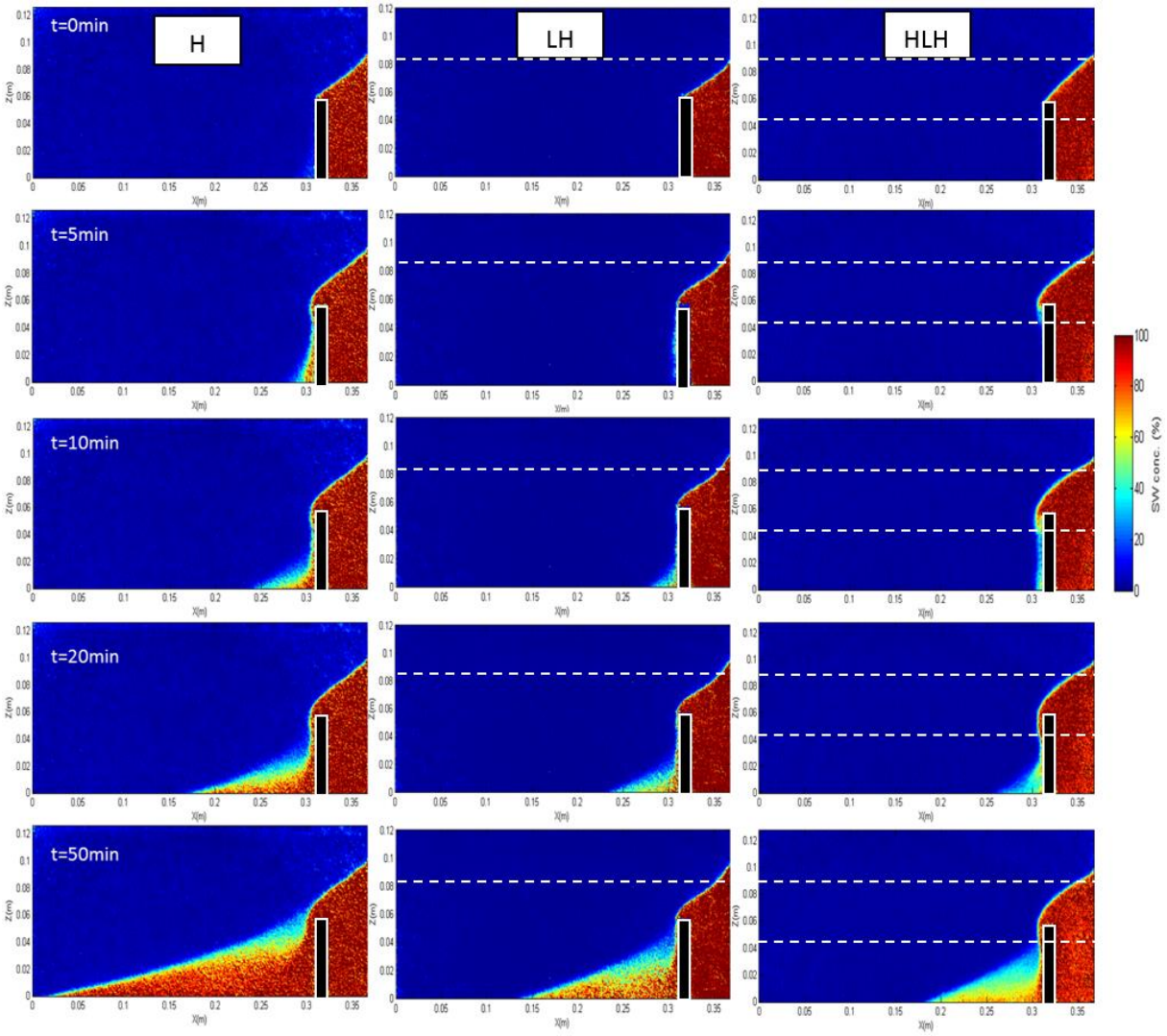

Figure 6.7 Transient experimental advancing-wedge phase in the subsurface dam case after decreasing the head difference from dh = 2.8 mm to dh = 2 mm

The rate of inland extension of the saline water was quantified in each case in order to assess the difference in time taken to reach the critical point X_{crit}, following the head decrement from dh = 2.8 mm to dh = 2 mm. The parameter $\Delta X_{adv}(t)$ was introduced to characterise the distance to be travelled by the toe before reaching X_{crit}, such that $\Delta X_{adv}(t) = abs[X(t) - X_{crit}]/ X_{crit}$; where X(t) is the toe length at time t. We considered that the critical point T_{crit} was reached when $\Delta X_{adv}(t)$ becomes smaller than 1%. The curves of $\Delta X_{adv}(t)$ are shown in Fig 6.8 and the recorded T_{spil} and T_{crit} values are presented in table 6.3. Note that in case HL the saline water has already intruded deeper into the freshwater zone prior to

applying dh = 2 mm; it was therefore not deemed necessary to include this case in this analysis.

The data show that the inland extension of the saline water was considerably lower in cases LH and HLH compared to the homogeneous scenario (Fig 6.8). This means that the rate of saline water spillage was much slower in presence of the low permeability layer in the central and top part of the aquifer. This slower intruding rate was clearly manifested by the milder slope observed in case LH and HLH, while a much steeper slope is exhibited in case H, indicating faster intrusion. This is further confirmed by the delayed starting times of spillage T_{spil} observed in the heterogeneous cases compared to the homogeneous setting, as well as the recorded values of T_{crit} , which are nearly twice in case LH and three times greater in HLH, compared to the homogeneous scenario.

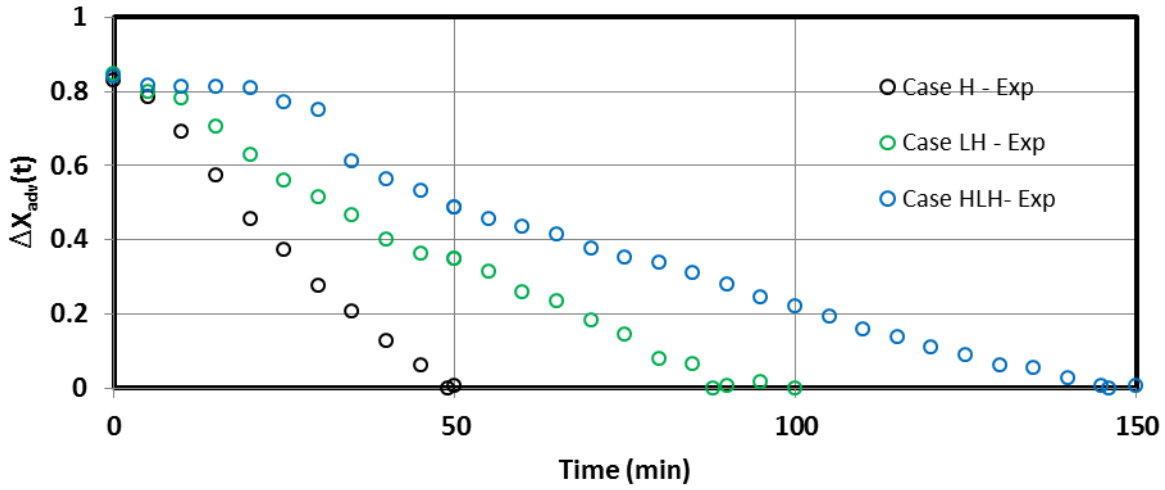

Figure 6.8 Transient experimental toe intruding rates following the saline water spillage in case H, LH, and HLH

Table 6.3 Experimental time required for the saline water to spill (T_{spil}) and to reach the critical point T_{crit} in case H, LH and HLH following the head decrement from dh = 2.8 mm to dh = 2 mm.

Cases	T_{spil}	T_{crit}
Case H	4 min	49 min
Case LH	7 min	88 min
Case HLH	10 min	146 min

Comparison between the numerical data and the experimental results for the advancing-wedge phase is shown in Fig 6.9 The simulation results yielded very good agreement with the experimental data in all cases. The numerical model confirms the ability of the dam to retain saline water for the all the various inland head previously applied to the bases cases, yielding a reduction of 77%, 76%, 77% and 78% in case H, LH, HLH and HL respectively. The model predicted the spillage of saltwater following the application of dh = 2.8 mm in case HL, while no spilling occurred in the other cases until dh = 2 mm was applied to the system, in perfect agreement with the experimental observations. The curves show that both the starting time of the spillage and the intruding rate of the saline water are consistent with the experimental data in all cases. The results demonstrate that the ability of subsurface dams to control saline water intrusion mechanism is strongly affected by the existence of stratified layers and the stratification pattern.

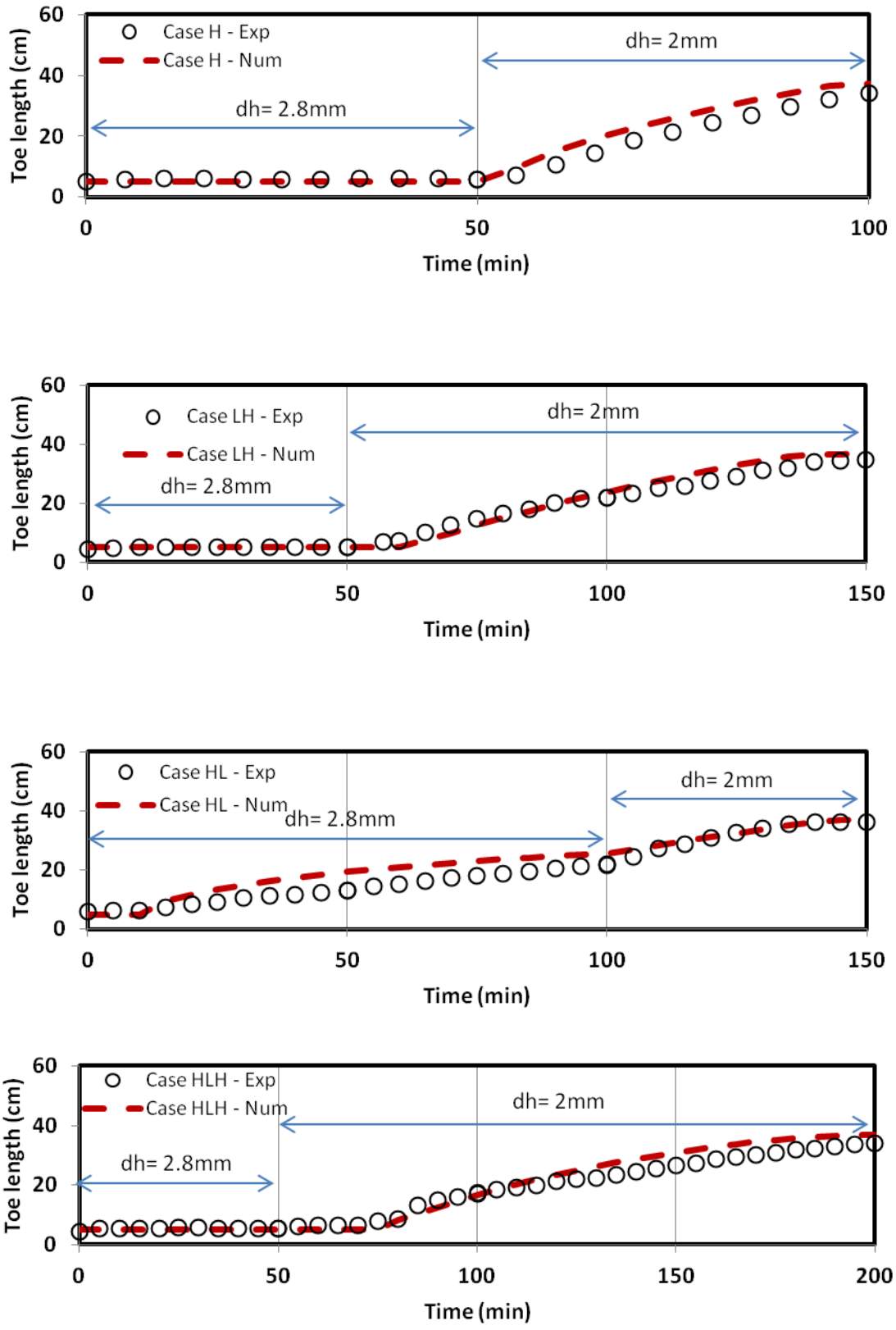

Figure 6.9 Comparison of the transient experimental and numerical toe length results of the subsurface dam cases during the intruding phase

An analysis of the flow velocity vectors was completed to gain an insight on the impact of each layering pattern on the flow dynamics before the spillage of saline water over the subsurface dam (Fig 6.10). The model-predicted inflow rate was also recorded in each aquifer setting, as shown in table 6.4. As expected, the inflow rate was maximal in the homogeneous case and the flow velocity vectors exhibited relatively similar magnitude throughout the system. Obviously, the magnitude of the vectors was very low at the bottom right corner, i.e within the location of the saltwater wedge, and very high at the top right corner of the model domain, i.e. where the freshwater exits the system. The magnitude of the flow velocity vectors was also substantially high at the crest of the subsurface dam, indicating that the freshwater discharge velocity increases over the wall, thereby exerting a downward pressure on the saline plume on the seaward side of the wall, which is in agreement with Luyun et al. (2009).

In the layered cases, the results show that there are basically three main processes that influence the saltwater intrusion mechanism which depend essentially on the location of the low permeability zone in the system. The first process, occurring in case LH, is the downwards channelling of the freshwater flow between the crest of the wall and the interlayer boundary. Hence, the freshwater flow increases in the reduced cross section, which result in more "pushing" effects exerted on the saltwater plume, thereby leading to a more effective resistance to the buoyancy forces which drive the intrusion of saline water. This is clearly shown in the figure, where the flow velocity vectors of highest magnitude were all located between the crest and the layer boundary, resulting in a visibly smaller saline plume and a rather curvier interface, in agreement with the experimental observations (Fig 6.5). In other words, the ability of the subsurface dam to resist SWI mechanism increased compared to the homogeneous case, despite the recorded inflow rate was decreased by 32% in this setting relative to the homogeneous scenario. It is also interesting to note that the inflow rate was

smaller than in case HL, which suggests that the flow magnitude at the crest of the wall has greater influence on the ability of subsurface dams to control SWI than overall freshwater inflow rate.

The second process, taking place in case HLH, is the weakening of the density contrast effects induced by intense mixing occurring as the seaward saline plume is forced to rise through low permeability material. The considerably lower solute concentration of the intruded saline water observed in case HLH at t = 50 min tends to support this explanation (Fig 6.7). Hence, this process directly reduces the density contrast effects and therefore helps the subsurface dam to withstand the SWI mechanism, despite the magnitude of the flow velocity at the crest as well as the inflow rate were both smaller than the homogeneous case.

The third process, occurring in case HL, is the subsequent slowdown of the freshwater flow in the lower part of the system leading to the lowering of the freshwater flow at the crest of the wall. This is clearly observable in Fig 6.10, where the red zone at the crest of the wall was much smaller than the homogeneous case. In other words, the flow at the crest exerted lesser resistance to the buoyancy forces driving the intrusion compared to the homogeneous case. This means that in such condition, the building up of the saline plume on the seaward side of the wall was facilitated. This process therefore caused the weakening of the ability of the subsurface dam to restrict the saline water intrusion mechanism, and induced easier saltwater spillage compared to a homogeneous scenario, following even lesser drop of the inland head boundary.

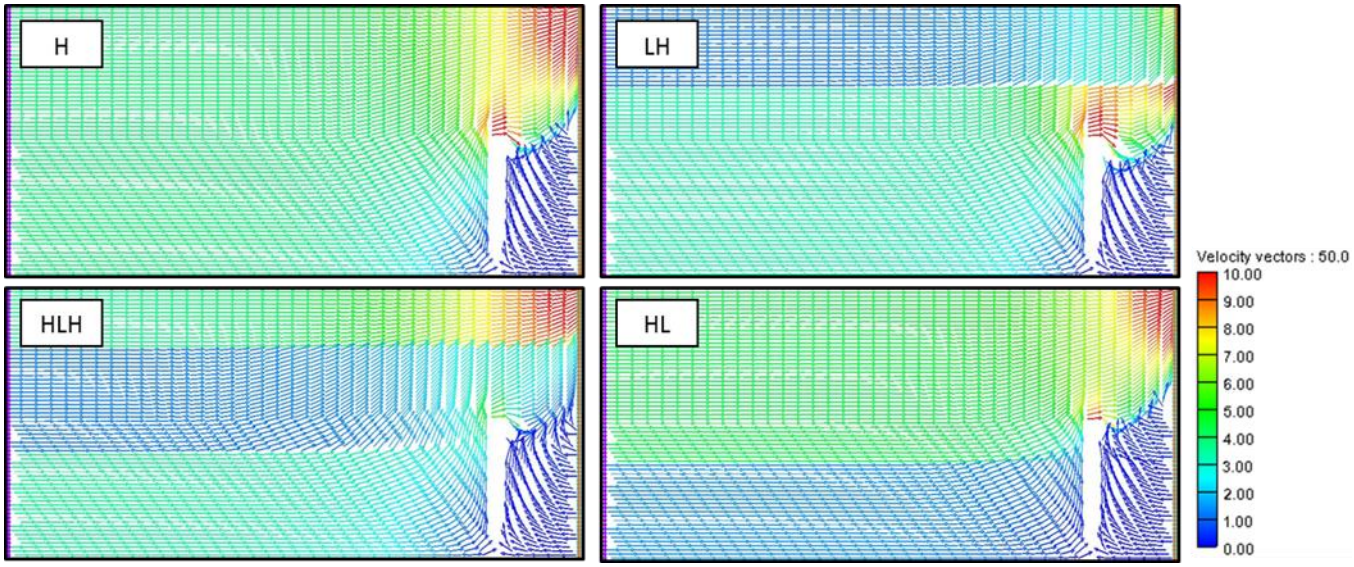

Figure 6.10 Maps of the flow velocity field at steady state after application of dh = 6mm. The velocity vectors are in cm/min.

Table 6.4 Model-predicted inflow rates Q_{in} at steady state (dh = 6 mm)

Cases	Case H	Case LH	Case HLH	Case HL
Q_{in} (cm^3/min)	15.9	10.8	12.3	13.6

Receding-wedge phase

The receding-wedge phase was initiated by instantaneously raising the freshwater level such that to increase the head difference from dh = 2 mm to the initial value dh = 6 mm. This subsequently caused a sharp increase of the freshwater flow throughout the system that abruptly repulsed the saline water towards the seaside (Fig 6.11). The receding process was associated with a significant widening of the transition-zone due to the sharp increase of the freshwater flow that transported saline flux along the freshwater-saltwater interface, especially in case HLH, where the lifted saline water passed through the lower permeability media. The removal of the saline water was not completed within 50 min in none of the investigated cases. Rather, the residual saltwater became relatively steady towards the end of

the test period, forming a smaller residual wedge on the landward side of the wall. At t = 50 min, the lengths of the residual wedge measured from landward edge of the wall were 5.4 cm, 5.2 cm, 5.1 cm and 7 cm in case H, LH, HLH and HL, respectively.

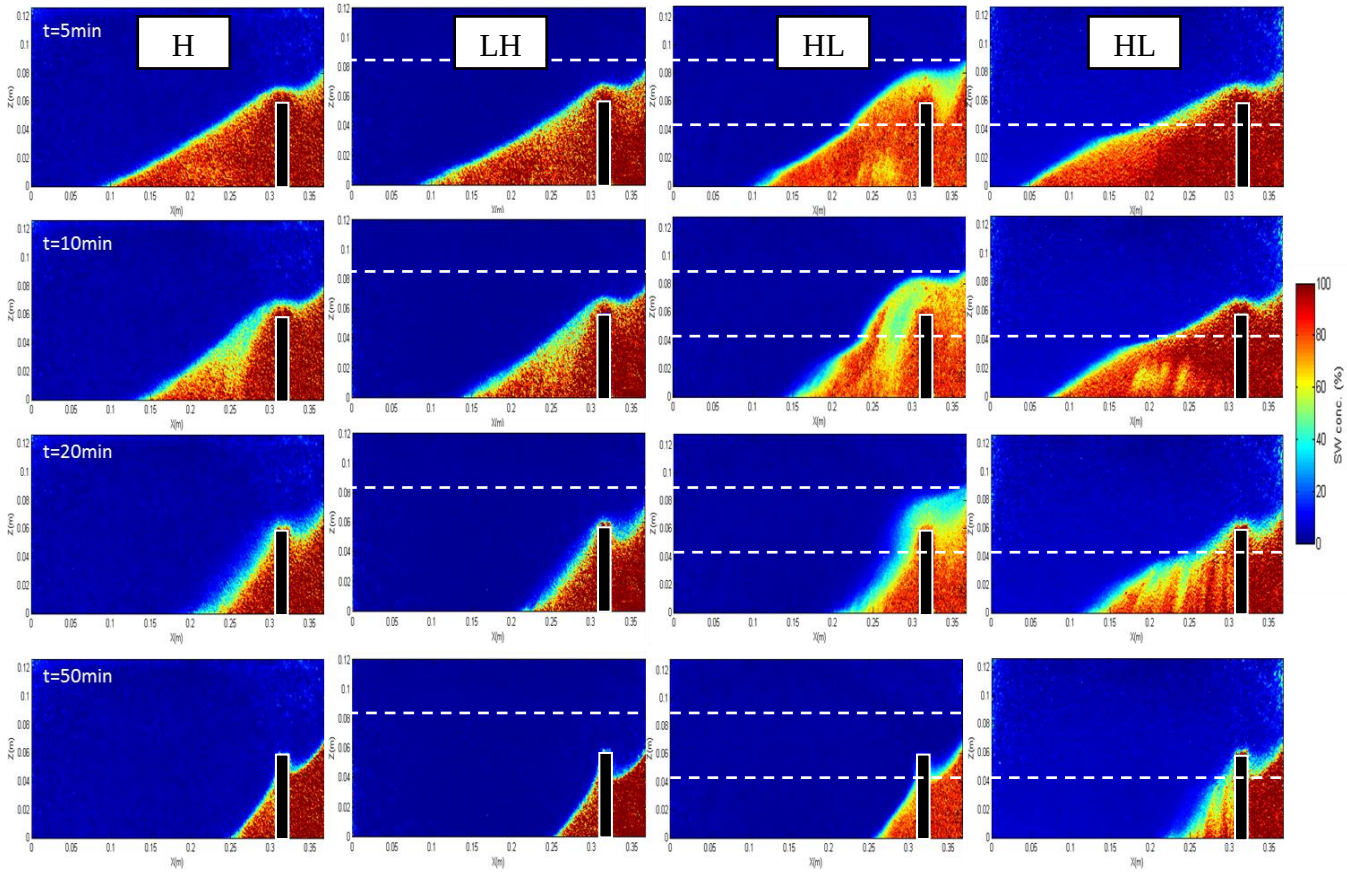

Figure 6.11 Transient experimental receding-wedge phase after returning the head difference back to dh = 6 mm.

The migration rate of the receding wedge was analysed in all the cases and the results are presented in Fig 6.12. The parameter $\Delta X_{rec}(t)$ was used to characterise the distance to be travelled by the toe until its position when the receding motion saltwater plume became steady forming a residual wedge on the landward side of the wall, i.e. at t = 50 min, such that $\Delta X_{rec}(t) = abs[X(t) - X_f\ ]/\ X(t_0)$; where $X(t_0)$ and X_f are the toe lengths at t = 0 min and t = 50 min, respectively. The small discrepancies at the initial condition (t = 0 min) are simply due to the minor differences of $X(t_0)$ upon the application of the inland head change. The data

show that the migrating saline water was much slower in case HL, while relatively similar in the other cases. This was expected because the bottom low K layer slows the transit of the freshwater flow in the lower part of the system, thereby preventing the effective upward lifting of saline water.

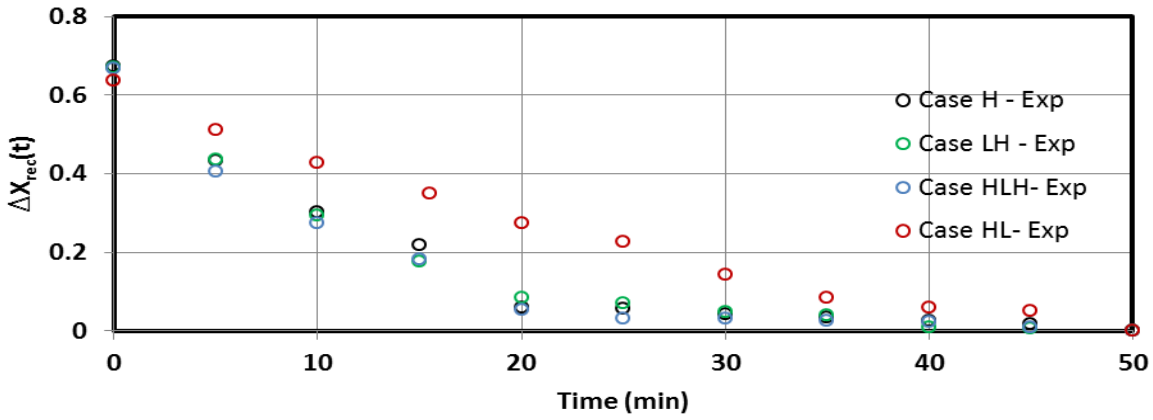

Figure 6.12 Transient experimental toe receding rates after resetting the initial head difference dh = 6 mm

Table 6.5 Time required for complete cleanup of the freshwater zone T_{flush}

Cases	Case H	Case LH	Case HLH	Case HL
Exp	135 min	155 min	160 min	200 min
Num	117 min	131 min	137 min	233 min

The complete cleanup of the freshwater zone required extending the test retreat time beyond 50 min. The freshwater zone was considered cleaned up when no saline water could be observable, even of low concentration. The time required for the saline water to be completely flushed from the freshwater zone T_{flush} was recorded in each aquifer setting (table 6.5). The presence of stratified layers generally prolonged the time needed for the residual

saline water to be flushed out. Unexpectedly, the time for complete saltwater removal in case LH was longer than the homogeneous scenario (15% longer).

This rather counter intuitive finding may be the result of two opposed influential factors associated with the presence of the overlying low K layer. The first is the downwards channelling of the freshwater flow by the upper low K layer, which increases the flow velocity in the lower part of the system and thus promotes the easier lifting of saline water. The second factor is the reduction of the total freshwater inflow, which leads to a reduction of the forces required to lift the denser saline water upward back over the wall. As a result, the time needed for complete flushing of the saltwater was longer. Our results therefore suggest that the second factor had more impact on the ability of the subsurface dam to clean up the freshwater area from SWI contamination. This is clearly shown in table 6.6, which shows the influence of the top low K layer thickness W_{top} on the cleanup time. The data show that T_{flush} initially decreased with increasing values of W_{top} (for $\leq 20\%$), mainly under the influence of the first process described above. For values of $W_{top} \geq 20\%$, the increasing values of $W_{top,}$ which obviously caused further reduction of the total freshwater inflow, led to increasing values of T_{flush}, thus mainly under the influence of the second process.

Table 6.6 Effect of the thickness of the top layer W_{top} on the flushing time. The values of W_{top} are given as percentage of the saturated thickness of the homogeneous case (h = 136 mm). The inflow rate Q_{in} were recorded after the flushing was completed

W_{top} (%)	Q_{in} (cm^3/min)	T_{flush} (min)
10 %	14.6	127
20 %	12.9	123
30 %	11.4	126
40 %	9.7	128
50 %	8.2	150

In case HL, the presence of the underlying low K layer induced a substantial delay in the time required for the saline water to be flushed out, as expected. It took nearly 50% more time for the residual saline water to be removed than the homogeneous setting. As explained above, this is because the underlying low K layer in this setting slows the freshwater flow that faces the residual saltwater wedge thus inhibits the effective upward lifting of saline flux. It is obvious that if the thickness of the low K layer was increased, the flushing time would be considerably increased, as this would not only cause a decrease in the total freshwater inflow, but it would also induce a greater zone where the flow velocity would be considerably lower. In case HLH, the freshwater flow at the crest is reduced by the middle layer low K layer, which partly compromises the landward-seaward transfer of saline flux above the wall. This can be seen in Fig 6.11, where the transition zone above the crest of the wall was noticeably wider and the wedge was more refracted relative to the homogeneous case. The impact of the low K layer was nonetheless much lessened than in case HL, since in case HLH the freshwater is allowed to flow freely along the aquifer bottom, where it is needed to initiate the lifting process.

The results show that the receding motion of the saline water in the numerical model yielded very good agreement with the experimental data in all the cases (Fig 6.13). The time required for complete removal of saline water from the landward side of the wall was also reported in table 6.12. The data show that it took relatively less time for the freshwater zone to be completely cleaned up in the numerical model for all the cases. The numerical results nonetheless confirm the negative impact of the stratified layers in prolonging the time needed to clean up the freshwater zone, in agreement with the experimental observations. These findings imply that the in cases of equivalent water table rise, the time required for the residual saline water to be completely removed from a coastal aquifer system would be substantially longer in presence of low permeability layers into the system, compared to an

idealized homogeneous aquifer system. In other words, the ability of subsurface dams to clean up coastal aquifer from intruded saline water may be largely overestimated when neglecting aquifer heterogeneity effect through the assumption of idealized homogeneous condition. While Oswald et al. (2002) and Luyun et al. (2009) demonstrated that full removal of saline water by the inland freshwater flow was a plausible phenomenon in homogeneous system, the present findings provide strong evidence of the plausibility of such a natural cleanup process of contaminated coastal ground waters in heterogeneous aquifer settings, with a rate of removal severely affected by the permeability and arrangement of the layers.

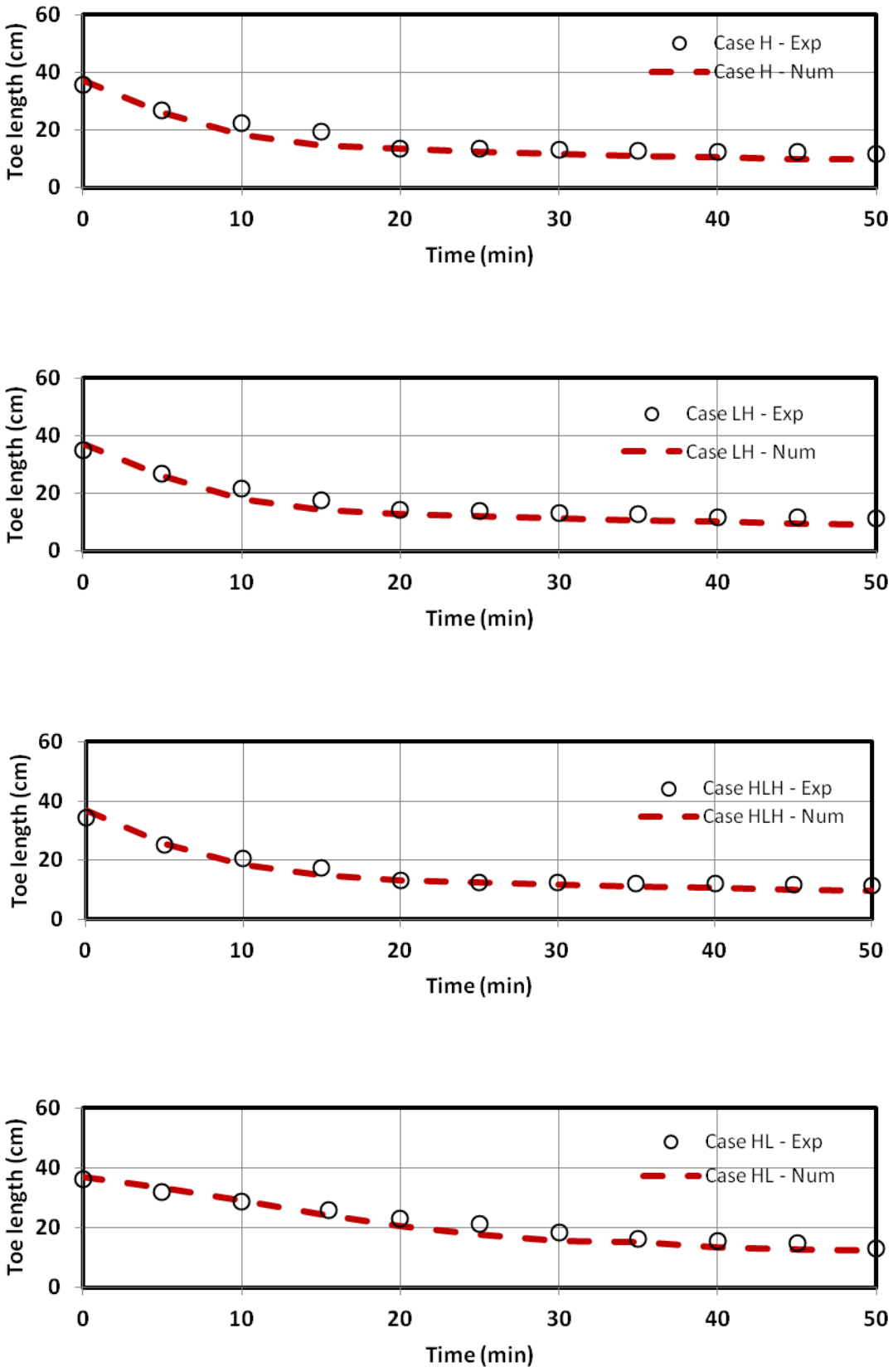

Figure 6.13 Comparison of the transient experimental and numerical toe length results of the subsurface dam cases during the receding-wedge phase

6.4 Summary and conclusions

In this study, laboratory experiments and numerical simulations were used to assess the impact of layered heterogeneity on the ability of subsurface dams to control saltwater intrusion and to clean-up salinized coastal aquifers. Three layering configurations were examined, where a low K layer was located in the top part of the system (case LH), in the middle part of the aquifer as interlayer (case HLH) and at the bottom part of the system (case HL). An idealized homogeneous aquifer (case H) was also examined for reference purposes. The performance of subsurface dams was tested for their ability (1) to restrict the saline water intrusion mechanism during the advancing-wedge phase, and (2) to clean up the freshwater zone from residual saline water in the receding-wedge phase. The main findings of this investigation are:

- The existence of a low permeability zone in the upper part of an aquifer system generally enhanced the ability of subsurface dams to restrict SWI mechanism and lower the rate of saltwater spillage when it occurs, compared to the homogeneous setting. The overlying low K layer forced the freshwater to flow in the reduced spacing between the crest of the wall and the bottom boundary of this low K layer, which pushed the saltwater wedge downwards and impeded its building up. The results showed that the time taken for the aquifer to be contaminated was nearly twice longer than in the homogeneous case.
- Conversely, the existence of the low permeability zone in the lower part of the aquifer substantially weakened the ability of subsurface dams to retain SWI. The underlying low K layer caused a reduced magnitude of the flow velocity over the crest of the wall, which allowed an easier building up of the saline plume on the seaward side of the wall and caused the saline water to spill over the wall at even larger head difference compared to the homogeneous scenario.

- The natural cleanup of SWI-contaminated coastal aquifers was evidenced for the first time in heterogeneous (multi-layered) geological formations. The presence of stratified layers nonetheless prolonged the cleanup time compared to the homogeneous case to various degrees, depending on the stratification pattern.
- In presence of a low K layer at the upper part of the system (case LH), the time for complete saltwater removal was longer than the homogeneous scenario (about 15%). This rather counter intuitive finding was because of the overall reduction of the total freshwater inflow into the aquifer associated with the presence of the low K zone, which induced a lessening of the forces required to lift the residual saline upward back towards the coastline.
- In case where a low permeability zone underlies the aquifer system (case HL), the time of completion of the cleanup process was at least about 50% longer than in the homogenous scenario. In such setting, the underlying low K zone significantly slowed the freshwater flow that faces the wedge and thus inhibited the effective upward lifting of saline flux on the seaward side of the wall.

The findings presented here are expected to have significant implications from water resources management prospective. Our results highlight the limitation of considering the common assumption of homogeneous condition when attempting to assess the performance of subsurface dams, which lead to large erroneous estimation of their ability to retain saltwater intrusion mechanism and clean-up previously contaminated coastal aquifers.

Our results also suggest that the residual saline water trapped in the landward side of the wall may be naturally removed from the freshwater zone without the need of mechanical removal techniques, despite the existence of such typical heterogeneous structures. The rate of removal would however be strongly dependent on the total groundwater inflow and the layering pattern, particularly the position of the low permeability layers in the aquifer. Other

factors such as the dispersion within the aquifer and the density contrast may also considerably influence the cleanup time.

Although real world stratified coastal aquifers may exhibit much more complex layering patterns, the findings of the study provide a first insight on the impact of the expected disruption of flow dynamics imposed by typical layered structures on the performance of subsurface dams in controlling SWI.

Chapter 7

A new physical barrier system to control SWI in coastal aquifers

The findings presented by Kaleris and Ziogas, (2013) demonstrated that the performance of cutoff walls located relatively close from the coastline would not only depend on the wall penetration depth, but also on the ratio of the groundwater inflow velocity over the density driven saltwater velocity. Thus, it is expected that that increasing this velocity ratio would not only improve the ability of the wall to repulse saltwater intrusion, but it would also allow an increased freshwater storage thus allowing a more optimal exploitation of the available freshwater resources. In this effort, this chapter investigates the performance of a new physical barrier system for seawater intrusion control purposes, which consist in the simultaneous application of an impermeable cutoff wall located close to the shore, and a short semi-permeable subsurface dam placed at the seaward side of the wall. The concept of combined actions on seawater intrusion (as applied to hydraulic barriers), has never been applied to physical barriers. The workability of this new barrier system, referred to as mixed physical barrier (MPB), was herein examined for various hydraulic gradients and compared to the traditionally-used barriers.

7.1 Experimental procedure

Fig 7.1 presents the various experimental cases investigated herein. The barriers were placed ahead of the packing of the beads. To form the semi-permeable dam, two dividers were inserted into the porous media chamber at the desired location, and fine beads of mean diameter 0.3 mm were siphoned into the spacing between them until the desired height. On completion of the packing, the dividers were carefully removed. The average hydraulic conductivity of the dam was also obtained by in situ measurement on the experimental flow tank (using finer mesh screens on both sides) and was K_d = 0.0017 m/s. Typical grouting

materials used field applications could exhibit hydraulic conductivities as low as 10^{-9} m/s. (Kaleris and Ziogas, 2013).

The cutoff wall was made of impermeable material (plasticine). Cutoff walls are generally located at distances from the coastline less than or equal to twice the aquifer height (Allow, 2012; Japan Green Resources Agency, 2004) and should be located within the area of the saltwater wedge to be effective (Luyun et al., 2011). To meet these conditions, the cutoff wall was placed at a distance in the order of half of the aquifer height in our investigations. It was ensured that the cutoff wall was located within the saltwater wedge area by first analysing the saltwater wedge extent in a synthetic aquifer free of barrier (base case), as described below. The cutoff wall depth was adjusted such that an opening smaller than 40% of the aquifer height from the bottom of the tank was left to ensure effective reduction of the saltwater intrusion length (Kaleris and Ziogas, 2013). Note that the maximum wall depth of construction applicable in real field aquifers is up to 100 m (Kaleris and Ziogas, 2013). Table 7.1 presents a summary of the dimensions and location of the dam and cutoff wall barriers. For the MPB experiment, the cutoff wall and the semi-permeable dam were both placed in the same positions as in the other experiments.

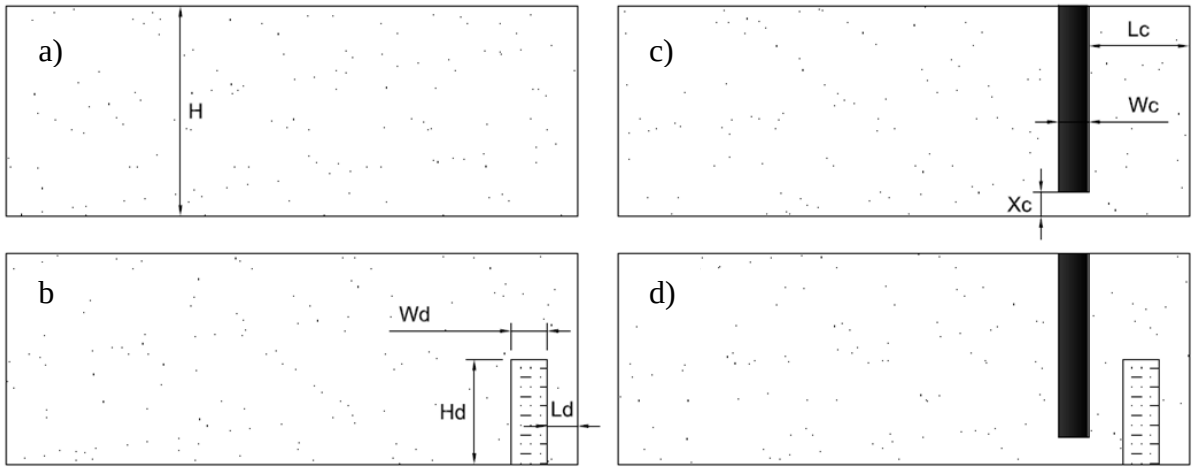

Figure 7.1 Investigated cases: a) baseline case; b) subsurface dam case; c) cutoff wall case; d) MPB case. The freshwater flow occurs from left to right.

Table 7.1 Values of the design variables

Variable	Symbol	Values
Subsurface dam		
Distance from seawater boundary	L_d	20 mm
Height	H_d	70 mm
Width	W_d	24 mm
Hydraulic conductivity	K_d	10 cm/min
Cutoff wall		
Distance from seawater boundary	L_c	66 mm
Opening	X_c	16 mm
Width	W_c	20 mm

The simulation of groundwater fluctuations was achieved by varying the freshwater level such that two different heads were successively forced at the freshwater boundary, namely 135.7 mm and 133.7 mm, yielding a head differences of dh = 6 mm (135.7-129.7 mm) and dh = 4 mm (133.7-129.7 mm). Each head difference was applied for 50 minutes to allow the system to reach a quasi-steady state condition. The head differences dh = 6 mm and dh = 4 mm corresponded to hydraulic gradients of 0.0158 and 0.0105, respectively. The initial condition was set by forcing a head of 135.7 mm at the freshwater boundary (dh = 6mm). The denser saltwater was allowed to intrude into a fully fresh aquifer, until the system reached the first quasi-steady state condition. The freshwater level was then decreased to 133.7 mm (dh = 4 mm), allowing the saltwater wedge to migrate further inland. The freshwater head was then returned to the initial value of dh = 6 mm, which forced the saltwater wedge to recede toward the seawater boundary. The use of the same head difference

dh = 6 mm as that used to set the initial condition was also to check if any hysteresis occurred over the course of the experiment.

To assess the effectiveness of the different barriers, a baseline case with no barrier installed was first studied to be used as a benchmark for the barrier cases investigated. The effectiveness of the barriers was characterised by the percentage of reduction $R = (TL_0 - TL_b)/TL_0$, where TL_0 and TL_b are the intrusion length before and after the installation of the barrier, respectively.

7.2 Numerical procedure

To simulate the transient saltwater intrusion, three stress periods were applied. After the initial condition was set in the first stress period, the freshwater level decreased from 135.7 mm to 133.7 mm. A constant-head of 129.7 mm was set on the saltwater side. These boundary conditions were forced on both sides and the system was allowed to reach a new steady state condition. The head and concentration resulting in each cell at the end of each stress period were used as initial condition for the following transient period. In the last stress period, the freshwater head was increased back to the initial value 135.7 mm. The subsurface dam was simulated into the numerical model by assigning the hydraulic conductivity K_d = 10 cm/min to the cells of interest, which corresponded to the value measured within the experimental setup as described below. The cutoff wall was assumed to be impermeable, i.e. the cells occupied by the wall were rendered inactive.

7.3 Results and discussion

7.3.1 Baseline case

Fig 7.2 presents the concentration colour maps of the base case, showing the intrusion of the saltwater wedges at the various steady state conditions observed in the experiment. The horizontal extent of the saltwater wedge was 8.8 cm in the physical model, at the end of the

first time period. The end of time period 1 was hereafter regarded as the zero time because the hydraulic gradient in time periods 1 and 3 was the same and results showed no difference in the length of the wedge between both time periods. Therefore, figures showing the transient TL will present only time period 2 (advancing wedge; dh = 4 mm) and time period 3 (receding wedge; dh = 6 mm).

The transient experimental and numerical TL data are presented in Fig 7.3. The numerical model results matched well with the experimental data. The model was able to accurately reproduce the movement of the toe for the two hydraulic gradients considered. After reducing the head difference to dh = 4 mm, the saltwater TL extended to 17.9 cm and 18.41 cm in the experimental and numerical, respectively. At time t = 50 min, the head difference was increased to dh = 6 mm which forced the wedge to retreat back to its original position. The agreement between the experimental and numerical results was generally good, with a maximum percentage difference up to 7% and 9%, in the advancing and receding wedge conditions, respectively. The shape of the saltwater wedge (transition zone and TL) at the end of the receding phase was identical to that of the initial condition, indicating that no hysteresis occurred throughout the experiment.

Fig 7.3 not only shows the reliability of the numerical model for the simulation of the remaining experiments, but it also demonstrates the accuracy of the recorded TL data used as baseline for estimating the performance of the barriers The two TL_0 values used for the calculation of R were therefore 8.8 cm and 17.9 cm. These were assumed to be the two extreme saltwater intrusion scenarios for the coastal aquifer system considered.

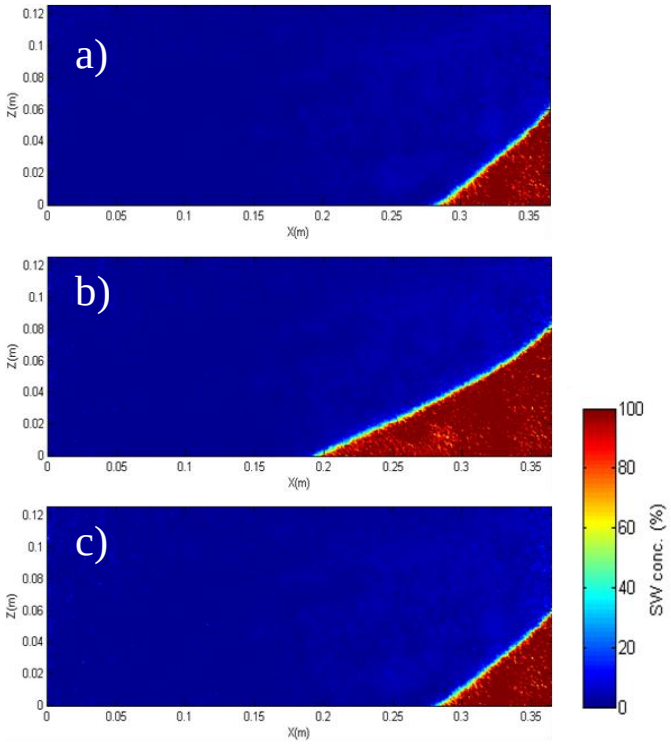

Figure 7.2 Steady-state experimental saltwater wedge in the base case; a) t = 0 min (initial condition); b) at t = 50 min (dh = 4 mm); c) at t = 100 min (dh = 6 mm)

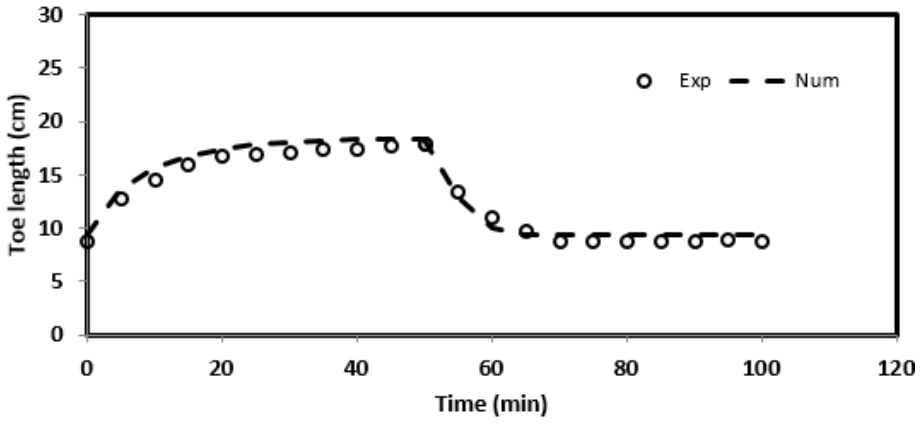

Figure 7.3 Transient experimental and numerical toe length results of the base case

7.3.2 Subsurface dam case

Fig 7.4 presents the experimental results of the steady state saltwater wedge for different hydraulic gradients. Upon setting the initial condition with dh = 6 mm, the saltwater

wedge slowly penetrated into the system until the TL reached 7 cm at steady state (Fig 7.4a). Following the application of head difference dh = 4mm, the intrusion length extended to 18.8 cm at steady state condition, which corresponds to a percentage of reduction R of -5 %. This negative reduction indicates that the TL exceeded that of the baseline case. Laboratory observations revealed that this extension was rather slow and occurred after the dam was almost fully saturated by the saline water (Fig 7.4b). As the saltwater supply into the system was partially disrupted by the semi-permeable dam, density difference effects caused the saline water in the landward side of the dam to gently slide under the freshwater flow, thereby causing a slight extension of the toe length. Similar observations were reported in Luyun et al. (2009).

After the head difference was reversed to dh = 6 mm at t = 50 min, the TL retreated and measured 7 cm at steady state, which corresponds to a percentage reduction R of 21%. This result indicates that the semi-permeable dam could achieve noticeable reduction of the intrusion length only when the hydraulic gradient was high enough to produce sufficient advective forces to help maintain the saltwater wedge on the seaward side of the dam. The final shape of the wedge was nearly identical to that of the initial condition, suggesting that no hysteresis occurred over the course of the experiment (Fig 7.4a, c).

The retreat of the wedge was associated again with a noticeable widening of the transition zone as the interface crosses the semi-permeable dam (Fig 7.4c). This can be clearly observed in Fig 7.5 that shows the transient receding wedge after dh = 6 mm was applied to the system. The penetration of the wedge through the dam induced a substantial widening of the transition zone. The low permeability material of the dam primarily restricted the movement of the wedge and decreased the freshwater flow velocity. The widening of the transition zone occurring in such conditions is expected to be the result of enhanced separation of streamlines

of the freshwater–saltwater mixture induced by flow refraction within the low permeability material of the dam (Lu et al, 2013).

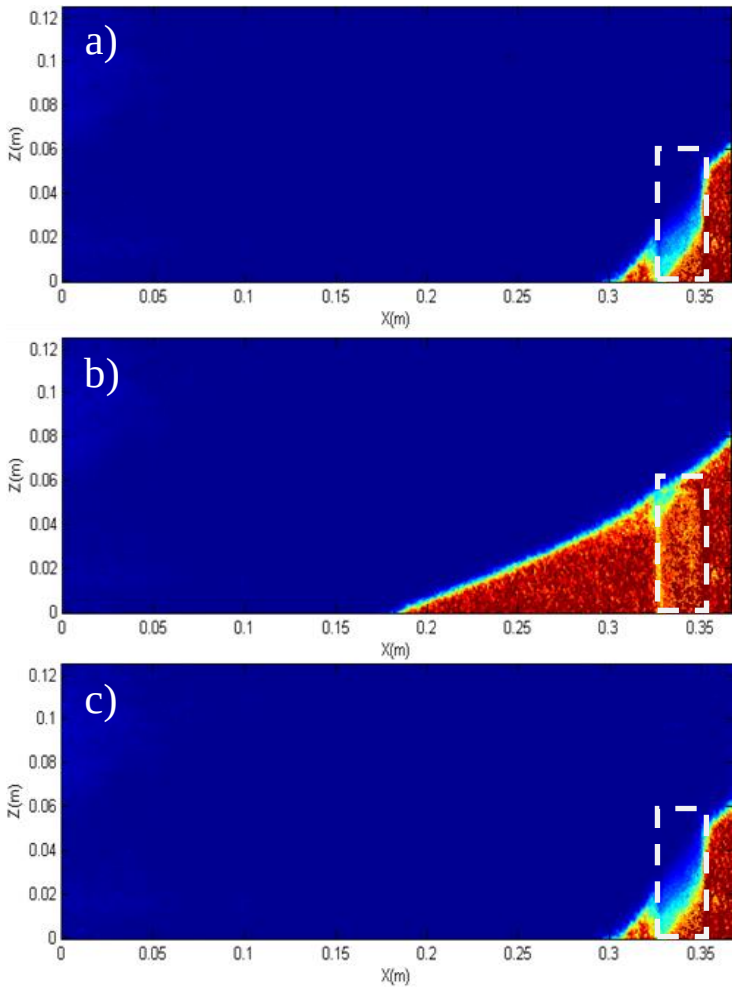

Figure 7.4 Experimental steady-state saltwater wedge in the subsurface dam case; a) t = 0 min (initial condition); b) at t = 50 min (dh = 4 mm); c) at t = 100 min (dh = 6mm)

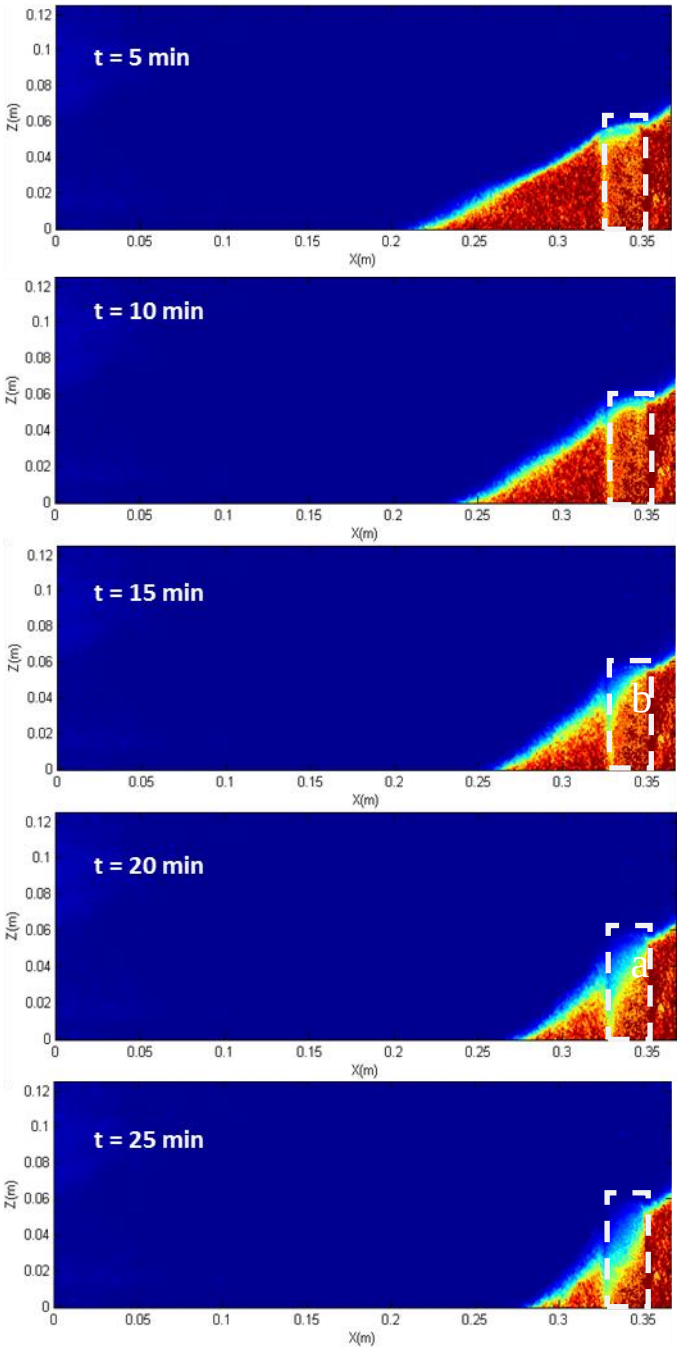

Figure 7.5 Transient experimental receding saltwater wedge in the subsurface dam case

The transient dynamics of the saltwater wedge compared to the numerical prediction is presented in Fig 7.6 for both the dam and baseline cases. The numerical model reasonably replicated the transient changes of the toe position in the presence of the subsurface dam, for both hydraulic gradients. Smaller values of the TL were recorded in the dam case until t=30

min in the experimental model, which suggests that the presence of the subsurface dam temporarily slowed down the rate of the intrusion at the start after which the wedge was forced to flow through the lower permeability material due to the build-up of the saline water pressure behind the dam.

The larger TL values observed in the subsurface dam case until t = 75-80 min in both the experimental and numerical model suggest that the dam temporarily slowed the natural retreat of saltwater wedge following the increment of the head difference to dh = 6 mm (t = 50-100 min). This observation indicates that initially the presence of the low permeability material partially prevented the increased freshwater flow from effectively repulsing the saline water towards the boundary, after which the TL values became smaller than the base case. In overall, the results suggest that the use of subsurface dams constructed from semi-permeable materials may not be an effective countermeasure for seawater intrusion control purposes.

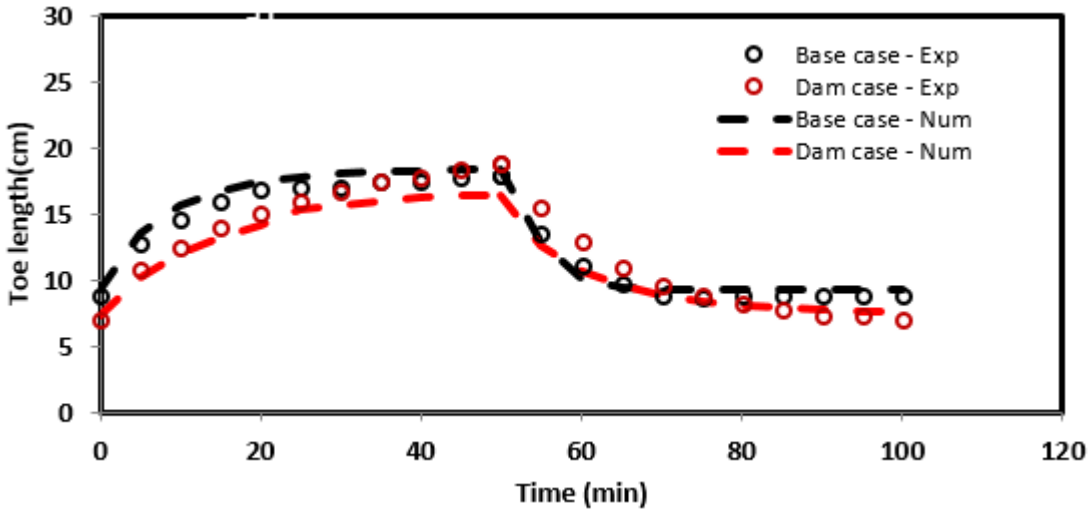

Figure 7.6 Transient experimental and numerical toe length results of the subsurface dam case

Sensitivity analysis was conducted to investigate the effect of the height of the dam and its hydraulic conductivity on the intrusion length. The hydraulic conductivity of the dam was expressed relative to that of the aquifer K_d/K and ranged between 0.02 and 0.12. The dam permeability had small effect on the TL for the steeper hydraulic gradient when dh = 6 mm (Fig 7.7). This is attributed to the greater freshwater flow that repulses the wedge and forces it to remain on the seaward side of the wall anyway. Hence, changing the dam permeability yields little effect in the saltwater wedge reduction. By contrast, the effect of the dam permeability was greater for the smaller head difference dh = 4 mm as the TL reduction ranged from R = 9% at K_d/K = 0.12 to R = 38% at K_d/K = 0.02. For this hydraulic gradient, the freshwater is unable to build great pressure that halts the wedge and hence in this case the dam is the primary obstacle in the way of the intruding saltwater wedge. Reducing the dam permeability in such case helps in impeding the wedge and thus yields noticeable TL reduction.

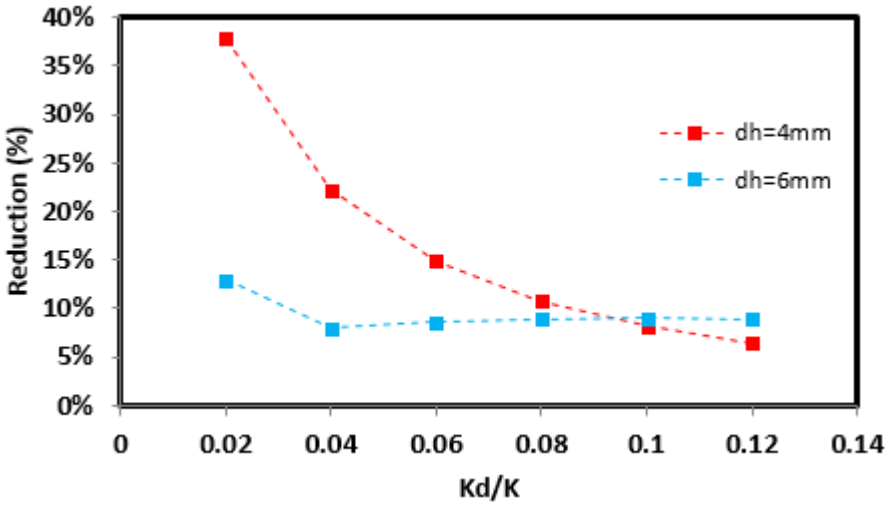

Figure 7.7 Sensitivity analysis of the effectiveness of the subsurface dam to the permeability ratio K_d/K

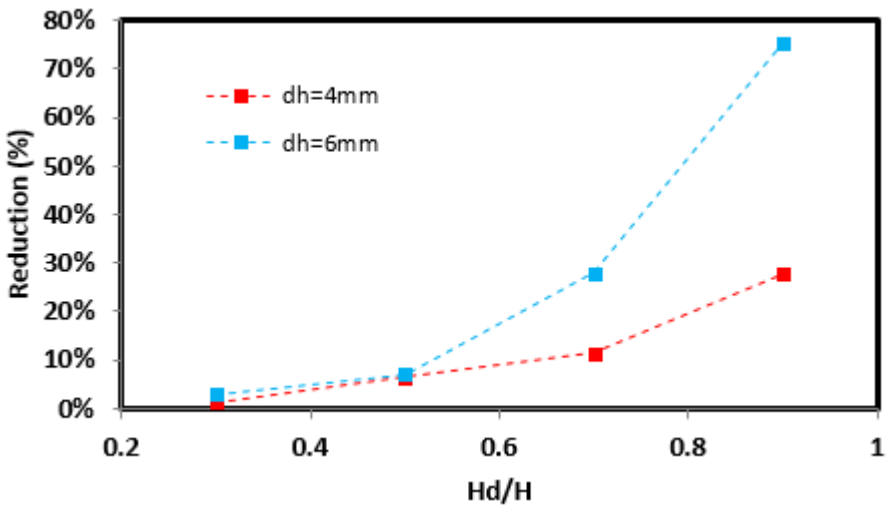

Figure 7.8 Sensitivity analysis of the effectiveness of the subsurface dam to the ratio H_d/H

The height of the dam was expressed relative to the depth of the aquifer H_d/H and was examined for a range 0.3 - 0.9 (Fig 7.8). The reduction values ranged from 1% to 28% for dh = 4 mm and between 3% and 75% for dh = 6 mm as H_d/H was varied from 0.3 to 0.9, respectively. The effect of the H_d/H ratio was pronounced in the steeper hydraulic gradient and had insignificant effect in case of dh = 4 mm. Again, this can be attributed to the insufficient freshwater pressure build-up in case of smaller head difference dh = 4 mm to a level that makes the subsurface dam alone unable to significantly prevent the saltwater from further intrusion, regardless of how much the semi-permeable dam covers the aquifer thickness.

7.3.3 Cutoff wall case

Fig 7.9 presents the experimental saltwater wedge for the various hydraulic gradients for the cutoff wall case. The first steady state (dh = 6 mm) was considered as the initial condition (Fig 7.9a), where the recorded toe was about 4.5 cm from the coastal boundary. Following the application of dh = 4 mm, the TL extended to 6.7 cm, which corresponds to reduction in the intrusion length of R = 63 % compared to the base case (Fig 7.9b).

Laboratory observations revealed that upon lowering the hydraulic gradient, the saltwater wedge rapidly migrated inland before it promptly stopped at the wall opening. The substantial reduction achieved by the cutoff wall resulted from the increased freshwater velocity as it flows through the reduced cross section below the wall, thereby effectively repulsing the saline water and forcing it to remain in the seaward side of the wall (Anwar, 1983; Kaleris and Ziogas, 2013; Luyun et al., 2011).

After increasing the head difference to dh = 6 mm at t = 50 min, the saltwater wedge receded toward the coastal boundary and the TL was 4.5 cm at steady state, similar to the observed TL at the initial condition (Fig 7.9c). This corresponds to a toe length reduction of 48% relative to the base case. Laboratory observations reveals that the saltwater retreat was associated with a distortion of the saltwater wedge (t = 2.5 min) and a widening of the transition zone (t = 5 and 7.5 min), as shown in Fig 7.10. This interesting observation may be the result of instantaneous increase of the hydraulic gradient which caused an increase of the freshwater flow transmitted to the system. The velocity of freshwater flow was sharply increased at the reduced cross section below the wall, thereby inducing a rather abrupt repulsion of the saltwater wedge associated with a substantial increase of the interface thickness. Such widening of the transition zone was also observed in Robinson et al. (2016) who attributed this to excessive dispersion occurring along the interface essentially induced by the unidirectional flow field that is typically associated with saltwater water retreat (Chang and Clement, 2012).

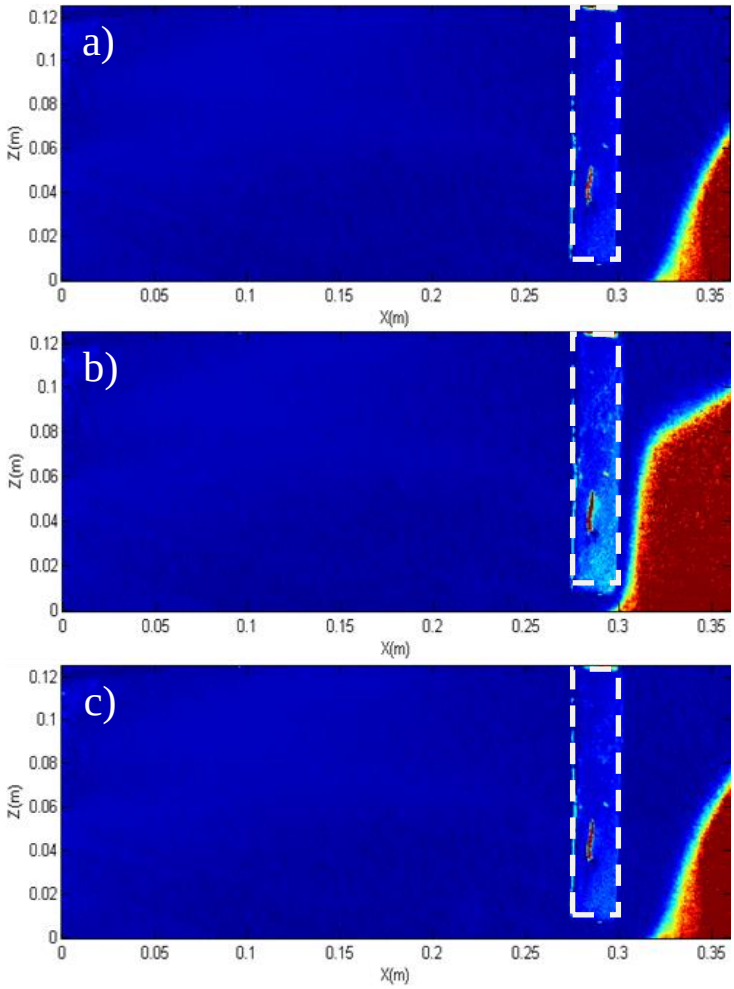

Figure 7.9 Steady-state experimental saltwater wedge for the cutoff wall case; a) t = 0 min (initial condition); b) at t = 50 min; c) at t = 100 min

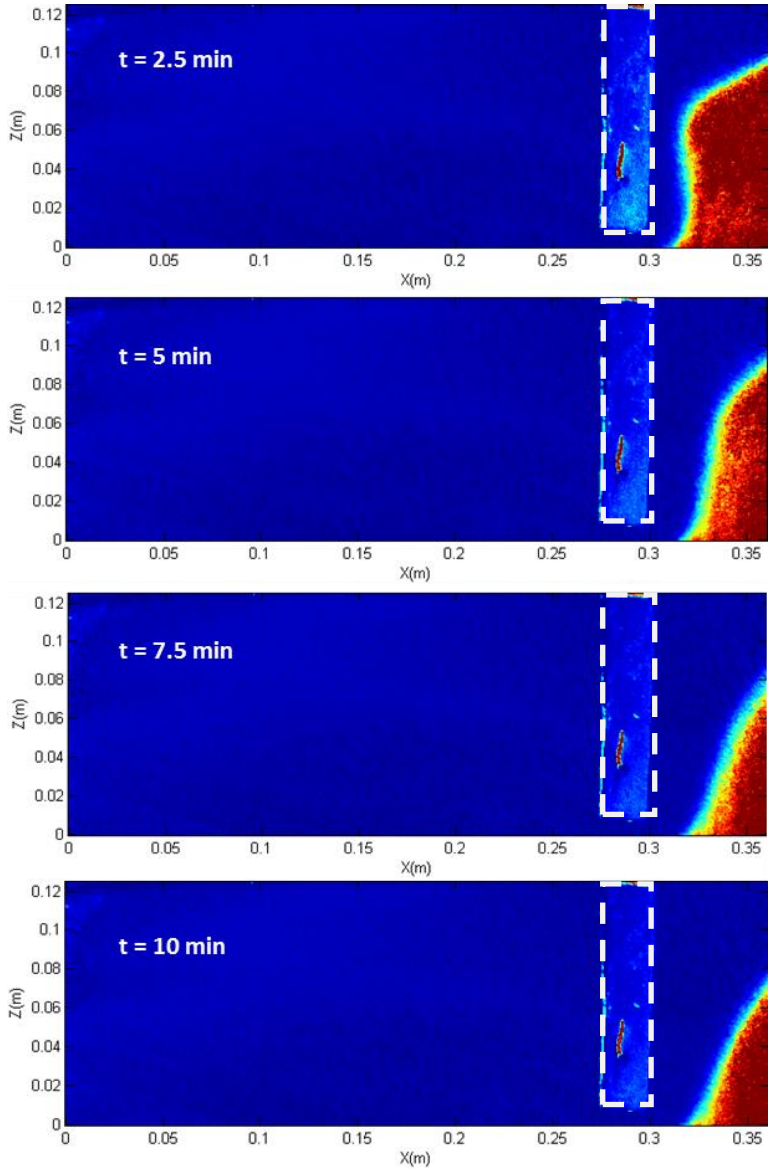

Figure 7.10 Transient experimental receding saltwater wedge for the cutoff wall case

Numerical results of the transient toe length for the cutoff wall case are well matched with the experimental data (Fig 7.11). The system rapidly reached a state of equilibrium within 10 minutes for both hydraulic gradients. The reduction achieved by the cutoff wall was significantly greater for the lower hydraulic gradient. Regardless of the extent of the saltwater wedge before the barrier installation, the cutoff wall was able to maintain the wedge on the seaward side for all the hydraulic gradients tested. Hence the reduction was higher for

the smaller hydraulic gradient which initially induced greater TL before the wall installation. This shows the long term reliability of cutoff walls in effectively reducing saltwater intrusion, where the reduction was more pronounced in smaller or shallower hydraulic gradients than steeper gradients. This result demonstrates that the worthiness of installing cutoff walls for seawater intrusion control purposes increases in shallower hydraulic gradients.

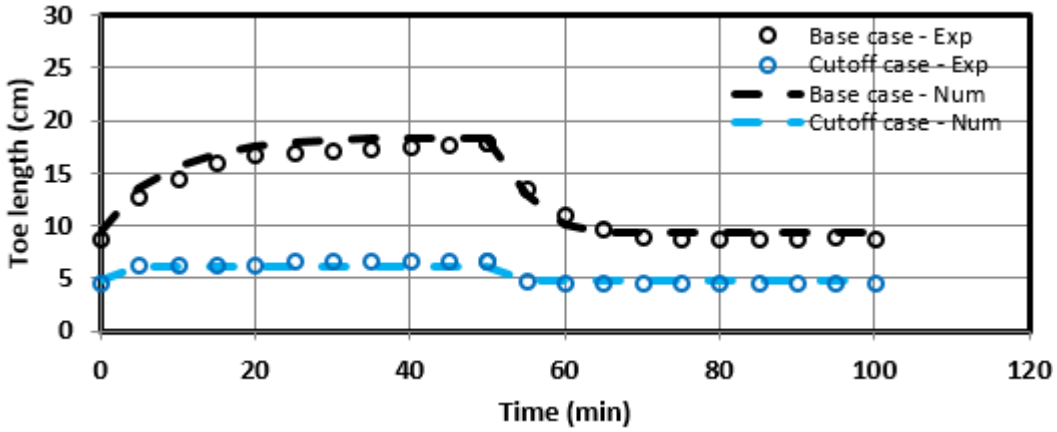

Figure 7.11 Transient experimental and numerical toe length results of the cutoff wall case

7.3.4 MPB case

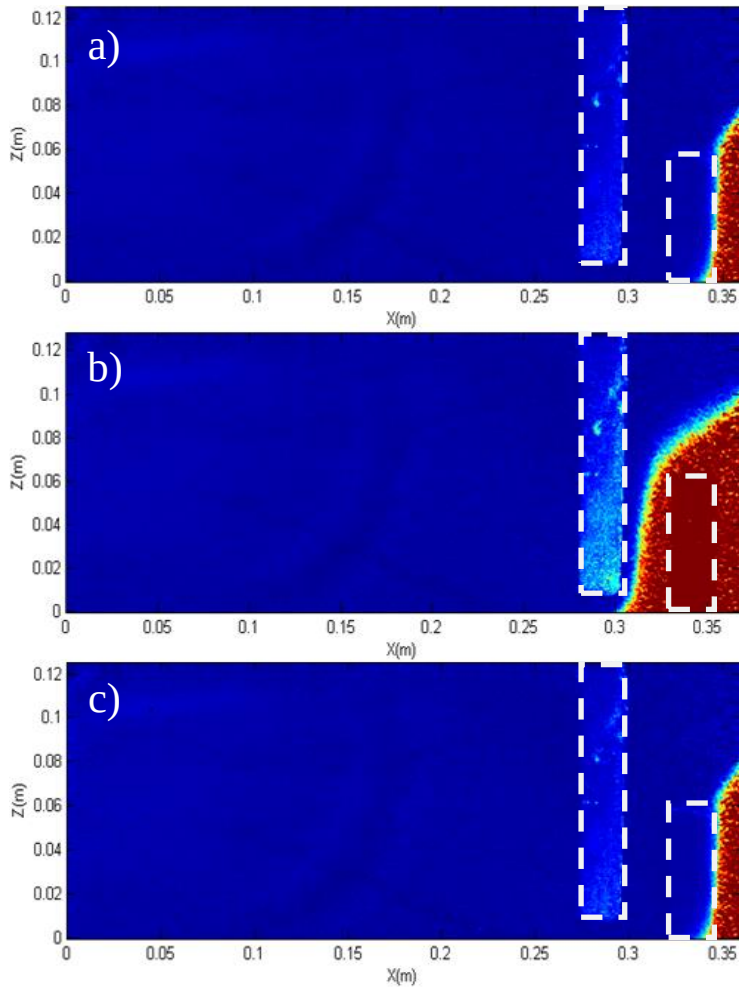

Figure 7.12 Steady-state experimental saltwater wedge in the MPB case; a) t = 0 min (initial condition); b) at t = 50 min; c) at t = 100 min

Fig 7.12 presents the experimental steady state saltwater wedges for the MPB case. The design parameters of the cutoff wall and the dam cases used here are the same as in the cutoff wall case and subsurface dam case, respectively. Upon imposing the first boundary conditions (dh = 6 mm), the saline water intruded the system before it was abruptly stopped at the position of the subsurface dam (Fig 7.12a). The initial intrusion length was 2.6 cm,

compared to TL = 8.8 cm recorded in the base case. It is interesting to note that unlike the subsurface dam case, the saline water did not penetrate through the dam here.

After applying a head difference of dh = 4 mm, the saltwater completely penetrated through the dam. The steady state TL was 6.9 cm, corresponding to a reduction R of 61% (Fig 7.12b). This result indicates that when the freshwater flow was not sufficiently high to prevent the complete saturation of the dam by the saline water, the MBP exhibited similar performance as the single cutoff wall. Laboratory observations revealed the existence of a saltwater lifting mechanism, whereby the residual saline flux was gradually lifted upward and transported over the dam toward the outlet (Fig 7.13a). This lifting also occurred over the course of the receding phase after increasing the head difference to dh = 6 mm (Fig 7.13b). To the best of our knowledge, this lifting mechanism has not been observed in previous studies. The images clearly show the freshwater flowing through the semi-permeable material of the dam and transporting the dense saline water along the interface.

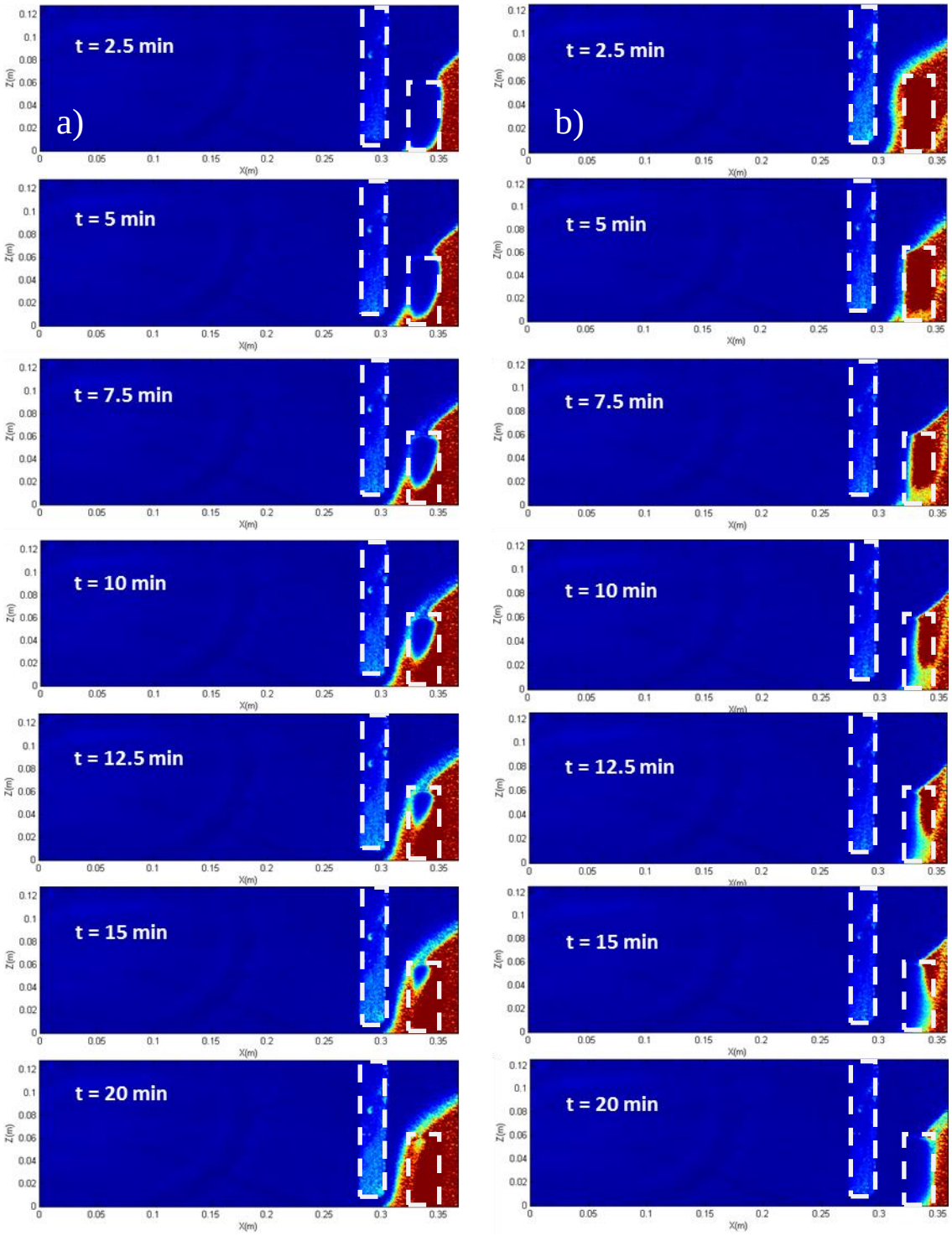

Figure 7.13 Experimental images of the saltwater lifting mechanism a) intruding condition (dh = 4 mm) b), receding condition (dh = 6 mm)

The performance of cutoff walls located nearby the coastline (less than half of the aquifer thickness) depends on the velocity ratio of the freshwater inflow velocity over the velocity of the intruding saltwater driven by density differences (Kaleris and Ziogas, 2013).

The combined effects of the cutoff wall and the semi-permeable dam induces an increase of the velocity ratio within the spacing between the barriers, which imposes more resistance to density contrast effects and allows the light freshwater to lift the denser liquid and discharge it outside the domain thereby ensuring an effective obstruction of the saltwater wedge on the seaward side of the dam. The recorded TL was 2.6 cm when the system reached final steady state, which corresponds to a reduction of 70% of the intrusion length (Fig 7.12c). In other words, the MPB achieved up to 62% and 42% more intrusion length reduction compared to the toe length recorded in the subsurface dam and the cutoff wall cases, respectively.

The transient dynamics of the saltwater wedge are shown in Fig 7.14. The transient toe movement was well reproduced by the numerical model for both hydraulic gradients. The experimental and numerical data show that the system reached steady state within 15 min for both hydraulic gradients. Additional simulations were conducted to investigate the influence of various key parameters on the saltwater intrusion length in presence of the MPB. The simulations were run solely for dh = 6 mm where the MPB exhibited the highest efficiency. Simulations were also run for single cutoff wall for the purpose of comparison. The TL was measured to characterize the effectiveness of the two barriers relative to each other. The MPB was found considerably more effective than the subsurface dam, even when the latter was impervious, and hence for this reason, the case of single semi-permeable dam was not included in the sensitivity analysis.

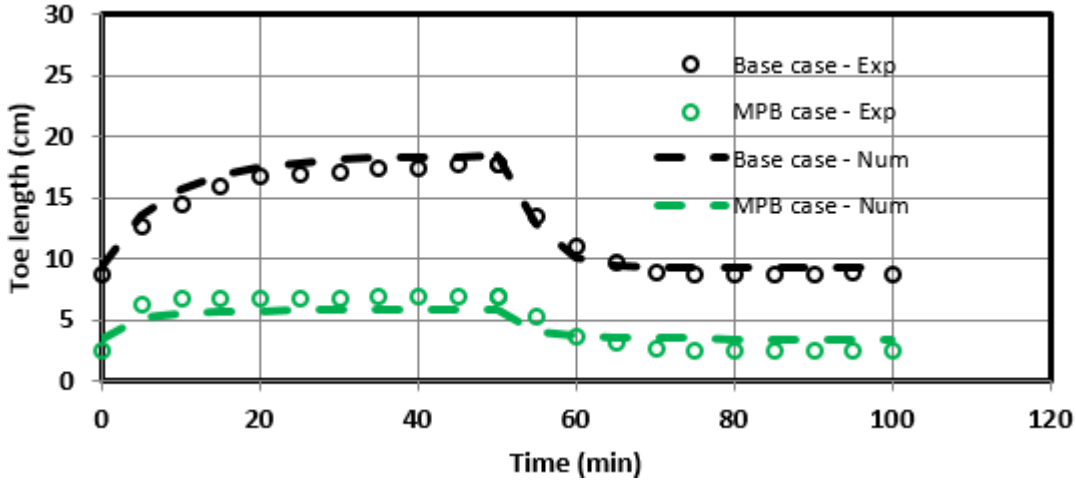

Figure 7.14 Transient experimental and numerical toe length results of the MPB case

The effect of the wall opening size (distance between the wall and aquifer bed) was first examined, where six X_c/H ratios over the range 0.1-0.6 were tested. Fig 7.15 shows the *TL* results in presence of a MPB and a single cutoff wall. The MPB induced 10% ($X_c/H = 0.1$) and 42% ($X_c/H = 0.6$) more reduction in the intrusion length than the cutoff wall. The smallest intrusion length was observed for $X_c/H = 0.3$ in the MPB case. The results indicate that the effect of MPB on the intrusion length was greater than that of the single cutoff as the wall opening size was increased. The MPB remains very effective up to opening size as large as $X_c/H = 0.6$, which may imply considerable construction cost saving. In addition, the 42% extra reduction introduced by the MPB system for $X_c/H = 0.6$ could not be achieved when using single cutoff wall even for wall penetration depth covering 90% of the aquifer thickness ($X_c/H = 0.1$). In such scenario, the MPB was not only substantially more effective in controlling the intrusion, but could also induce considerable construction cost savings, depending on the site specific hydrogeological conditions. This may be of particular importance for deep aquifers where the difference in the penetration depth between the MPB and the cutoff wall may induce significant saving, even considering the need to construct semi-permeable dam in the MPB case.

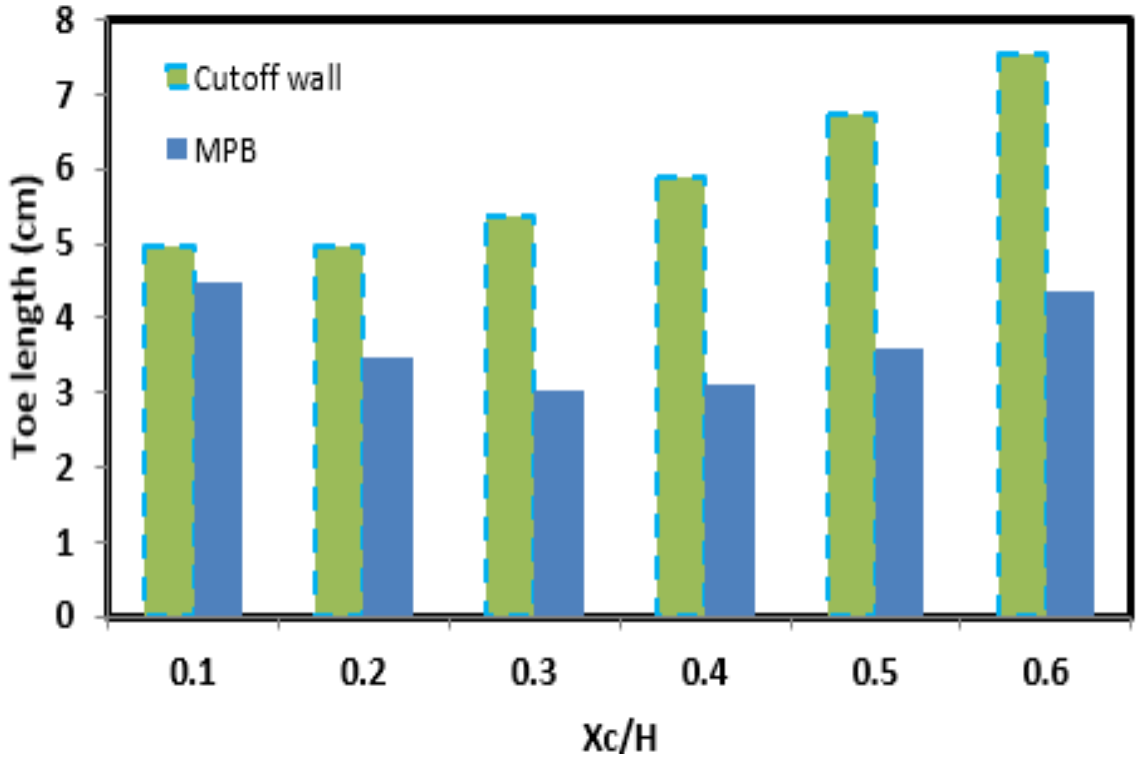

Figure 7.15 Effect of the ratio X_c/H on the intrusion length in presence of the MPB

The effect of the spacing X_s between the cutoff and the dam was also investigated. The subsurface dam was maintained at the same position, while the cutoff was moved seaward, such that six values of X_s ranging between 0.2 and 2.2 cm were investigated (Fig 7.16). The reduction of the TL achieved by the MPB increased by decreasing the spacing X_s, with a more pronounced reduction than a single cutoff. The smallest intrusion length was recorded at X_s = 0.2 cm in the MPB case, albeit this may be hardly feasible in practical situation. Note that for the range 0.2-1.0 cm, only little effect on the toe length was observed in the case of the MPB, while the performance of the single cutoff wall reached a maximum value for a wall position corresponding to X_s = 0.2 cm, i.e. when the wall was installed at 4.6 cm from the coastline boundary. The TL was 1.82 cm and 3.02 cm for the MPB and single cutoff, respectively. In other words, the MPB achieved 40% more saltwater wedge reduction than the single cutoff for the smallest spacing considered. Given that moving the cutoff in the seaward direction would allow greater fresh groundwater storage, this finding implies that a

more optimal use of the available freshwater could be associated with a more effective control of the saltwater intrusion process using an MPB system compared to a single cutoff wall system, for equivalent seaward displacement of the impermeable wall.

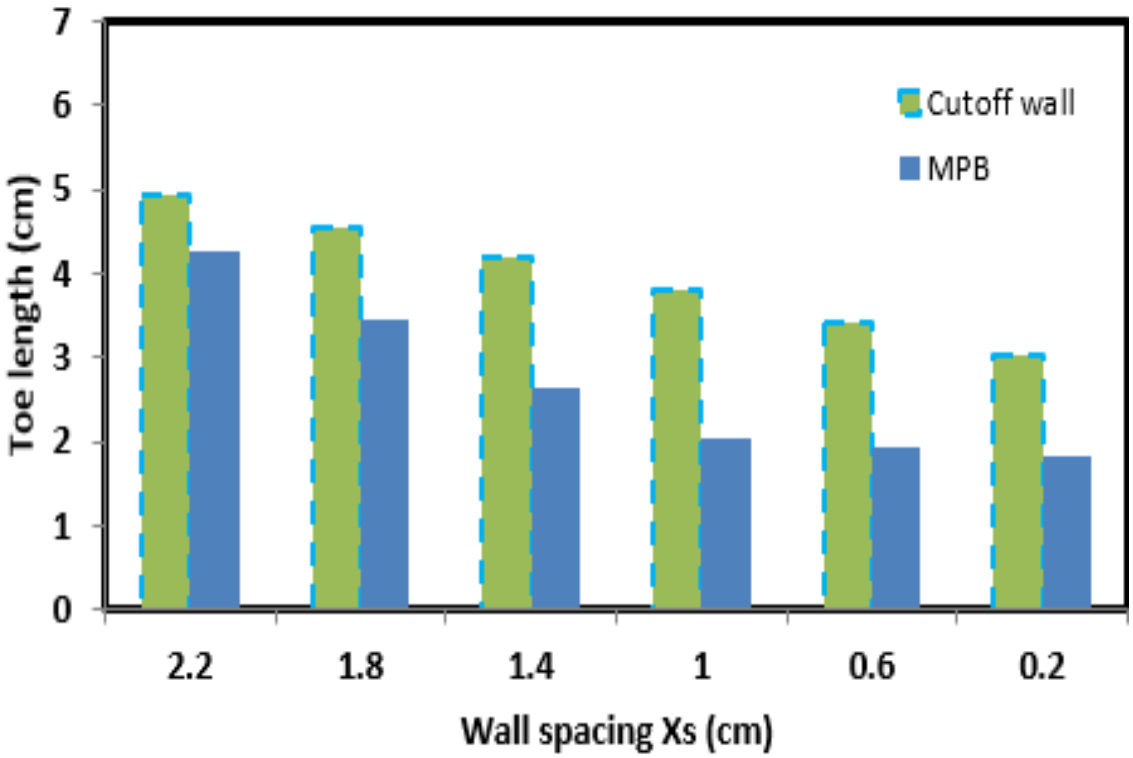

Figure 7.16 Effect of the spacing Xs on the intrusion length in presence of the MPB

The effect of the hydraulic conductivity of the porous medium on the barrier performance was examined over the range 35-300 cm/min (Fig 7.17). While the TL remained nearly the same in presence of single cutoff wall for the various K values, it continuously decreased with increasing K when using the MPB barrier system. The effect of hydraulic conductivity in the MPB case may be attributed to the permeability contrast between the dam and the background aquifer permeability, which keeps varying for different aquifer permeability. As the latter increases, this contrast ratio becomes bigger. The MPB induced between 5% and 21% more reduction than the cutoff wall as K varied from 35 to 300 cm/min

respectively. This result indicates that the relative effectiveness of MPB compared to a single cutoff would be expected to increase with increasing aquifer hydraulic conductivity.

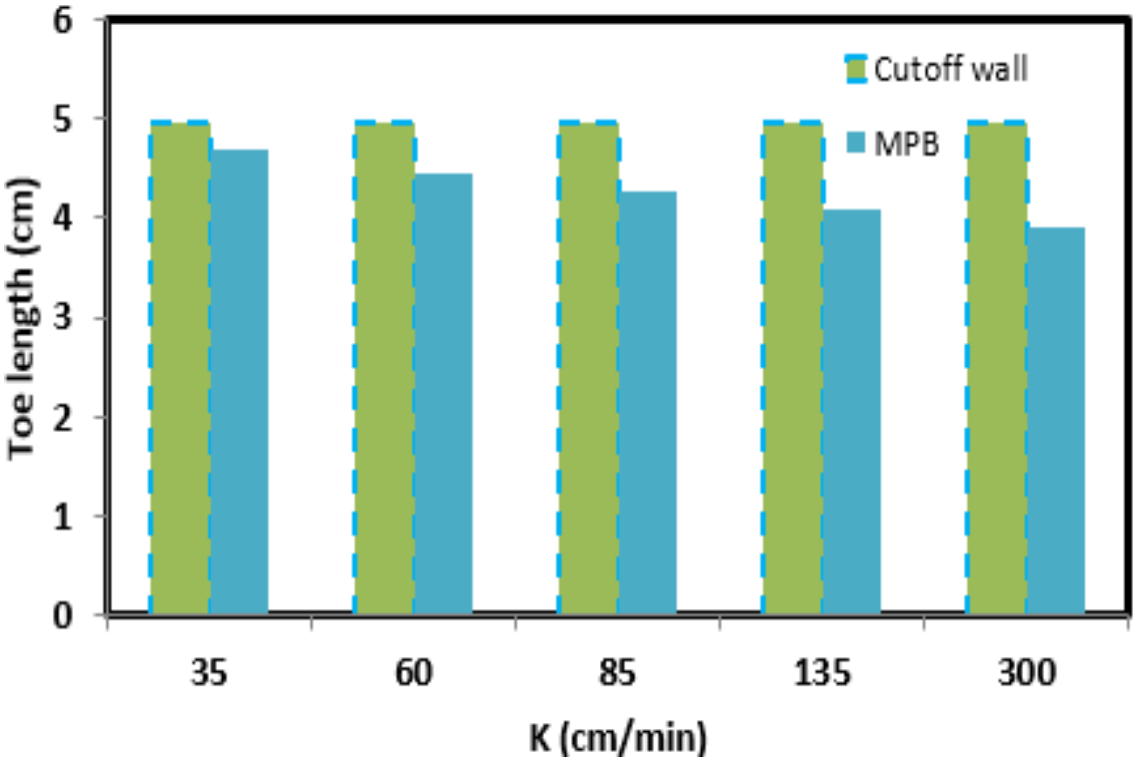

Figure 7.17 Effect of the aquifer hydraulic conductivity on the intrusion length in presence of the MPB

The effect of the dispersivity coefficients on the performance of MPB was also investigated (Fig 7.18). Three values of longitudinal dispersivity were tested: 0.001, 0.05 and 0.2 cm. The transversal to longitudinal dispersivity ratio remained constant. The net TL reduction was estimated at 2.5% and 2.8%, for the MPB and the cutoff wall, respectively. For the lowest and highest dispersivity values considered, the MPB induced about 14% additional reduction in the TL for the two extreme dispersivity values considered. The results show that the effectiveness of the MPB increased for systems with higher dispersivity. The impact of MPB on the saltwater intrusion length compared to that of a single cutoff wall would thus be expected to be greater in highly dispersive coastal groundwater systems.

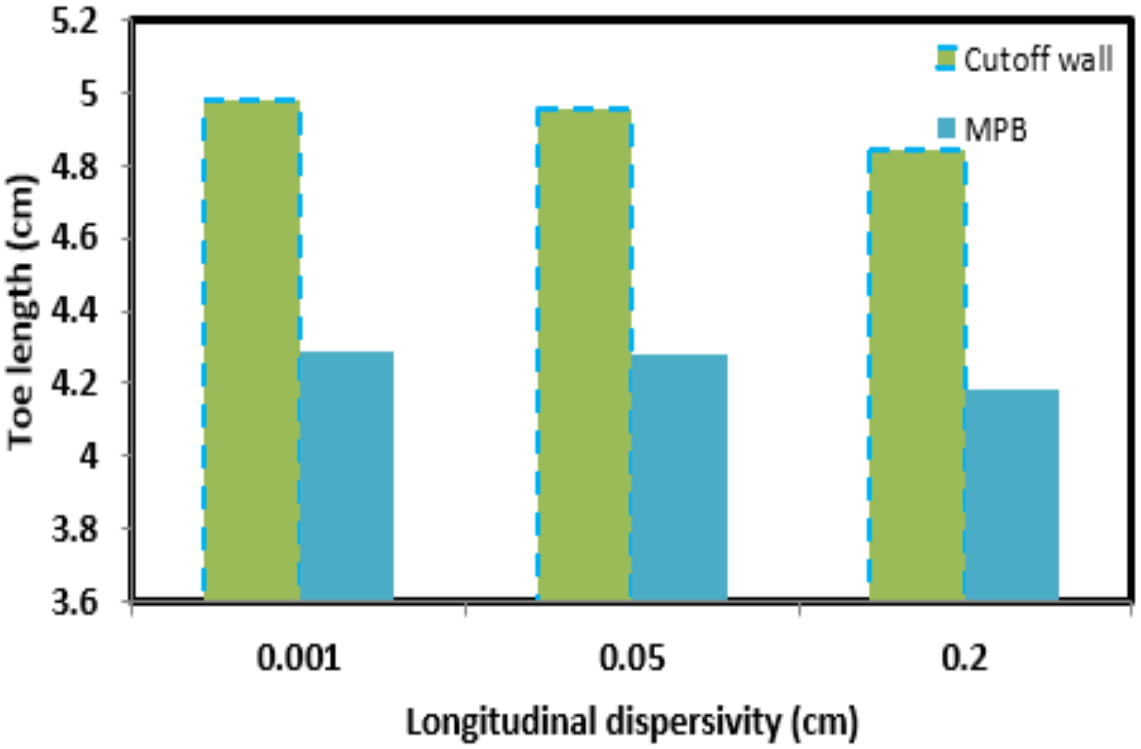

Figure 7.18 Effect of the longitudinal dispersivity of the aquifer on the intrusion length in presence of the MPB

Results of the influence of the density contrast on TL are presented in Fig 7.19, where three saltwater density contrast between seawater and freshwater of 1.020, 1.025 and 1.030 were examined. The increase in density contrast induced an increase of the intrusion length by 57% for the MPB case, and 18% for the single cutoff case. For the lowest density, the MPB achieved 44% more reduction than the single cutoff wall. By contrast, for the highest density difference considered, the single cutoff achieved about 7.8% more reduction of the TL than the MPB. The results show that the effectiveness of the MPB increases substantially for lower saltwater density. Obviously, the decrement of the saltwater density eases the lifting of saline flux by the MPB. This result implies that the MPB may display good efficiency in real scale aquifer setting, particularly in zones where wide transition zone generally occurs, where saltwater concentration is subsequently reduced as a result of micro/macro scale heterogeneity. The results suggest that more reduction of the intrusion length may be

achieved with the MPB than a single cutoff in coastal groundwater systems with saltwater solutions inferior or equal to 1025 kg/m^3. The performance of the MPB may however be lower for higher saltwater density values.

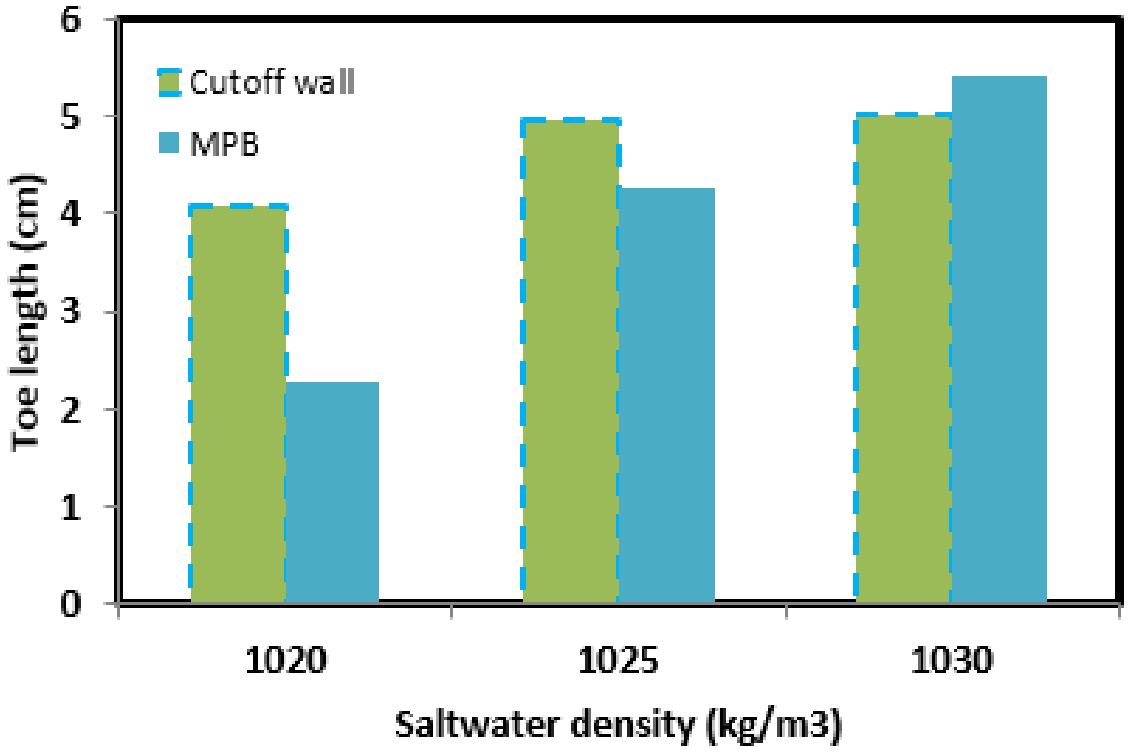

Figure 7.19 Effect of the saltwater density on the intrusion length in presence of the MPB

7.4 Summary and conclusions

This study provides a thorough analysis of the effect of subsurface physical barriers on saltwater intrusion dynamics under transient conditions. A new barrier system was suggested as saltwater intrusion control method: the mixed physical barrier MPB, which combines an impermeable cutoff wall and semi-permeable subsurface dam located on its seaward side. Using laboratory experiments and numerical simulations, the effect of the semi-permeable subsurface dam, cutoff wall and MPB on saltwater intrusion dynamics was investigated for different hydraulic gradients. The sensitivity of the performance of these different barriers to some key design and hydrogeological parameters was then explored. The main findings of the study are:

- Subsurface dams constructed from semi-permeable material do not provide suitable control of the saltwater intrusion process. A reduction in the toe length may be exhibited provided that the groundwater flux is sufficiently high to assist dam in retaining the intruding saltwater wedge. They primarily affect the rate of the saltwater transport process but this effect is rapidly dissipated after complete saturation of the dam by the saline water. In the cases investigated here, the semi-permeable dam eventually induced a negative effect on wedge length when the hydraulic gradient was lower, causing the toe length to extend beyond the toe location observed prior the dam installation.
- The worthiness of installing cutoff walls for saltwater intrusion control purposes increases as the hydraulic gradient becomes smaller or shallower. In the cases considered here, the cutoff wall was able to reduce the toe length by up to 63%.
- The MPB induced a visible saltwater lifting process, whereby freshwater flowing below the wall opening with increased velocity transported dispersive flux of saltwater above the subsurface dam and discharged it towards the outlet. This lifting mechanism has significant effect on the intrusion length, especially when the hydraulic gradient was

relatively steep, where it yielded up to 70% reduction of the initial intrusion length, corresponding to 42% more reduction than the single cutoff wall and 62% more than the semi permeable subsurface dam alone.

- While the effectiveness of single cutoff walls is limited to wall opening sizes not exceeding 40% of the aquifer thickness, the MPB exhibited good reduction for wall opening size extending up to 60% of the aquifer thickness, where it could exhibit up to 42% more reduction than a single cutoff wall. This reduction could not be achieved using single cutoff wall even for wall penetration depth covering 90% of the aquifer thickness. This finding therefore implies that there may be a potential for construction cost savings by installing impermeable wall with shorter penetration depth when using MPB (especially in deep coastal aquifer systems), and at the same time best ensuring the repulsion of intruding saline water.
- For equivalent seaward displacement of the impermeable wall, the MPB displayed better obstruction of the intruding saline water, achieving up to 40% more intrusion length reduction than the single cutoff wall. This finding implies that displacing the impermeable wall of the MPB seaward would not only ensure a more reliable prevention against saltwater intrusion, but also allow a more optimal use of the available freshwater volume, which is essential from a prospective of water resources management.
- The effectiveness of the MPB was found to increase with increasing hydraulic conductivity, dispersivity and decreasing saltwater density (<1025 kg/m3) of the coastal groundwater system.

In field applications, the installation of the MPB is expected to be more suitable in high hydraulic conductivity aquifers (e.g. sand, gravel), where the groundwater flow velocity is high. In such conditions, the effect of the MPB in increasing the freshwater inflow velocity over the velocity of the intruding saltwater within the spacing between the wall and the semi-

permeable dam will be more feasible. In addition, real aquifers generally exhibit higher dispersion often associated with micro/macro scale heterogeneity, which results in considerable widening of the freshwater-saltwater transition zone with different salt concentrations. Consequently, the toe of a marine saltwater intrusion may meet the inland freshwater with only slightly elevated concentrations (brines). This low density contrast between the intruding saline water and fresh groundwater may therefore further enhance the ability of the MPB to lift up saline flux and repulse it seaward.

Additional experiments and modelling would however be recommended for future work to further explore the field practicability of this system. For instance, the effect of large-scale model, 3D effects and the bottom boundary morphology are clearly worthy of further analyses. Our ongoing work focus on this and also on exploring the effectiveness of the MPB in heterogeneous aquifers and this shall be the subjects of future publications.

Chapter 8

Conclusions and recommendations

The purpose of this research was to provide, using laboratory and numerical modelling tools, an insight on the impact of subsurface physical barriers on saltwater intrusion and the associated flow and transport process in unconfined coastal aquifer systems incorporating typical layered heterogeneity and to assess the performance of the MPB as a new countermeasure for SWI control purposes.

The first result chapter (chapter 3) provides laboratory evidence that the expansion of the transition zone was less observable during the landward displacement of freshwater-saltwater interface, whether it occured as a result of water table drop or sea level rise and regardless of the magnitude of the head change. By contrast, the results showed that receding saltwater wedges exhibited a noticeable widening of the transition zone with similar amplitude when induced by a rise of the water table or a drop of the sea level, provided that the magnitude of head changes are comparable but opposite directions. In addition to be promoted by excessive dispersion along the interface, experimental observations revealed that the transition zone widening mechanism was also enhanced by possible sliding of some freshwater into the wedge during the saltwater retreat process, which was thereafter sucked upward because of density difference effects towards the transition zone, thereby exacerbating its widening. It seems conceivable that such mechanism could possibly occur in real coastal aquifer systems where the common non-uniformity of aquifer bedrocks could further enhance preferential flow and thus facilitate the leakage of some freshwater below the wedge, albeit field evidence of such effect have never been reported in previous studies. Further investigations involving larger aquifer models would enable further examination of the transition zone dynamics and explore the reproducibility of this observed phenomenon at

larger scale. The transient analysis of the saltwater toe length showed that timescale asymmetry between saltwater intrusion and retreat processes could also be observed in scenarios involving sea level fluctuations. Further work would be needed to assess saltwater migration rates in response to water level fluctuations in more complicated scenarios, involving for instance typical subsurface heterogeneity effects. The steady state toe length analysis showed that in such (highly) idealized homogeneous coastal system with horizontal bed and vertical slope a reasonable estimate of the logarithmic extent of the saltwater intrusion could be obtained based on the difference between the level of the water table and the sea level. The regression coefficients of the linear relationship would only require a minimum of two values of toe lengths associated with two water level differences for prediction purposes. It is important to underline that this finding is not meant to, and could not, be directly extrapolated to practical management situations. Future works involving the of larger and/or 3D aquifer models would nonetheless be beneficial in enabling using more data points to further verify the linear relationship suggested herein.

The findings reported in chapter 4 reveal that the vulnerability of pumping wells to salinization through upconing process would be higher in low permeability aquifer systems. In such environment, the results showed that the pumping rate needed to observe the upconing was relatively smaller than in the higher permeability system. In addition, the landward migration rate of the saltwater toe was also relatively faster, for equivalent pumping rate increment which suggests faster salinization rate of the aquifer. Further investigations including assessment of 3D effects would be desirable to support these interesting findings. Experimental observations showed that the widening of the freshwater-saltwater transition zone commonly observed as the saltwater wedge draws closer to the well location was more pronounced with decreasing permeability. The results suggest that the process of restoration of salinized aquifers after interruption of the (contaminated) well would be slower in low

permeability systems, which implies a longer time required before it possible to reuse freshwater from the restored aquifer. Flow velocity field analysis revealed that the saltwater upconing mechanism was associated with a large local reduction of the flow velocity along the upper part of the interface leading a subsequent local reduction of the repulsion forces exerted by the seaward freshwater flow, which thus facilitated the vertical rise of the saline plume toward the well. Sensitivity analysis showed that the critical pumping rate and critical time (defined as the time required for the 1% salt contour line to reach the well) were more sensitive to the variations in the well location than the well depth. The critical time increased with the increasing location and depth ratios following relatively simple linear equation. For all configurations tested, the lowest critical pumping rate was found for the lowest hydraulic conductivity, which further reflects the vulnerability of low permeability aquifer systems to salinization of pumping wells. Results showed that for the well configurations considered, higher saltwater densities would tend to facilitate the saltwater upconing mechanism. The influence of the saltwater density on the critical time was more significant for wells located farther away from the initial position of the interface. Results showed that increasing the dispersivity only induced negligible effects on the critical pumping rate. However, for a fixed pumping rate, the critical time decreased with increasing dispersivity, which suggests that higher dispersive systems would tend to induce faster upconing mechanism, for equivalent pumping rate,

Chapter 5 provides laboratory evidence of the performance of cutoff walls as a SWI control measures in various heterogeneous (multi-layered) coastal aquifer settings and for different hydraulic gradients. Albeit the stratification patterns found in real field applications may be more complex than the rather simplified and idealised approached adopted herein, the study provides nonetheless for the first time a valuable first-hand insight on the potential of cutoff walls to achieve substantial reduction of the saltwater intrusion length in typical

stratified scenarios. The experimental observations showed that their effectiveness would nonetheless be affected by the stratification (compared to simplified homogeneous conditions), to various degrees, depending on the arrangement of the layers. The existence of stratification would basically impose a disruption of the flow dynamics, and therefore likely affect the freshwater velocity at the opening wall opening. The results showed that the existence of a low permeability layer in the lower part of the aquifer in the system would induce a local reduction of the flow velocity at the wall opening, thereby decreasing the repulsion ability of the cutoff wall and thus allowing more inland penetration of the saline water. The results also showed that the presence of a low permeability layer in the middle portion of an aquifer system would affect the downward motion of the freshwater that is usually associated with the installation of cutoff calls, thereby also resulting in lowering the flow velocity at the wall opening relative to the homogeneous scenario, and thus reducing the repulsion force facing the intruding saltwater. Sensitivity analysis revealed that in such aquifer setting, the effectiveness of cutoff walls would be further reduced with decreasing the middle layer hydraulic conductivity, increasing its thickness and increasing the saltwater density. Their performance would nonetheless be improved by decreasing the distance to coastline and increasing wall penetration depth. Given that most of the real field sites exhibit prevalently layering stratification patterns, the results presented herein emphasizes the necessity to consider ground variability prior to planning and designing of cutoff walls for saltwater intrusion control purposes, for a more realistic assessment of their performance. Further works would include the assessment of the impact of the 3D effects on the present findings, which would also enable examination of the repulsion ability of cutoff walls with partial lateral coverage. Investigation of the effect of the slope of the aquifer bed on the performance of cutoff walls would also be desirable.

Chapter 6 provides valuable insights on the impact of layered heterogeneity on the ability of subsurface dams to control saltwater intrusion and to clean-up salinized coastal aquifers. The performance of subsurface dams was tested for their ability to restrict the saline water intrusion mechanism (prior to saltwater spillage) and to clean up the freshwater zone from residual saline water (post saltwater spillage). The results suggest that the existence of a low permeability zone in the upper part of an aquifer system would tend to enhance the ability of subsurface dams to restrict SWI mechanism and delay the time of salinization of the aquifer compared to an idealised homogeneous scenario. In such setting, the overlying low permeability layer would force the freshwater to flow through the reduced spacing between the crest of the wall and the bottom boundary of the low permeability layer, thereby effectively pushing the saltwater wedge downwards and obstructing its building up on the seaward side of the wall. Conversely, the existence of a low permeability layer in the lower part of the aquifer substantially would tend to substantially weaken the ability of subsurface dams to retain SWI, given the subsequent reduction of the flow velocity over the crest of the wall, which would allow easier building up of the saltwater on the seaward side of the wall and thus enable faster spillage of saline water into the freshwater storage area. Although real systems would exhibit more complex layering patterns, the results showed, for the first time under controlled laboratory conditions, strong evidence that the natural cleanup of SWI-contaminated coastal aquifers can eventually occur in heterogeneous (multi-layered) geological formations. The presence of stratified layers was nevertheless found to prolong the cleanup time compared to simplified homogeneous conditions, especially in the case where the aquifer is underlain by a low permeability layer, whereby the associated restriction of the freshwater flow that faces the wedge would considerably jeopardise the effective upward lifting of saline flux back over the wall. These findings further highlight the limitation of assuming simplified homogeneous conditions when attempting to assess the performance of

subsurface dams, which may lead to misleading estimation of their ability to restrict SWI and clean-up salinized coastal aquifers. Future works exploring the impact of the type of inland boundary (head controlled versus flux controlled) on the performance of subsurface dams and the associated time required for salinized aquifer systems to be restored would be of great interest.

Chapter 7 provides a thorough analysis of the effect of subsurface physical barriers on saltwater intrusion dynamics under transient conditions and proposes a new barrier system for saltwater intrusion control purposes, referred to as the mixed physical barrier MPB, which combines an impermeable cutoff wall and semi-permeable subsurface dam located on its seaward side. The results provided in this chapter show that subsurface dams constructed with semi-permeable material would tend not provide suitable control of SWI. On the other hand, the results showed that the worthiness of installing cutoff walls for SWI control would increase as the hydraulic gradient becomes shallower. This means that the expected reduction of toe length (compared to prior wall installation) would increase with decreasing hydraulic gradient of the aquifer system. The investigation of the MPB gives initial promising results as to its effectiveness in repulsing SWI, particularly for relatively steep hydraulic gradient where its performance was substantially greater than the other barriers investigated. The introduction of the MPB was associated with a visible lifting of the dense saline water towards the outlet by the (lighter) freshwater flow. Such interesting mechanism, observed for the very first time under controlled laboratory conditions, has never been documented in previous studies. The sensitivity analysis results showed that the effectiveness of the MPB was superior to the single cutoff wall for a wide range of wall design (wall opening and distance to coastline) and hydrogeological (hydraulic conductivity, dispersivity, density contrast) parameters tested. The results also suggested a possible potential for construction cost savings by installing impermeable wall with shorter penetration depth when using the

MPB (especially in deep coastal aquifer systems), and at the same time best ensuring the repulsion of intruding saline water. In addition, the results indicated that for equivalent seaward displacement of the impermeable wall, the MPB would ensure a more reliable prevention against saltwater intrusion than a single cutoff wall, which implies a more optimal use of the available freshwater volume, which is essential from a water resources management stand point. The results indicated that the performance of the MPB would be expected to increase in high hydraulic conductivity aquifers (e.g. sand, gravel), where the groundwater flow velocity is relatively high, which would enable best the increase of the ratio of the freshwater inflow velocity over the intruding saltwater velocity within the spacing between the wall and the semi-permeable dam and thus allow faster repulsion. The relatively high dispersion commonly found in real aquifer systems, often associated with micro/macro scale heterogeneity, would be expected to break down density contrast and thus further enhance the ability of the MPB to lift up saline flux, thereby facilitating its seaward repulsion. Additional experiments and modelling would however be recommended for future work to further explore the field practicability of this new system. Future investigations involving larger scale models, 3D effects, and the influence of the bottom boundary morphology on the effectiveness of the MPB as well as the reproducibility of the observed saltwater lifting mechanism are clearly worthy of further analyses.

References

Abarca, E., Carrera, J., Sánchez-Vila, X., Dentz, M., 2007. Anisotropic dispersive Henry problem. Adv.Water Resour. 30, 913-926.

Abarca, E., Clement, T.P., 2009. A novel approach for characterizing the mixing zone of a saltwater wedge. Geophys.Res.Lett. 36, L06402.

Abarca, E., Vázquez-Suñé, E., Carrera, J., Capino, B., Gámez, D., Batlle, F., 2006. Optimal design of measures to correct seawater intrusion. Water Resour.Res. 42, W09415

Abdoulhalik, A., Ahmed, A.A., 2017a. The effectiveness of cutoff walls to control saltwater intrusion in multi-layered coastal aquifers: Experimental and numerical study. Journal of Environmental Management. 199, 62-73.

Abdoulhalik, A., Ahmed, A.A., 2017b. How does layered heterogeneity affect the ability of subsurface dams to clean up coastal aquifers contaminated with seawater intrusion? Journal of Hydrology. 553, 708-721.

Abdoulhalik, A., Ahmed, A., Hamill, G.A., 2017. A new physical barrier system for seawater intrusion control. Journal of Hydrology. 549, 416-427.

Allow, K.A., 2012. The use of injection wells and a subsurface barrier in the prevention of seawater intrusion: a modelling approach. Arabian Journal of Geosciences. 5, 1151-1161.

Anwar, H., 1983. The effect of a subsurface barrier on the conservation of freshwater in coastal aquifers. Water Res. 17, 1257-1265.

Archwichai, L., Mantapan, K., & Srisuk, K., 2005. Approachability of subsurface dams in the Northeast Thailand. In International conference on geology, geotechnology and mineral resources of Indochina . 28-30.

Attanayake, P., Sholley, M., Evaluation of the hydraulic gradient at an island for low-level nuclear waste disposal, IAHS publication 312, 2007, 237-243.

Basdurak, N. B., Onder, H., & Motz, L. H. 2007. Analysis of Techniques to Limit Saltwater Intrusion in Coastal Aquifers. In World Environmental and Water Resources Congress 2007: Restoring Our Natural Habitat. 1-8.

Bear, J., 1972. Dynamics of flow in porous media. Dover, New York.

Bear, J., 1979. Hydraulics of groundwater, MacGraw-Hill, New-york.

Bear, J., Cheng, A.H., Sorek, S., Ouazar, D., Herrera, I., 1999. Seawater intrusion in coastal aquifers: concepts, methods and practices, Springer Science & Business Media.

Botero-Acosta, A., Donado, L.D., 2015. Laboratory Scale Simulation of Hydraulic Barriers to Seawater Intrusion in Confined Coastal Aquifers Considering the Effects of Stratification. Procedia Environmental Sciences. 25, 36-43.

Chang, S.W., Clement, T.P., 2012. Experimental and numerical investigation of saltwater intrusion dynamics in flux-controlled groundwater systems. Water Resour.Res. 48, W09527.

Chang, S.W., Clement, T.P., Simpson, M.J., Lee, K., 2011. Does sea-level rise have an impact on saltwater intrusion? Adv.Water Resour. 34, 1283-1291.

Comte, J.-., Wilson, C., Ofterdinger, U., González-Quirós, A., 2017. Effect of volcanic dykes on coastal groundwater flow and saltwater intrusion: A field-scale multiphysics approach and parameter evaluation. Water Resour.Res. 53, 2171-2198.

Dagan, G., Bear, J., 1968. Solving the problem of local interface upconing in a coastal aquifer by the method of small perturbations. Journal of Hydraulic Research. 6, 15-44.

de Louw, P.G.B., Vandenbohede, A., Werner, A.D., Oude Essink, G.H.P., 2013. Natural saltwater upconing by preferential groundwater discharge through boils. Journal of Hydrology. 490, 74-87.

Diersch, H.-., Prochnow, D., Thiele, M., 1984. Finite-element analysis of dispersion-affected saltwater upconing below a pumping well. Applied Mathematical Modelling. 8, 305-312.

Dose, E.J., Stoeckl, L., Houben, G.J., Vacher, H.L., Vassolo, S., Dietrich, J., Himmelsbach, T., 2014. Experiments and modeling of freshwater lenses in layered aquifers: Steady state interface geometry. Journal of Hydrology. 509, 621-630.

Essink, G.H.O., 2001. Improving fresh groundwater supply—problems and solutions. Ocean Coast.Manage. 44, 429-449.

Ferguson, G., Gleeson, T., 2012. Vulnerability of coastal aquifers to groundwater use and climate change. Nature Climate Change. 2, 342-345.

Goswami, R.R., Clement, T.P., 2007. Laboratory-scale investigation of saltwater intrusion dynamics. Water Resour.Res. 43, W04418.

Guo, W., Langevin, C.D., 2002, User's guide to SEAWAT; a computer program for simulation of three-dimensional variable-density ground-water flow.

Harbaugh, A.W., Banta, E.R., Hill, M.C., McDonald, M.G., 2000. MODFLOW-2000, The U. S. Geological Survey Modular Ground-Water Model-User Guide to Modularization Concepts and the Ground-Water Flow Process. Open-file Report.U.S.Geological Survey., 134.

Hasan Basri, M., 2001. Two new methods for optimal design of subsurface barrier to control seawater intrusion, PhD thesis, The Univ. of Manitoba, Canada.

Hussain, M.S., Javadi, A.A., 2016. Assessing impacts of sea level rise on seawater intrusion in a coastal aquifer with sloped shoreline boundary. Journal of Hydro-environment Research. 11, 29-41.

IPCC, 2014, Climate change, Intergovernmental Panel On Climate.

Jakovovic, D., Werner, A.D., Simmons, C.T., 2011. Numerical modelling of saltwater up-coning: Comparison with experimental laboratory observations. Journal of Hydrology. 402, 261-273.

Japan Green Resources Agency, 2004. Technical Reference for Effective Groundwater Development.

Johannsen, K., Kinzelbach, W., Oswald, S., Wittum, G., 2002. The saltpool benchmark problem – numerical simulation of saltwater upconing in a porous medium. Advances in Water Resources. 25, 335-348.

Kaleris, V.K., Ziogas, A.I., 2013. The effect of cutoff walls on saltwater intrusion and groundwater extraction in coastal aquifers. Journal of Hydrology. 476, 370-383.

Kashef, A.I., Smith, J.C., 1975. Expansion of salt-water zone due to well discharge, Journal of the American Water Resources Association. 11, 1107-1120.

Ketabchi, H., Mahmoodzadeh, D., Ataie-Ashtiani, B., Simmons, C.T., 2016. Sea-level rise impacts on seawater intrusion in coastal aquifers: Review and integration. Journal of Hydrology. 535, 235-255.

Ketabchi, H., Mahmoodzadeh, D., Ataie-Ashtiani, B., Werner, A.D., Simmons, C.T., 2014. Sea-level rise impact on fresh groundwater lenses in two-layer small islands. Hydrol.Process. 28, 5938-5953.

Kim, K., Seong, H., Kim, T., Park, K., Woo, N., Park, Y., Koh, G., Park, W., 2006. Tidal effects on variations of fresh–saltwater interface and groundwater flow in a multilayered coastal aquifer on a volcanic island (Jeju Island, Korea). Journal of Hydrology. 330, 525-542.

Klassen, J., Allen, D.M., 2017. Assessing the risk of saltwater intrusion in coastal aquifers. Journal of Hydrology. 551, 730-745.

Kumar, C., 2006. Management of groundwater in salt water ingress coastal aquifers. Groundwater Modelling and Management., 540-560.

Langevin, C.D., Shoemaker, W.B., W.B., Guo, W., 2003, MODFLOW-2000, the US Geological Survey Modular Ground-Water Model--Documentation of the SEAWAT-2000 Version with the Variable-Density Flow Process (VDF) and the Integrated MT3DMS Transport Process (IMT). USGS Open-File Report 03-426. Tallahassee, Florida.

Liu, Y., Mao, X., Chen, J., Barry, D.A., 2014. Influence of a coarse interlayer on seawater intrusion and contaminant migration in coastal aquifers. Hydrol. Process. 28, 5162-5175.

Lu, C., Chen, Y., Zhang, C., Luo, J., 2013. Steady-state freshwater–seawater mixing zone in stratified coastal aquifers. Journal of Hydrology. 505, 24-34.

Lu, C., Werner, A.D., 2013. Timescales of seawater intrusion and retreat. Adv.Water Resour. 59, 39-51.

Lu, C., Xin, P., Li, L., Luo, J., 2015. Seawater intrusion in response to sea-level rise in a coastal aquifer with a general-head inland boundary. Journal of Hydrology. 522, 135-140.

Luyun Jr, R.A., 2010. Effects of Subsurface Physical Barrier and Artificial Recharge on Seawater Intrusion in Coastal Aquifers. PhD thesis, Kagoshima University, Japan.

Luyun Jr., R., Momii, K., Nakagawa, K., 2009. Laboratory-scale saltwater behavior due to subsurface cutoff wall. Journal of Hydrology. 377, 227-236.

Luyun, R., Momii, K., Nakagawa, K., 2011. Effects of recharge wells and flow barriers on seawater intrusion. Ground Water. 49, 239-249.

Mehdizadeh, S.S., Vafaie, F., F., Abolghasemi, H., 2015. Assessment of sharp-interface approach for saltwater intrusion prediction in an unconfined coastal aquifer exposed to pumping. Environmental Earth Sciences. 73, 8345-8355.

Mehdizadeh, S.S., Karamalipour, S.E., Asoodeh, R., 2017. Sea level rise effect on seawater intrusion into layered coastal aquifers (simulation using dispersive and sharp-interface approaches). Ocean & Coastal Management. 138, 11-18.

Mehdizadeh, S.S., Werner, A.D., Vafaie, F., Badaruddin, S., 2014. Vertical leakage in sharp-interface seawater intrusion models of layered coastal aquifers. Journal of Hydrology. 519, 1097-1107.

Michael, H.A., Russoniello, C.J., Byron, L.A., 2013. Global assessment of vulnerability to sea-level rise in topography-limited and recharge-limited coastal groundwater systems. Water Resour.Res. 49, 2228-2240.

Morgan, L.K., Bakker, M., Werner, A.D., 2015. Occurrence of seawater intrusion overshoot. Water Resour.Res. 51, 1989-1999.

Morgan, L.K., Stoeckl, L., Werner, A.D., Post, V.E.A., 2013. An assessment of seawater intrusion overshoot using physical and numerical modeling. Water Resour.Res. 49, 6522-6526.

Morris, B.L., Lawrence, A.R., Chilton, P., Adams, B., Calow, R.C., Klinck, B.A., 2003. Groundwater and its susceptibility to degradation: a global assessment of the problem and options for management, United Nations Environment Programme.

Noorabadi, S., Nazemi, A., Sadraddini, A., Delirhasannia, R., 2017. Laboratory investigation of water extraction effects on saltwater wedge displacement. Global Journal of Environmental Science and Management. 3, 21-32.

Oki, D.S., Souza, W.R., Bolke, E.L., Bauer, G.R., 1998. Numerical analysis of the hydrogeologic controls in a layered coastal aquifer system, Oahu, Hawaii, USA. Hydrogeol.J. 6, 243-263.

Oostrom, M., Hayworth, J.S., Dane, J.H., Güven, O., 1992. Behavior of dense aqueous phase leachate plumes in homogeneous porous media. Water Resour.Res. 28, 2123-2134.

Oswald, S.E., Scheidegger, M.B., Kinzelbach, W., 2002. Time-dependent measurement of strongly density-dependent flow in a porous medium via nuclear magnetic resonance imaging. Transp.Porous Media. 47, 169-193.

Oswald, S.E., Kinzelbach, W., 2004. Three-dimensional physical benchmark experiments to test variable-density flow models. Journal of Hydrology. 290, 22-42.

Oude Essink, G.H.P., 2001. Improving fresh groundwater supply—problems and solutions. Ocean Coast.Manage. 44, 429-449.

Oude Essink, G.H.P., van Baaren, E.S., de Louw, P.G.B., 2010. Effects of climate change on coastal groundwater systems: A modeling study in the Netherlands. Water Resour.Res. 46, W00F04.

Pool, M., Carrera, J., 2010. Dynamics of negative hydraulic barriers to prevent seawater intrusion. Hydrogeol.J. 18, 95-105.

Rasmussen, P., Sonnenborg, T., Goncear, G., Hinsby, K., 2013. Assessing impacts of climate change, sea level rise, and drainage canals on saltwater intrusion to coastal aquifer. Hydrology and Earth System Sciences. 17, 421-443.

Reilly, T.E., Goodman, A.S., 1987. Analysis of saltwater upconing beneath a pumping well. Journal of Hydrology. 89, 169-204.

Riva, M., Guadagnini, A., Dell'Oca, A.., 2015. Probabilistic assessment of seawater intrusion under multiple sources of uncertainty. Adv.Water Resour. 75, 93-104.

Robinson, G., Ahmed, A.A., Hamill, G.A., 2016. Experimental saltwater intrusion in coastal aquifers using automated image analysis: Applications to homogeneous aquifers. Journal of Hydrology. 538, 304-313.

Robinson, G., Hamill, G.A., Ahmed, A.A., 2015. Automated image analysis for experimental investigations of salt water intrusion in coastal aquifers. Journal of Hydrology. 530, 350-360.

Schmork, S., Mercado, A., 1969. Upconing of Fresh Water—Sea Water Interface Below Pumping Wells, Field Study. Water Resour.Res. 5, 1290-1311.

Sebben, M.L., Werner, A.D., Graf, T., 2015. Seawater intrusion in fractured coastal aquifers: A preliminary numerical investigation using a fractured Henry problem. Adv.Water Resour. 85, 93-108.

Sherif, M.M., Singh, V.P., 1999. Effect of climate change on sea water intrusion in coastal aquifers. Hydrol.Process. 13, 1277-1287.

Shi, L., Cui, L., Park, N., Huyakorn, P.S., 2011. Applicability of a sharp-interface model for estimating steady-state salinity at pumping wells—validation against sand tank experiments. Journal of Contaminant Hydrology. 124, 35-42.

Simmons, C.T., Fenstemaker, T.R., Sharp, J.M., 2001. Variable-density groundwater flow and solute transport in heterogeneous porous media: approaches, resolutions and future challenges. Journal of Contaminant Hydrology. 52, 245-275.

Simpson, M.W., Allen, D.M., Journeay, M.M., 2014. Assessing risk to groundwater quality using an integrated risk framework. Environmental earth sciences. 71, 4939-4956.

Sriapai, T., Walsri, C., Phueakphum, D., Fuenkajorn, K., 2012. Physical model simulations of seawater intrusion in unconfined aquifer. Songklanakarin Journal of Science & Technology. 34, 679-687.

Stoeckl, L., Houben, G.J., Dose, E.J., 2015. Experiments and modeling of flow processes in freshwater lenses in layered island aquifers: Analysis of age stratification, travel times and interface propagation. Journal of Hydrology. 529, 159-168.

Strack, O.D.L., 1976. A single-potential solution for regional interface problems in coastal aquifers. Water Resour.Res. 12, 1165-1174.

Strack, O.D.L., Ausk, B.K., 2015. A formulation for vertically integrated groundwater flow in a stratified coastal aquifer. Water Resour.Res. 51, 6756-6775.

Strack, O.D.L., Stoeckl, L., Damm, K., Houben, G., Ausk, B.K., de Lange, W.J. 2016. Reduction of saltwater intrusion by modifying hydraulic conductivity. Water Resour.Res. 52, 6978-6988.

Sugio, S., Nakada, K., Urish, D.W., 1987. Subsurface seawater intrusion barrier analysis. J.Hydraul.Eng. 113, 767-779.

Todd, D.K., 1959. Ground water hydrology, John Wiley and Sons, Inc, New York.

Van Dam, J., 1999. Exploitation, restoration and management,Seawater Intrusion in Coastal Aquifers—Concepts, Methods and Practices, Springer, 73-125.

Voss, C.I., Souza, W.R., 1987. Variable density flow and solute transport simulation of regional aquifers containing a narrow freshwater-saltwater transition zone. Water Resour.Res. 23, 1851-1866.

Watson, T.A., Werner, A.D., Simmons, C.T., 2010. Transience of seawater intrusion in response to sea level rise. Water Resour.Res. 46, W12533.

Webb, M.D., Howard, K.W.F., 2011. Modeling the Transient Response of Saline Intrusion to Rising Sea-Levels. Ground Water. 49, 560-569.

Werner, A.D., Bakker, M., Post, V.E.A., Vandenbohede, A., Lu, C., Ataie-Ashtiani, B., Simmons, C.T., Barry, D.A., 2013. Seawater intrusion processes, investigation and management: Recent advances and future challenges. Advances in Water Resources. 51, 3-26.

Werner, A.D., Jakovovic, D., Simmons, C.T., 2009. Experimental observations of saltwater up-coning. Journal of Hydrology. 373, 230-241.

Werner, A.D., Simmons, C.T., 2009. Impact of Sea-Level Rise on Sea Water Intrusion in Coastal Aquifers. Ground Water. 47, 197-204.

WHO, 2011. Guidelines for drinking-water quality. World Health Organization. 216, 303-304.

Wirojanagud, P. and Charbeneau, R. J., 1985, Saltwater upconing in unconfined aquifers, Journal of Hydraulic Engineering, 111, 417–434.

Zheng, C., Wang, P.P., 1999, MT3DMS: a modular three-dimensional multispecies transport model for simulation of advection, dispersion, and chemical reactions of contaminants in groundwater systems.